Molecular mechanisms used by *Staphylococcus aureus* to access iron from human haemoglobin

Claire F. Dickson
Menzies Research Institute

Submitted in fulfilment of the requirements for the degree of Doctor of Philosophy
University of Tasmania, October 2014

Declarations

This thesis contains no material which has been accepted for a degree or diploma by the University or any other institution, except by way of background information and duly acknowledged in the thesis, and to the best of my knowledge and belief no material previously published or written by another person except where due acknowledgement is made in the text of the thesis, nor does the thesis contain any material that infringes copyright.

The publishers of the papers comprising Chapter 3 and part of Chapter 5 hold the copyright for that content, and access to the material should be sought from the respective journals. The remaining non-published content of the thesis may be made available for loan and limited copying and communication in accordance with the Copyright Act 1968.

Claire Dickson
May 2014

Authority of access

This thesis may be made available for loan and limited copying and communication in accordance with the Copyright Act 1968.

Statement of co-authorship

The following people and institutions contributed to the publication of work undertaken as part of this thesis:

Claire Dickson, Menzies Research Institute Tasmania = Candidate
Kaavya Krishna Kumar, The University of Sydney = **Author 1**
David A. Jacques, MRC Laboratory of Molecular Biology, United Kingdom = **Author 2**
G. Reza Malmirchegini, University of California Los Angeles, USA = **Author 3**
Thomas Spirig, The University of California Los Angeles, USA = **Author 4**
Joel P. Mackay, The University of Sydney = **Author 5**
Robert T. Clubb, The University of California Los Angeles, USA = **Author 6**
J. Mitchell Guss, The University of Sydney = **Author 7**
David A. Gell, University of Tasmania = **Author 8**
Gleb Pishchany, Vanderbilt University School of Medicine, USA = **Author 9**
Jessica R. Sheldon, University of Western Ontario, Canada = **Author 10**
Md Tauqeer Alam, Emory University School of Medicine, USA = **Author 11**
Timothy D. Read, Emory University School of Medicine, USA = **Author 12**
David E. Heinrichs, University of Western Ontario, Canada = **Author 13**
Eric P. Skaar, Vanderbilt University School of Medicine, USA = **Author 14**

Author details and their roles:
Paper 1, "Structure of the Hemoglobin-IsdH Complex Reveals the Molecular Basis of Iron Capture by *Staphylococcus aureus*", published in The Journal of Biological Chemistry (2014) 289, 6728-6738:
Located in Chapter 3.
Candidate was the primary author and, with Authors 1–3 and Authors 5–8, contributed to the idea, its formalisation and development.
Author 1 contributed 1 from 5 data figures/tables in Paper 1 (the crystal structure of $IsdH^{N2}$, which is not presented in this thesis).
Author 2 assisted with data collection and analysis.
Author 3 prepared some of the protein samples used for experiments presented in Paper 1.
Author 4 made the DNA construct that was used to produce the protein provided by Author 3.
Candidate contributed 4 from 5 data figures/tables in Paper 1.

Paper 2, "IsdB-dependent Hemoglobin Binding Is Required for Acquisition of Heme by *Staphylococcus aureus*", published in The Journal of Infectious Diseases *doi* 10.1093/infdis/jit817, first published online December 13, 2013:
Located in Section 5.2 of Chapter 5.
Candidate and Authors 8–14 contributed to the idea, its formalisation and development.
Candidate contributed 1 from 6 data figures in Paper 2.

We the undersigned agree with the above stated "proportion of work undertaken" for each of the above published (or submitted) peer-reviewed manuscripts contributing to this thesis:

Signed: _____ _____

David Gell
Supervisor
Menzies Research Institute
University of Tasmania

Tom Marwick
Head of School
Menzies Research Institute
University of Tasmania

Date: 09-05-2014

Abstract

Iron is used as a co-factor in a range of biological reactions and is an essential nutrient across all domains of life. During infection, pathogens must acquire iron from their host environment. The tetrameric oxygen transport protein, haemoglobin A (Hb), represents the largest pool of mammalian iron, accounting for ~ 65 % of iron in a healthy individual. Genes encoding for Hb receptors are found in the genomes of Gram-positive and Gram-negative pathogens and their deletion results in attenuated virulence, suggesting that Hb is an important source of iron during host colonization. As yet, the mechanisms by which these receptors interact with Hb and capture the haem co-factor (containing the iron) are largely unknown.

Staphylococcus aureus is a Gram-positive human pathogen and is a significant health burden in both community and health care settings. *S. aureus* expresses an elaborate system of proteins known as the iron regulated surface determinant (Isd) system, which is specialized to strip iron from Hb. Two related Hb receptors have been identified in the staphylococcal genome, IsdB and IsdH. IsdB and IsdH bind to Hb on the bacterial cell surface, actively remove the haem cofactor and relay it to the down stream haem binding proteins IsdA and IsdC in the cell wall. IsdB and IsdH are multi-domain proteins, with separate domains dedicated to Hb binding and haem binding. Recent structural studies have revealed how Hb and haem are bound by the isolated domains, however, as the isolated domains do not liberate the haem cofactor from Hb these studies provide limited insight into the receptor mechanism. The aim of this project was to characterize the structure and function of the intact Hb receptors and reveal the molecular mechanism by which they capture the haem from Hb and relay it through the Isd pathway.

Small angle X-ray scattering studies were used to show that a conserved three-domain region of IsdB and IsdH, which includes one Hb-binding and one haem-binding domain, adopts a conserved bi-lobed structure. Two X-ray crystal structures of IsdB and IsdH at 4.2 Å and 3.7 Å resolution, respectively, indicate that this architecture is maintained upon binding to Hb. Each α and β Hb globin chain is bound independently by one receptor molecule and functional studies confirmed that haem is captured from all four globin haem pockets, suggesting a mechanism where the receptors can access all the globin haem groups regardless of the Hb oligomeric state.

The Hb-binding domains of the full-length receptors bind to a surface of Hb that is distant from the globin haem coordination site. The haem-binding domain is positioned via a scaffolding linker domain directly adjacent to the globin haem pocket suggesting that a second set of specific interactions is involved in liberating the haem cofactor. As this interface is not well resolved in the low-resolution structures, rational mutagenesis was used to alter the Hb-binding properties of IsdH. A version of IsdH that bound through only the α subunit of Hb yielded crystals that diffracted to 2.5 Å resolution. The higher resolution structure revealed specific contacts on the haem transfer interface, and a conformational change in the globin haem pocket, which begin to illustrate how the haem cofactor is extracted from the globin.

To investigate the mechanism of haem relay through the Isd pathway, haem transfer assays were designed. IsdH and IsdB captured haem from Hb with similar efficiency. However, IsdB showed superior activity in transferring haem to IsdA and IsdC. Haem capture from Hb required the specific recognition of Hb though the Hb-targeting domain, but, the speed of haem relay to IsdA/C was inversely related Hb-binding affinity suggesting that haem relay activity relies on a weak interaction with the Hb molecule. Using site directed mutagenesis, Hb binding affinity was attenuated or enhanced in a range of IsdB constructs. The activity of these mutants in haem relay experiments was consistent with the hypothesis that Hb binding affinity is fine tuned to allow for a specific interaction while maximizing the transfer speed of the haem cargo.

Hb utilization is a common strategy employed by pathogenic bacteria to enhance growth and survival during infection. This work has contributed to our understanding of how the human pathogen, *S. aureus,* interacts with and utilizes host Hb, and is the first study to characterize the molecular mechanism by which the haem ligand is captured from Hb by a bacterial receptor.

Acknowledgements

Firstly, thank you to my supervisor Dave. It has been a privilege to work with, and learn from such a brilliant scientist.

Thank you to Lisa and Adele for looking out for my welfare and being my mothers at Menzies.

To Joel, Jacqui, Margie, Ann and Mitchell, thank you for welcoming me into your labs, mentoring me and being such amazing, interesting people.

Dave J. and Kaavya – I am lucky to have shared this experience with you and have learnt so much from you both. To Dave J. especially, thank you for believing in me, encouraging me and providing me with a friendship that I will value forever.

To Kate and Kaz, thank you for running with me, eating too much chocolate with me, and keeping me sane throughout this degree. To the rest of my peers at UTAS and USYD, it would not have been the same without you!

Vanessa and Katrina – the best things to come to me through science!

Thank you to the MX and SAXS/WAXS beamline scientists at the Australian Synchrotron for your help and incredible knowledge and enthusiasm.

To my family, who have helped me through all the tough times and celebrated with me every success - I could not love or respect you more and I thank you for all you have done for me. Finally, thank you to Lucy "pukas" the cat, for the love, loyalty and whiskers!

Table of Contents

Abbreviations

ATP	Adenosine tri-phosphate
ABC	ATP binding cassette
AHSP	α-haemoglobin stabilising protein
Blsk	*Bacillus anthracis* S-layer protein K
CD	circular dichroism
Da	daltons
D_{max}	maximum dimension
DMT1/NRAMP2	divalent metal transporter 1
DTT	dithiothreitol
DtxR	diphtheria toxin repressor
EDTA	ethylenediaminetetraacetic acid
ELISA	enzyme-linked immunosorbent assay
ExbB	biopolymer transport protein ExbB
ExbD	biopolymer transport protein ExbD
FbpA	ferric binding protein A of *Neisseria meningitidis*
FeoB	ferrous iron transport protein B
FhuCBG-D1/D2	ferric hydroximate uptake system of *Staphylococcus aureus*
Fur	ferric uptake regulator
GTPase	guanosine triphosphate hydrolase
Hb	haemoglobin
HbCO	carbon monoxide liganded haemoglobin
HbO_2	oxygen liganded haemoglobin
Hal	heme-acquisition leucine-rich repeat protein of *B. anthracis*
Hbp1	haem/Hb binding protein 1 of *Listeria monocytogenes*
Hbp2	haem/Hb binding protein 2 of *Listeria monocytogenes*
HemR	Haem receptor of *Yersinia pestis*
HgbA	Hb receptor A of *Haemophilus ducreyi*
HmbR	Hb receptor of *N. meningitidis*
Hp	haptoglobin
HrtAB	haem regulated transporter complex, proteins A and B of *S. aureus*
HtsABC	haem transport system proteins A, B and C of *S. aureus*
HxuA	haem/haemopexin utilization protein A of *Haemophilus influenzae*
HxuC	haem/haemopexin utilization protein B of *H. influenzae*
IFN-γ	interferon gamma
IL-1	interleukin 1
IL-6	interleukin 6
IlsA	Iron-regulated leucine rich surface protein of *Bacillus cereus*
IMAC	immobilized-metal affinity chromatography
IPTG	isopropyl β-D-thiogalactopyranoside
Isd	iron regulated surface determinant
IsdA	iron regulated surface determinant protein A of *S. aureus*
IsdB	iron regulated surface determinant protein B of *S. aureus*
$IsdB^{N1}$	iron regulated surface determinant protein B, NEAT domain 1
$IsdB^{N2}$	iron regulated surface determinant protein B, NEAT domain 2
IsdC	iron regulated surface determinant protein C of *S. aureus*
IsdE	iron regulated surface determinant protein E of *S. aureus*
IsdF	iron regulated surface determinant protein F of *S. aureus*
IsdG	iron regulated surface determinant protein G of *S. aureus*
IsdH	iron regulated surface determinant protein H of *S. aureus*
$IsdH^{N1}$	iron regulated surface determinant protein H, NEAT domain 1
$IsdH^{N2}$	iron regulated surface determinant protein H, NEAT domain 2
$IsdH^{N3}$	iron regulated surface determinant protein B, NEAT domain 3

IsdI	iron regulated surface determinant protein I of *S. aureus*
IsdX1	iron regulated surface determinant protein X1 of *B. anthracis*
IsdX2	iron regulated surface determinant protein X2 of *B. anthracis*
ITC	isothermal titration calorimetry
K_d	equilibrium dissociation constant
LB	Luria-Bertani broth
MQW	Milli-Q® water
LRR	leucine rich repeat
Mb	myoglobin
MS	mass spectrometry
M_w	weight average molecular weight
NEAT	near iron transporter domain
NMR	nuclear magnetic resonance
PCR	polymerase chain reaction
PDB	protein data bank
RALS	right angle light scattering
R_g	radius of gyration
PMB	*p*-hydroxymercuribenzoate
PRR	pattern recognition receptor
r.m.s.d	root-mean-square deviation
RP-HPLC	reverse phase high pressure liquid chromatography
rpm	revolutions per minute
SAXS	small angle X-ray scattering
SAXS-WAXS	small angle X-ray scattering – wide angle X-ray scattering
S.E.	standard error of the mean
S.D.	standard deviation
SDS-PAGE	sodium dodecyl sulfate polyacrylamide gel electrophoresis
SEC	size-exclusion chromatography
Shp	haem associated protein Shp of *Streptococcus pyogenes*
Shr	streptococcal hemoprotein receptor
ShuA	Shigella heme uptake protein A
SiaABC	Staphylococcal iron regulated transporter complex ABC
SirABC	Staphylococcal iron acquisition transporter complex ABC
SLH	S-layer homology domains
SstABCD	Staphylococcal siderophore transporter complex ABC
s1IsdB	iron regulated surface determinant protein B of *S. lugdunensis*
TbpA	transferrin-binding protein A of *Neisseria meningitidis*
TbpB	transferrin-binding protein B of *N. meningitidis*
TMED	N,N,N',N'-tetramethylethylenediamine
TonB	Gram-negative bacterial TonB protein
Tris	tris(hydroxymethyl)methylamine
UV	ultraviolet
vis	visible
WT	wild type

Chapter 1: Introduction

1.1 Iron is required for life

The element iron is a vital nutrient across all domains of life. The ability to cycle between stable oxidation states, together with a redox potential that can be tuned across a broad range (+300 mV to -500 mV) by binding to protein ligands, allows iron to act as a catalyst for many important biochemical reactions[1]. Iron-containing proteins are involved in vital processes such as: metabolism, including electron transport; oxygen transport and storage; generation of and detoxification of reactive oxygen species; DNA synthesis and regulation of gene expression. Thus iron is crucial to many aspects of organism function.

Most pathogens display the same requirements for iron as their host and, hence, competition for iron ensues during infection[2,3]. In a mammalian host, several systems act to limit the accessibility of host iron; however, pathogens employ a range of machinery to access these reservoirs. The ability of a pathogen to grow and survive in the host environment is linked to its fitness to access host iron[4]. Iron-uptake pathways that target specific iron-containing proteins of the host provide a significant advantage to the infecting organism. Such targeted iron-acquisition systems are often unique to pathogenic strains and are only expressed under conditions of infection, making them ideal targets for novel antibiotic therapies[5,6]. The iron-regulated surface determinant (Isd) system of the human pathogen *Staphylococcus aureus* has evolved to target iron found in human haemoglobin (Hb)[7,8], the largest pool of iron in the body. The mechanisms behind Hb receptor function in the Isd pathway form the focus of this thesis.

1.2 *Staphylococcus aureus*

Alexander Ogston first identified the pathogenic bacterial genus, *Staphylococcus*, in the early 1880s[9]. Ogston observed that *Staphylococcus* and other bacteria were consistently present in abscesses that formed at surgical wounds and demonstrated that *Staphylococcus* was a causative agent of abscess formation and bacteremia[10]. Soon after Anton J. Rosenbach distinguished the major human pathogen *Staphylococcus aureus*

from the less virulent strain *Staphylococcus albus* (now *epidermidis*), and named it such to reflect its characteristic golden pigmentation[11]. *S. aureus* is now recognised as the leading cause of surgical site infections, skin and soft tissue infections and infective endocarditis[12].

S. aureus is a Gram-positive bacterial pathogen that persistently and asymptomatically colonises the anterior nares of 20-30% of the population[13]. Upon dissemination, *S. aureus* can produce infections of the skin and invasive disease in many tissues and organs. Before the penicillin class of antibiotics was available, up to 80% of individuals with invasive *S. aureus* infection succumbed to the disease, hence S. aureus is a highly effective and virulent pathogen[14]. Contributing to the success of *S. aureus* is the ability to rapidly acquire antibiotic resistance genes. The penicillins prevent bacterial growth by binding to the bacterial transpeptidase, known as penicillin-binding protein, and inhibiting peptidoglycan (cell wall) synthesis. Resistance to the penicillins is afforded by penicillinase, enzyme that hydrolyses the β-lactam ring of the penicillin. Penicillin-resistant strains of *S. aureus*, expressing penicillinase, began to emerge in the early-1940s, only two years the antibiotic was introduced, and *S. aureus* resistance to penicillin remains high today[15].

Methicillin, a variant of penicillin that is not cleaved by penicillinase, was developed in 1960. In 1961, Patricia Jevons isolated the first methicillin-resistance clone of *S. aureus* from one of her patients[16]. The incidence of methicillin-resistant *S. aureus* (MRSA) infection now ranges from ~25 % to almost 70 % globally[14] and MRSA strains that are resistant to all β-lactam antibiotics are a leading cause of nosocomial infections and have high mortality rates[17,18].

The gene responsible for methicillin resistance (*mecA*) encodes for an alternative transpeptidase enzyme, penicillin-binding protein 2a (PBP2a), which is not bound by penicillins or methicillin[19,20]. *MecA* is found on the staphylococcal chromosome in a mobile genetic element known as the staphylococcal cassette chromosome mec (SCC*mec*). Horizontal gene transfer is thought to allow for the rapid spread of SCC*mec* between staphylococcal strains and uses the activity of sight specific recombinases, also encoded for in the SCC[21].

β-lactam antibiotics are derived from fungi, which naturally produce and secrete these molecules. The *mecA* gene is thought to have evolved to allow *Staphlococci* to grow alongside β-lactam secreting fungi, however, was lost upon human colonisation where the immune system eliminates such fungi[22]. *S. fleurettii*, an ancient staphylococcal species which is found as a commensal of a number of animals, encodes for a homologue of the *mecA* gene with ~99% sequence identity to *SCCmec*[23]. Importantly *mecA* in *S. fleurettii* is found in region of its chromosome that is not associated with SCC and hence *S. fleurettii* is thought to be the origin of methicillin resistance in present day MRSA[23].

Eleven variants of SCC*mec*, have been described, to date[22]. Hospital-associated strains of MRSA commonly carry SCC*mec* types I-III[24], which in addition to the *mecA* gene, carry resistance genes for a number of additional classes of antibiotics, including quinolones, tetracyclines, macrolides and aminoglycosides[25]. SCC*mec* may also carry other fitness genes for adaptation to varied environments[22].

In the early 1990's new strains of MRSA emerged amongst healthy individuals in the community. These strains were called community-associated (CA) MRSA as they infected healthy individuals with no known risk factors for MRSA infection including no prior exposure to health care environments. CA-MRSA is genetically distinct from traditional health care associated MRSA strains[26]. The CA strains typically harbor the smaller SCC*mec* types IV, V and occasionally VII, which carry resistance only to methicillin. Despite providing narrow antibiotic resistance, these smaller mobile elements are thought to provide other advantages including reduced metabolic demand and reduced doubling times when compared with the larger SCC*mec* type I[27]. In addition the compact size allows for rapid spread between staphylococcal strains. Furthermore, the ability for CA-MRSA strains to cause invasive disease in healthy young individuals is attributed to a plethora of additional virulence factors, not present in the HA-MRSA strains, for example the toxin Panton-Valentine leukocidin (PVL)[26,28,29].

CA-MRSA infections are of particular importance to indigenous health in Australia. One of the earliest reported outbreaks of CA-MRSA occurred in a remote Aboriginal community in Western Australia in 1993[30]. Since then, several CA-MRSA strains have spread around Australia[31] and cause invasive disease with appreciable mortality[32,33]. The

spread of CA-MRSA around Australia is reflected globally[26]. In addition, the distinction between HA- and CA-MRSA infections is beginning to break down as MRSA with CA genetic backgrounds become established in hospitals.

Since the 1980s, vancomycin, a glycopeptide antibiotic, has been used to treat multi-drug resistant MRSA infections. It is not surprising that vancomycin resistance has since been established[34,35]. As the reserve of effective antibiotics dwindles and pharmaceutical companies shy away from new drug discovery and development, new antibacterial treatments are urgently needed, but their development requires a better understanding of the mechanisms that underlie *S. aureus* pathogenesis[36,37]. In this thesis I present a structure-function study of an iron-uptake protein from *S. aureus* that contributes to pathogenesis.

1.3 The distribution of iron in the body and relevant iron sources for infecting pathogens

Under normal conditions, an adult human contains ~4–5 g of iron and significant deviations from this value lead to a variety of disease states. Despite this large reservoir of iron, under normal conditions, the concentration of free iron within a mammalian system is extremely low: in the order of 10^{-24} M[38]. Iron is highly reactive in the presence of oxygen and, without proper regulation, it is toxic to the organism. To prevent toxicity, iron is coordinated to specific iron-binding proteins allowing for the modulation of its reactivity, i.e., its reduction potential and accessibility to ligands[39]. The majority of iron is also contained within cells and compartmentalised to ensure that reactions only occur in the appropriate context. In the subsequent sections, the most abundant iron-binding proteins are introduced, followed by a brief discussion of their relevance to infection.

1.3.1 Haem-iron and non-haem-iron

When considering the forms of iron available to infecting pathogens, biological iron can be divided into two main pools: haem-iron and non-haem-iron. Haem is a macrocyclic molecule that is synthesised in the liver and bone marrow and binds approximately 80% of mammalian iron. Haem consists of protoporphyrin IX complexed with iron, and is a prosthetic group for many proteins. Protoporphyrin IX bound to Fe(III) is called haemin, while haem may refer to protoporphyrin IX bound to Fe(III) or Fe(II); the term haem is

used throughout this thesis to refer to both species and the oxidation state is specified where necessary. The aromatic ring of protoporphyrin IX is made up of four pyrrole rings, joined together by methine groups and is decorated by four methyl, two vinyl and two propionic acid functional groups, (Fig. 1.1). Both Fe(II) and Fe(III) species (which are the common species found in biology) prefer an octahedral coordination geometry. Iron is chelated in the centre of the porphyrin ring by the four pyrrole nitrogens and the available axial coordination sites may be bound by the side chains of histidine, tyrosine, methionine or cysteine residues, allowing for incorporation into the haem protein. Non-haem iron is directly coordinated to protein side chains or found in motifs such as iron-sulphur (Fe-S) clusters, which play structural or enzymatic roles in a range of proteins[40,41].

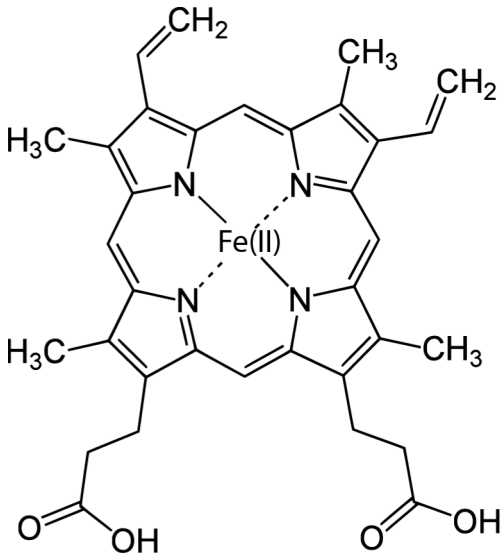

Figure 1.1. The chemical structure of Fe(II)-Protoporphyrin IX, or haem.

1.3.2 Extracellular iron-binding proteins

Iron-binding proteins are present in intracellular and extracellular locations. Iron that is absorbed in the gut, or released in cell lysis, is transported in complex with extracellular iron-binding proteins. Dietary iron entering the duodenum is reduced by duodenal cytochrome b to Fe(II) iron[42] and imported into the intestinal epithelium via divalent metal transporter 1 (DMT1/NRAMP2)[43]. Inside enterocytes, iron is oxidised back to the

ferric state by hephaestin[44,45] and released into the circulation by ferroportin 1, an iron exporter expressed by duodenal enterocytes, hepatocytes and macrophages[46,47]. In the serum, ferric iron is immediately complexed to transferrin, a carrier protein that transports iron to cells in the periphery or to the liver for storage. The transferrin protein contains two homologous lobes, designated the N- and C-lobe, which each contain a single iron-binding site (Fig. 1.2 A)[48]. Each lobe is further divided into two subdomains (N1/N2 and C1/C2), which both contribute iron coordinating side chains to a central binding site. Transferrin has an exceptionally high affinity for iron (greater than 10^{20} M^{-1})[49,50], and under normal conditions, the circulating pool is only 25–40% saturated, pushing the equilibrium state towards no free iron and providing a buffer against changes in iron concentration. Iron-loaded transferrin binds to the transferrin receptor 1, which is present on all cells, and the complex is internalised via receptor-mediated endocytosis[51,52]. Acidic conditions in the early endosomes promote release of iron from transferrin through protonation of several basic residues at the inter-domain interface. This has the effect of destabilising the iron-bound (or closed) conformation[48,53] (Fig. 1.2 A), hence transferrin shows decreasing affinity for iron with decreasing pH[54]. Lactoferrin is a homologue of transferrin that is found in lymph and mucosal secretions and is released by neutrophils under conditions of infection (Fig. 1.2 B)[55]. Lactoferrin has an even higher affinity for iron 10^{22}–10^{24} M^{-1} than transferrin[49,50]. Both apo-lactoferrin and apo-transferrin have a bacteriostatic effect by limiting iron availability while lactoferrin has additional bactericidal activity mediated by a direct interaction with bacterial membranes and protease activity[56,57].

Figure 1.2. Ribbon diagrams of the human iron-binding proteins, transferrin (A) and lactoferrin (B). Transferrin (PDB 3QYT) is shown with the N-lobe (blue and cyan) in the open conformation and the C-lobe (yellow and orange) in the closed conformation. Both the N- (green and lime) and C- (pink and purple) lobes of lactoferrin are in the closed conformation (PDB 1LFG). Iron is shown as brown spheres and the iron-coordinating residues are shown as red sticks. Figure adapted from *Mizutani et. al.*[48].

Figure 1.2

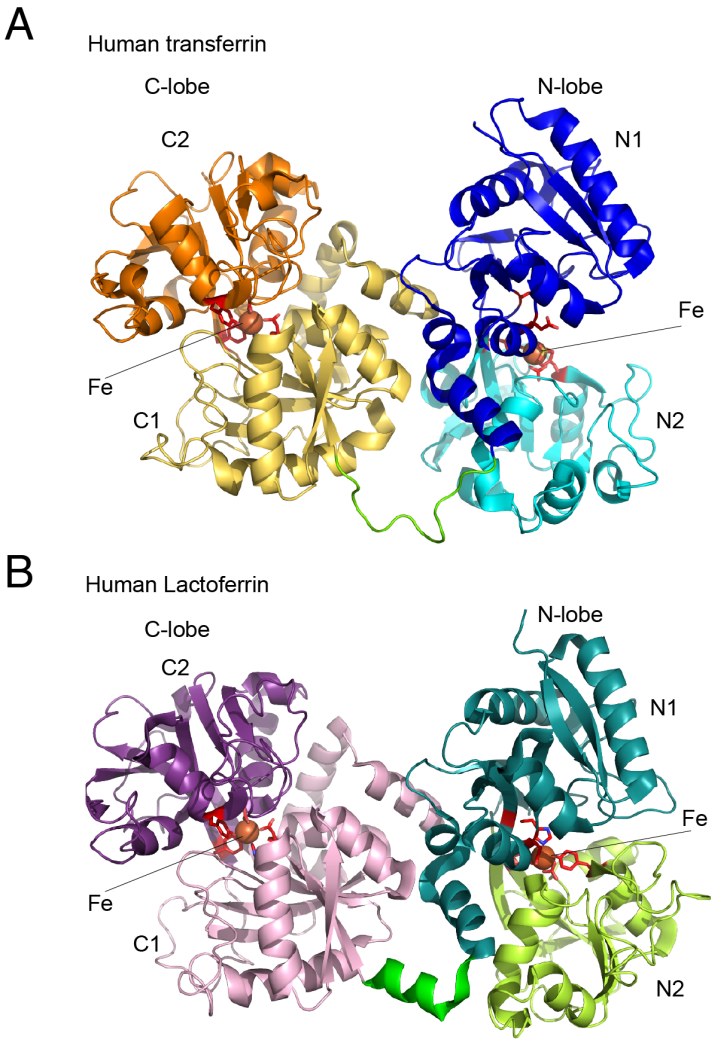
A
Human transferrin
C-lobe
N-lobe
C2
N1
Fe
Fe
C1
N2
B
Human Lactoferrin
C-lobe
N-lobe
C2
N1
Fe
Fe
C1
N2

Transferrin only accounts for ~0.1 % of total body iron and lactoferrin accounts for a much smaller percentage[56,58], however, both proteins are used as a source of iron by pathogenic bacteria. These proteins are iron sources for bacteria that thrive extracellularly, as well as intracellular bacteria, such as *Mycobacterium tuberculosis,* which can access transferrin in endosomal compartments[59,60].

1.3.3 Intracellular iron-binding proteins

The largest demand on iron availability is the process of erythropoiesis, during which erythrocytes, the cells responsible for oxygen transport, are made. Erythroblasts take up circulating transferrin and use the released iron in the production of haemoglobin (Hb). Hb is a haem protein and, under normal circumstances, accounts for ~ 65–75 % of the total iron pool[61]. It is a tetrameric protein, consisting of two α Hb and two β Hb chains, which each coordinate a haem cofactor (Fig. 1.3 A). One oxygen molecule can be bound reversibly to each the four prosthetic haem groups allowing oxygen delivery from the lungs to the tissues. Each globin chain has a conserved α-helical fold with the β chains comprised of eight helical regions (A–H; Fig. 1.3 B), and the α chains containing seven helical regions (A–C and E–H by homology with sperm whale myoglobin; Fig. 1.3 C). The haem group is bound in a pocket between the E and F helices and is coordinated by a single histidine residue that lies on the F-helix (His87 in α Hb and His92 in β Hb; Fig. 1.3 B,C). Oxygen binds to the remaining axial coordination position on the distal side of the haem plane and is stabilised by a hydrogen bond with the imidazole ring of the distal histidine (His58 in α Hb and 63 in β Hb; Fig. 1.3 B,C). The monomeric oxygen storage protein, myoglobin (Mb), is found in muscle cells, and has a similar fold with eight α-helices (A–H), coordinating the haem group via His94. Hb utilisation has been demonstrated in bacterial[62], protozoan[63] and fungal pathogens[64,65], illustrating the importance of Hb as a nutrient source during infection in a mammalian host environment.

Figure 1.3. The structure of human Hb. (A–C) α chains are shown in pink and β chains are shown in red. Each chain binds to a single haem group (yellow) and the central iron (brown sphere) is coordinated by the imidazole group of the proximal histidine. Oxygen (red spheres) is coordinated to the remaining axial position and is held in place be a hydrogen bond to the distal histidine. The helical globin fold of a single β or α chain are shown in (B) and (C) respectively.

Figure 1.3

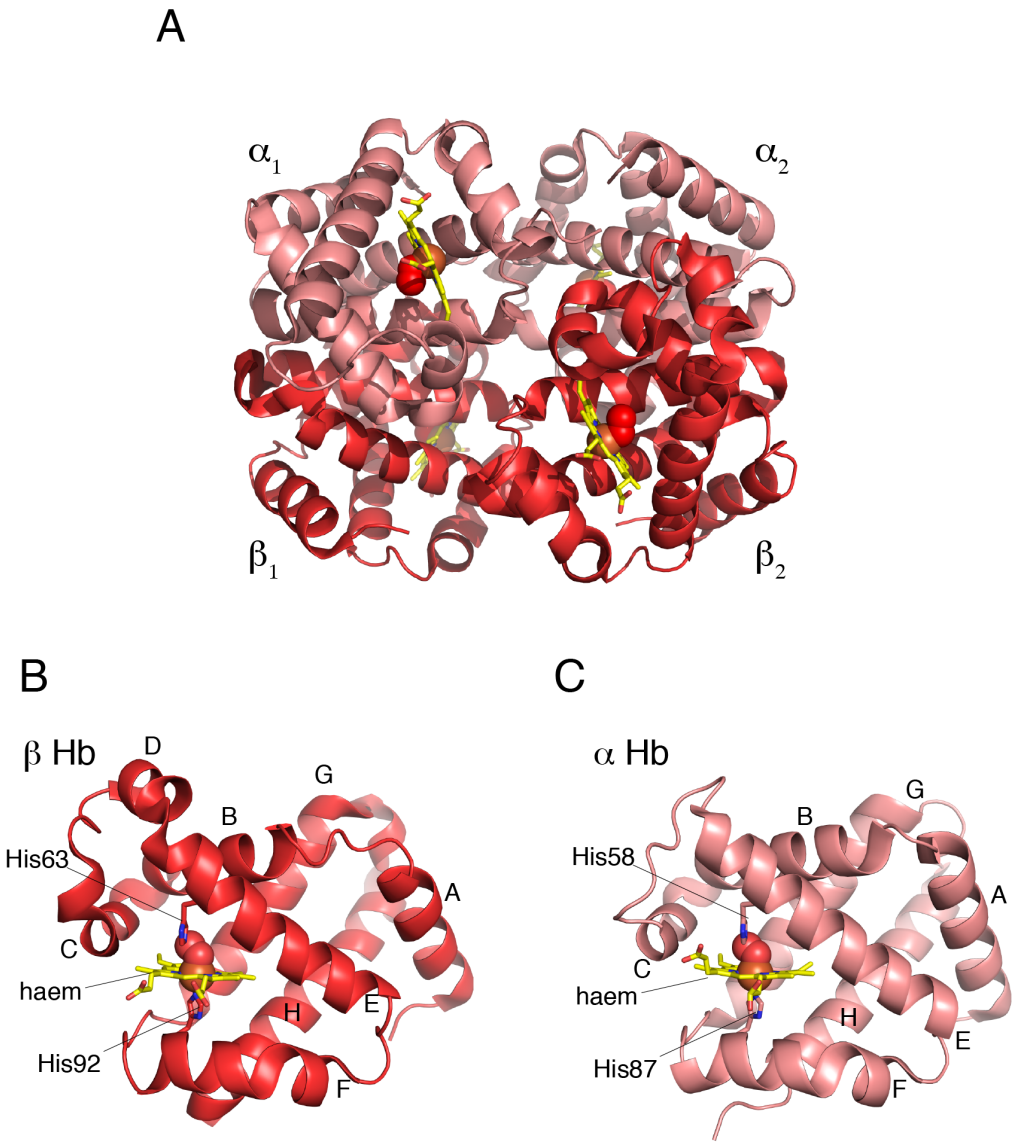
A
α1
α2
β1
β2
B
β Hb
D
G
B
His63
A
C
haem
H
E
His92
F
C
α Hb
G
B
His58
A
C
haem
H
E
His87
F

Inside cells, the iron storage protein, ferritin, accounts for ~30% of total body iron under normal iron loading conditions[58,61]. Ferritin is made up of 24 heavy and light chains that form a cage-like shell[66]. Iron enters the cavity inside the shell and is oxidised at a catalytic site present in the heavy chains and then undergoes mineralisation to be stored as ferrihydrite[67,68]. In this way, up to 4500 iron atoms can be stored by a single ferritin molecule. Pathogens such as *Bacillus cereus* make use of this iron store[69,70].

1.3.4 Mechanisms to limit iron availability are up-regulated during infection

As well as minimising iron toxicity, mechanisms for limiting the concentration of free iron in the body are also up-regulated during infection. Pro-inflammatory cytokines induce iron-restricting proteins, and can target the response to the intracellular or extracellular location of the pathogen[59,71]. Mechanisms to limit iron availability during infection are found in plants[72], insects[73], birds[74] and reptiles[75] and, hence, are recognised as a conserved innate immune defence strategy.

The innate immune system recognises pathogen-associated molecular patterns through pattern recognition receptors (PRRs) that are expressed by a range of cell types. Signaling via PRRs leads to secretion of the pro-inflammatory cytokines IL-1 and IL-6, which in turn lead to the production and secretion of hepcidin by the liver[59]. Hepcidin is a peptide hormone that acts to decrease iron uptake from the gut, as well as secretion of iron from macrophages and hepatocytes into the plasma. Hepcidin interacts directly with ferroportin 1 leading to the internalisation and degradation of ferroportin 1[76]. With reduced levels of ferroportin 1 to release iron into circulation, iron accumulates inside cells and, as a result, transferrin saturation drops below 20% limiting its utility to pathogens[3]. While effective at limiting iron from extracellular pathogens, this response is inappropriate for pathogens that reside in intracellular compartments, such as *Mycobacterium tuberculosis, Chlamydia psittaci* and *Legionella pneumophila*[59,60]. These pathogens persist inside macrophages and induction of hepcidin leading to macrophage iron loading has been shown to enhance the growth of *Chlamydia psittaci* and *Legionella pneumophila*[77]. In contrast, activation of macrophages though IFN-γ signaling leads to up-regulation of ferroportin 1 and down-regulation of the transferrin receptor[71]. This activity of IFN-γ was shown to decrease macrophage iron levels resulting in decreased bacterial iron uptake and reduced survival of *Salmonella enterica* Typhimurium inside the activated phagocytes.

Cytokine signaling during infection also leads to production of acute phase proteins (proteins expressed in the acute phase of infection) involved in sequestering iron from infective agents. The role of these proteins is to minimise harmful effects of free iron, haem or iron/haem binding proteins that are released from their appropriate compartments during tissue damage. These proteins also act to withhold iron from pathogens and subvert attempts to access iron through induced tissue degradation. One such acute phase protein is haptoglobin (Hp), a serum glycoprotein that complexes with haemoglobin that is released from lysed erythrocytes. The Hp:Hb complex is rapidly cleared by macrophages of the spleen expressing the CD163 receptor[78]. Haemopexin is another acute phase glycoprotein and binds to free haem with extremely high affinity (K_d of 0.1 pM)[79]. The haem-haemopexin complex is internalised after binding to its receptor, which is expressed on most cell types but primarily in the liver[80]. The haemopexin structure consists of two domains, each with a β-propeller fold (Fig. 1.4). Extensive loop regions form a contact surface between the two domains. The haem-binding site is situated at the domain interface and contains two histidines that coordinate the haem iron (Fig. 1.4)[79]. Like other haem-binding proteins in the host, haemopexin can be exploited as a source of iron by pathogens such as *Haemophilus influenza*[81].

To overcome these strategies used by the host to withhold iron, many pathogens have acquired aggressive iron uptake pathways that strip iron directly from the host proteins. *S. aureus* can utilise transferrin iron[82], Hb, Hb:Hp complexes and Mb, but not haemopexin[83,84]. Multiple iron uptake pathways are commonly found in the genomes of both Gram-positive[5,85,86] and Gram-negative[87] bacterial pathogens, highlighting the importance of iron to bacterial survival and infection.

Figure 1.4. The structure of rabbit haemopexin. Haem (yellow sticks) is bound between the N (yellow) and C (blue) domains. The two haem-coordinating histidine residues (red) are contributed by extensive loops. The loop joining the two domains is coloured green.

Figure 1.4

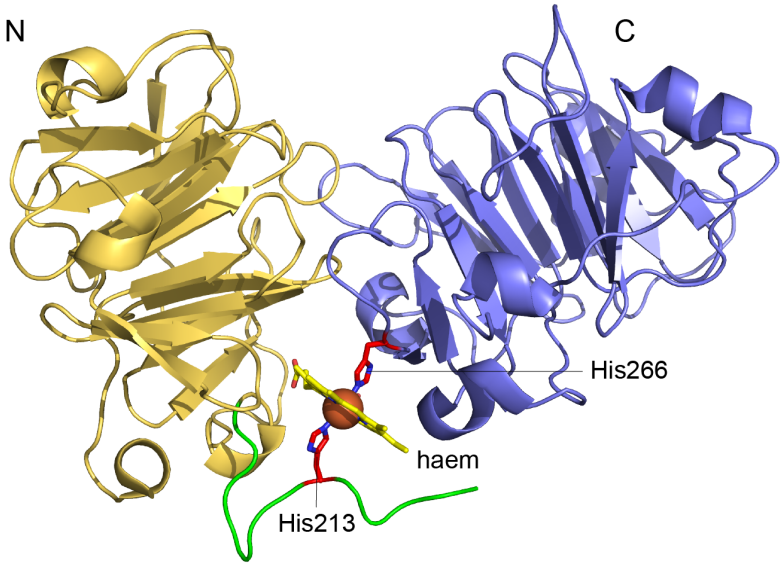

1.4 The importance of iron in infection

1.4.1 Experimental models and disease states of iron overloading

Evidence that the availability of iron can be a determinant of disease severity is seen under conditions of iron overload. In animal models of infection, administration of iron or iron-containing compounds to artificially elevate iron levels has been shown to enhance infection by *Escherichia coli*[88], *Pasteurella pestis*[89], *Listeria monocytogenes*[90] and *Vibrio vulnificus*[91] as well as numerous other bacterial, fungal and protozoan pathogens[92].

Individuals with iron overload diseases have increased risk of infection. Hereditary haemochromatosis is associated with an increase in iron absorption from the gut and a concomitant increase in transferrin saturation as well as iron loading in the liver, heart and pancreas. Individuals with haemochromatosis have higher susceptibility to bacterial, viral and fungal pathogens and are at risk of infection from bacterial strains that are avirulent in healthy individuals[4,93]. For example, an attenuated strain of *Yersinia pestis* lacking genes involved in uptake of iron from host iron proteins, was able to cause opportunistic and lethal infection in an individual with haemochromatosis as well as in a mouse model of haemochromatosis[94]. In contrast, macrophages from individuals with hereditary haemochromatosis may be deficient in iron and *M. tuberculosis,* which has an intracellular lifestyle, shows attenuated growth in macrophages from individuals with haemochromatosis[95]. Additionally, numerous studies have observed a correlation between increased risk of infection and iron supplementation in human infant and adult populations[3].

1.4.2 Iron regulates bacterial gene expression during infection

Low iron conditions, such as those experienced during infection, signal through bacterial iron-sensing proteins such as the ferric uptake regulator (Fur) and the iron-dependent diphtheria toxin repressor (DtxR). Fur and DtxR respond to changes in environmental iron concentrations by regulating the expression of a large number of bacterial proteins (~390 in *S. aureus*)[96-99]. The Fur protein is found in both Gram-positive and Gram-negative bacteria where it regulates genes involved in iron uptake, stress response pathways and other virulence factors involved in host colonisation. Under iron-replete

conditions, Fur complexes with iron and binds to its consensus sequence, resulting in transcriptional repression[100]. Iron-limiting conditions lift Fur/DtxR mediated repression of gene expression. Many of the well-known toxins responsible for the "morbidity and mortality" of infection are regulated this way. For example, the diphtheria toxin, expressed by *Corynebacterium diphtheriae* during infection, is regulated by DtxR[101] while the Shiga-like toxin, expressed by *Escherichia coli,* is regulated by Fur[102]. Genomic and proteomic studies have shown that, in *S. aureus,* Fur regulates the expression of toxins involved in tissue degradation (cytotoxins and hemolysins) and genes involved in metabolism, immunomodulation, biofilm formation, and iron uptake[98,103].

1.5 Mechanisms used by bacteria to access host iron during infection

Pathogenic bacteria employ multiple mechanisms to access host iron. Some of these mechanisms, such as the production of siderophores (iron chelators discussed in Section 1.5.1) are shared with free-living bacteria. Other mechanisms have evolved to specifically target haem and haem/iron-proteins of a host.

Highly successful pathogens express surface-exposed or secreted receptors that bind to the host protein and remove the iron/haem for transport into the cell. Several obligate pathogens, such as, Gram-negative *Neisseria* spp., *Moraxella catarrhalis* and *Haemophilus influenza,* rely entirely on targeted interactions with host proteins and do not produce siderophores[104-106]. These pathogens exclusively colonise humans and produce receptors highly evolved to use human Hb, transferrin, lactoferrin or haemopexin[105,107].

Gram-negative bacteria are encased by a lipopolysaccharide-rich outer membrane, whereas Gram-positive bacteria lack a second outer membrane and are instead surrounded by a much thicker peptidoglycan cell wall of ~15–50 nm (~40 nm in staphylococci[108]). Hence, the cell-surface proteins that interact with the host are different for Gram-negative (Sections 1.5.2, 1.5.3) and Gram-positive (Section 1.5.4) bacteria. A haem uptake system of *S. aureus* that specifically targets human Hb is the subject of this

thesis and is described in detail in Section 1.5.4. and in the introduction sections of the results chapters.

1.5.1 Capture of 'free' iron by siderophores, porins and FeoB

Fe(II) is relatively soluble at neutral pH (10^{-2} M), while Fe(III) is sparingly soluble (10^{-18} M). In an oxygenated environment, Fe(II) is oxidised to Fe(III) and deposited in insoluble compounds such as iron oxides and iron hydroxides. However, the concentration of soluble iron may be higher in niche environments: anaerobic conditions limit oxidation of Fe(II) to less soluble Fe(III), while acidic conditions (pH < 5) increase the solubility of both Fe(II) and Fe(III). Low oxygen conditions are found in the mammalian stomach and gastrointestinal tract, and the stomach is also highly acidic. Fe(II) is thought to diffuse through the Gram-positive cell wall and through porins in the Gram-negative outer membrane (Fig. 1.5 A,B). Import of Fe(II) across the plasma membrane proceeds by the ferrous iron transporter, FeoB[109], which is an integral membrane protein with 8–12 membrane-spanning helices and a cytoplasmic G-protein domain[110,111]. GTPase activity of the cytoplasmic domain provides the energy required for import of Fe(II) across the inner membrane. Under anaerobic conditions Fe(III) can be reduced to Fe(II) through the action of bacterial assimilatory ferric reductases[112]. Fe(III) reduction can occur extracellularly or in the periplasm allowing for uptake via the Feo system. Secreted, membrane-bound, periplasmic and cytoplasmic reductases have been identified[112].

The Feo import system is the primary iron uptake system of *Helicobacter pylori*[113] reflecting adaptation of the bacteria to growth in the acidic conditions of the stomach, where Fe(II) is bioavailable. The Feo system is required for *H. pylori* virulence as genetic deletion of the Feo operon reduced colonisation in mouse models of infection[113]. Similarly, FeoB contributes to intestinal colonisation by *Escherichia coli* and *Salmonella enterica* Typhimurium reflecting the availability of Fe(II) under the anaerobic conditions experienced in the gastrointestinal tract[114,115].

A strategy employed by terrestrial, marine, and pathogenic bacteria to import iron is the secretion of iron-binding molecules, known as siderophores[116]. Siderophores are chelating agents (< 2000 Da) that bind to Fe(III) with extremely high affinity (up to 10^{30} M)[56,117]; siderophores capture free iron in the environment, or iron that is released from host proteins, to form almost irreversible Fe(III)-siderophore complexes. Fe(III)-siderophore

complexes freely diffuse across the Gram-positive cell wall or are recaptured by Gram-negative outer membrane receptors (Fig. 1.5 A,B). The Gram-negative siderophore receptors use the TonB-ExbB-ExbD system to actively transport captured siderophores across the outer membrane (Fig. 1.5 A). TonB is a periplasmic protein that is anchored via an N-terminal domain to the cytoplasmic membrane. TonB interacts with numerous classes of outer membrane receptors and with the integral membrane proteins ExbB and ExbD located in the cytoplasmic membrane (Fig. 1.5 A)[118]. ExbB and ExbD use the proton gradient across the inner membrane to drive transport of a substrate (in this case a siderophore) into the periplasm where it is bound by a specific substrate binding protein, and ferried to a transporter in the plasma membrane (Fig. 1.5 A; Section 1.5.3). Siderophore import across the cytoplasmic membrane is conserved in both Gram-positive and Gram-negative bacteria and utilises an ABC transporter permease complex (transport across the cytoplasmic membrane is described in Section 1.5.3; Fig. 1.5 A,B). In the cytoplasm iron is release by enzymatic degradation of the siderophore or reduction of the iron. While hundreds of different siderophores have been described, these commonly bind iron though catechol, hydroxamate or α-hydroxy carboxylate functional groups[119].

In a pathogenic setting, siderophores provide a non-specific iron acquisition system allowing infection in a wide range of hosts and have been shown to strip iron from a range of mammalian proteins including transferrin, lactoferrin and ferritin[119]. Exploitation of siderophores produced by other microorganisms can provide an advantage for growth in bacterial communities and expression of uptake pathways for xeno-siderophores is common[120,121].

S. aureus synthesises the α-hydroxy carboxylate siderophores, Staphyloferrin A and Staphyloferrin B[122]; however, is also able to use hydroxamate siderophores that are secreted by other bacterial species[123]. In addition, *S. aureus* favours fermentative metabolism under conditions of low iron availability, producing lactate as a by-product[103,124]. Lactate is secreted from the cell, reducing the local pH and increasing iron solubility and taking advantage of the accelerated rates of iron loss from transferrin with decreasing pH[54,103].

Figure 1.5. Non-specific iron uptake pathways of Gram-negative (A) and Gram-positive (B) bacteria. Fe(III) may be reduced to Fe(II) by ferric reductase enzymes (yellow) allowing for diffusion through porins in the Gram-negative outer membrane (A) or through the Gram-positive cell wall (B). Fe(II) is actively imported across the cytoplasmic membrane via the conserved transmembrane protein, FeoB (blue). Alternatively, free Fe(III) or Fe(III) derived from host proteins may be bound by chelating siderophores that are secreted by the bacteria or other microorganisms. In Gram-negative bacteria siderophores are actively imported across the outer membrane (OM) via siderophore-receptor-TonB-ExbBD complexes **(A).** In Gram-positive bacteria siderophores freely diffuse through the cell wall **(B)**. Once in the periplasm, siderophores are bound by periplasmic binding proteins **(A)** or lipoproteins **(B)** that deliver the siderophore to a conserved ABC-transporter complex in the cytoplasmic membrane. Transport across the cytoplasmic membrane requires the use of energy in the form of ATP hydrolysis. Inside the cell, the siderophores are either degraded or reduced to release iron.

Figure 1.5

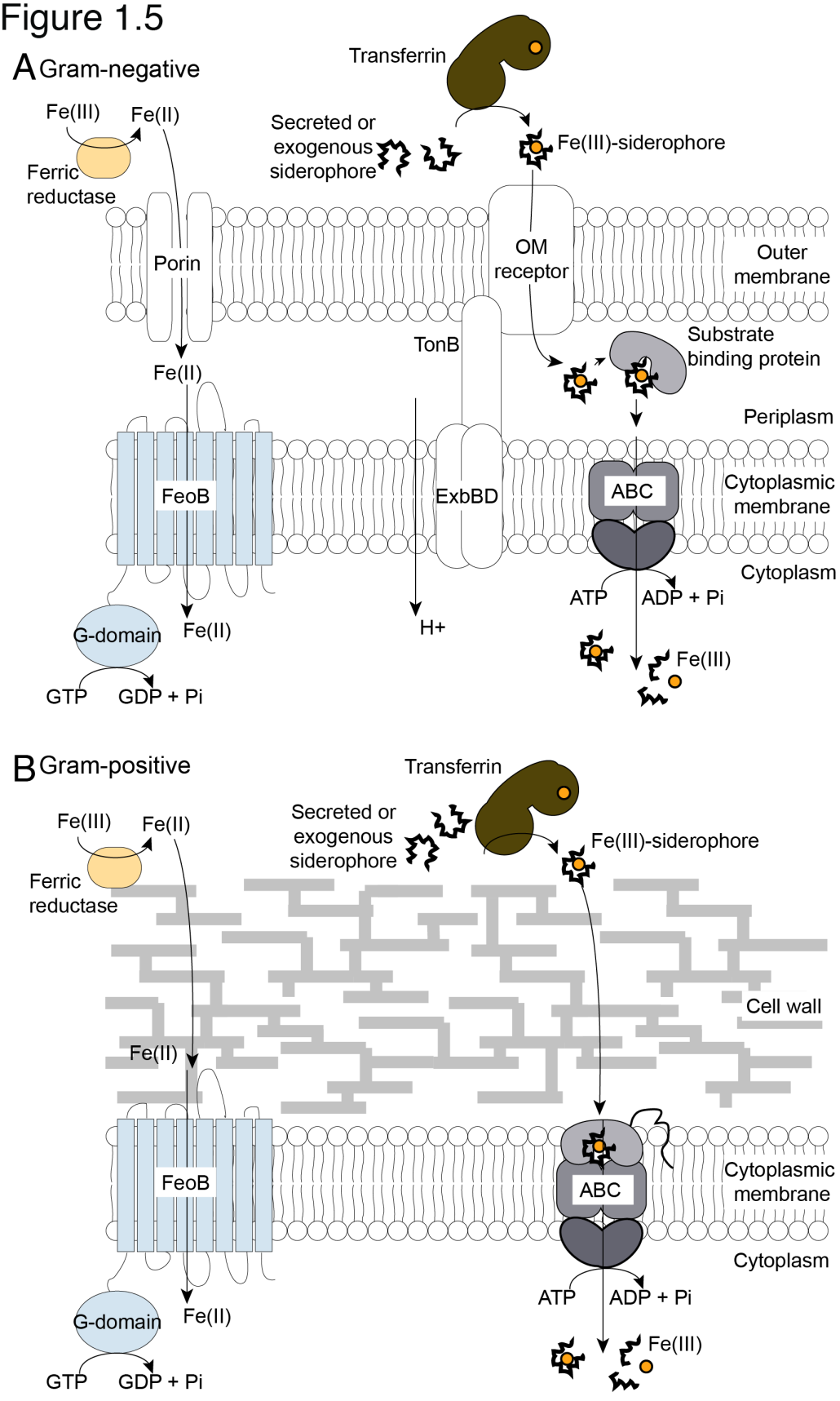
A Gram-negative
Transferrin
Fe(III)
Fe(II)
Ferric reductase
Secreted or exogenous siderophore
Fe(III)-siderophore
Porin
OM receptor
Outer membrane
TonB
Substrate binding protein
Fe(II)
Periplasm
FeoB
ExbBD
ABC
Cytoplasmic membrane
Cytoplasm
ATP
ADP + Pi
G-domain
Fe(II)
H+
Fe(III)
GTP
GDP + Pi
B Gram-positive
Transferrin
Fe(III)
Fe(II)
Secreted or exogenous siderophore
Fe(III)-siderophore
Ferric reductase
Cell wall
Fe(II)
FeoB
ABC
Cytoplasmic membrane
Cytoplasm
ATP
ADP + Pi
G-domain
Fe(II)
Fe(III)
GTP
GDP + Pi

1.5.2 Gram-negative secreted haemophores

Haemophores are secreted or surface proteins that capture haem-iron via competition with host proteins and are retrieved from the extracellular environment by haemophore receptors. Unlike siderophores, haemophores may make defined interactions with specific host proteins and are not imported into the bacterial cell but instead offload their cargo to the surface-exposed haemophore receptors[119]. Gram-negative bacterial species produce haemopores with no homology existing between the different protein families.

HasA, one of the best-characterised haemophores of Gram-negative bacteria, is secreted by *Serratia marcescens*[125], *Pseudomonas aeruginosa*[87], and *Yersinia pestis*[126]. HasA acquires haem that is passively released from Hb[127], haemopexin and myoglobin[128] by virtue of its very high affinity for haem $K_d << 10^{-8}$ M [129]. The HasA fold is formed from two structural motifs, one composed of seven β-strands and the other of four α-helices[130]. Haem is bound at the interface between the two motifs and residues of two extended loops provide the haem ligands. The iron is coordinated by one histidine and one tyrosine sidechain. A second histidine is involved in a stabilising interaction with the tyrosine phenolyate. Haem-loaded HasA delivers its ligand to a surface-exposed receptor, HasR (which belongs to the family of outer membrane receptors described below). The haemophore and its receptor form a stable interaction (K_d of 5 nM). While HasR has a lower affinity for haem than free HasA, receptor binding sterically destabilises the HasA-haem interaction, allowing for haem transfer[131]. The haem is then imported into the periplasm by the outer membrane receptor and HasA is recycled in an energy-dependent manner[132].

1.5.3 Gram-negative outer-membrane receptors

1.5.3.1 Gram-negative outer-membrane haem transporters

Gram-negative bacteria have a family of outer membrane receptors that capture host haem-containing proteins, remove the haem and import it into the periplasm (Fig. 1.6)[133-135]. These outer membrane receptors show homology to outer membrane siderophore receptors[136] and outer membrane haemophore receptors[132].

The receptors may be highly specific for one host protein, such as the Hb receptor, HmbR, from *Neisseria meningitidis*[135,137]. Other outer membrane receptors can utilise a range of host proteins, such as HemR from *Yersinia enterocolitica*, which can use Hb, Mb, human or bovine serum albumin, haemopexin and Hb:Hp complexes[137]. Each member of the outer membrane receptor family shows a high degree of structural homology consisting of a 22-stranded β barrel that spans the membrane, a periplasmic plug domain and a Ton-B box (a sequence of seven hydrophobic residues that is recognised by TonB; Fig. 1.6 A,B)[118,135,137]. The substrate-binding site may consist of surface-exposed loops, the interior of the barrel and/or extracellular surface of the plug domain[133-136,138,139]. Energy required for passage of the bound substrate through the membrane is provided by an interaction with the TonB-ExbB-ExbD system.

Recent advances have been made in understanding how the outer membrane receptors recognise and interact with host proteins. Haemoglobin receptors have been identified in a number of Gram-negative pathogenic and commensal bacteria[133,135,137-139]. The function of haem release from Hb has been attributed to extracellular loop 7 of HemR[137], HgbA from *Haemophilus ducreyi*[134,139], ShuA in *Shigella dysenteriae* and both loop 7 and neighbouring loop 6 of HmbR from *Neisseria meningitidis*[135]. Loop 7 contains two motifs (FRAP/YRVP, NXXL) and an intervening histidine residue, which are highly conserved amongst outer-membrane Hb receptors. A combination of these elements (and occasionally the plug domain) have been shown to be important for utilisation of haem from Hb. Interestingly, this region is not involved in Hb binding, and the two functions of Hb capture and haem removal, are carried out at distinct interfaces. Mutagenesis studies have indicated that Hb binding is mediated by loops 2 and 3 in HmbR[135] and loop 5 in HgbA[134], however, it is currently unknown which surface of Hb is targeted or by which molecular mechanism the haem group is released.

HxuC of *Haemophilus influenzae* is an outer membrane receptor that can import free haem or haem from Hb[81]. In the presence of the receptor HxuA, HxuC can also import haem from haemopexin. HxuA is an extracellular protein that is linked to the outer membrane. HxuA binds with high affinity to both apo- and holo-haemopexin but does not bind directly to haem[81]. Instead, binding of HxuA to holo-haemopexin induces haemopexin to release haem into the solution. As yet it is unknown how HxuA causes

haem release from haemopexin but possible mechanisms include steric interactions with the haem or a conformational change in the haemopexin haem pocket. The liberated haem group may be used by any available haem importer. As HxuA does not bind haem and binds with high affinity to apo-haemopexin it has been suggested that the primary role of this protein may be to deactivate haemopexin to prevent clearance of haem by the host. Alternatively, HxuA may directly associate with a haem transporter such as HxuC to ensure that the released haem is channeled for uptake.

1.5.3.2 Gram-negative outer-membrane transferrin receptors

Neisseria. spp. do not express siderophores but capture iron through direct binding to transferrin[140]. The transferrin outer membrane receptor, TbpA and co-receptor TbpB are highly specific for human transferrin[107,141]. Structural studies have recently revealed the molecular mechanism by which TbpA releases iron from transferrin. TbpA interacts with the C-lobe of human transferrin, over a very large interface (Fig. 1.6 B)[142]. A small helical segment on surface-exposed loop 3 reaches into the iron-binding cleft formed between the C1 and C2 lobes of transferrin and weakens the interaction between the iron and the coordinating side-chains (Fig. 1.6 B). The co-receptor, TbpB, binds to a distinct surface of the transferrin C-lobe and enhances the efficiency of transferrin utilisation. TbpB is linked to the outer membrane via a long unstructured polypeptide chain and is proposed to provide an advantage in transferrin capture. In addition, TbpA and TbpB can simultaneously bind to transferrin encasing the iron coordination site in a chamber, assumed to direct the iron towards the TbpA transport channel.

1.5.4 Gram-positive haem uptake systems

Protein networks transport haem across the cell wall in Gram-positive *Firmicutes* bacteria[143,144]. These networks start with secreted or surface-exposed haem-binding proteins that capture haem from host proteins (Fig. 1.6 C). The captured haem molecule is then relayed through the cell wall via one or more intermediate haem carrier proteins to an inner membrane transporter complex for passage into the cell. The best-characterised Gram-positive haem import system is the iron regulated surface determinant (Isd) system of *S. aureus,* which specifically targets Hb, and is discussed below.

1.5.4.1 The iron regulated surface determinant system of S. aureus

To access Hb found in erythrocytes, *S. aureus* produces haemolytic toxins, including α-toxin/α-haemolysin, β-haemolysin and γ-haemolysin, which cause erythrocyte lysis and release Hb into the serum. Two surface-exposed receptors, IsdB and IsdH, capture the released Hb from the serum and remove the haem ligand (Fig. 1.6 D)[7,84,145-147]. The haem is then transferred to the cell-wall haem-binding proteins IsdA and IsdC, which relay the ligand to the haem-binding lipoprotein, IsdE, and membrane permease IsdF[148,149]; transport across the inner membrane is described in section 1.5.3.

IsdA, B, C and H are anchored to the cell wall by sortase enzymes, which catalyse the formation of a covalent linkage between the C-terminal amide group of the protein and the peptide crossbridge of the cell wall. IsdA, B and H are substrates of the constitutively expressed sortase A, which is ubiquitous amongst *Firmicutes* bacteria[150]. In contrast, IsdC is the only substrate of sortase B[151], which recognises a distinct sorting motif present in the C-terminal domain of IsdC[7,151,152]. Sortase A and sortase B attach their substrates to different cell wall building blocks[153], locating IsdA/B/H on the extracellular surface of the cell wall and IsdC closer to the periplasmic space[7]. As IsdC has a higher affinity for haem than IsdA/B/H, this distribution of Isd proteins polarises the cell wall to favour movement of haem towards the cytoplasmic membrane (Fig. 1.6 D).

Figure 1.6. Targeted iron uptake pathways of Gram-negative (A, B) and Gram-positive (C, D) bacteria. (A) In Gram-negative bacteria, outer membrane receptors bind to host iron/haem containing proteins or secreted haemophores. These receptors show homology to the outer membrane siderophore receptors. The outer membrane receptors remove the haem/iron from the host protein or haemophore and together with the TonB-ExbBD complex import the haem/iron through an energy dependent mechanism. In the periplasm the haem/iron is bound by a periplasmic substrate binding protein and delivered to a cytoplasmic membrane ABC transporter complex for passage into the cell. **(B)** The structure of the outer membrane transferrin receptor, TbpA, of *Neisseria meningitides,* bound to human transferrin (PDB 3V8X). The β-barrel domain is coloured green while the plug domain is shown in purple. A short helical segment (red) in one of the extracellular loops interacts with the iron-binding site (red spheres) of the transferrin C-lobe (orange and yellow). The transferrin N-lobe (blue and cyan) does not contact the bacterial receptor. Once inside the periplasm, Fe(III) is bound to FbpA (grey; PDB 1O7T) for transport to a cytoplasmic membrane ABC-transporter complex. **(C)** Schematic diagram showing the elements that make up the haem import pathways of Gram-positive *Firmicutes* bacteria. Surface-exposed or secreted receptors interact with Hb (red and pink) and remove the haem cofactor. Haem is then relayed through a series of haem carrier proteins attached to the cell wall before being offloaded to a haem binding lipoprotein. Finally haem is imported though the cytoplasmic membrane by an ABC-transporter complex in a step that is conserved across bacteria. **(D)** The Isd haem import pathway of *S. aureus.* Hb (red and pink) is bound on the bacterial surface by the cell wall anchored receptors IsdH and IsdB (blue), which capture the haem cofactor via an unknown mechanism. Haem is then passed to the haem relay proteins IsdA and IsdC in the cell wall, before being transferred to IsdE, the substrate-binding component of an ABC-transporter permease. The known structures of the haem binding-proteins IsdA and IsdC (cyan and green respectively; PDB 2ITF, 2O6P) and the haem binding lipoprotein IsdE (grey; PDB 2Q8Q) are shown as ribbon diagrams.

Figure 1.6

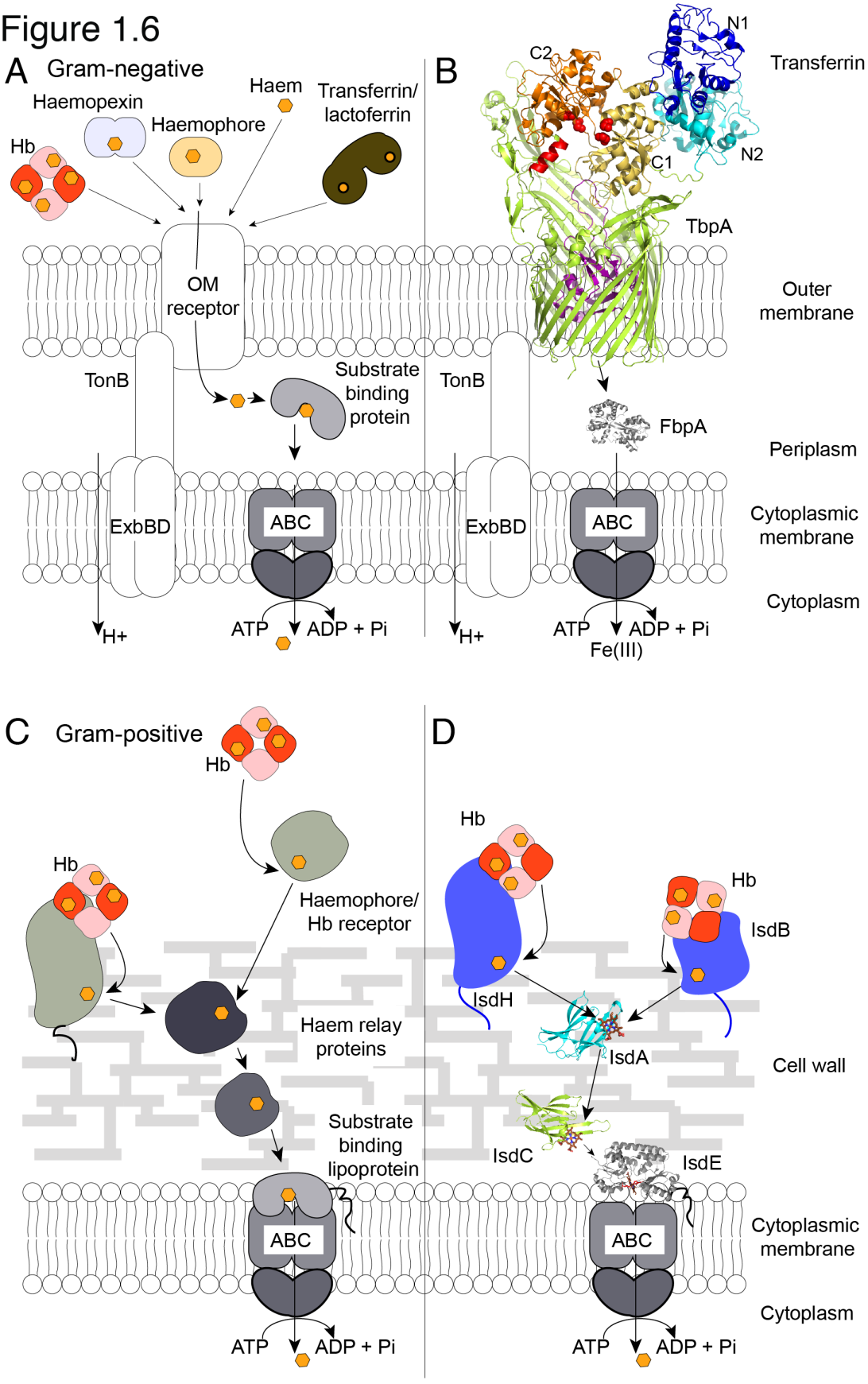
A Gram-negative
Haemopexin
Haem
Transferrin/
lactoferrin
Haemophore
Hb
OM
receptor
TonB
Substrate
binding
protein
ExbBD
ABC
H+
ATP
ADP + Pi
B
N1
C2
C1
N2
Transferrin
TbpA
Outer
membrane
TonB
FbpA
Periplasm
ExbBD
ABC
Cytoplasmic
membrane
H+
ATP
ADP + Pi
Fe(III)
Cytoplasm
C Gram-positive
Hb
Haemophore/
Hb receptor
Haem relay
proteins
Substrate
binding
lipoprotein
ABC
ATP
ADP + Pi
D
Hb
IsdB
IsdH
IsdA
Cell wall
IsdC
IsdE
ABC
Cytoplasmic
membrane
Cytoplasm
ATP
ADP + Pi

1.5.4.2 The NEAT domain

Haem relay through the Isd pathway is mediated by NEAr Transporter (NEAT) domains. The NEAT domain was originally identified in genes located in or near an operon encoding for a putative iron ABC transporter[143]. Subsequently, it was shown that NEAT domain containing proteins bind to haem or Hb and are involved in uptake of haem from Hb[7]. NEAT domains are ~130 residues in length and have an immunoglobulin like fold comprising an 8-stranded β-sandwich and one or more short helical segments (Fig. 1.7 A)[154-160]. The majority of characterised NEAT domains bind to either haem or Hb; however, they may also make additional interactions with other host factors[83,161-163].

IsdA, B, C and H all contain one NEAT domain that mediates binding to haem (Fig. 1.7 B, black box)[147,155,156,159,160,162,164]. Two highly conserved tyrosine residues on the β7–β8 hairpin are involved in haem binding (Fig. 1.7 A). Structural and spectroscopic studies indicate that one tyrosine phenolate directly coordinates the iron and the second acts to position the first[155,156,159,160,164]. In most cases, the sixth axial coordination site remains empty. The haem group is bound in a hydrophobic pocket, formed between the β7–β8 hairpin, and a short helical segment, with the two propionate groups pointing out of the pocket into the solvent. The haem group is partially exposed on the surface of the protein (~35–45% solvent exposed in IsdA/B/C and H), which is consistent with a role in haem transport, and differs from proteins such as Hb that bind haem as a functional cofactor and largely bury the haem group.

Proteins belonging to the NEAT domain family are widely distributed in (and exclusive to) Gram-positive bacteria of the phylum of *Firmicutes* suggesting that these bacteria have evolved for growth in environments abundant in haem. Numerous significant human pathogens, including *S. aureus, S. pyogenes, Listeria monocytogenes, B. anthracis, B. cereus, Clostridium perfringens,* and *Clostridium tetani,* contain NEAT domains in their genome[143,144].

1.5.4.3 Mechanism of haem transfer between NEAT domains

A direct transfer of haem between Isd proteins was determined by UV visible spectrophotometry and mass spectrometry[148,149,165]. Only IsdH or IsdB can capture haem from Hb. IsdH and IsdB can transfer haem to IsdA or to IsdC. IsdA can transfer haem to

IsdC. Several independent measurements of the affinity of the Isd proteins for haem have been made, giving values from μM to sub-nM, depending upon the technique used[149,155,165-167]. However, in each case the relative ranking of affinities was the same, with the affinity of IsdB for haem being ~10 fold greater than Hb, IsdA being ~2.5 fold greater than IsdB and IsdC being ~2–10 fold greater than IsdA. Hence the haem transfer process may be thermodynamically driven by an increase in the relative affinity for haem. Only IsdC can transfer haem to the lipoprotein IsdE[149,168]. Taken together these data suggest that the pathway for haem uptake proceeds from Hb to IsdB/H, directly to IsdC or via IsdA, and finally to IsdE (Fig. 1.6 D).

Kinetic studies of haem transfer in the Isd pathway have shown that the rate of haem transfer between NEAT domains is much faster than the spontaneous dissociation of haem from the donor protein[149,155,165]. IsdB captures haem from Hb, at ~2000× and 80× the rate of passive haem dissociation from the α and β chains of the Fe(III)-Hb dimer, respectively[149,169]. Transfer of haem from IsdB to IsdC occurs 8000-fold faster than passive haem loss from IsdB, and to IsdA ~2–8 fold greater again[149,155]. Finally, transfer of haem from IsdA to IsdC is > 70 000 times faster than passive haem loss from IsdA[165]. Hence Hb:Isd and Isd:Isd complexes must form in order to rapidly and directly transfer haem.

The Isd:Isd interactions that achieve rapid haem transfer are extremely weak (K_d > 5 mM in the case of IsdA and IsdC) making them difficult to characterise[170,171]. Low-affinity or transient interactions are common in ligand relay pathways, allowing for rapid and repeated turnover of the cargo[172,173]. Paramagnetic resonance excitation NMR and crosslinking studies, which can detect or capture very weak interactions, have shown that IsdA and IsdC form homo- and hetero-associations in a ‘handclasp’ conformation, which juxtaposes the haem pockets of the two proteins[170,171]. The haem pocket β7–β8 hairpin of IsdC is also the binding site used in transient interactions with IsdE[170]. Interestingly, similar NEAT:NEAT interactions are observed in the crystal packing in X-ray crystallography structures of haem bound IsdA, IsdB, IsdC and IsdH^{N3} (Fig. 1.7 C; PDB 2ITF, 3RTL, 3QUG, 3QUH). This suggests that a similar mode of haem pocket interactions may be common to all haem-binding NEAT domains.

Figure 1.7. The cell wall anchored Isd proteins bind haem and Hb via NEAT domains. (A) The haem binding NEAT domain of IsdC (PDB 2O6P) showing the β-sandwich domain fold common to all NEAT domains. The haem cofactor (yellow sticks) is bound between a short helical segment in loop 2 (blue) and the β7–β8 hairpin. The haem coordinating tyrosine (Tyr132) and supporting tyrosine (Tyr136) are shown as cyan spheres. **(B)** The domain architecture of the four cell wall anchored Isd proteins. Haem-binding domains are represented by black rectangles while Hb binding domains are represented by white rectangles. Helical linker domains are coloured grey. Small while squares indicate cell wall anchoring motifs. **(C)** Haem pocket interactions between adjacent NEAT domains in the crystal packing of IsdC (red; PDB 2O6P), IsdH (pink; PDB 3QUG), IsdB (yellow; PDB 3RTL) and IsdA (orange; PDB 2ITF). The haem pocket tryosines are shown in stick representation and coloured cyan. Helical regions are coloured blue.

Figure 1.7

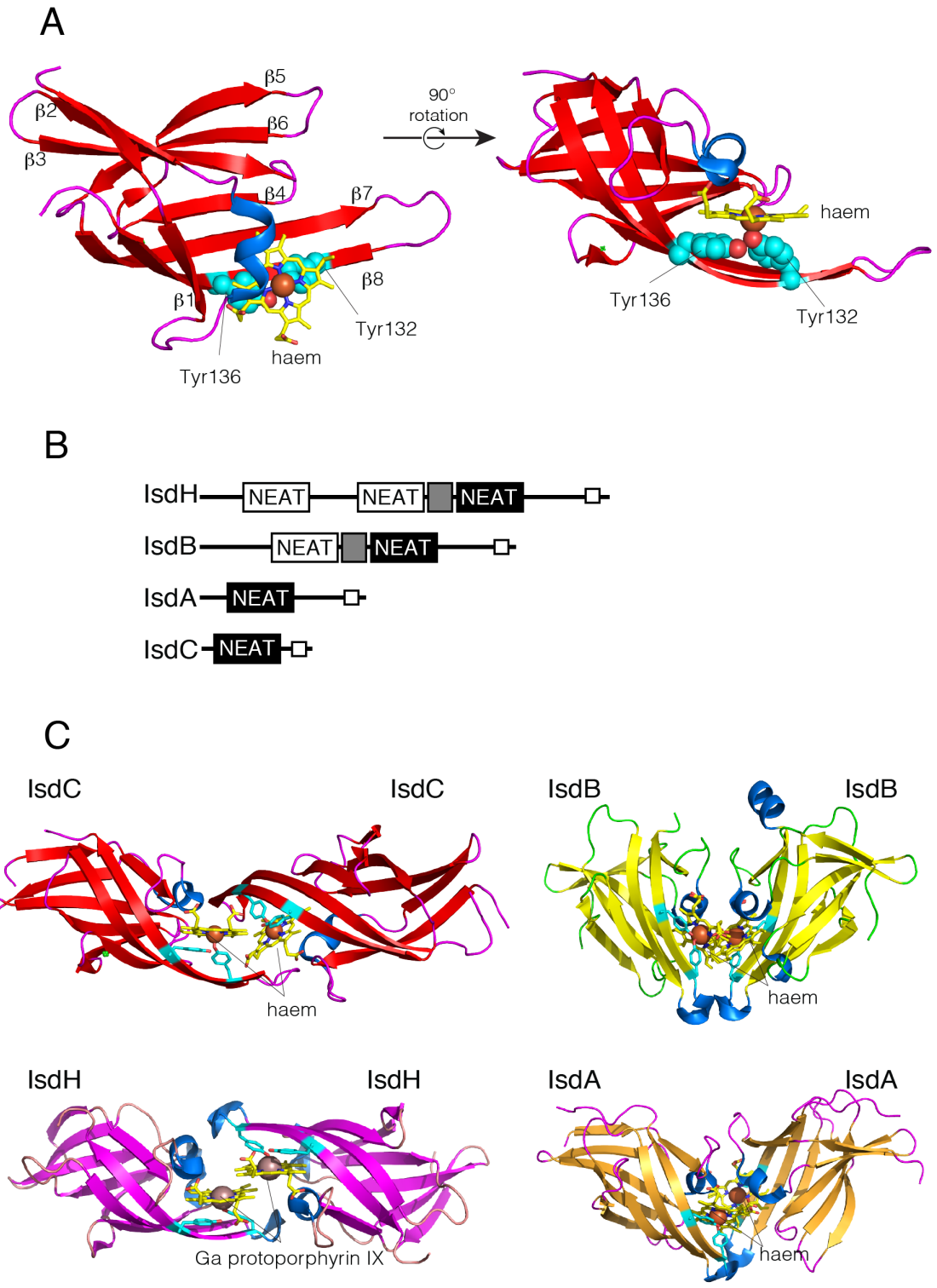
A
β5
β2
β6
β3
β4
β7
β8
β1
Tyr132
haem
Tyr136
90°
rotation
haem
Tyr136
Tyr132
B
IsdH
NEAT
NEAT
NEAT
IsdB
NEAT
NEAT
IsdA
NEAT
IsdC
NEAT
C
IsdC
IsdC
haem
IsdB
IsdB
haem
IsdH
IsdH
Ga protoporphyrin IX
IsdA
IsdA
haem

1.5.4.4 Hb receptors of S. aureus

Unlike IsdA and IsdC, which are comprised of a single NEAT domain, IsdB and IsdH, both contain one ($IsdB^{N1}$) or two ($IsdH^{N1}$ and $IsdH^{N2}$) additional N-terminal NEAT domains respectively (Fig., 1.7 B and 1.8 B, white boxes). While $IsdB^{N1}$, $IsdH^{N1}$ and $IsdH^{N2}$ adopt the conserved β-sandwich fold, common to all NEAT domains, the haem-binding tyrosine motif is absent and these NEAT domains do not bind to haem[147,174]. Instead the isolated $IsdH^{N1}$ and $IsdH^{N2}$ have been shown to bind to Hb[146,147,158]. The affinity of $IsdH^{N1}$ for Hb has been measured to be 17–30 nM[145,147]. The full-length IsdB protein or an N-terminal fragment of IsdB (containing $IsdB^{N1}$) also binds to Hb[7,83,145,174]. The full-length IsdB protein has a similar affinity for Hb (K_d ~55 nM) as $IsdH^{N1}$ [145] $IsdH^{N1}$ and $IsdH^{N2}$ each bind to the α chain of Hb, while a second, weaker, binding site for $IsdH^{N2}$ exists on β chain of Hb[146]. $IsdB^{N1}$ has greater primary sequence homology with $IsdH^{N2}$ (65 % identity) than $IsdH^{N1}$ (46 % identity) predicting that it will show similar interactions with α and β Hb chains to $IsdH^{N2}$. Mutagenesis studies of $IsdH^{N1}$ and structural studies with isolated $IsdH^{N1}$ and $IsdH^{N2}$ have identified the Hb binding surface, which includes a short α helix in loop 2 as well as loops 4, 6 and 8 (Fig. 1.8 A, orange)[146,147,175]. This is the same surface that is used by the haem-binding NEAT domains to contact haem. Interactions of the Hb-binding NEAT domains are discussed in more detail in Section 3.1 where it is directly relevant to the aims of the chapter.

IsdB and IsdH capture haem from Hb at faster rates than can be explained by the passive loss of haem from Hb alone[149,167]. In addition, IsdB has been shown to catalyse the transfer of haem from Hb to the haem carrier protein IsdC[149] and hence perform all of the functions expected for a Hb receptor involved in haem uptake *in vitro*. Enzymatic relay of haem from Hb to IsdA/C by IsdH has not yet been demonstrated. However, the isolated haem-binding NEAT domain of IsdH was shown to transfer haem to IsdC[148] and to IsdA [176], predicting that IsdH will also function in haem relay. As yet, the mechanism by which IsdB and IsdH extract haem from Hb and function in haem relay is unknown.

1.5.4.5 Putative Hb receptors in other Gram-positive bacteria

Proteins containing NEAT domains have been identified as Hb receptors in *Firmicutes* bacteria, other than *S. aureus*. These proteins have a range of domain architectures that are dissimilar from IsdB and IsdH (Fig. 1.8 B).

Shr from *Streptococcus pyogenes* is anchored in the cytoplasmic membrane via a C-terminal tail that spans the distance of the cell wall and is exposed on the cell surface[177]. A large protein at 145 kDa, Shr contains an N-terminal region with two domains of unknown function (DUF1533), two NEAT domains, a series of leucine rich repeats and an EF hand[163]; the domain architecture is shown in Figure 1.8 B. The two NEAT domains bind to haem[163,178], and the full-length protein was shown to bind to Hb with a K_d of ~50 nM, measured by ELISA, which is comparable to IsdH and IsdB[145,147,163,179]. A region in the N-terminus of the protein, adjacent to the N-terminal NEAT domain, was implicated in Hb binding[163]; however, the sequence and structure of the Hb-binding site is currently unknown. Shr captures haem from Hb at rates that are 7 and 60 fold faster than passive haem release from the β and α chains of Fe(III)-Hb respectively[179] supporting a physical interaction between the receptor and Hb that facilitates haem transfer. Shr can also catalyse the transfer of haem from Hb to Shp[178,179]. Shp is a functional homologue of IsdC, which despite limited sequence identity to the *S. aureus* protein also has a NEAT domain fold[180]. Like IsdC, Shp can relay haem to HtsA, the haem binding lipoprotein component of an ABC membrane permease[181]. Hence, Shr can promote haem release from Hb and catalyse its transfer to Shp, and appears to perform an analogous function in haem uptake in *S. pyogenes* to that of IsdB and IsdH in *S. aureus*.

IlsA from *Bacillus cereus* comprises a single NEAT domain, a series of leucine rich repeats and three SLH domains that are predicted to embed the receptor in the proteinaceous S-layer, which is associated with the cell wall (Fig. 1.8 B)[69]. IlsA was shown to bind to Hb by ELISA, with an estimated affinity of 3 nM, and also to haem. Haem binding is likely to occur through the single NEAT domain of IlsA as the primary sequence contains the haem-coordinating tyrosines and other recognised haem pocket residues. Both IlsA and Shr contain leucine rich repeats (LRR). LLR are known to mediate protein-protein interactions in many other proteins[182] and are candidates for Hb

binding domains. Interestingly, IlsA was also shown to interact with ferritin *in vitro* and assist in iron uptake from ferritin[69,70]. *B. cereus* can infect both insect and mammalian hosts and the IlsA protein has been suggested to mediate haem/iron uptake in both host environments through Hb and ferritin interactions. While direct haem uptake from Hb has not be shown, IlsA was required for *in vitro* growth on Hb as an iron source and an Isd-like operon was identified in the *B. cereus* genome, providing a potential haem relay network for IlsA to function in.

The *B. anthracis* proteins, IsdX1 and IsdX2, contain one or five NEAT domains respectively (Fig. 1.8 B). Unlike the *S. aureus* and *S. pyogenes* Hb receptors, the IsdX proteins are secreted, although a small percentage of IsdX2 may remain associated with the cell wall[183]. The *B. anthracis* proteins also differ from IsdB/H and Shr, in that single NEAT domains can perform both Hb and haem binding functions. For example four of the five NEAT domains of *B. anthracis* IsdX2 bind to both haem and Hb with Hb binding affinities ranging from ~ 2 μM to 41 nM. Two of these NEAT domains can bind haem derived from Hb and three can transfer the haem to *B. anthracis* IsdC[184]. The single NEAT domain of the *B. anthracis* receptor, IsdX1, was also shown to interact weakly with Hb with a K_d of ~8 μM, and transfer haem to IsdC[183,185]. Importantly, IsdX2 and IsdX1 have not yet been demonstrated to accelerate haem release from Hb and little is known about the IsdX-Hb interaction. The X-ray crystal structures of IsdX1 and IsdX-NEAT5 reveal a conserved structure and mechanism of haem binding to the *S. aureus* haem binding NEAT domains[154,157]. In contrast, residues involved in Hb binding, which were identified though mutagenesis studies, are absent from the *S. aureus* receptors, indicating that the mechanism behind haem scavenging is likely to be distinct[154,157].

B. anthracis also encodes for a cell wall associated putative Hb receptor, Hal[186]. Hal contains a single NEAT domain, with homology to IsdX2-NEAT5 and a series of leucine rich repeats (Fig. 1.8 B). Like IsdX2-NEAT5, the NEAT domain of Hal binds to haem and Hb, and can extract haem from Hb; however, no structural or kinetic information is available. The relative roles IsdX1, IsdX2 and Hal in growth using Hb as an iron source have not been determined although each have been implicated in this function *in vitro*[154,183,186].

L. monocytogenes produces two secreted NEAT domain containing proteins, Hbp1 and Hbp2, that are implicated in haem uptake from Hb. Hbp2 (also called SvpA) contains three NEAT domains (Fig. 1.8 B) and, like IsdX2, a small portion of this protein may be associated with the cell wall[187]. Hbp2 binds to haem and contributes to haem utilisation under conditions of low haem abundance[188]. In addition, the cell wall anchored form of Hbp2 is involved in growth on Hb as an iron source *in vitro*[188]. However, interaction between Hbp1 or Hbp2 and Hb is yet to be demonstrated.

Of the above putative Hb receptors, evidence for direct haem transfer from Hb to the receptor in a protein complex is available for Shr, which has been shown accelerate haem release from Hb. Evidence of facilitated haem release is missing for IlsA, IsdX1, IsdX2, Hal and Hbp2. Further characterisation of the interaction between the putative receptors and Hb is required to determine whether they function like the Hb receptors of *S. aureus* or form a family of Gram-positive haemophores, which compete for but do not directly liberate haem from the host protein.

Figure 1.8. Putative Hb receptors of Gram-positive *Firmicutes* bacteria (A) The structure of the first Hb-binding NEAT domain of IsdH ($IsdH^{N1}$; PDB 3SZK). The Hb-binding face (orange) is the same face used by the haem-binding NEAT domains to bind haem. **(B)** The domain architecture of putative Hb receptors. One or more NEAT domains are present in each. Domains shown to bind to haem are coloured black. All proteins contain a secretion signal (small black circle). The Hb-binding proteins may be anchored to the cell wall via a sortase anchoring motif (small white square), imbedded in the cell membrane via a transmembrane domain (TM) or in the S-layer via S-layer homology domains (SLH). Shr, IslA and Hal also contain leucine rich repeat domains (LLR).

Figure 1.8

A

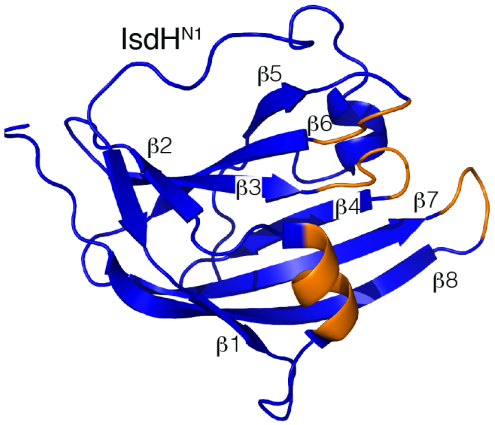
IsdH^N1
β5
β6
β2
β3
β4
β7
β8
β1

B

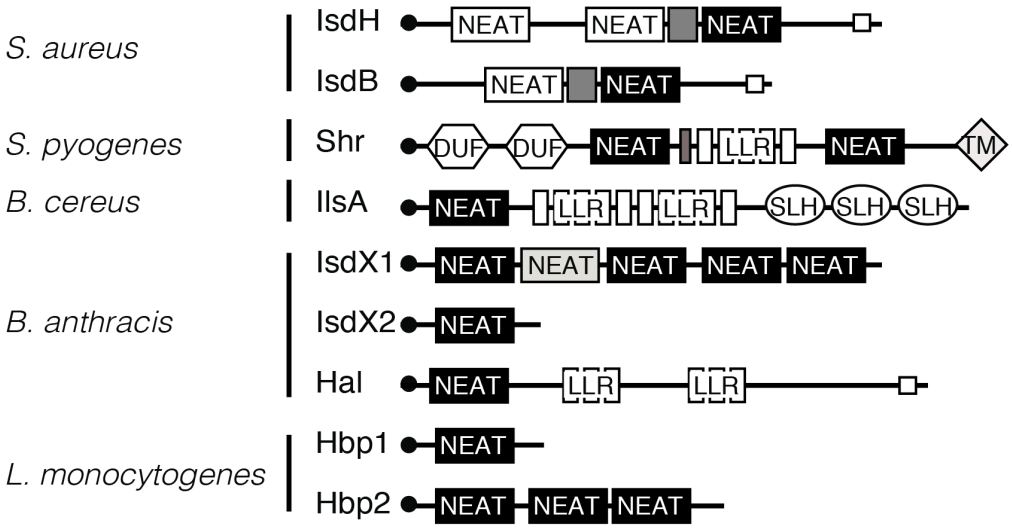
S. aureus
IsdH
NEAT
NEAT
NEAT
IsdB
NEAT
NEAT
S. pyogenes
Shr
DUF
DUF
NEAT
LLR
NEAT
TM
B. cereus
IlsA
NEAT
LLR
LLR
SLH
SLH
SLH
B. anthracis
IsdX1
NEAT
NEAT
NEAT
NEAT
NEAT
IsdX2
NEAT
Hal
NEAT
LLR
LLR
L. monocytogenes
Hbp1
NEAT
Hbp2
NEAT
NEAT
NEAT

1.5.5 Import across the inner membrane

The machinery used to import haem or Fe(III)-siderophore complexes across the cytoplasmic membrane is conserved across Gram-negative and Gram-positive bacteria (Fig. 1.5&1.6). Despite significant differences in the chemical composition of haem and siderophores, the inner membrane transporters for both of these substrates are structurally related and belong to the same protein families. Gram-negative and Gram-positive inner membrane transporters consist of one or more substrate-binding proteins and an adenosine tri-phosphate (ATP) binding cassette (ABC) transporter permease comprising one or two trans-membrane proteins and one or two ATPases.

The periplasmic substrate-binding proteins belong to the helical backbone metal receptor superfamily, characterised by a bi-lobed structure bridged by a backbone formed from one or more α-helices[189-191]. The substrate-binding site is formed between the two lobes, however residues involved in contacts with substrate vary to allow for diverse ligand transport. In Gram-negative bacteria these substrate-binding proteins diffuse though the periplasm, shuttling the cargo from the outer membrane to the inner membrane. In Gram-positive bacteria, the substrate binding proteins are lipoproteins and are displayed on the periplasmic surface of the inner membrane. The substrate binding protein docks to an adenosine tri-phosphate (ATP) binding cassette (ABC) transporter permease allowing substrate transport though membrane.

Seven operons encoding for putative ABC iron/haem transporter systems (including a substrate binding protein and homo- or hetero-dimeric permease) are found in the *S. aureus* genome[82]. Several of these operons have now been characterised, including four involved in the uptake of siderophore iron, as follows. The staphylococcal iron regulated (SirABC) transporter is responsible for the uptake of Staphyloferrin B (also called Staphylobactin)[189]. The haem transport system (HtsABC) was originally suggested to act as a haem importer[82], but subsequently shown to bind to Staphyloferrin A in structural studies[190,192]. The ferric hydroximate uptake system (FhuCBG-D1/D2) has broad substrate specificity allowing for uptake of a range of ferric hydroxamate siderophores[123]. The Staphylococcal siderophore transporter (SstABCD) has unknown substrate specificity[144,193]. In addition, two ABC transporter permease complexes are involved in haem uptake: the iron regulated surface determinant transporter (IsdEF)[7], and the haem

regulated transporter HrtAB[103]. Interestingly, the only ATPase component to be characterised is FhuC of the ferric hydroximate uptake system. FhuC has been shown to perform the ATPase role for FhuCBG, SiaABC[194] and HtsABC[192], and may be important for the functioning of all seven *S. aureus* ABC transporter iron uptake systems[195].

1.5.6 Haem catabolism

Once haem reaches the bacterial cytoplasm it can either be directly incorporated into bacterial haem-binding proteins or broken down to release iron. Haem-degrading enzymes, known as haem oxygenases, are found in bacteria through to humans. The haem oxygenases of Gram-negative bacteria show structural homology to the human haem oxygenase 1[196] and use a conserved mechanism for haem catabolism[197]. In contrast, the Gram-positive haem oxygenases are structurally distinct to haem oxygenase 1, and degrade haem via several unique mechanisms[198-200]. IsdG and IsdI of *S. aureus* fall into the latter category and degrade haem to produce free iron, staphylobillin (a chromophore), and formaldehyde[200,201].

1.6 The role of the Isd system in infection

Proteins of Isd system are highly up-regulated in response to conditions of iron restriction *in vitro*[5,98,202], during growth in human blood and serum[6] and during infection[5]. In addition, *S. aureus* strains in which the *isdA, isdB, isdC, isdH, sortB* genes or the haem oxygenase genes (*isdG* and *isdI*) have been deleted show impaired growth in animal infection models, suggesting that the ability to utilise haem is important for full virulence[84,174,203-205].

1.6.1 Role of the Hb receptors of S. aureus in infection

It was originally observed that gene deletion of *isdB* but not *isdH* causes a significant defect in growth using Hb as a sole iron source *in vitro*[8,84]. However, Hurd *et al*., did not observe a growth defect for *S. aureus* strains inactivated for *isdB, isdH* or *IsdA,* when grown in the presence of Hb as a sole iron source[206]. In the latter studies, Hb that had been lyophilised was provided at ~80 nM. It was subsequently shown that lyophilised Hb but not Hb purified fresh from blood could sustain growth of Δ*isdB* strains when provided at ~40 nM[207]. Lyophilised Hb is known to release free haem due alterations in the Hb structure and free haem has been shown to support *S. aureus* growth independently of IsdB and IsdH activity[84,207]. More recently, it was demonstrated that haem uptake from

Hb by IsdB is only required in the presence of low concentrations of Hb (10–20 nM)[208]. This is consistent with a role for IsdB in Hb utilisation *in vivo*, where extracellular Hb concentrations are expected to be in the nanomolar range under physiological conditions and may be further limited depending up the site of infection. In these studies, deletion of *isdB* virtually abolishes growth on human Hb, suggesting that IsdB is the primary receptor for haem uptake from Hb[207,208].

Despite the difference observed in *in vitro* growth assays, IsdB and IsdH each contribute to bacterial virulence based on the following observations. Deletion of either *isdB* or *isdH* from *S. aureus* increased survival time of mice after systemic infection[174,205]. In addition, passive transfer of antibodies raised against IsdB into *S. aureus*-infected mice caused increased survival rates following lethal infection. The protection provided by passive immunisation was attributed to loss of Hb receptor function, as anti-IsdB antibodies blocked IsdB binding to Hb but did not enhance phagocytosis and killing during growth in mouse blood[174]. Hence haem uptake by the Isd system is an important aspect of *S. aureus* virulence and an understanding of the mechanisms behind this pathway may inform targeted drug design. Interestingly, while IsdB and IsdH are both important for pathogenesis, they appear to play distinct roles in infection, as IsdB but not IsdH is involved in abscess formation in spleen and kidneys[84,174,203]. This suggests that the Hb binding and haem capture functions of these two proteins may not be redundant but contribute to different aspects of the infection process.

1.6.2 Other roles for the Isd proteins in infection

The Isd proteins may play other roles in infection, in addition to iron uptake. This may explain why different Isd proteins are more, or less, important for the colonisation of different of organs. For example, IsdA has been proposed to have a role in cell adhesion, skin and nasal colonisation, and innate immune evasion. These activities are mediated through binding to a diverse range of ligands, including fibrinogen[162], lactoferrin[57] and extracellular matrix proteins cytokeratin K10, loricrin, and involucrin[161] and by reducing the hydrophobicity of the bacterial surface to prevent the antimicrobial activity of fatty acids present in the skin[209]. IsdB has been found to induce aggregation of platelets through direct binding to the platelet integrin $\alpha_{IIb}\beta_3$[210]. The integrin-binding activity of IsdB was also shown to promote bacterial entry into a range of non-immune cells for intracellular growth, and was independent of Hb binding activity[211]. An alternative role in

immune evasion has also been suggested for IsdH. *S. aureus* cells expressing IsdH show reduced phagocytosis and increased survival in whole blood when compared to a Δ*isdH* strain[205,212]. The increased survival was linked to enhanced degradation of complement; however, binding of IsdH to Hb may still be involved as residues on the IsdH Hb-binding interface were necessary for *S. aureus* survival in human blood[205]. Hence, while the Isd proteins have a primary role in haem uptake from Hb, they also carry out a range of other roles that contribute to infection.

1.7 Project aims

Currently, little is known about the structural mechanisms that achieve iron uptake from host haem proteins. Although progress has been made in understanding the structure, function and haem transfer mechanism of the haem binding Isd proteins, there is a significant gap in our knowledge of the Isd Hb receptors and the mechanism of haem capture from Hb at the top of the Isd pathway. This project had two broad aims. The first aim was to determine the molecular mechanisms used by the Hb receptors, IsdB and IsdH to liberate haem from Hb. The second aim was to investigate how haem is relayed to IsdA and C, following haem capture by IsdB and IsdH.

Chapter 2. Materials and methods

Materials

2.1 Consumables, reagents and suppliers

1 kb DNA ladder	Invitrogen (Mount Waverley, VIC)
Acetone	Merk millipore (Kilsyth, Vic)
Acetonitrile (HPLC grade)	Merk millipore (Kilsyth, Vic)
Acetic Acid	Merk millipore (Kilsyth, Vic)
Acrylamide	Bio-Rad (Gladesville, NSW)
Agar	Oxoid (Thebarton, SA)
Additive screen	Hampton Research (Aliso Viejo, CA, USA)
Agarose (DNA grade)	Astral Scientific (Caringbah, NSW)
Ammonium persulfate (APS)	Sigma-Aldrich (Castle Hill, NSW)
Ammonium sulphate	Sigma-Aldrich (Castle Hill, NSW)
Ampicillin (AMP)	Sigma-Aldrich (Castle Hill, NSW)
Antarctic phosphatase	New England Biolabs (Ipswich, MA, USA)
*Bam*HI	New England Biolabs (Ipswich, MA, USA)
Bovine serum albumin (BSA)	Sigma-Aldrich (Castle Hill, NSW)
1-butanol	Merk millipore (Kilsyth, Vic)
Casein peptone	Oxoid (Thebarton, SA)
Cat whiskers	Lucy (Ingleside, NSW)
Chloramphenicol (CAM)	Sigma-Aldrich (Castle Hill, NSW)
Complete, EDTA-free protease inhibitor tablets	Roche Diagnostics (Castle Hill, NSW)
Coomassie® Brilliant Blue R	Sigma-Aldrich (Castle Hill, NSW)
Diammonuim citrate	Sigma-Aldrich (Castle Hill, NSW)
Disodium hydrogen orthophosphate	Sigma-Aldrich (Castle Hill, NSW)
Dithiothreitol (DTT)	Gold Biotechnology (St. Louis, MO, USA)
dNTPs	New England Biolabs (Ipswich, MA, USA)
Dpn1	New England Biolabs (Ipswich, MA, USA)
Ethanol (HPLC grade)	Merk millipore (Kilsyth, Vic)
Ethylenediaminetetraacetic acid (EDTA)	Sigma-Aldrich (Castle Hill, NSW)
Ethylene glycol	Hampton Research (Aliso Viejo, CA, USA)
Glycerol	Sigma-Aldrich (Castle Hill, NSW)
Glycine	Sigma-Aldrich (Castle Hill, NSW)
Guanidine hydrochloride	Astral Scientific (Caringbah, NSW)
His-select® Ni Affinity Gel	Sigma-Aldrich (Castle Hill, NSW)
Hydrochloric acid	Sigma-Aldrich (Castle Hill, NSW)
Imidazole	Sigma-Aldrich (Castle Hill, NSW)
Isopropyl β-D-thiogalactopyranoside (IPTG)	Gold Biotechnology (St. Louis, MO, USA)
Isopropanol	Merk millipore (Kilsyth, Vic)
Kanamycin sulphate	Sigma-Aldrich (Castle Hill, NSW)
Methanol (HPLC grade)	Ajax Finechem (Taren Point, NSW)
Mark 12® protein standards	Invitrogen (Mount Waverley, VIC)
NeXtal Classic suite	Qiagen (Doncaster, VIC)
NeXtal JCSG+ suite	Qiagen (Doncaster, VIC)
NeXtal Pact suite	Qiagen (Doncaster, VIC)
Nickel sulphate	Sigma-Aldrich (Castle Hill, NSW)
PEG-3350	Hampton Research (Aliso Viejo, CA, USA)
Phusion DNA polymerase	New England Biolabs (Ipswich, MA, USA)
PMSF	Sigma-Aldrich (Castle Hill, NSW)

Potassium chloride	Sigma-Aldrich (Castle Hill, NSW)
QIAprep® Spin miniprep kit	Qiagen (Doncaster, VIC)
SmaI	New England Biolabs (Ipswich, MA, USA)
Snakeskin™ 3500 MWCO pleated dialysis tubing	Quantum Scientific (Lane Cove West, NSW)
Sodium dihydrogen orthophosphate	Sigma-Aldrich (Castle Hill, NSW)
Sodium chloride	Sigma-Aldrich (Castle Hill, NSW)
SYBR safe	Invitrogen (Mount Waverley, VIC)
T4 DNA ligase	New England Biolabs (Ipswich, MA, USA)
T4 Polynucleotide Kinase	New England Biolabs (Ipswich, MA, USA)
N,N,N',N'-tetramethyldiamine (TEMED)	Sigma-Aldrich (Castle Hill, NSW)
Tris(hydroxymethyl)methylamine (TRIS)	Sigma-Aldrich (Castle Hill, NSW)
Trifluoroacetic acid (TFA)	Sigma-Aldrich (Castle Hill, NSW)
Tryptone T	Oxoid (Thebarton, SA)
XhoI	New England Biolabs (Ipswich, MA, USA)
Yeast extract	Oxoid (Thebarton, SA)
Zero blunt® TOPO® PCR Cloning Kit	Invitrogen (Mount Waverley, VIC)

Methods

2.2 Primers, genomic DNA, plasmids and bacterial strains

Single-stranded DNA oligonucleotides for cloning and site directed mutagenesis were purchased from Sigma Genosys (Castle Hill, NSW; see Appendix A for sequences). Genomic DNA from the *Staphylococcus aureus* strain TCH1516 was purchased from ATCC (Manassas, VA, USA).

The IsdH^{N1}, pRM208 and pRM216 vectors were a kind gift from Dr Rob Clubb. The pRM208 vector consists of the IsdH gene (residues 326-660) cloned into the pHis-SUMO backbone vector, which encodes for a Kanamycin resistance gene. pRM216 was generated from pRM208 and carries a Tyr642 to Ala mutation. Details of the construction of these vectors can be found in Spirig, *et al.,*[167].

Cloning and mutagenesis was performed in the *Escherichia coli* DH5α strain (F^- Φ80*lacZ*ΔM15 Δ(*lacZYA-argF*) U169 *rec*A1 *end*A1 *hsd*R17(r_k^-, m_k^+) *pho*A *sup*E44 *thi*-1 *gyr*A96 *rel*A1 λ^-).

The *E. coli* Rosetta2 (DE3) pLysS strain (F^- *ompT* *hsdS*$_B$(r_B^- m_B^-) *gal* *dcm* (DE3) pLysSRARE2 (Cam^R)) was used for recombinant protein production.

2.3 Cloning of recombinant Isd protein constructs

The genes encoding for IsdA, B, C and H were amplified from *Staphylococcus aureus* strain TCH1516 genomic DNA by polymerase chain reaction (PCR). The forward and reverse primer sequences contained a *XhoI* or a *BamHI* restriction endonuclease cleavage site respectively. Primer sequences can be found in Appendix A. A typical PCR reaction contained 1–100 ng template DNA, 0.5 μM primes, 0.25 mM dNTPs, 1× Phusion HF polymerase buffer and of 1U Phusion polymerase. Thermocycling was carried out in a T100 Thermal cycler (Bio Rad, Gladesville, NSW) and conditions included an initial incubation at 98 °C for 45 sec, followed by thirty cycles of (98 °C for 30 sec, 55 °C for 30 sec and 72 °C for 15–30 sec/kb) and a final incubation at 72 °C for 10 min.

For blunt insertion into the pBluescript cloning vector, 5' phosphates were added to the PCR products in a 2 h incubation with T4 Polynucleotide Kinase at 37 °C. T4 Polynucleotide Kinase was heat inactivated at 65 °C for 20 min. The vector was linearized in a 2-h incubation with *SmaI* at 25 °C and the 5' phosphate groups were removed by incubation with Antarctic phosphatase for 1h at 37 °C. Antarctic phosphatase was heat inactivated at 65 °C for 20 min. The PCR products were then ligated to the blunt ends of pBluescript in a 1-h incubation with T4 DNA ligase at room temperature.

The IsdB gene was cloned blunt into the pCR®-Blunt II-TOPO® vector using the Zero blunt® TOPO® PCR Cloning Kit (Invitrogen).

For direct cloning or sub-cloning into pET15b (Novagen) the PCR products or parent vectors containing the gene of interest were digested with XhoI/BamHI for 2 h at 37 °C. The pET15b vector was similarly treated and the digestion products were purified via agarose gel electrophoresis. To prevent re-ligation of partially digested vector, the digested plasmid was incubated with Antarctic phosphatase for 1 h at 37 °C. The digested products were then ligated as above.

Plasmids were transformed into *E. coli* DH5α cells for colony screening. Single colonies were grown overnight at 37 °C in LB broth containing 100 $\mu g \cdot ml^{-1}$ ampicillin. Plasmid DNA was isolated via the alkaline lysis method according to Sambrook *et al*.,[213] or using

the Qiagen QIAprep® Spin Miniprep Kit and confirmed to be correct by DNA sequencing (AGRF, Westmead, Sydney).

2.4 Site directed mutagenesis

The modified QuikchangeTM method of Liu and Naismith was used to introduce single or multiple mutations, insertions and deletions in a single step into the Isd expression vectors[214]. Primer sequences and parent vectors can be found in Appendix B. Forward and reverse primers contained a complementary sequence with a Tm (Tmpp) 5–10 °C lower than the non-complementary 3' overhangs (Tmno). Reaction components were the same as for standard PCR, with the modification of 2–10 ng template vector. The reaction conditions included an initial incubation at 95°C for 5 min, twelve cycles of (95 °C for 1 min, Tmno – 5 °C for 1 min and 72 °C for 10–15 minutes) followed an annealing step Tmpp – 5 °C for 1 min and a final extension step at 72 °C for 30 min.

To remove template DNA, the PCR reaction products were incubated with 5U *Dpn1,* an enzyme that only digests methylated DNA, for 2 h at 37°C. *E. coli* DH5α cells were then transformed with 250 ng of the *Dpn1* digested DNA for colony screening. All mutations were confirmed by DNA sequencing (AGRF, Westmead, Sydney).

2.5 Recombinant protein expression and purification

2.5.1 Protein expression

For recombinant protein overexpression, expression vectors were transformed into *E. coli* Rosetta2 (DE3) pLysS cells and grown overnight on LB-agar plates containing 34 $\mu g \cdot ml^{-1}$ Chloramphenicol and either 100 $\mu g \cdot ml^{-1}$ Ampicillin for pET15b backbone vectors or 50 $\mu g \cdot ml^{-1}$ Kanamycin for pHis-SUMO backbone vectors. Several colonies were inoculated into 20 mL of LB broth and were grown overnight with shaking at 37 °C. The overnight culture was diluted 50–100 fold into 2 L of LB broth to give a starting OD_{600} of ~ 0.05 and grown with shaking at 37 °C. When the OD_{600} had reached ~0.7 the culture was equilibrated to the expression temperature and induced with 1 mM IPTG. For production of haem binding proteins in their holo form, 5-10 $\mu g \cdot ml^{-1}$ haem was also added to the culture at induction.

IsdA, IsdC and IsdH constructs were expressed at 37 °C for 4 hours before harvesting by centrifugation. IsdB was degraded over time in the growing cells. Expression trials were conducted and the highest yield of intact protein was achieved in a 30–45 minute induction at 37 °C before harvesting. $IsdB^{N2}$ was expressed for 4–5 h at 22 °C. Cell pellets were resuspended in 50 mM NaP, pH 7.4, 10 mM imidazole, 300 mM NaCl, 0.1 μM PMSF. For IsdB constructs, 1× complete mini-EDTA free protease inhibitor cocktail (Roche) was also included. Cell suspensions were snap frozen in liquid nitrogen and stored at –80 °C.

2.5.2 Immobilized metal affinity chromatography (IMAC)

Proteins cloned into the pET15b vector were expressed with an N-terminal affinity tag with the sequence MGSSHHHHHHSSGLVPRGSHMLE. Similarly, proteins expressed from the pHis-SUMO vector contained an N-terminal fusion including a hexa-His tag with the sequence MGSSHHHHHHSSGLVPRGSHMAS followed by the 11.3 kDa, ubiquitin-like protein, SMT3, from *Saccharomyces cerevisiae.*

The His-tagged proteins were purified at 4 °C over 5 mL IMAC resin (HIS-Select Nickel Affinity gel, Sigma) and the eluted proteins were analysed by SDS-PAGE (see Section 3.2.1, Fig. 3.3, 3.4). For IsdH constructs, the load condition was 50 mM NaP, pH 7.4, 300 mM NaCl, 20 mM imidazole. The bound protein was washed in equilibration buffer containing 20 mM imidazole and eluted with 100 mM imidazole. IsdB constructs were applied to the Ni-resin in 50 mM NaP pH, 7.4, 300 mM NaCl, 10 mM imidazole and washed in equilibration buffer containing 20 mM imidazole. Apo-proteins were eluted in equilibration buffer containing 100 mM imidazole, while the holo-protein was eluted in 250 mM imidazole. IsdA was loaded onto the Ni-resin in 50 mM NaP, pH 7.4, 300 mM NaCl, 10 mM imidazole. IsdA was washed in the load buffer and eluted in 50 mM NaP, pH 7.4, 300 mM NaCl, 30 mM imidazole. Finally, IsdC was loaded onto the Ni-resin 50 mM NaP, pH 7.4, 300 mM NaCl, 10 mM imidazole, washed in equilibration buffer containing 30 mM imidazole, and eluted in 100 mM imidazole.

2.5.3 Cleavage of the his-SUMO affinity tag

Fractions eluted off Ni-resin containing His-Sumo tagged proteins were identified by SDS-PAGE. Pooled fractions were mixed with 1/100 His-tagged ubiquitin-like protein 1

(Ulp1) protease for 1 h at room temperature. An overnight dialysis step at 4 °C was then used to buffer exchange the protein into 20 mM Tris, pH 8.0, 300 mM NaCl. The dialysed protein was applied to a 5 mL IMAC column equilibrated in 50 mM NaP pH, 7.4, 300 mM NaCl, 10 mM imidazole and washed 5x 1CV of equilibration buffer. The cleaved recombinant protein was obtained in the flow through and wash fractions, while the His-SUMO tag and His-Ulp1 were maintained on the column. The SUMO tag and Ulp1 were eluted from the Ni-resin in 50 mM NaP pH, 7.4, 300 mM NaCl, 250 mM imidazole. A representative SDS-PAGE analysis of the Sumo tag cleavage and separation can be found in Figure 3.9.

2.5.4 Anion Exchange chromatography

Additional purification of $IsdH^{N1N2N3}$ and $IsdH^{N2N3}$ was performed by anion-exchange chromatography (Q-sepharose, GE Healthcare). Proteins were loaded in 10 mM NaP, pH 7.0 and eluted over a gradient of 100–250 mM NaCl.

$IsdH^{N2}$ was subject to cation exchange chromatography over SP-sepharose resin (GE Healthcare). The load condition was 50 mM NaP, pH 6.5 and extensive washing of the bound protein was performed in the same condition. $IsdH^{N2}$ was eluted in 50 mM NaP, pH 6.5, 50 mM NaCl.

IsdC was subject to anion exchange chromatography over DEAE sepharose resin (GE Healthcare). The protein was loaded onto the column in 10 mM Tris, pH 8.0 and washed in the same condition. For preparations of IsdC that were expressed without the addition of exogenous haem, apo-IsdC could be collected in the flow through and wash fractions. The holo protein was eluted in 20 mM Tris, pH 8.0, 200 mM NaCl.

2.5.5 Gel filtration chromatography

A final gel filtration step over a Superose 12 column, (GE Healthcare) equilibrated in 150 mM NaP pH 7.0, was performed where necessary.

2.5.6 Measuring haem content in recombinant Isd proteins

Haem saturation was measured by first unfolding the protein in 0.1 M NaOH, or 6 M guanidine hydrochloride, to release the haem. The concentration of haem was then determined from the absorbance at 390 nm using the reported extinction coefficients for haem (Table 2.1). The contribution of haem to the absorbance at 280 nm was back

calculated from its concentration and subtracted from the observed A_{280} value. The resulting A_{280} was used to determine the protein concentration using the theoretical extinction coefficient calculated from the primary protein sequence (appendix A). This method of determining the protein concentration was validated with refractive index measurements made during SEC.

Table 2.1. Extinction coefficients of haem at 280 and 390 nm

Wavelength (nm)	ε ($M^{-1}\cdot cm^{-1}$)	
	6M guanidine HCl	NaOH
390	47700	58400
280	17530	18080

2.5.7 Production of Apo-Isd proteins by acid acetone haem extraction

Haem was removed from IsdA, IsdB, IsdC and IsdH constructs by acid acetone haem extraction method of Ascoli *et al.,*[215]. The haem bound proteins were desalted via buffer exchange over a 10 mL G-25 Sepharose column ($IsdH^{N2N3}$ and $IsdB^{N1N2}$) or dialysis ($IsdH^{N1N2N3}$ and IsdC) into MQW or 10 mM Tris, pH 8.0. Proteins were concentrated to ~1 mM haem and added drop-wise to 10 mL acetone containing 25 μL of 2 M HCl that had been precooled to –20 °C. The reaction was carried out on ice with constant stirring. The precipitated protein was recovered by centrifugation at 6000 rpm for 20 min at –10 °C. The supernatant containing the extracted haem was discarded and the protein pellet dissolved in 2 mL of MWQ. The apo protein was dialysed or buffer exchanged into 150 mM NaP, pH 7.0.

2.6 Purification of human Hb from blood

Human haemoglobin was prepared from blood as described previously[216]. Briefly, red blood cells from freshly collected blood were washed in saline solution and then lysed under hypotonic conditions. Hb was purified from the haemolysate via cation exchange chromatography over an SP-sepharose column, followed by anion exchange chromatography over Q-sepharose resin (Fig. 2.1 A). Oxygenated Hb can undergo autooxidation, a reaction producing superoxide (O_2^-) and Fe(III) haem[217]. The oxidised iron can participate in further reduction-oxidation reactions, producing a range of reactive oxygen species that can damage the polypeptide chains[39]. During Hb purification the globin was maintained in the carbon monoxide (CO)-liganded state to inhibit autooxidation and limit protein degradation[218]. HbCO was formed by bubbling CO through the red blood cells before lysis. This procedure avoids the excessive frothing that

would occur if gas was bubbled through the highly concentrated protein solution obtained after cell lysis. CO and O_2 exchange rapidly across the red blood cell membrane and the ~220-fold higher affinity of Hb for CO compared to O_2[219] results in essentially complete conversion to HbCO. At all subsequent protein purification steps Hb solutions were re-charged with CO. The concentration of purified HbCO was determined by UV-visible absorption spectroscopy using the published absorption coefficients of 192000 and 13900 $M^{-1} \cdot cm^{-1}$ at 419 and 539 nm (Fig. 2.1 B, Table 2.2)[220].

When red blood cells become lysed in the body, the iron centre of Hb that is released is rapidly oxidised to Fe(III), and so it is likely that the Hb receptors will predominantly encounter oxidised Hb. Both IsdH and IsdB can capture haem from Fe(III)-Hb[149,167]. In addition, IsdH has much higher affinity for Fe(III)-haem (values between 2 μM and 40 nM have been obtained)[167,176,221] than Fe(II) haem (which does not show specific binding to IsdH), indicating that haem capture is likely to be more effective from oxidised Hb. To prepare Fe(III)-Hb, HbCO was first converted to HbO_2 by photolysis of the CO ligand. This involved passing a stream of pure oxygen over the HbCO solution, which was held on ice and illuminated with a focussed beam from a LED lamp (11,000 lux at 1 m). HbO_2 was reacted with a five-fold molar excess of potassium ferricyanide at ~10 °C and monitored using UV-visible spectrophotometry at 5 min intervals. When the spectrum resembled that of Fe(III)-Hb, the oxidant was removed by buffer exchange over G-25 sepharose (GE Healthcare Life Sciences). The spectrum of Fe(III)-Hb is shown in Figure 2.1 B.

Table 2.2. Visible absorption properties of human Hb in different ligation and oxidation states

Hb ligation state	Wavelength (nm)	ε_{280nm} ($M^{-1} \cdot cm^{-1}$) *
HbCO	419	192000
	539	13900
	569	13900
HbO_2	515	129000
	576	14900
Fe(III)-Hb	405	169000
	500	9000

*Values are from Eaton and Hofrichter[220]

Figure 2.1

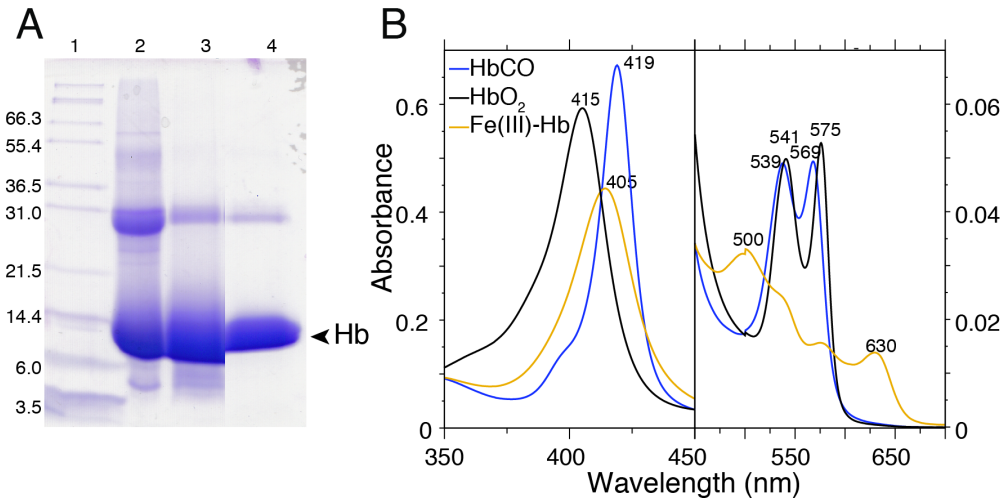

Figure 2.1. Purification of Hb from blood. (A) Purification of Hb from haemolysate by ion-exchange chromatography: *lane 1*, Mark 12 protein standards (Invitrogen); *lane 2*, haemolysate; *lane 3*, Hb eluted from SP-sepharose resin; *lane 4*, Hb eluted from Q-sepharose resin. **(B)** The UV-visible absorption spectra of HbCO (blue), HbO2 (black) and Fe(III)-Hb (yellow) have distinct absorption maxima.

2.7 Haem transfer assays

Haem transfer was monitored by UV-visible spectroscopy. Hb at 1.5 μM tetramer concentration, equivalent to 6 μM haem, was mixed with apo-Isd proteins at the ratios indicated in Results. Reactions were performed in 150 mM NaP, pH 7.0 at 4 °C. Absorbance spectra (350–700 nm) were recorded at 40-second intervals on a JASCO UV-630 spectrophotometer equipped with a temperature controlled sample chamber. To determine the percentage of haem transferred from Hb to the Isd protein at each time point, the acquired UV-visible spectrum was fit to a linear combination of Fe(III)-Hb and fully haem-loaded holo-IsdH^{N2N3} spectra .

2.8 Size exclusion chromatography

Size exclusion chromatography (SEC) experiments were performed on a Superose 12 or Superose 6 columns (GE Healthcare Life Sciences) equilibrated in 150 mM NaP pH 7.0. Proteins were mixed at the concentrations indicated in the results chapters and 100 μL samples loaded onto the column. Elution of protein samples was monitored at 280 nm with a Jasco UV2070 detector.

2.9 Static light scattering

The molecular weight of proteins eluting from a gel filtration column was determined from in-line measurements of static (Rayleigh) light scattering based on the relationship

$$R(\theta) = K \cdot c \cdot M_{\mathrm{W}}$$

where $K = K_f \cdot n_0^2 \cdot \left(dn/dc\right)^2$ and $K_f = \dfrac{4\pi^2}{\lambda^4 \cdot N_A}$

In the above expressions: $R(\theta)$ is the excess Rayleigh ratio, which is the *excess* scattering intensity of the sample over that of the pure solvent, divided by incident light intensity; c is the solute concentration (g·mL^{-1}); n_0 is the refractive index (dimensionless) of the solvent; dn/dc is the specific refractive index increment with respect to sample concentration (g·mL^{-1}); N_{A} is Avogadro's number; λ is the wavelength of incident light (nm). This method yields the weight-average molecular weight (M_{W}) of protein species in the solution, which is defined

$$M_W = \frac{\sum_i c_i M_i}{\sum_i c_i}$$

where c_i is the weight concentration of each species with molecular weight M_i.

Right-angle light scattering (RALS) intensity and refractive index (RI) were measured on a Viscotek 305 Triple Detector Array (TDA) instrument (Malvern). The detectors in this instrument are housed in an insulated oven, which was set to maintain a temperature of 30 °C. Gel filtration columns were placed outside of the detector/column oven, which led to some baseline drift if there were large changes in laboratory temperature. Runs with excessive baseline drift were discarded. The light scattering cell had a volume of 18 μL and was illuminated by a Laser diode (670 nm). Light scattered at an angle of 90° was measured by a photodiode detector. The refractive index detector was a dual cell design in which one compartment is filled solvent from the equilibrated column and sealed, and the other compartment receives solvent/solute mixtures eluting from the column during the experiment. At the interface between the two compartments a light beam is deflected due to differences in refractive index of the solution and solvent. Calibration of the detectors and calculation of sample M_W was performed using the OMNISEC software (Malvern). The detectors were calibrated (by D. Gell) using the following standards and data: BSA (Sigma A1900), ε_{279} = 0.667 mL·g^{-1}·cm^{-1}, M_W = 66,300 Da, dn/dc (670 nm) = 0.185 mL·g^{-1}; α Hb stabilizing protein (AHSP, residues recombinant), ε_{280} = 11,460 M^{-1}·cm^{-1}, M_W = 10810 Da; hen egg lysozyme (Hampton Research HR7110), $\varepsilon_{281.5}$ = 2.64 mL·g^{-1}·cm^{-1}, M_W = 14,600 Da; and polyethylene oxide (PEO) Viscotek TDA calibration standard, 20.17 mg vial (Malvern), M_W = 22,252, dn/dc (670 nm) = 0.132. The dn/dc values of AHSP and lysozyme were not obtained from physical data and were assumed to be 0.185 mL·g^{-1}.

To calibrate the RI detector, a known mass (m, units g) of standard was injected. The total RI signal – (RI) – was obtained by summing the detector voltage across the whole peak volume using OMNISEC. A calibration constant for the RI detector (K_{RI}), which is an instrument constant that incorporates geometric properties of the cell and detector response, was obtained from a plot of m against (RI) for multiple samples according to

$$(RI) = K_{RI} \cdot \frac{m \cdot (dn/dc)}{n_0}$$

A straight line fit with a coefficient of determination, $r^2 = 0.998$, gave $K_{RI} = 9.648 \times 10^6$.

The calibration constant for the RALS detector (K_{LS}) was obtained by plotting $M_W \cdot (RI)$ against (LS) – the total RALS signal summed over the peak – according to the formula

$$M_W = \frac{(LS)}{(RI)} \cdot \frac{K_{RI} \cdot K_{LS}}{n_0^3 \cdot K_f \cdot (dn/dc)}$$

A straight-line fit with a coefficient of determination, $r^2 = 0.997$, gave $K_{LS} = 4.415 \times 10^{-8}$. The above procedure assumes that samples of carefully prepared concentration elute from the chromatography column with zero loss of material. It was noted that some material binds to new in-line filters, so it was necessary to inject multiple standards or samples after replacing any components of the system, or after in-place cleaning, prior to commencing measurements or calibration runs. To calculate sample M_W across a peak, OMNISEC software accounts for dilution (peak spreading) between the RI and RALS detectors using additional parameters that were obtained from BSA standard runs. The value of dn/dc (670 nm) was assumed to be 0.185 $mL \cdot g^{-1}$ for all experimental protein samples. Although calibration was performed only once, BSA was used periodically to monitor system performance. The value of M_W for BSA obtained from repeated measurements over the course of these analyses was 67.3 ± 1.7 kDa (n = 14).

2.10 Small angle X-ray scattering

Samples of $IsdH^{N2N3}$(Y642A) were buffer exchanged by gel filtration into 20 mM NaP, pH 7.5, 500 mM NaCl and matched buffer controls were collected from the same column flow through. SAXS data were collected at the University of Sydney on an Anton Paar SAXSess instrument with line collimation (10-mm slit and integration width) and CCD detector; details of the experimental setup can be found in[222]. Data were collected from the buffer control, followed by the protein sample, which were sequentially loaded into the same quartz capillary (1 mm diameter). Images were collected at 10 °C over four, 15 minute intervals, allowing for radiation damages to be assessed. SAXSquant2D (Anton-Paar, Austria) was used to average the 2D images and generate I(q) versus q (q

$= (4 \cdot \pi \cdot \sin\theta)/\lambda$, where 2θ is the scattering angle and $\lambda = 1.54$ Å) profiles. Solvent subtraction was performed using SAXSquant1D (Anton Parr). *I(0)*'s and *P(r)* curves were calculated using GIFT (Anton Paar, Austria) and PRIMUS[223] and experimental molecular weights were calculated from the calibrated *I(0)*'s[224]. *Ab initio* shape reconstruction was carried out as described in Chapter 3.

$IsdB^{(Y440A)}$ samples formed aggregates which could be removed by gel filtration. To remove interference from aggregates, IsdB was subjected to SEC-SAXS at the Australian Synchrotron SAXS-WAXS beamline and data reduction was performed using SCATTERBRAIN (Australian Synchrotron). The experiment was performed at 27 °C and data were placed on an absolute scale by normalizing to the scattering of water. Twenty images of two-second exposures recorded across the main elution peak were averaged. The buffer control that was subtracted from the peak consisted of the average of 50 curves from a region of the SEC run with no scattering signal. The resulting scattering curve was processed with PRIMUS[223]. A camera distance of 1 m was used with an X-ray energy of 11 KeV giving a Q range from 0.01 to 0.5 $Å^{-1}$. Data were collected on a Pilatus 1M detector (Dektris).

Ensemble Optimization Method (EOM)[225] was performed using the EOM web interface of ATSAS online. The structured domains used to generate a pool of 10000 conformers were taken from PDB files 4FC3, 2LHR, 2E7D and 3RTL.

2.11 X-ray crystallography

Isd proteins were mixed with Fe(III)-Hb at a 2:1 ratio, buffer exchanged into 20 mM HEPES pH 7.5 and concentrated so that the starting samples contained 5 $mg \cdot ml^{-1}$ Hb. Crystallisation was performed by hanging drop vapour diffusion. Initial crystallisation screens were performed in 24-well plates and included conditions in the NeXtal Classic, JCSG+ and Pact suites (Qiagen, Doncaster, VIC). Details of crystallisation conditions, data collection, molecular replacement and refinement are presented in Chapters 3 and 6. A comprehensive overview of the theory behind protein crystallography can be found in Bernhard Rupp's 'Biomolecular Crystallography'[226].

Chapter 3. The three domains of IsdH^{N2N3} and IsdB are assembled into a higher-order structure that positions the globin haem pocket to achieve haem transfer from both α and β Hb chains.

3.1 Introduction

The two Hb receptors of *S. aureus*, IsdB and IsdH, share a region of approximately 360 amino acids with ~62% sequence identity (Fig. 3.1, indicated by red dashed line) and close to 80% sequence similarity. These regions of IsdB and IsdH, referred to hereafter as IsdB^{N1N2} and IsdH^{N2N3}, each contain one NEAT domain that binds only to Hb[145-147], a helical linker domain[167], and one NEAT domain that binds only to haem[147,155,160,227]. IsdB^{N1N2} captures haem from Hb, at ~2000× and 80× the rate of passive haem dissociation from the α and β chains of the Fe(III)-Hb dimer, respectively[149,169]. Studies by Spirig *et al.,* suggest that IsdH^{N2N3} removes haem from Fe(III)-Hb at similar rates to IsdB^{N1N2} [167]. These rapid rates of haem transfer imply that haem is actively released from Hb via specific interactions with the receptor that destabilise the globin fold. All three domains of IsdH^{N2N3} are necessary for haem uptake from Hb, as the isolated domains, or protein constructs containing an unstructured linker in place of the helical linker domain, do not capture haem from Hb[167]. IsdH contains an additional N-terminal NEAT domain, not present in IsdB, which is attached via a 100-residue unstructured linker (Fig. 3.1). This additional domain of IsdH also has Hb binding functionality[146,147], however, a role in haem capture from Hb has not been established.

Figure 3.1. Domain architecture of IsdH and IsdB. Schematic of the Isd protein domain architectures shows NEAT domains with Hb binding (white boxes) or haem binding (black boxes) activity. The sequence identity between domains is indicated by black dashed lines, and between the homologous three domain region by red dashed lines. Known structures of the isolated N-terminal Hb binding NEAT domains (PDB 4F3C and 3SZK)[146,147,175], the helical Linker (PDB 2LHR)[167] and the C-terminal haem binding NEAT domain (PDB 2Z6F)[160] of IsdH are shown. IsdH and IsdB, share a region of extended homology indicated by the red dashed line. $IsdH^{N1}$, the first NEAT domain of IsdH relative to the N-terminus of the protein; $IsdH^{N2}$, the second NEAT domain of IsdH; $IsdH^{N3}$, the third NEAT domain of IsdH; $IsdB^{N1}$, the first NEAT domain of IsdB relative to the N-terminus of the protein; $IsdB^{N2}$, the second NEAT domain of IsdB.

Figure 3.1

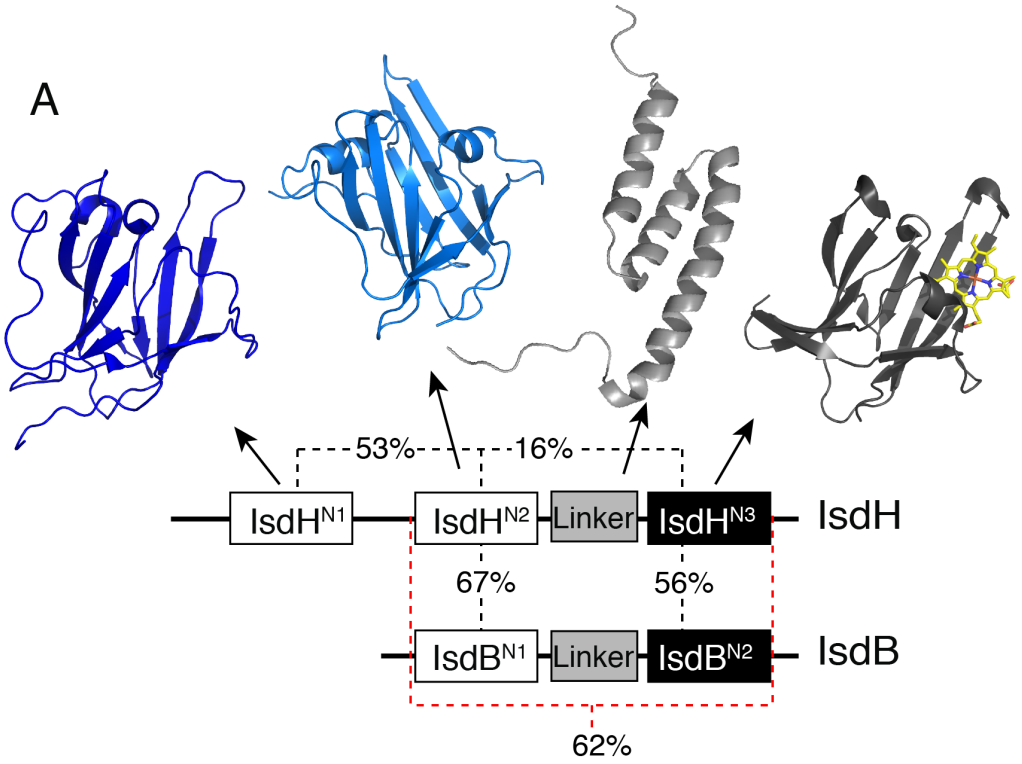
A
53%
16%
IsdH^N1
IsdH^N2
Linker
IsdH^N3
IsdH
67%
56%
IsdB^N1
Linker
IsdB^N2
IsdB
62%

Isolated NEAT domains from IsdB and IsdH have been structurally characterised, revealing how these NEAT domains bind to their ligands. The first ($IsdH^{N1}$)[146] and second ($IsdH^{N2}$)[175] NEAT domains of IsdH have been co-crystallized with Hb. In these structures $IsdH^{N1}$ and $IsdH^{N2}$ bind to a surface of α Hb comprising the A and E helices, that is distant from the haem pocket, and the globin retains its native fold (Fig. 3.2 A, B). The α Hb recognition face of $IsdH^{N1}$ (and $IsdH^{N2}$) consists of a short aromatic helix and three loops. Similar contacts are made with α Hb by both NEAT domains.

Several structures of $IsdH^{N3}$ and a single structure of $IsdB^{N2}$ have been reported that provide a detailed understanding of how these domains bind to the haem cofactor[155,160,176]. Both domains sandwich the haem ligand in a hydrophobic groove that exists between the β-hairpin formed by strands β7 and β8, and a short α helix (α1) (Fig. 3.2 C, D). This haem binding face corresponds to the same surface of $IsdH^{N1}$ and $IsdH^{N2}$ that is used to contact Hb. Haem-iron is penta-coordinate, being bound to the protein through a conserved tyrosine side chain (Tyr642 in IsdH and Try440 in IsdB). Neither $IsdH^{N3}$ nor $IsdB^{N2}$ form a stable interaction with Hb, and although they can bind haem from solution they cannot remove haem from Hb (Section 3.2.4)[167,174].

The aim of this chapter was to investigate the functional and structural properties of the intact Hb receptors to answer the question: how do the structured domains of $IsdB^{N1N2}$ and $IsdH^{N2N3}$ work together to free haem from Hb?

Figure 3.2. Crystal structures of the isolated NEAT domains of IsdH and IsdB bound to Hb or haem. (A, B) Structures of the Hb-binding NEAT domains, $IsdH^{N1}$ (PDB 3SZK) (A) and $IsdH^{N2}$ (PDB 4FC3) (B), bound through the α chain of Hb (red). **(C, D)** Structures of the haem binding NEAT domains: $IsdH^{N3}$ (PDB 2Z6F) (C) and $IsdB^{N2}$ (PDB 3RTL) (D). Residues that line the haem pocket are shown as sticks. The haem group is coloured yellow and residues that directly coordinate the haem iron are coloured blue. Residues involved in hydrophobic interactions with the porphyrin ring are coloured green.

Figure 3.2

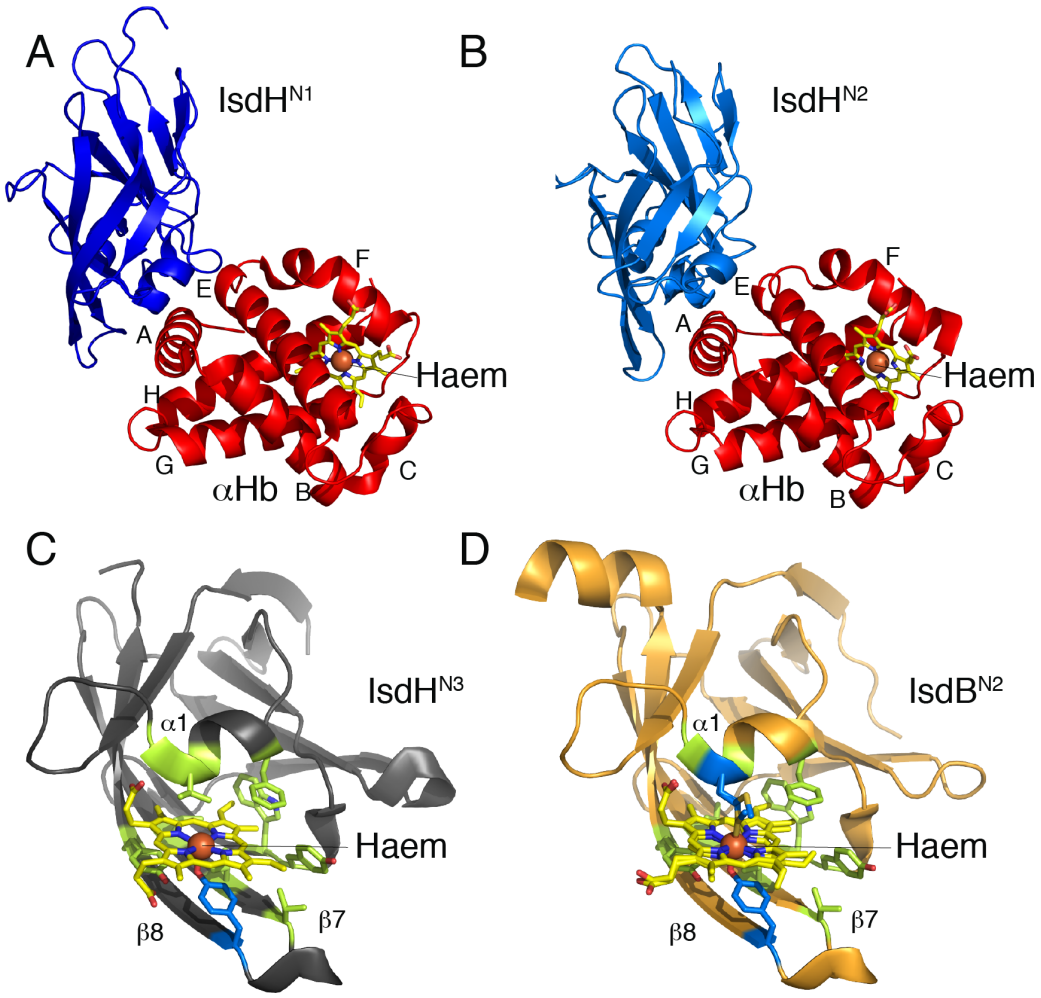
A
IsdH^{N1}
F
E
A
H
G
αHb
B
C
Haem
B
IsdH^{N2}
F
E
A
H
G
αHb
B
C
Haem
C
IsdH^{N3}
α1
Haem
β8
β7
D
IsdB^{N2}
α1
Haem
β8
β7

3.2 IsdB^{N1N2} and IsdH^{N2N3} capture haem from α and β Hb chains through a direct interaction

3.2.1 Preparation of Isd proteins

To obtain constructs of IsdH and IsdB for functional studies, a region of the *isdH* gene containing the three NEAT domains (to express IsdH^{N1N2N3}) and the full-length *isdB* gene lacking the N-terminal secretion signal and C-terminal sortase anchor sequences (protein expressed from this construct is referred to simply as IsdB hereafter), were cloned from the *S. aureus* strain TCH1516 genomic DNA into pET15b (Novagen). Gene fragments corresponding to IsdB^{N1N2} and IsdH^{N2N3}, and the isolated NEAT domains thereof, were then sub-cloned into pET15b (see Section 2.3 and table A1). Proteins were expressed from pET15b with an N-terminal histidine-tag MGSSHHHHHHSSGLVPRGSHMLE, which allows for binding to Ni-agarose resin. Optimised expression conditions can be found in Section 2.5.1. The Isd proteins were purified from bacterial lysates using Ni-affinity chromatography and analysed by SDS-PAGE (Fig. 3.3 A, B, C and 3.4 A, B, C, D). Each of the recombinant proteins migrated as a single band of the expected molecular weight (arrowhead) except for IsdH^{N3}, which migrated as three bands (Fig. 3.3 C). The abundance and relative ratio of the three bands did not change with expression time or protease inhibitor type and concentration. Elution fractions from the metal affinity step were subjected to RP-HPLC, however only a single polypeptide peak was detected. Mass spectrometry revealed that the major species corresponded to the expected protein construct lacking the N-terminal methionine, however two minor species were present with mass differences that corresponded to an alpha-N-6-gluconolyl modification (178 Da) and an alpha-N-6-phosphogluconolyl modification (258 Da) of the N-terminal histidine tag. Phosphogluconolylation of histidine tagged proteins expressed in *E. coli* is common and, as the modification occurs on the affinity tag rather than the protein, it is not expected to effect protein function[228]. His-tagged Isd proteins bind to Hb and haem, and transfer haem, with similar efficiency to the native untagged proteins and so the N-terminal affinity tag was left un-cleaved following Ni affinity chromatography[146,147,149,165]. The Isd proteins were subjected to a final purification step involving ion-exchange chromatography, or gel filtration and were ~90–95% pure (See Sections 2.5.4 and 2.5.5; Fig. 3.3 D, E and Fig. 3.4 E, F, G).

Figure 3.3. SDS-PAGE analysis of expression and purification of IsdH constructs.
(A) Purification of $IsdH^{N2N3}$ by Ni-affinity chromatography: *lane 1*, Mark 12 protein standards (Invitrogen); *lane 2*, bacterial lysate; *lane 3*, flow through; *lane 4*, 20 mM imidazole wash; *lanes 5–8*, 100 mM imidazole elution fractions. **(B)** Purification of $IsdH^{N2}$ by Ni-affinity chromatography: *lane 1*, Mark 12 protein standards; *lane 2*, bacterial lysate; *lane 3*, flow through; *lanes 4–5*, 5 mM imidazole wash; *lanes 6–10*, 150 mM imidazole elution fractions. **(C)** Purification of $IsdH^{N3}$ by Ni-affinity chromatography: *lane 1*, Mark 12 protein standards; *lane 2*, bacterial lysate; *lane 3*, flow through; *lane 4*, 10 mM imidazole wash; *lane 5*, 25 mM imidazole wash; *lane 6*, 50 mM imidazole wash; *lanes 7–8,* 100 mM imidazole elution fractions, *lanes 9–10*, 175 mM imidazole elution fractions. **(D)** Purification of $IsdH^{N2N3}$ by anion exchange chromatography: *lane 1*, Mark 12 protein standards; *lane 2*, load condition; *lanes 3–6*, eluted fractions over a 100–250 mM NaCl gradient. **(E)** Purification of $IsdH^{N2}$ by cation exchange chromatography: *lane 1*, Mark 12 protein standards; *lane 2*, load condition; *lanes 3–6*, flow through; *lanes 7–11*, wash fractions; *lane 12*, pooled fractions eluted in 500 mM NaCl. Arrows indicate the positions of over-expressed recombinant proteins. Stars indicate fractions collected from the final purification step.

Figure 3.3

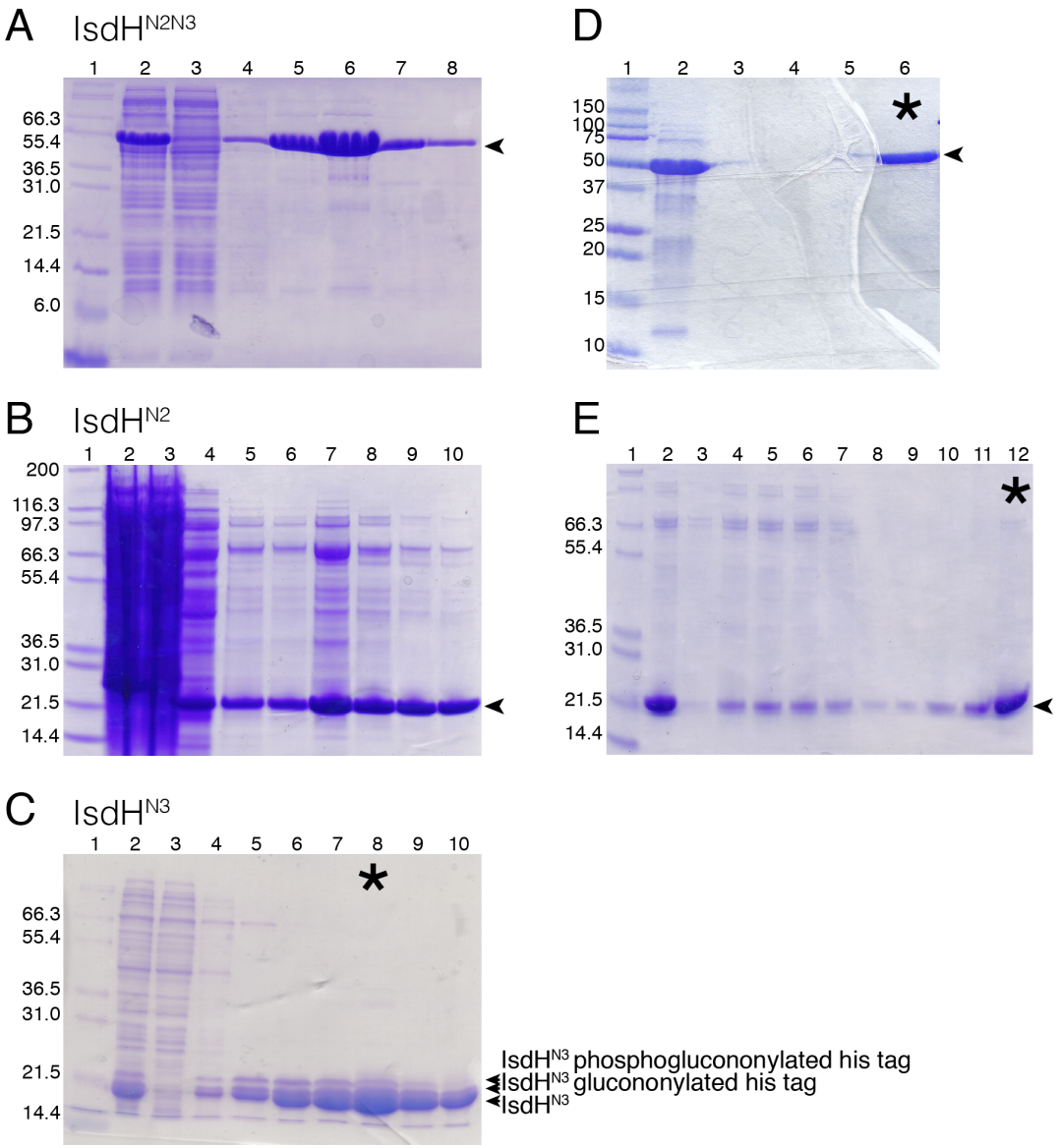
A
IsdH^N2N3
1 2 3 4 5 6 7 8
66.3
55.4
36.5
31.0
21.5
14.4
6.0
D
1 2 3 4 5 6
150
100
75
50
37
25
20
15
10
*
B
IsdH^N2
1 2 3 4 5 6 7 8 9 10
200
116.3
97.3
66.3
55.4
36.5
31.0
21.5
14.4
E
1 2 3 4 5 6 7 8 9 10 11 12
66.3
55.4
36.5
31.0
21.5
14.4
*
C
IsdH^N3
1 2 3 4 5 6 7 8 9 10
66.3
55.4
36.5
31.0
21.5
14.4
*
IsdH^N3 phosphogluconolylated his tag
IsdH^N3 gluconolylated his tag
IsdH^N3

Figure 3.4. SDS-PAGE analysis of expression and purification of IsdB constructs. Purification of **(A)** IsdB, and **(B)** $IsdB^{N1N2}$ by Ni-affinity chromatography: *lane 1*, Mark 12 protein standards; *lane 2*, bacterial lysate; *lane 3*, flow through; *lane 4*, 20 mM imidazole wash; *lanes 5–7*, 250 mM imidazole elution fractions. **(C)** Purification of $IsdB^{N1}$ by Ni-affinity chromatography: *lane 1*, Mark 12 protein standards; *lane 2*, bacterial lysate; *lane 3*, flow through; *lane 4*, 10 mM imidazole wash; *lanes 5–7*, fractions eluted in 150 mM imidazole. **(D)** Purification of $IsdB^{N2}$ by Ni-affinity chromatography: *lane 1*, Mark 12 protein standards; *lane 2*, bacterial lysate; *lane 3*, flow through; *lane 4*, 25 mM imidazole wash; *lanes 5–8*, fractions of apo-$IsdB^{N2}$ eluted in 100 mM imidazole; *lanes 9–10*, fractions of holo-$IsdB^{N2}$ eluted in 250 mM imidazole. **(E)** Purification of IsdB by cation exchange chromatography: *lane 1*, Mark 12 protein standards; *lane 2*, load condition; *lane 3*, flow through; *lane 4*, 50 mM NaCl wash; *lane 5*, 100 mM NaCl wash; *lane 6–9*, fractions eluted in 200 mM NaCl. **(F)** Purification of $IsdB^{N1N2}$ by cation exchange chromatography: *lane 1*, Mark 12 protein standards; *lane 2*, load condition; *lane 3*, proteins present in precipitate; *lane 4*, flow through; *lane 5*, 100 mM NaCl wash; *lane 6*, 150 mM NaCl wash; *lanes 7–10*, fractions eluted in 250 mM NaCl. **(G)** Purification of $IsdB^{N1}$ by SEC: *lane 1*, Mark 12 protein standards; *lane 2*, load; *lanes 3–6*, fractions collected from SEC. Arrows indicate the positions of over-expressed recombinant proteins. Stars indicate fractions collected from the final purification step.

Figure 3.4

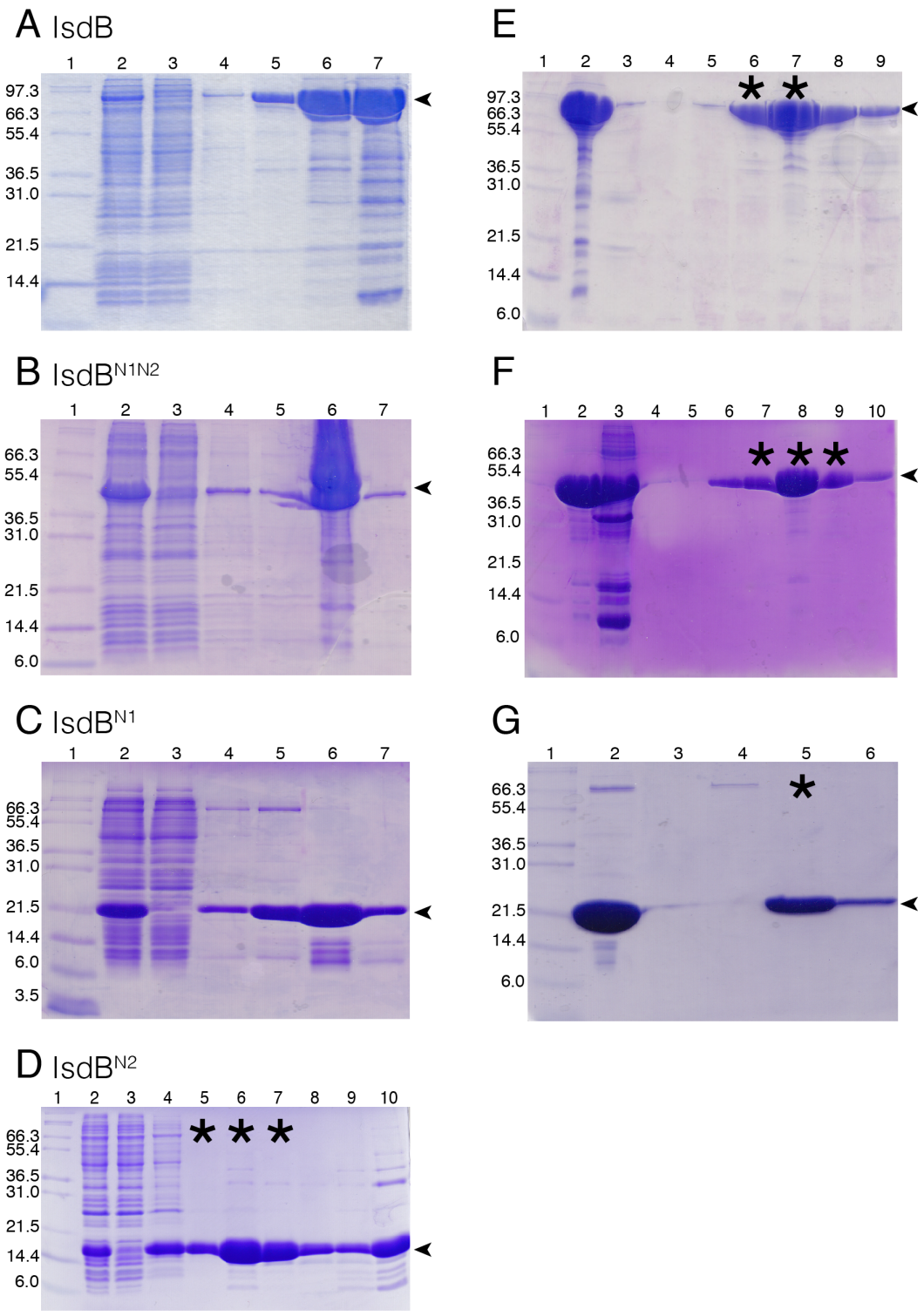
A IsdB
1 2 3 4 5 6 7
97.3
66.3
55.4
36.5
31.0
21.5
14.4
B IsdB^N1N2
1 2 3 4 5 6 7
66.3
55.4
36.5
31.0
21.5
14.4
6.0
C IsdB^N1
1 2 3 4 5 6 7
66.3
55.4
36.5
31.0
21.5
14.4
6.0
3.5
D IsdB^N2
1 2 3 4 5 6 7 8 9 10
66.3
55.4
36.5
31.0
21.5
14.4
6.0
E
1 2 3 4 5 6 7 8 9
97.3
66.3
55.4
36.5
31.0
21.5
14.4
6.0
F
1 2 3 4 5 6 7 8 9 10
66.3
55.4
36.5
31.0
21.5
14.4
6.0
G
1 2 3 4 5 6
66.3
55.4
36.5
31.0
21.5
14.4
6.0

Proteins that bind to haem absorb visible light in the region between 350 and 750 nm and display a major peak, known as the Soret band, at ~400 nm, which arises from a $\pi \rightarrow \pi^*$ transition of the porphyrin ring[220]. IsdB and IsdH constructs that contained the haem binding NEAT domains bound to endogenous haem during expression in *E. coli* cells and the purified proteins displayed a peak in their UV-visible absorption spectra at ~ 400 nm, as reported previously[156,229]. To estimate the level of haem contamination the purified proteins were unfolded in 0.1 M NaOH and the concentration of haem and protein determined according to the extinction coefficients of free haem and protein at 390 and 280 nm, respectively (See Section 2.5.6, Appendix A). When haem was added to the bacterial expression culture at a concentration of 5–10 $\mu g \cdot ml^{-1}$ $IsdH^{N2N3}$ and $IsdB^{N1N2}$ obtained were 80–100% haem saturated (UV-visible absorption spectra of the holo-proteins are shown in Figure 3.5).

Apo-proteins were prepared either by chromatographic separation of apo- and holo-protein fractions, or by haem extraction in acidified acetone. Apo-$IsdB^{N2}$ was separated from the haem bound protein during Ni-affinity chromatography, as reported by Gaudin *et. al.,* 2011 and Bowden *et. al.,* 2014[155,230]. Both apo-$IsdB^{N2}$ and holo-$IsdB^{N2}$ bound to the Ni affinity resin. Apo-$IsdB^{N2}$ eluted at low imidazole concentrations (100 mM) while the haem bound protein was collected in fractions containing 250 mM imidazole. Native histidine, tryptophan and cysteine residues can promote binding to Ni-affinity resin. $IsdB^{N2}$ has three native histidine residues. The topology of the environment around a histidine residue affects its accessibility and pKa and hence ability to bind to Ni-resin[231]. The three histidine residues of $IsdB^{N2}$ may contribute differently to the binding affinity for Ni resin in the apo and holo forms of the protein, allowing for separation of the two species during the chromatography. Similarly, apo-$IsdH^{N3}$ could be separated from the haem bound protein by passage over Q-sepharose anion-exchange resin in a salt gradient of 0–1 M NaCl. Apo-$IsdH^{N3}$ was eluted under low salt conditions, while the haem-containing fraction (a mixture of partially-liganded $IsdH^{N3}$ species) was recovered at higher salt concentrations. Apo-$IsdB^{N1N2}$ and apo-$IsdH^{N2N3}$ were prepared by extraction of the haem in acidified acetone (see Section 2.5.7). The acidic conditions caused unfolding of the protein and released the haem group to the organic solvent. The polypeptide chain was precipitated, recovered by centrifugation and dissolved in water. As a final step, remaining acetone was removed by extensive dialysis or gel filtration.

The percentage of contaminating haem remaining in each apo-prep was consistently less than 8 % (the apo proteins show negligible absorption from 350–750 nm; Fig. 3.5 A, B).

To determine if the apo proteins retained function after solvent extraction of the haem group, their ability to re-bind to haem was assessed. The UV-visible absorption spectrum of a haem coordinating protein is extremely sensitive to chemical environment around the haem cofactor[232], making it possible to distinguish between the spectrum of haem bound specifically to a haem coordination site and haem that is free in solution or bound non-specifically to the protein. Haem was titrated into unliganded $IsdB^{N1N2}$, $IsdB^{N2}$, $IsdH^{N2N3}$ and $IsdH^{N3}$. The spectrum was measured 2 minutes after each addition of haem and the absorbance at 400 nm (IsdH) or 404 nm (IsdB) was plotted against haem concentration (Fig. 3.5 C–F). The spectral change could be fit with two straight-lines, with a break point, suggesting that each addition of haem was quantitatively bound up to a point of haem saturation, where after the absorbance increased according to the molar absorptivity of free haem. The Isd:haem ratio at the break point of the curve (Fig. 3.5 C–F, dashed line) suggested the formation of a complex with 1:1 stoichiometry for all proteins.

Figure 3.5. Haem binding properties of IsdH^{N2N3} and IsdB^{N1N2}. (A) The UV-visible absorption spectra of holo- (black) and apo-IsdH^{N2N3} (grey). **(B)** The UV-visible absorption spectra of holo- (black) and apo-IsdB^{N1N2} (grey). Only Isd proteins bound to haem absorb visible light. **(C–F)** Haem titration experiments demonstrating specific binding to haem by IsdH^{N2N3} (C), IsdH^{N3} (D), IsdB^{N1N2} (E). Data points were fit, by linear regression, in two groups. A perfect 1:1 binding stoichiometry (assuming accurate concentration determination and K_d << working concentration) would see the linear fits intersect at the vertical dashed line.

Figure 3.5

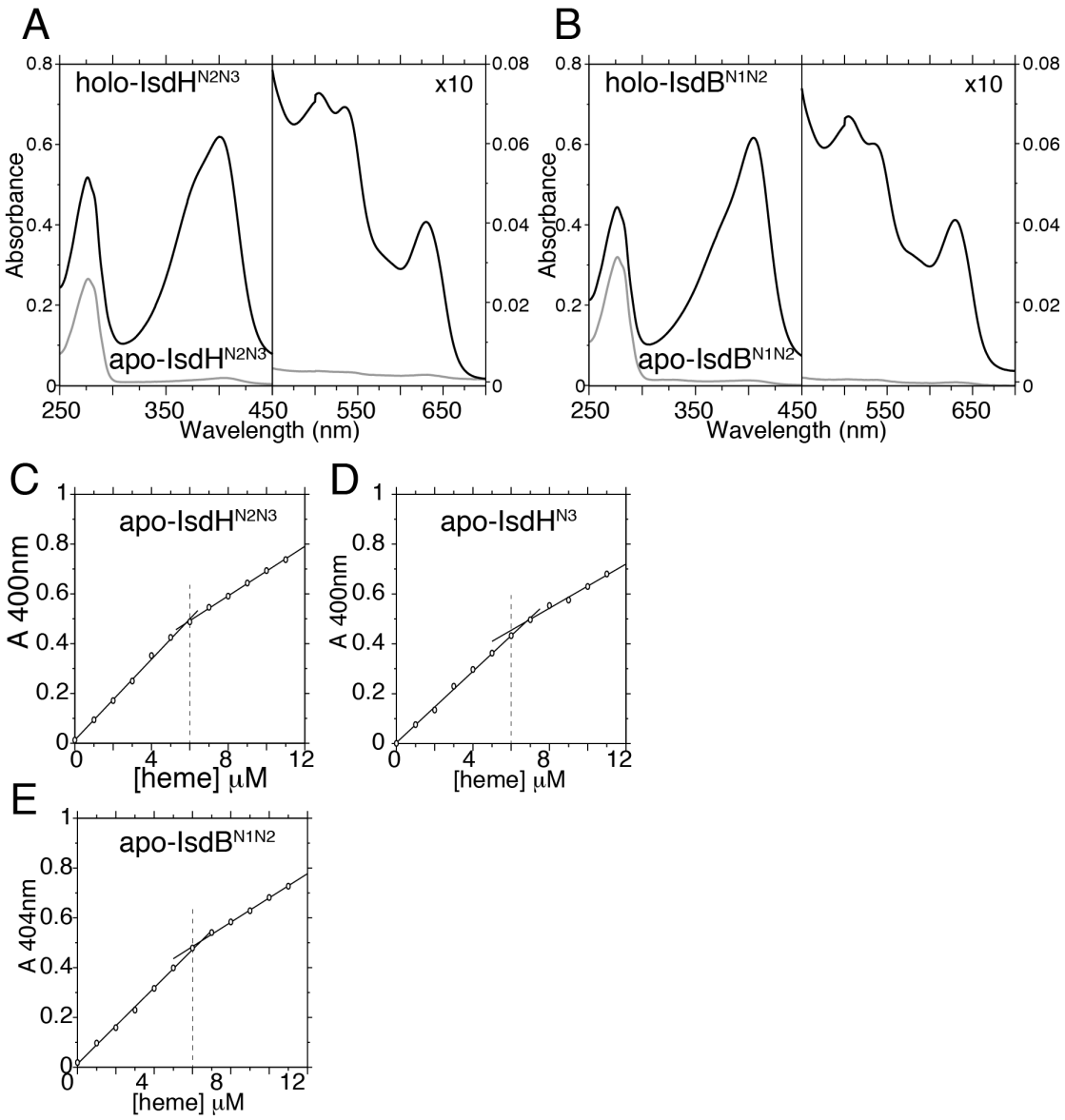
A
holo-IsdH^{N2N3}
x10
apo-IsdH^{N2N3}
Absorbance
Wavelength (nm)
B
holo-IsdB^{N1N2}
x10
apo-IsdB^{N1N2}
Absorbance
Wavelength (nm)
C
apo-IsdH^{N2N3}
A 400nm
[heme] μM
D
apo-IsdH^{N3}
A 400nm
[heme] μM
E
apo-IsdB^{N1N2}
A 404nm
[heme] μM

3.2.3 IsdH^{N2N3} and IsdB^{N1N2} rapidly acquire all four haem groups from human Hb.

Haem-bound IsdB^{N1N2} and IsdH^{N2N3} each have a distinct UV-visible absorption spectrum to Fe(III)-Hb (Fig. 3.6 A and 3.7 A), allowing haem transfer to the Isd proteins to be detected. To show that apo-IsdH^{N2N3} can capture haem from Hb, Fe(III)-Hb was mixed with excess apo-IsdH^{N2N3} and the UV-visible spectrum was recorded after a 10 min incubation. The spectrum resembled that of holo-IsdH^{N2N3} indicating that haem had been transferred from Fe(III)-Hb to IsdH^{N2N3} (Fig. 3.6 A).

A single Hb tetramer contains four haem groups, one bound to each of the α and β subunits. To determine whether IsdH^{N2N3} can interact with the haem sites of both α and β Hb subunits, Fe(III)-Hb was mixed with a 1, 2, 3, 5 or 7-fold molar excess (per Hb tetramer) of apo-IsdH^{N2N3} and the UV-visible absorption spectra acquired at 40 s intervals. Representative spectra for a 5:1 mixing ratio (per globin haem) of IsdH^{N2N3} to Fe(III)-Hb are shown in Figure 3.6 B. The change in absorbance at 406 nm, which represents the largest difference between the spectrum of Fe(III)-Hb and haem bound IsdH^{N2N3}, plotted against time is shown in Figure. 3.6 C. The reaction was essentially complete within ~10 min at all mixing ratios. The absorbance at 406 nm after 10 min was plotted against the apo-IsdH^{N2N3}:Hb mixing ratio (Fig. 3.6 D). The spectral change at 406 nm was linear up to an apo-IsdH^{N2N3}:Hb molar ratio of ~3.5:1, suggesting an interaction with all four globin haem pockets.

To determine whether all four haem groups of Fe(III)-Hb were transferred to IsdH^{N2N3}, the fraction haem bound Hb contributing to the recorded spectrum was determined at different points across the time course. This was done by least squares fitting of the each of the measured spectra to a linear combination of the spectrum of Fe(III)-Hb and holo-IsdH^{N2N3}. The spectra of Fe(III)-Hb, recorded 10 min after mixing with a 1-, 2- or 5-fold excess of apo-IsdH^{N2N3}, are shown in Figure 3.6 E (black); overlaid are the fitted curves generated from the sum of the spectra of Fe(III)-Hb and holo-IsdH^{N2N3} (red). Small residuals (blue) indicate that a combination of the two species provides a reasonable model for the reaction. Upon addition of 1, 2 or 5 molecules of receptor per Hb tetramer, 23%, 49±0.3% or ~ 94±0.6% of haem was removed after 10 min at 4 °C (errors are given as ± S.E. from two experiments). In summary, IsdH^{N2N3} quantitatively captures haem from both chains of human Hb.

Figure 3.6. IsdH^{N2N3} rapidly captures haem from all four globin sites. (A) UV-visible absorption spectra of Fe(III)-Hb (6 μM haem, corresponding to 1.5 μM tetramer), holo-IsdH^{N2N3} (6 μM) and apo-IsdH^{N2N3} (7.5 μM), showing that they are distinct. The spectrum of a mixture of Fe(III)-Hb (1.5 μM) and apo-IsdH^{N2N3} (7.5 μM) is shown after a 10-min incubation at 4 °C (solid black line). **(B)** The figure shows spectra taken at 40-s intervals of a mixture of Fe(III)-Hb (1.5 μM) and apo-IsdH^{N2N3} (7.5 μM) incubated at 4 °C. The spectrum of Fe(III)-Hb (1.5 μM) is overlaid for comparison (red, dashed line). Arrows indicate the direction of spectral change. **(C)** The figure shows absorbance at 406 nm recorded over 35 min for the mixture in B. The spectral change is rapid, and essentially complete after 10 min at 4 °C. **(D)** The plot shows absorbance at 406 nm, recorded after a 10-min incubation of apo-IsdH^{N2N3}:Hb, prepared at different molar mixing ratios. The linear relationship between spectral change and [IsdH$^{N2–N3}$]/[Hb] ratio is consistent with a model in which 3–4 IsdH$^{N2–N3}$ molecules interact with four heme sites per Hb tetramer. **(E)** The figure shows spectra of Fe(III)-Hb (1.5 μM) recorded 10 min after mixing with a 1-, 2- or 5-fold excess of apo-IsdH^{N2N3}. Overlaid are the fitted curves generated from a linear combination of the spectra of Fe(III)-Hb and holo-IsdH^{N2N3} (red). The residuals are shown in blue.

Figure 3.6

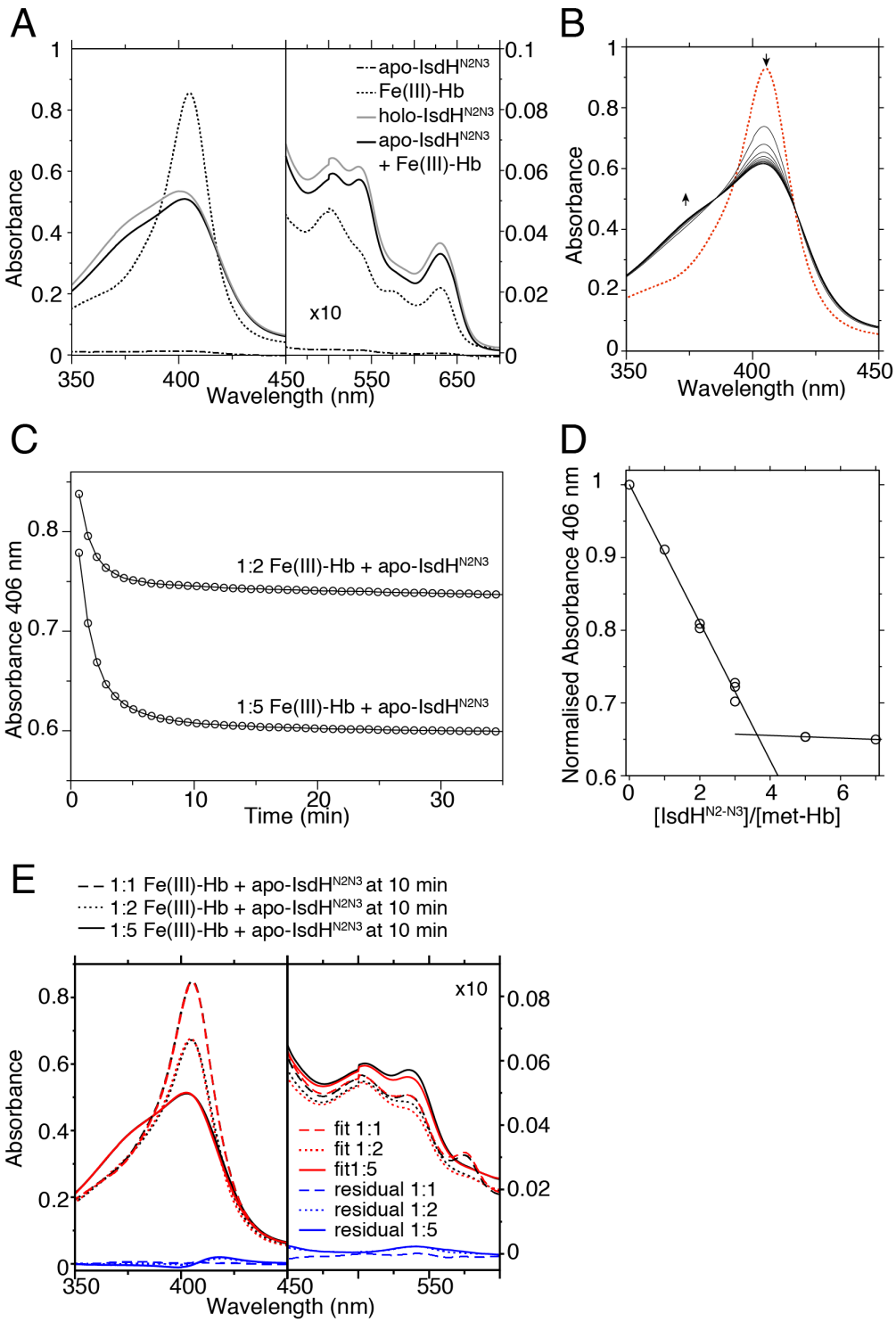
A
apo-IsdH^N2N3
Fe(III)-Hb
holo-IsdH^N2N3
apo-IsdH^N2N3 + Fe(III)-Hb
x10
Absorbance
Wavelength (nm)
B
Absorbance
Wavelength (nm)
C
1:2 Fe(III)-Hb + apo-IsdH^N2N3
1:5 Fe(III)-Hb + apo-IsdH^N2N3
Absorbance 406 nm
Time (min)
D
Normalised Absorbance 406 nm
[IsdH^N2-N3]/[met-Hb]
E
1:1 Fe(III)-Hb + apo-IsdH^N2N3 at 10 min
1:2 Fe(III)-Hb + apo-IsdH^N2N3 at 10 min
1:5 Fe(III)-Hb + apo-IsdH^N2N3 at 10 min
x10
fit 1:1
fit 1:2
fit1:5
residual 1:1
residual 1:2
residual 1:5
Absorbance
Wavelength (nm)

IsdB^{N1N2} was also able to capture haem from Fe(III)-Hb as the spectrum of a mixture of apo-IsdB^{N1N2} and Fe(III)-Hb, taken after a 10 min incubation, resembled that of holo-IsdB^{N1N2} (Fig. 3.7 A). The change in spectra for a 5:1 mixture (per globin haem) of IsdB^{N1N2} and Fe(III)-Hb are shown in Figure 3.7 B. The spectra recorded at 10 min for a 2:1 and 5:1 mixture of apo-IsdB^{N1N2} and Fe(III)-Hb and their fitted curves (comprising a linear combination of the spectrum of Fe(III)-Hb and holo-IsdB^{N1N2}) are shown in Figure 3.7 C. At 2:1 and 5:1 molar ratios of IsdB^{N1N2}:Hb-tetramer 45±0.5% and 89±0.3% of total haem was transferred after ~10 min at 4 °C (errors are given as ± S.E. from three-to-four experiments). Hence IsdB and the homologous region of IsdH both access all four globin haem groups and take up haem from Fe(III)-Hb with similar efficiency.

Figure 3.7. IsdB^{N1N2} captures haem from all four globin sites. (A) UV-visible absorption spectra of Fe(III)-Hb (6 μM haem, corresponding to 1.5 μM tetramer), holo-IsdB^{N1N2} (6 μM) and apo-IsdB^{N1N2} (7.5 μM), showing that they are distinct. The spectrum of a mixture of Fe(III)-Hb (1.5 μM) and apo-IsdB^{N1N2} (7.5 μM) is shown after a 10-min incubation at 4 °C. **(B)** The figure shows spectra taken at 40-s intervals of a mixture of Fe(III)-Hb (1.5 μM) and apo-IsdB^{N1N2} (7.5 μM) incubated at 4 °C. The spectrum of Fe(III)-Hb (1.5 μM) is overlaid for comparison (red, dashed line). Arrows indicate the direction of spectral change. **(C)** The figure shows spectra of Fe(III)-Hb (1.5 μM) recorded 10 min after mixing with a 2- or 5-fold excess of apo-IsdB^{N1N2}. Overlaid are the fitted curves generated from a linear combination of the spectra of Fe(III)-Hb and holo-IsdH^{N2N3} (red). The residuals are shown in blue.

Figure 3.7

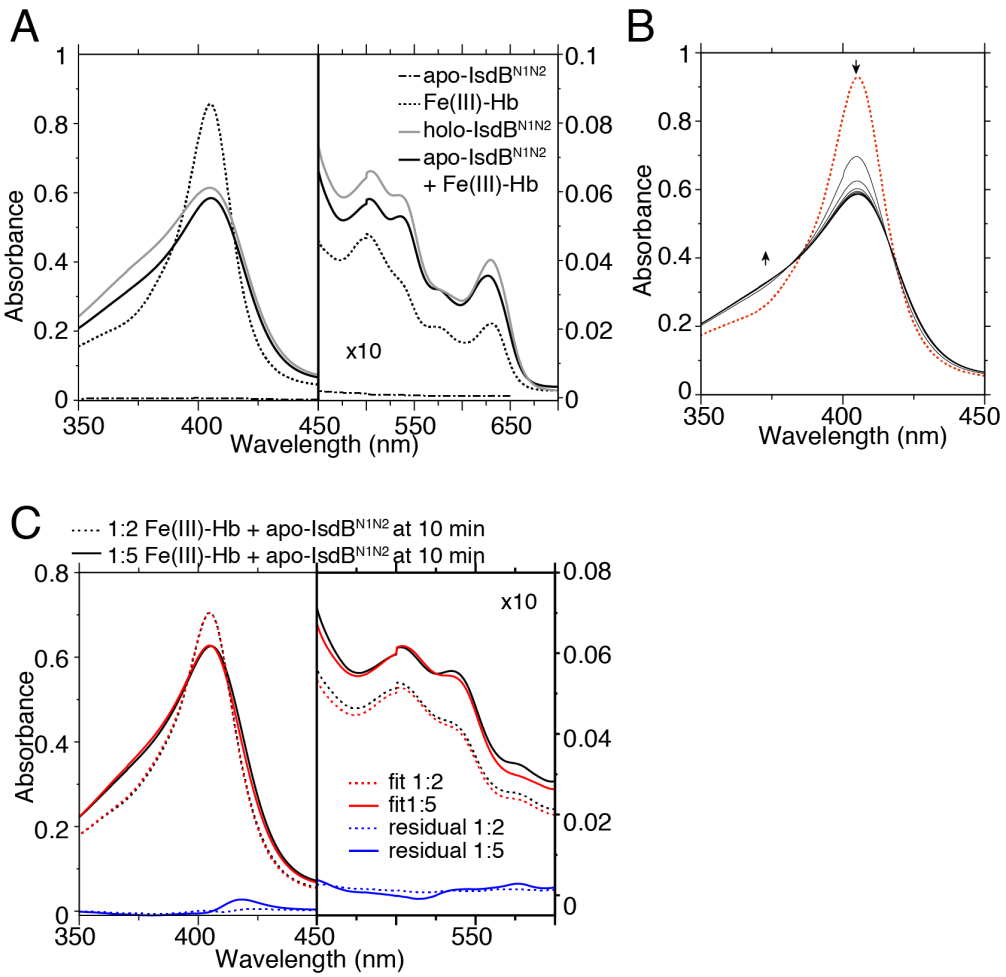
A
apo-IsdB^{N1N2}
Fe(III)-Hb
holo-IsdB^{N1N2}
apo-IsdB^{N1N2} + Fe(III)-Hb
x10
Absorbance
Wavelength (nm)
B
Absorbance
Wavelength (nm)
C
1:2 Fe(III)-Hb + apo-IsdB^{N1N2} at 10 min
1:5 Fe(III)-Hb + apo-IsdB^{N1N2} at 10 min
x10
fit 1:2
fit1:5
residual 1:2
residual 1:5
Absorbance
Wavelength (nm)

3.2.4 $IsdB^{N1N2}$ and $IsdH^{N2N3}$ require the Hb-binding domains, $IsdH^{N2}$ and $IsdB^{N1}$, to capture haem from both α and β Hb chains.

The haem cofactor is necessary for correct folding of Hb chains[146,233] and hence removal of a haem group from one subunit might cause disruption to Hb tertiary and quaternary structure. In turn, quaternary subunit interactions must have an important role in stabilising the globin:haem interaction because monomeric globin chains lose haem ~30-fold more rapidly than Hb tetramers[169,234]. Thus, one possible mechanism through which IsdB/H could accelerate haem loss would be to disrupt Hb quaternary structure. Upon interaction with IsdH or IsdB, removal of the first globin haem may sufficiently destabilise the remaining globin haem interactions to accelerate passive haem loss. Hence, although $IsdH^{N2N3}$ and $IsdB^{N1N2}$ can quantitatively deplete haem from Hb, it was possible that haem can be released into solution from destabilised Hb and scavenged by Isd receptors that are not physically bound to Hb chains. To investigate if such a mechanism operates, I asked whether the isolated $IsdH^{N3}$ haem-binding domain was able to scavenge haem from sub-stoichiometric (2:1) $IsdH^{N2N3}$:Hb mixtures. The isolated $IsdH^{N3}$ domain is fully functional to bind haem from solution (section 3.2.1, Fig. 3.4 E) but is unable to capture haem from native Fe(III)-Hb over the course of 10 min (Fig. 3.8 A, grey circles), as previously shown by Spirig *et al.*[167]. When $IsdH^{N2N3}$:Hb was mixed in a 2:1 ratio, in the presence or absence of additional $IsdH^{N3}$, the haem transfer curves were identical, with ~50% of haem groups removed from Hb in each case (Fig. 3.8 A, compare dashed and solid curves). Similarly, the isolated $IsdB^{N2}$ was also unable to liberate haem from Fe(III)-Hb. Again, haem was not released to $IsdB^{N2}$ when it was added to a 2:1 mixture of $IsdB^{N1N2}$:Hb tetramer. (Fig. 3.8 B). Hence haem transfer from Hb to $IsdB^{N1N2}$ or $IsdH^{N2N3}$ occurs through a specific complex and requires contacts mediated by the Hb binding NEAT domain ($IsdB^{N1}$ or $IsdH^{N2}$).

Figure 3.8

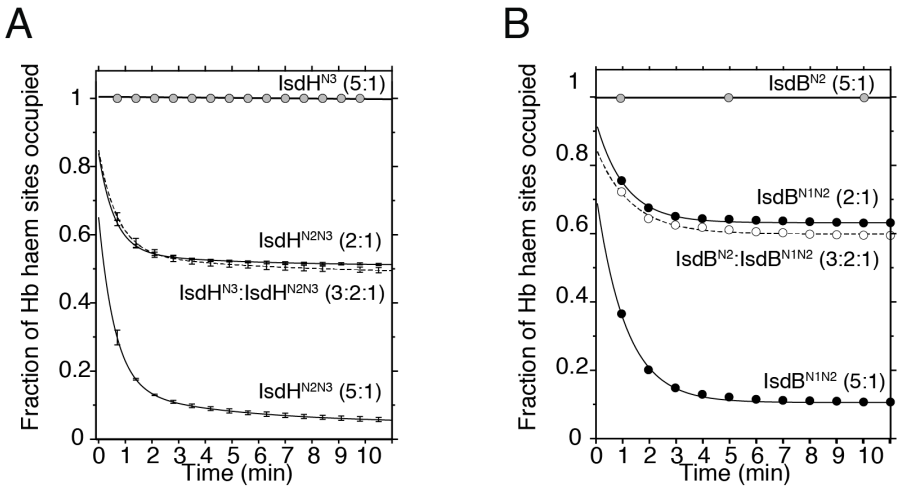

Figure 3.8. Haem capture from all four globin sites requires the Hb-binding domain, IsdH^{N2} or IsdB^{N1}. (A) The fraction of occupied haem sites in Fe(III)-Hb (6 μM haem, corresponding to 1.5 μM tetramer) in the presence of apo-IsdH^{N2N3} or apo-IsdH^{N3} was calculated by fitting individual spectra, taken at 40 s intervals, to a linear combination of the spectrum of Fe(III)-Hb and holo-IsdH^{N2N3} as shown in Fig 3.7.c. Mixing ratios indicated in the figure are per tetramer. Haem transfer in a 3:2:1 molar mixture of IsdH^{N3}:IsdH^{N2N3}:Hb (dashed curve) was very similar to that of 2:1 IsdH^{N2N3}:Hb indicating that haem was not released to apo-IsdH^{N3}. Error bars are ± S.E. from two experiments. **(B)** Data for IsdB^{N1N2} or IsdB^{N2} obtained using the same parameters as in A. These data are from single measurements.

3.3 IsdH^{N2N3} and IsdB^{N1N2} adopt a similar compact globular structure in solution.

Experiments from Spirig *et al*., show that the three domains of IsdH^{N2N3} are needed to achieve haem capture from Hb, suggesting that a higher-order structural organisation of these domains may be involved[167]. To investigate the multi-domain structure of IsdH^{N2N3} and IsdB^{N1N2}, small-angle X-ray scattering (SAXS) analysis was performed.

3.3.1 Preparation of Isd mutant proteins deficient in haem binding

In order to capture a stable complex of IsdH^{N2N3} or IsdB^{N1N2} bound to Hb for structural studies it was expected that haem transfer might need to be disabled to prevent complex dissociation. A Tyr-to-Ala mutation, which removes the haem coordinating side chain, has been characterised previously in both IsdH and IsdB and leads to a reduced affinity for haem[155,167,221]. The single mutation (Tyr642-to-Ala in IsdH and Tyr440-to-Ala in IsdB) was introduced into the haem binding domains of IsdH^{N2N3} or IsdB^{N1N2} using the modified QuickChange mutagenesis protocol of Liu and Naismith[214] (primer sequences can be found in Appendix B). IsdH^{N2N3}(Y642A) was expressed from a pHis-SUMO vector (Appendix A; construct 216) and contained an N-terminal His tag followed by a SUMO tag. An initial Ni-affinity chromatography step was performed as for IsdH^{N2N3}. The His-SUMO tag was then removed by incubation with ULP1 followed by a second affinity chromatography step, during which the IsdH^{N2N3}(Y642A) was collected in the flow through and the SUMO and ULP1 proteins were retained on the Ni resin. SDS-PAGE analysis of the IsdH^{N2N3}(Y642A) purification is shown in Figure 3.9 A.

Expression and purification of IsdB^{N1N2}(Y440A) was performed as for the wild type protein. IsdB^{N1N2}(Y440A) preparations were partially contaminated with porphyrin. IsdB has a distal Met in the haem pocket that may coordinate haem in the absence of Tyr440. In addition, haem may bind with low affinity into the hydrophobic pocket in the absence of a coordinating residue. The majority of the haem-bound IsdB^{N1N2}(Y440A) protein could be separated from the apo protein during the Ni-affinity or cation exchange chromatography (see Section 2.5.2).

To assess haem capture activity, a five fold excess of $IsdH^{N2N3}$(Y642A) or $IsdB^{N1N2}$(Y440A) was mixed with Fe(III)-Hb (per tetramer) and the visible absorption spectra were monitored over time. A plot of the change in absorbance at 406 nm is shown in Figure 3.9 B. Unlike the wild type proteins, the constructs carrying the Tyr-to-Ala mutation produced a minimal change in the spectrum of Fe(III)-Hb over time. Hence the two proteins were largely attenuated in haem capture function as observed previously[167].

$IsdH^{N2N3}$(Y642A) and $IsdB^{N1N2}$(Y440A) were determined to be monomeric by SEC-RALS with weight-average molecular weights (M_W) of 39.7 kDa and 46.3 kDa respectively (compared to theoretical molecular weights of 38.9 kDa and 42.2 kDa). SAXS data for $IsdH^{N2N3}$(Y642A) were recorded at three concentrations (2, 4 and 7 $mg \cdot ml^{-1}$). $IsdB^{N1N2}$(Y440A) samples occasionally showed evidence of aggregation, which could be removed by gel filtration. To remove interference from aggregates, $IsdB^{N1N2}$(Y440A) was subjected to SEC-SAXS at the Australian Synchrotron SAXS-WAXS beamline.

Figure 3.9. Production and haem capture properties of SUMO-IsdH^{N2N3}(Y642A) and IsdB^{N1N2}(Y440A). **(A)** *lane 1*, Mark 12 protein standards; *lane 2*, bacterial lysate; *lane 3*, flow through; *lane 4*, fractions eluted with 100 mM imidazole and incubated with ULP1; *lane 5*, IsdH^{N2N3}(Y642A) eluted in the flow through after reapplication to the Ni-affinity column. **(B)** The figure shows absorbance at 406 nm recorded over 35 min for: Fe(III)-Hb (6 μM haem corresponding to 1.5 μM Hb tetramer; magenta); Fe(III)-Hb (1.5 μM) mixed with 7.5 μM IsdH^{N2N3}(Y642A) (blue); Fe(III)-Hb (1.5 μM) mixed with 7.5 μM IsdB^{N1N2}(Y440A) (orange); Fe(III)-Hb (1.5 μM) mixed with 7.5 μM apo-IsdH^{N2N3} (black); Fe(III)-Hb (1.5 μM) mixed with 7.5 μM apo-IsdB^{N1N2} (grey). These data are from single measurements.

Figure 3.9

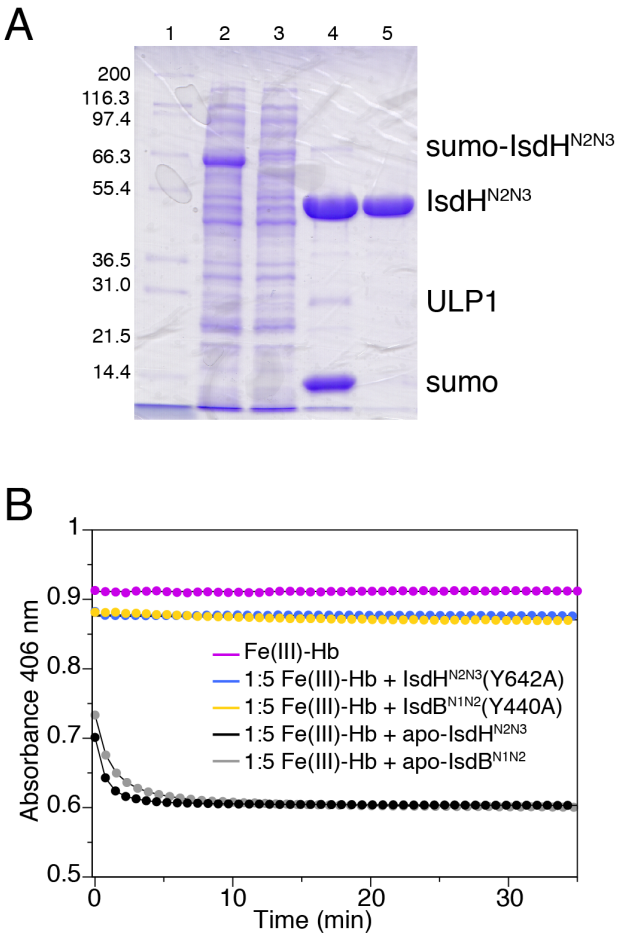
A
1
2
3
4
5
200
116.3
97.4
66.3
55.4
36.5
31.0
21.5
14.4
sumo-IsdH^N2N3
IsdH^N2N3
ULP1
sumo
B
Absorbance 406 nm
Time (min)
Fe(III)-Hb
1:5 Fe(III)-Hb + IsdH^N2N3(Y642A)
1:5 Fe(III)-Hb + IsdB^N1N2(Y440A)
1:5 Fe(III)-Hb + apo-IsdH^N2N3
1:5 Fe(III)-Hb + apo-IsdB^N1N2

3.3.2 SAXS analysis of IsdH^{N2N3}(Y642A) and IsdB^{N1N2}(Y440A)

No significant aggregation or inter-particle interference was detected by Guinier analysis for IsdH^{N2N3}(Y642A) or IsdB^{N1N2}(Y440A) (Fig. 3.10 A, B). Model-free analysis of the SAXS data collected for IsdH^{N2N3}(Y642A) yielded the expected molecular weights for all samples (Table 3.1), which were within 10% of the theoretical molecular weight calculated from the sequence.

Table 3.1. Molecular parameters from SAXS

Structural parameters	IsdH^{N2N3}(Y642A)*			IsdB^{N1N2} (Y440A)	SUMO-IsdH^{N2N3} (Y642A)
Sample concentration (mg·ml^{-1})	7	4.5	3	—	9.5
I(0) (cm^{-1}) (P(r) analysis)	0.1770[a] 0.183± 0.001[b]	0.1186[a] 0.122 ± 0.001[b]	0.0807[a] 0.0821 ±0.0006[b]	0.0034 ± 0.000056[b]	0.3669 [a] 0.366 ± 0.005[b]
R_g (Å) (P(r) analysis)	27.75[a] 28.1 ± 0.2[b]	28.96[a] 30.4 ± 0.2[b]	28.99[a] 30.2 ± 0.02[b]	32.6 ± 0.773[b]	45.4 [a] 45.3 ± 1.2 [b]
I(0) (cm^{-1}) (Guinier analysis)	0.183 ± 0.001[b]	0.121 ± 0.001 [b]	0.082 ± 0.001[b]	0.003 ± 0.000	0.358 ± 0.005 [b]
R_g (Å) (Guinier analysis)	27.7 ± 0.4[b]	29.5 ± 0.5[b]	29.6 ± 0.8[b]	31.05 ± 0.682	41 ± 0.9[b]
D_{max} (Å)	85[a]	90[a]	85[a]	120 [b]	165 [b]
Molecular mass determination					
Partial specific volume (cm^3 g^{-1})	0.732	0.732	0.732		0.730
Contrast ($\Delta\rho$ x 10^{10} cm^{-2})	2.808	2.808	2.808		2.831
Mean molecular mass (from $I(0)$)	36405[a] 37639[b]	36830[a] 37575[b]	38470[a] 39090[b]		54455 [a]
M_r calculated from primary sequence (monomer)	38788	38788	38788		52500

[a] Values generated with GIFT
[b] Values generated with primus
*The IsdH^{N2N3}(Y642A) protein used for this experiment, was produced by G. Reza Malmirchegini.

Both proteins had a bimodal pair-distance distribution function, *P(r)* with a major peak at ~23 Å, which is consistent with the dimensions of an individual NEAT domain based on

X-ray crystallography, and a shoulder peak at around 40–50 Å, indicating that the two molecules have a similar compact bi-lobed shape (Fig. 3.10 C).

Ab initio shape reconstruction of IsdH^{N2N3}(Y642A) was carried out using the experimental scattering data and the program DAMMIF[235]. Ten independent models were averaged using the DAMAVER[236]. Although there was some variation between the models (normalised spatial discrepancy = 0.983), no outliers were identified and filtering of the average envelope to retain the most highly occupied area gave a dumbbell shaped molecule, with two lobes separated by a central rod (Fig.3.10 D). The rod shaped region of the envelope had dimensions similar to the NMR structure of the helical linker domain. This region of the envelope was more intimately associated with one of the two lobes, suggesting a more substantial interaction interface between the linker and one of the NEAT domains. As the IsdH^{N2} and IsdH^{N3} domains are similar in shape and volume it was not possible to designate which of the lobes corresponded to the IsdH^{N2} or IsdH^{N3} domains.

In an attempt to assign the two NEAT domains to the two lobes of the scattering envelope a SUMO-tagged IsdH^{N2N3}(Y642A) was produced. It was reasoned that, with inclusion of the additional SUMO domain, an *ab initio* envelope would be asymmetrical allowing for unambiguous placement of the NEAT domains. Guinier and model free analysis of the scattering data (Table 3.1 and Fig. 3.10 E) indicated that the protein was free of aggregates, and had the expected molecular weight of 52.5 kDa. The *P(r)* curve for SUMO-IsdH^{N2N3}(Y642A) contained two maxima at 23 and 43 Å respectively, consistent with IsdH^{N2N3}(Y642A) and IsdB^{N1N2}(Y440A), however the curve had a tail indicating a much more extended molecule (Fig. 3.10 F). *Ab initio* shape reconstruction was performed as for IsdH^{N2N3}(Y642A), and produced an extended, symmetrical rod shape into which it was not possible to unambiguously place the four domains (Fig. 3.10 G).

Figure 3.10. SAXS analysis of the domain structure of IsdB^{N1N2} and IsdH^{N2N3}. The solution scattering intensity distribution, I(q), is shown for: **(A)** IsdH^{N2N3}(Y642A) **(B)** IsdB^{N1N2}(Y440A). Insets show linear Guinier plots, indicating that there is no aggregation or inter-particle interference. **(C)** The pair distance distribution function, *P(r)*, indicates that IsdH^{N2N3}(Y642A) and IsdB^{N1N2}(Y440A) are compact bi-lobed molecules with a D_{max} of 85 and 120 Å. **(D)** *Ab initio* model of IsdH^{N2N3}(Y642A). The average envelope of 10 DAMMIF runs are shown as dots while the filtered average envelope is shown as spheres. **(E)** The solution scattering intensity distribution, I(q), of SUMO-IsdH^{N2N3}(Y642A). The insert shows a linear Guinier plot. **(F)** The pair distance distribution function, *P(r)*, of SUMO-IsdH^{N2N3}(Y642A). IsdH^{N2N3}(Y642A) is shown for comparison. **(G)** *Ab initio* model of SUMO-IsdH^{N2N3}(Y642A). The average envelope of 8 DAMMIF runs are shown as dots while the filtered average envelope is shown as spheres.

Figure 3.10

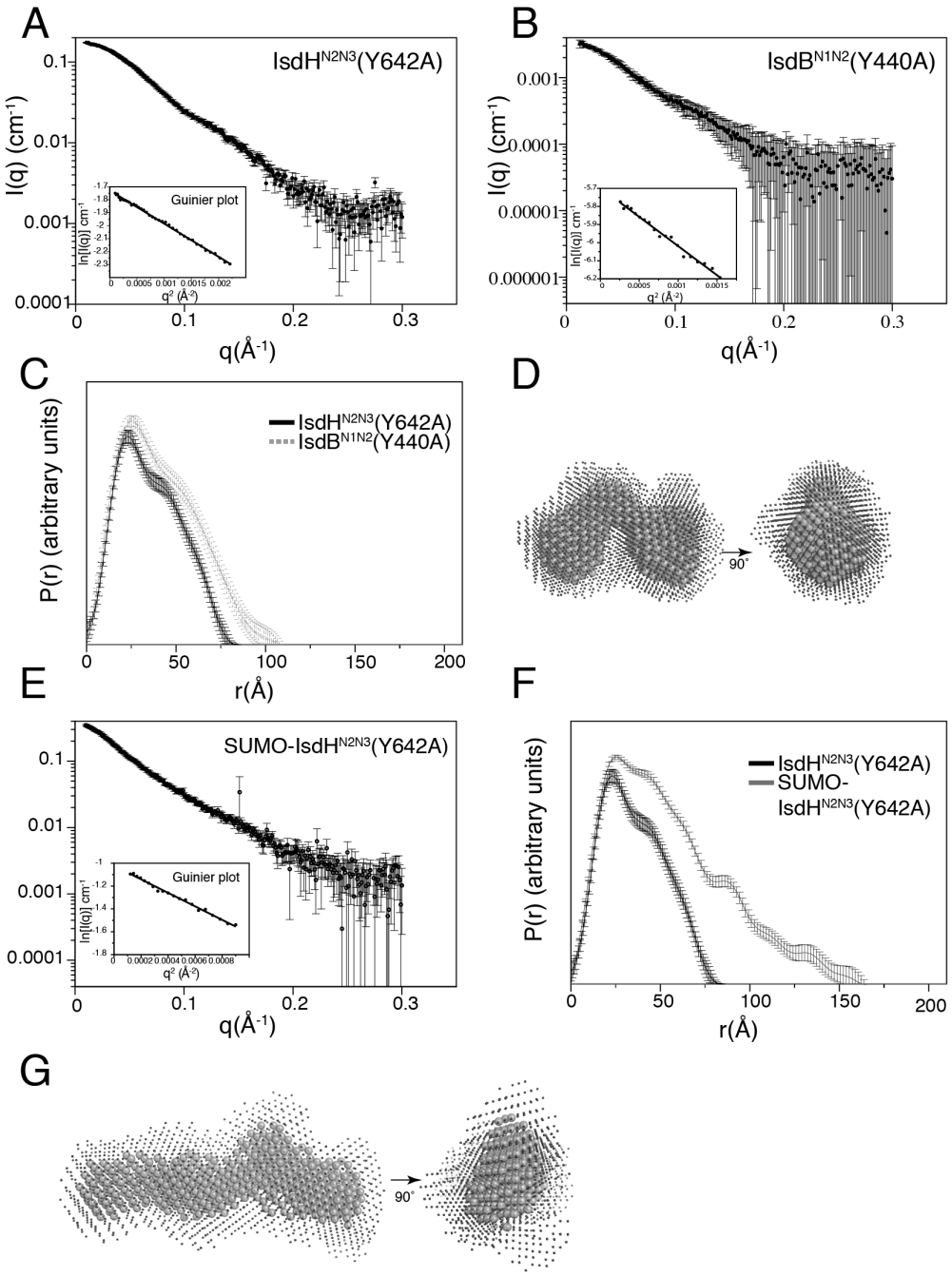
A
IsdH^{N2N3}(Y642A)
I(q) (cm^{-1})
q(Å^{-1})
Guinier plot
ln[I(q)] cm^{-1}
q^2 (Å^{-2})
B
IsdB^{N1N2}(Y440A)
I(q) (cm^{-1})
q(Å^{-1})
ln[I(q)] cm^{-1}
q^2 (Å^{-2})
C
P(r) (arbitrary units)
IsdH^{N2N3}(Y642A)
IsdB^{N1N2}(Y440A)
r(Å)
D
90˚
E
SUMO-IsdH^{N2N3}(Y642A)
I(q) (cm^{-1})
q(Å^{-1})
Guinier plot
ln[I(q)] cm^{-1}
q^2 (Å^{-2})
F
P(r) (arbitrary units)
IsdH^{N2N3}(Y642A)
SUMO-
IsdH^{N2N3}(Y642A)
r(Å)
G
90˚

To determine whether IsdB and IsdH contain unstructured regions a dimensionless Kratky plot, which is independent of protein size and molecular weight, was generated. A well-ordered globular protein is expected to have a maximum with an ordinate value of 1.1 (at qR_g = 1.73) (Fig. 3.11, dashed line). The curve for $IsdH^{N2N3}$(Y642A) has the features of a globular protein with, a maximum of 1.2 at qR_g = 2 (Fig. 3.11, grey). Small deviations from a single bell curve are consistent with a multi-domain structure[237-239]. $IsdB^{N1N2}$(Y440A) displays similar features to $IsdH^{N2N3}$(Y642A) indicating a similar proportion of structured residues (Fig. 3.11, grey dashed). For comparison, the Kratky plot for $IsdH^{N1N2}$, which comprises two NEAT domains separated by an unstructured linker, is shown (Fig. 3.11, black). The structured and unstructured regions of $IsdH^{N1N2}$ give rise to an increase in the maximum of the bell-shaped portion of the curve and a trend to higher scattering ratios with increasing q; features that are clearly distinct from the $IsdH^{N2N3}$(Y642A) and $IsdB^{N1N2}$(Y440A) curves.

Figure 3.11. Kratky analysis of the solution scattering of $IsdB^{N1N2}$ and $IsdH^{N2N3}$. The figure shows a dimensionless Kratky plot for $IsdH^{N2N3}$(Y642A) and $IsdB^{N1N2}$(Y440A). The Kratky plot obtained from SAXS data of $IsdH^{N1N2}$, which is known to have an unstructured linker, is shown for comparison (data provided by K. Krishna Kumar). The dashed vertical line indicates the peak position of the bell curve expected for the case of a single-domain globular protein.

Figure 3.11

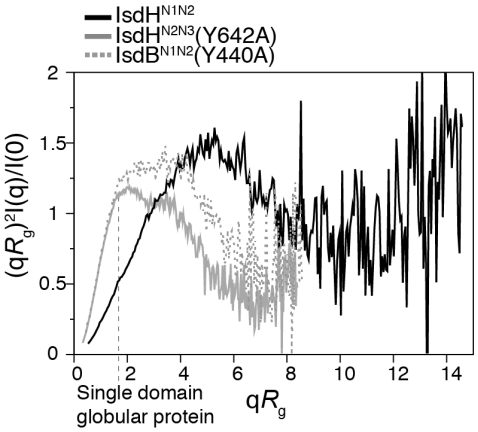
IsdH^N1N2
IsdH^N2N3(Y642A)
IsdB^N1N2(Y440A)
(qR_g)^2I(q)/I(0)
2
1.5
1
0.5
0
0
2
4
6
8
10
12
14
Single domain
globular protein
qR_g

To further characterise the flexibility of IsdH^{N2N3}(Y642A) and IsdB^{N1N2}(Y440A), the distribution of conformations that was required to completely describe the scattering data was assessed using Ensemble Optimisation Method (EOM)[225]. A pool of 10000 random conformers consisting of two NEAT domains and the helical linker of IsdH were generated, and ensembles of structures from the pool were fit to the scattering data. The ensemble with the best fit to the scattering data for IsdH^{N2N3}(Y642A) and IsdB^{N1N2}(Y440A) had a narrow R_g distribution, indicating a similar spacing between the two NEAT domains in all members of the ensemble (Fig. 3.12 A–D, dashed lines). For an unbiased comparison with the IsdH^{N1N2} protein, the analysis was repeated with an ensemble generated from the two NEAT domains joined by a linker composed of dummy residues. A very similar R_g distribution was obtained if the α-helical linker was replaced with the dummy atom linker (Fig. 3.12 A–D, solid lines). In contrast, the ensemble that fits to scattering data for IsdH^{N1N2} has a bimodal R_g distribution. This distribution suggests that the IsdH^{N1N2} protein adopts compact and extended states (Fig. 3.12 E, F, black curve). Similar EOM size distributions have previously been observed for proteins that contain unstructured inter-domain linkers[240]. In summary these results show that IsdB^{N1N2} and IsdH^{N2N3} adopt a similar, compact, multi-domain architecture.

Figure 3.12. IsdB^{N1N2} and IsdH^{N2N3} adopt compact structures. Ensemble optimization method (EOM) indicated that IsdH^{N2N3}(Y642A) (A, B) and IsdB^{N1N2}(Y440A) (C, D) are restricted to relatively compact conformers (χ^2=0.920, χ^2=0.272 respectively). Dashed lines indicate ensembles generated assuming a helical linker (PDB 2LHR) while solid lines represent ensembles generated with a dummy atom linker. For comparison, EOM indicated that a mixture of extended (R_g ~ 60 Å) and more compact (R_g ~ 40 Å) conformers was required to adequately describe the scattering data obtained from IsdH^{N1N2} (χ^2 =0.910) (E, F; data provided by K. Krishna Kumar).

Figure 3.12

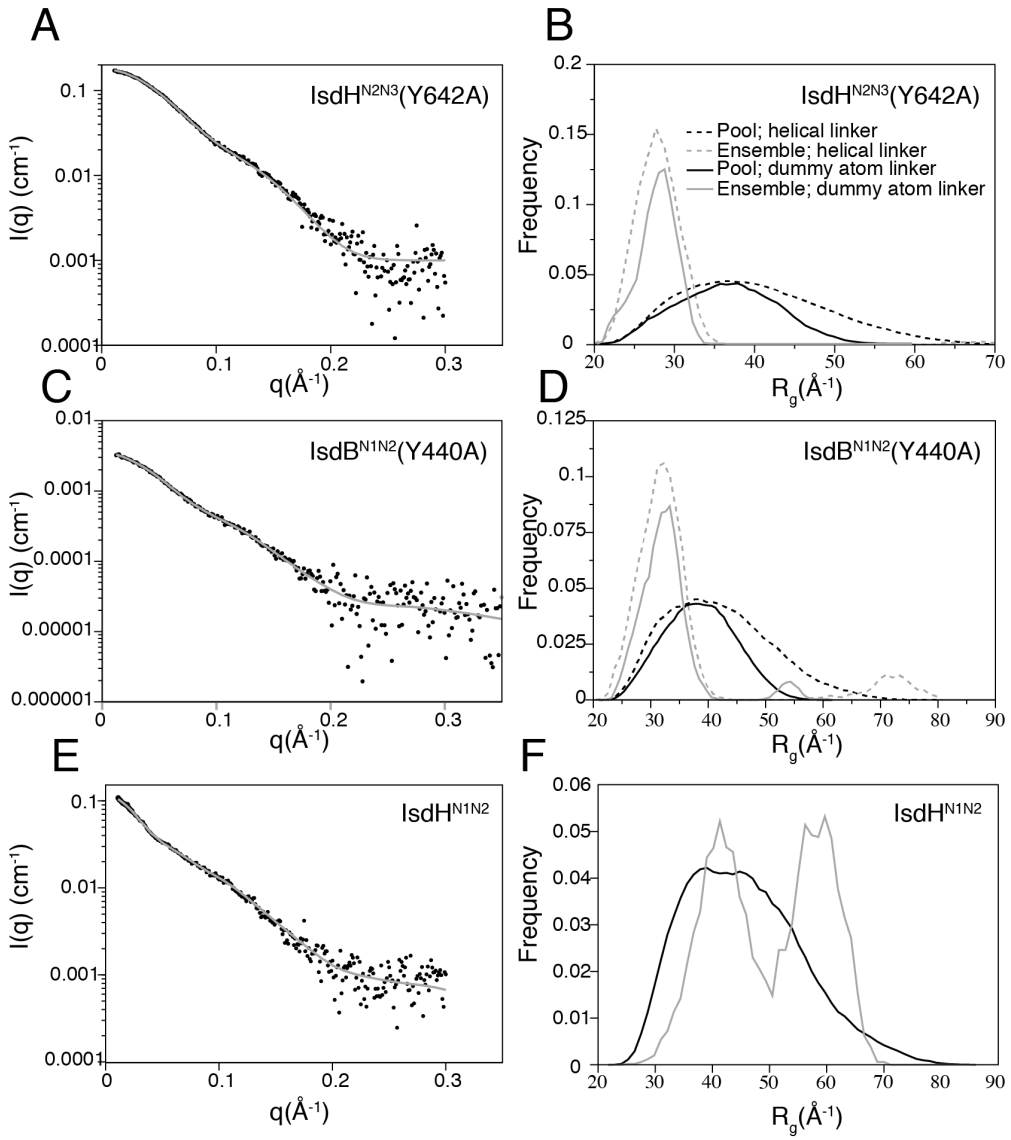
A
IsdH^{N2N3}(Y642A)
I(q) (cm^{-1})
q(Å^{-1})
B
IsdH^{N2N3}(Y642A)
Pool; helical linker
Ensemble; helical linker
Pool; dummy atom linker
Ensemble; dummy atom linker
Frequency
R$_g$(Å^{-1})
C
IsdB^{N1N2}(Y440A)
I(q) (cm^{-1})
q(Å^{-1})
D
IsdB^{N1N2}(Y440A)
Frequency
R$_g$(Å^{-1})
E
IsdH^{N1N2}
I(q) (cm^{-1})
q(Å^{-1})
F
IsdH^{N1N2}
Frequency
R$_g$(Å^{-1})

3.4 IsdH^{N2N3}:Hb complex indicates how the NEAT domains assemble on Hb and work synergistically to capture the haem group.

3.4.1 Crystallisation of the IsdH^{N2N3}:Hb complex

Hb exists in equilibrium between dimeric and tetrameric states and binds weakly to IsdB and IsdH. Previous SAXS studies of mixtures of Hb with isolated NEAT domains, performed in our lab, have shown that these complexes are heterogeneous and give complicated SAXS profiles that cannot be directly interpreted. This was not predicted to be a problem for X-ray crystallography, which also provides higher information content and so crystallography was chosen to investigate the structure of IsdH^{N2N3} and IsdB^{N1N2} in complex with Hb. To choose a suitable mixing ratio of IsdH^{N2N3} and Hb for crystallisation screening, SEC and static light scattering experiments were performed. IsdH^{N2N3}(Y642A) and Fe(III)-Hb eluted as single peaks with M_W's of 40.7 and 30.3 kDa respectively (Fig. 3.13 A). When two IsdH^{N2N3}(Y642A) molecules were mixed with one Hb tetramer a single peak was observed with a M_W of 92.7. At a 4:1 mixing ratio, the M_W of the complex peak was only moderately changed (M_W: 95.3 kDa) and an additional peak of unbound IsdH^{N2N3}(Y642A) was observed. This is consistent with a primary interaction site for the IsdH^{N2} domain on the α chains of Hb and a much weaker interaction with a secondary site on the β chains of Hb[146]. Hence a 2:1 mixing ratio, with the receptors likely bound through the α chains, was chosen for crystallisation.

The complex of IsdH^{N2N3}(Y642A) with Fe(III)-Hb was subject to sparse matrix crystallisation screening at 21 °C. Crystalline formations were obtained in three initial hit conditions but were only reproducible in 0.2 M diammonium citrate, pH 5.0, 20% (w/v) PEG3350, (see Materials and Methods section for details, Fig. 3.13 B). An initial grid screen changing pH by 0.2 pH units and precipitant concentration by 2% followed by a finer screen changing precipitant concentration by 1% resulted in crystals with a flaky appearance that did not diffract (Fig. 3.13 C). An additive screen (Additive screen HT; Hampton Research, Aliso Viejo, CA, USA) was used to identify conditions that would change the crystal habit. Large single crystals (200–500 μm) that diffracted to ~5 Å were grown when an organic solvent such as ethanol, 1-butanol or isopropanol was added to

0.2 M diammonium citrate, pH 4.6, 13% (w/v) PEG3350, (Fig. 3.13 D). Initial attempts to improve the diffraction properties of the crystals included streak seeding and changing the molar mixing ratio to 4:1 $IsdH^{N2N3}$(Y642A):Fe(III)-Hb. Each of these strategies produced large single crystals that diffracted to ~5 Å. As the crystals had a solvent content of 60%, which is higher than the average of ~50% for a protein crystal (but within the normal range), dehydration was attempted but did not improve the diffraction resolution. Crystal annealing was also unsuccessful in improving the diffraction resolution. Numerous cryoprotectants were tested at a range of concentrations, however, diffraction data collected from crystals mounted in capillaries at room temperature also had a resolution limit of ~5 Å. Poor diffraction was therefore deemed to be a property of the crystals and not due to damage during cryo-soaks or the freezing process.A single crystal of the 2:1 $IsdH^{N2N3}$(Y642A):Fe(III)-Hb complex, cryo-protected in 23% ethylene glycol, allowed X-ray diffraction data to be collected to 4.2 Å using synchrotron radiation (Table 3.2). Integration and scaling were performed with HKL-2000 and SCALEPACK[241].

Figure 3.13. Crystallisation of the IsdH^{N2N3}(Y642A):Fe(III)-Hb complex. (A) An SEC experiment indicating that a stable complex is formed between 2 IsdH^{N2N3}(Y642A) molecules and one Hb tetramer. **(B)** Initial crystalline formations obtained in the sparse matrix screen. **(C)** A grid screen to optimize pH and precipitant produced flaky crystals. **(D)** Addition of an organic solvent produced large single crystals.

Figure 3.14. Anomalous signal in the four Hb haem pockets. Anomalous signal (blue) was present in the α Hb (orange) and β Hb haem pockets.

Figure 3.13

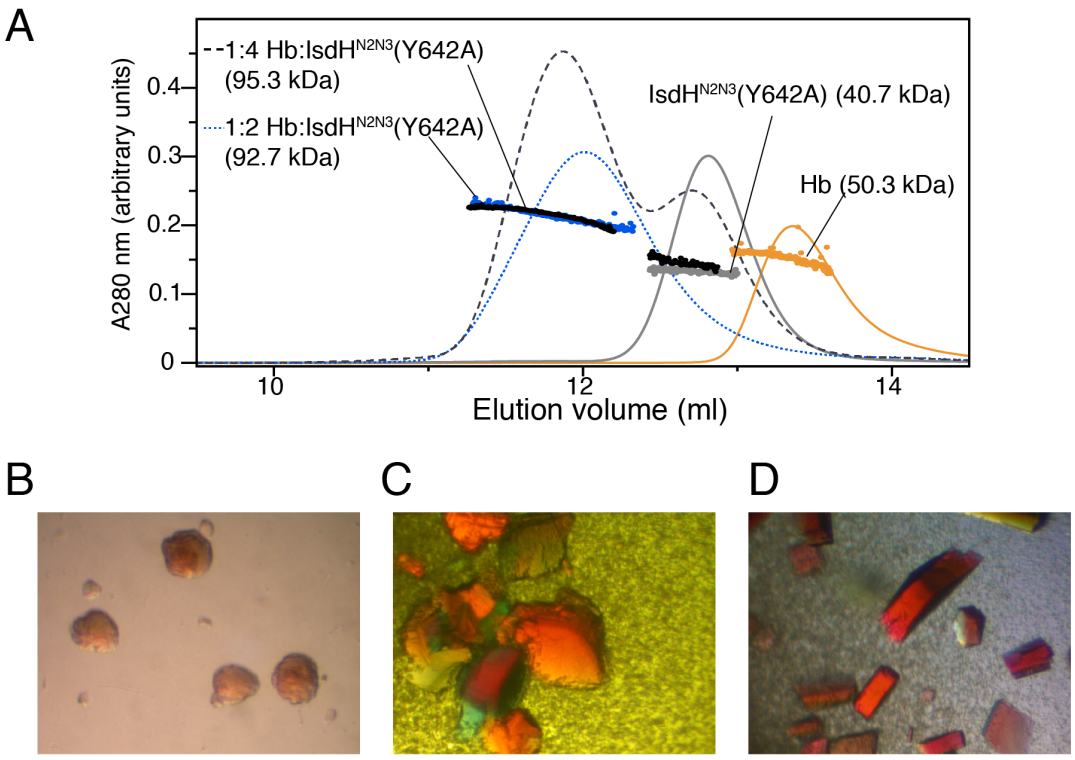

Figure 3.14

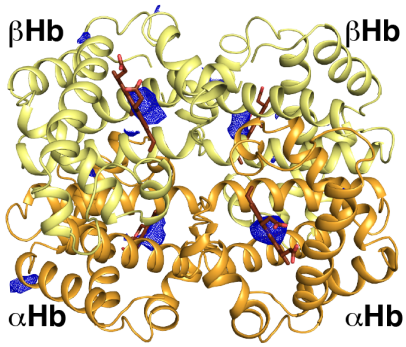

3.4.2 Molecular replacement and refinement

The structure was solved using molecular replacement by searching in a stepwise fashion for domains using the crystal structures of dimeric Fe(III)-Hb (PDB 3P5Q), IsdH^{N2} (PDB 4FC3) and IsdH^{N3} (PDB 2E7D and 2Z6F) as search models. CHAINSAW[242] was used to prune side chains from the IsdH^{N2} PDB file and produce a poly-alanine search model as the intact model could not be placed in the asymmetric unit. An NMR model of the linker domain (PDB 2LHR) was also available, however, PHASER[243] was unable to find a unique solution with this model. An initial search with PHASER placed two Hb dimers, four copies of the poly-alanine model of IsdH^{N2} and two IsdH^{N3} domains into the asymmetric unit, suggesting that four receptors were present in the complex, consistent with the volume of the asymmetric unit. Although the IsdH^{N2} and IsdH^{N3} domains are structurally very similar, PHASER unambiguously placed them in unique locations within the complex. Four regions of helical electron density corresponding to the linker domain for each of the IsdH molecules were evident in the F_O-F_C map providing confidence in the experimental model. The four linker domains were placed manually into the model as rigid bodies using the NMR structure 2LHR (the unstructured N- and C-terminal residues of 2LHR were first removed). Haem groups were not included in the initial model, however, an anomalous signal was observed at the expected iron positions in the four globin chains, and haem groups were included in the final low resolution structure (Fig. 3.14). MOLREP[244] was used to search for the two additional IsdH^{N3} domains expected in the structure, however only one domain could be placed successfully. The electron density observed for the fourth IsdH^{N3} domain, which was expected to lie over the haem pocket of the other β Hb subunit, was not sufficiently strong to place the IsdH^{N3} domain with confidence (dashed ellipse in Fig. 3.15 A), and it was therefore not included in the model.

The solution was refined with Buster version 2.10.0[245]. Refinement was weighted heavily towards the geometry of the high-resolution structures used for molecular replacement, and included non-crystallographic symmetry restraints[246] and translation/liberation/screw (TLS) refinement; groups were defined as single domains. MolProbity[247] was used to verify the geometry and the Ramachandran statistics were as follows: 96.2 % of residues were found in favoured regions; 99.9% in allowed regions; 0.06% in disallowed regions. Coordinates and structure factors can be found at RCSB PDB, entry 4IJ2.

Table 3.2. **Data collection and refinement statistics (molecular replacement)**

	$IsdH^{N2N3}$(Y642A):Hb
Data collection	
Wavelength (Å)	0.95369 Å
Space group	P 2_1 2_1 2
Cell dimensions	
a, *b*, *c* (Å)	132.90, 185.30, 103.21
α, β, γ (°)	90, 90, 90
Resolution (Å)	49.7–4.23 (4.32–4.24)
R_{merge} (%)	9.2 (72.7)
$I / \sigma I$	10.17 (1.83)
Completeness (%)	99.9 (100)
Redundancy	3.8 (3.8)
Refinement	
Resolution (Å)	29.15–4.24 (4.5–4.24)
No. reflections	18511 (2862)
R_{work} / R_{free}	0.299 /0. 310 (0.2911/0.2786)
No. atoms	
Protein	13375
Ligand/ion	172
Water	-
B-factors	
Protein	86.14
Ligand/ion	65.65
Water	-
R.m.s. deviations	
Bond lengths (Å)	0.008
Bond angles (°)	0.84

Diffraction data were collected from a single crystal. Values in parentheses are for the highest-resolution shell.

3.4.3 The $IsdH^{N2-N3}$:Hb complex

The structure of the $IsdH^{N2N3}$(Y642A):Fe(III)-Hb complex is shown in Figure 3.15. Four IsdH molecules were bound to one Hb tetramer in the asymmetric unit, with each α or β Hb globin chain bound independently to one complete receptor molecule (3.15 A–C). The three domains of the receptor were arranged in a dumbbell structure with the globular $IsdH^{N2}$ and $IsdH^{N3}$ domains separated by the intervening helical linker domain (3.15 B–E). This arrangement is consistent with inter-domain interactions detected in an NMR spectroscopic analysis of the free receptor[167], which identified a minimal interface between $IsdH^{N2}$ and the N-terminal end of the helical linker and a distinct interface between $IsdH^{N3}$ and the C-terminal end of the three-helix bundle. The residues identified by NMR chemical shift differences are mapped on the crystal structure of the receptor in Figure 3.15 D and localise to the domain interfaces in the crystal structure. The $IsdH^{N2}$

domains were bound to equivalent sites on the α and β chains and their positions relative to the Hb subunits were consistent with the known IsdH^{N2} binding site (Fig. 3.15 B, C)[175].

The three complete IsdH^{N2N3}(Y642A) molecules in the complex have essentially identical structures (backbone r.m.s.d <1.2 Å in pair-wise comparisons), indicating that IsdH^{N2N3} binds to α and β Hb in the same conformation. Some difference electron density was observed in the F_O-F_C map between the three domains of the receptors (Fig. 3.15 E, green mesh) suggesting that the missing residues (465–472 and 531–534), which are flexible in the NMR structure of the isolated linker domain[167], are ordered in the context of the multi-domain receptor bound to Hb. In addition, positive heteronuclear NOEs for these residues, recorded from the three-domain IsdH^{N2N3}(Y642A) receptor, argue that the inter-domain linking residues are ordered in the context of the three-domain assembly[167]. No attempt was made to build into this density due to the low resolution and absence of obvious secondary structure.

The helical linker domain positions the IsdH^{N3} domain directly over the haem pocket of the bound globin subunit, such that the haem would need to move only ~12 Å, through the entrance to the globin haem pocket, to transfer to IsdH (Fig. 3.15, B, C, F). Hence positioning of the IsdH^{N3} domain appears to be a critical feature of the receptor mechanism. Electron density at the haem-binding site of the IsdH^{N3} domains (Fig. 3.15 F), together with weak anomalous signal (Fig. 3.15 E), suggests that the receptors have partial haem occupancy despite the inactivating Tyr642 to Ala mutation. It is not clear if this haem is derived from the bound globin, however reducing the occupancy of the haem groups bound to the globin chains resulted in residual density in the F_O-F_C map, suggesting that the globin haem sites are fully occupied. An alternative explanation is that IsdH^{N3} domain picked up haem that was released into the solution by denatured Hb present in the crystallization drop. Extensive precipitation of denatured Hb was evident as a thick brown skin on the surface of the crystallisation drop. On the basis that IsdH^{N2N3}(Y642A) receptor cannot actively capture haem from Hb in solution (Section 3.3.1)[167] it is more likely the haem derived from solution may have bound weakly in the hydrophobic cleft. This is consistent with the observation that IsdH^{N2N3}(Y642A) was expressed partially saturated (< 10%) with porphyrins derived from *E. coli*.

Juxtaposition of the two haem coordination sites provides a direct route for haem to transfer from Hb to the receptor (Fig. 3.15 F). In addition, rapid rates of haem transfer[149,167] indicate that haem is actively removed from the globin through destabilisation of the globin-haem interaction. With the X-ray data at 4.2-Å resolution it was not possible to say if the globin haem pocket structure is altered by interaction with $IsdH^{N3}$. In addition, the haem binding β-strands (residues Val-637–Gln-645) of $IsdH^{N3}$ are not well defined in the electron-density. It was possible to model this β-hairpin for one of the receptors bound to an α Hb chain, using the high resolution structures of isolated $IsdH^{N3}$ (PDB 2Z6F and 2E7D). The conformation of the β-hairpin is substantially different in apo- and holo-$IsdH^{N3}$ and the best fit to the density was that of the haem-bound domain (PDB 2Z6F). In this conformation the β-hairpin is in closer proximity to the globin haem pocket. Strategies that led to successful acquisition of X-ray diffraction data at higher resolution are described in Chapter 5.

Figure 3.15 Crystal structure of IsdH$^{N2–N3}$ bound to Hb. **(A)** four IsdH$^{N2–N3}$ receptors bind to one Hb tetramer in the asymmetric unit of the crystal. **(B-C)** Detail of the IsdH^{N2N3}(Y642A):α (B, blue/orange) and IsdH^{N2N3}(Y642A):β (C, teal/yellow) interaction complexes. Residues from the loop regions, which are not modeled in the structure, are shown with dashed lines. **(D)** Inter-domain interface residues identified by an NMR study of the free receptor (red)[167] are shown mapped onto the crystal structure of IsdH^{N2N3} receptor. **(E)** A stereo diagram showing the $2F_O$-F_C electron density map for one full IsdH^{N2N3} receptor contoured at 1σ (grey mesh). F_O-F_C electron density (green mesh) is shown at 3σ, suggesting that the linking residues between the domains are ordered. Anomalous signal present at the haem coordination site (blue) is also shown at 3σ. **(F)** The IsdH^{N2N3}(Y642A):α Hb interface with F_O-F_C difference map shown at 3σ (green), indicating electron density that is not accounted for by atoms of the IsdH^{N2N3}:Hb model. The structure of haem-bound IsdH^{N3} (PDB 2Z6F, red) is superimposed to indicate the expected binding position of the haem group (sticks), which coincides with a peak of F_O-F_C difference electron density in the IsdH^{N2N3}:Hb complex (green). Haem transfer from globin to the IsdH receptor requires a relatively small translation of only 12 Å between the E and F helices of the globin.

Figure 3.15

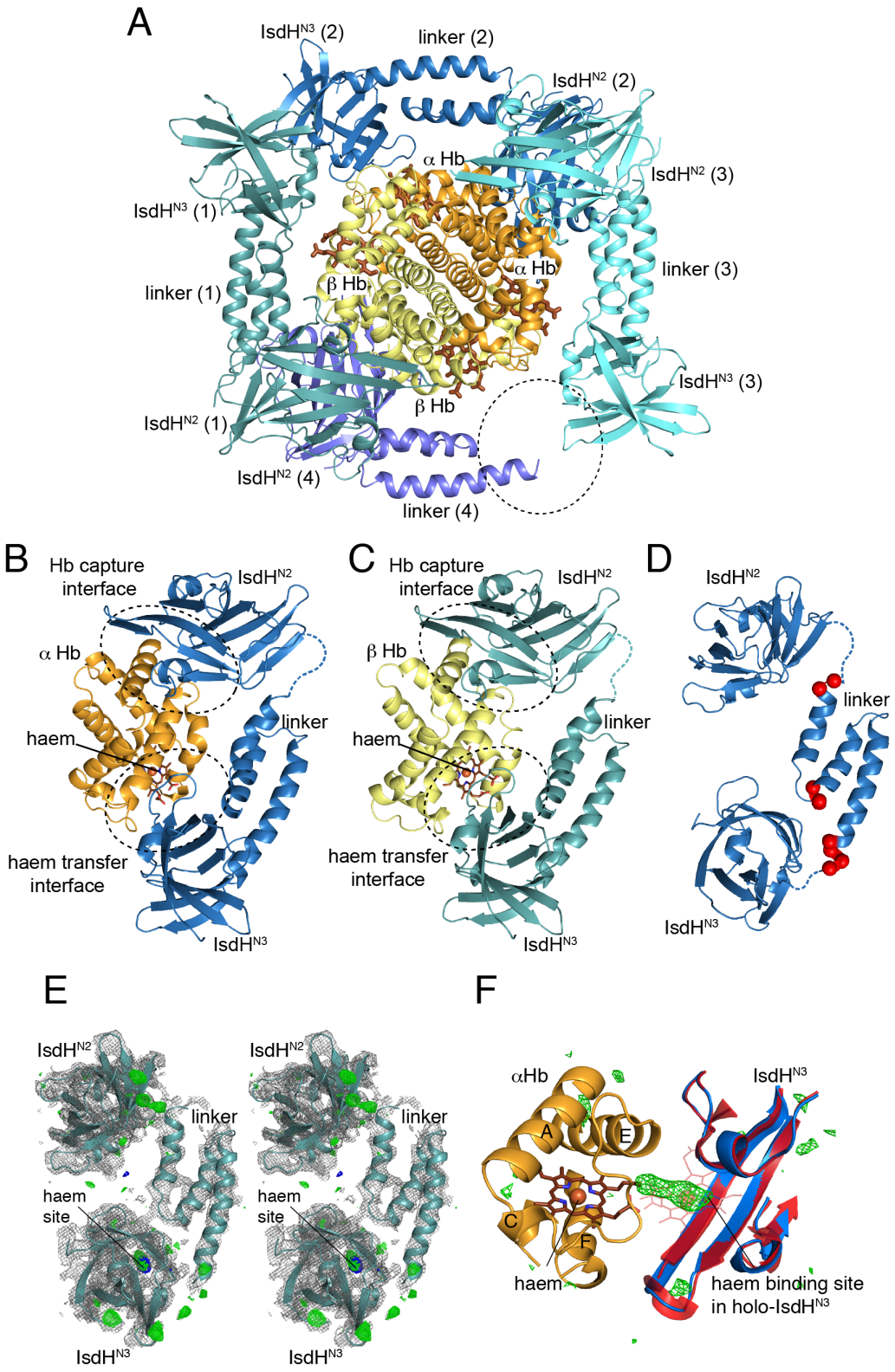
A
IsdH^N3 (2)
linker (2)
IsdH^N2 (2)
α Hb
IsdH^N2 (3)
IsdH^N3 (1)
linker (3)
α Hb
β Hb
linker (1)
IsdH^N3 (3)
β Hb
IsdH^N2 (1)
IsdH^N2 (4)
linker (4)
B
Hb capture interface
IsdH^N2
α Hb
linker
haem
haem transfer interface
IsdH^N3
C
Hb capture interface
IsdH^N2
β Hb
linker
haem
haem transfer interface
IsdH^N3
D
IsdH^N2
linker
IsdH^N3
E
IsdH^N2
linker
haem site
IsdH^N3
IsdH^N2
linker
haem site
IsdH^N3
F
αHb
A
E
C
F
haem
IsdH^N3
haem binding site in holo-IsdH^N3

3.5 IsdH^{N2N3} adopts the same conformation when free and in complex with Hb

The crystal structure of IsdH^{N2N3} bound to Hb was used to evaluate the SAXS data obtained for IsdH^{N2N3} free in solution to see whether any large changes in the conformation of the receptor occur upon binding to Hb. Theoretical X-ray scattering curves for the three full receptors present in the crystal structure were generated using the program CRYSOL[248]. These theoretical curves were fit to the solution scattering of IsdH^{N2N3}(Y642A). All three theoretical curves fit extremely well to the experimental scattering, with χ values of 0.925 (chain E), 0.904 (chain F) and 0.866 (chain G) (Fig. 3.16 A), suggesting that no major structural change occurs upon receptor binding and providing independent validation of the 4.2 Å crystal structure. Superposition of the crystal structure of the bound receptor and the *ab initio* model of IsdH^{N2N3}(Y642A) using SUPCOMB[249] reveals close agreement between the free model and bound structure (Fig. 3.16 B). These results argue that the domains of the receptor are pre-organized to position the haem acceptor site over the globin haem pocket.

Figure 3.16 The domain organization of IsdH^{N2N3} in solution is same as that shown in the crystal structure. **(A)** Fit of the experimental solution scattering of free IsdH^{N2N3} to the theoretical scattering curve generated for a single IsdH^{N2N3} molecule (chain E) from the crystal structure of IsdH^{N2N3}(Y642A):Hb. **(B)** *Ab initio* shape reconstruction of the IsdH^{N2N3} receptor (spheres), overlaid with the crystal structure of IsdH^{N2N3}(Y642A) (ribbon and sticks).

Figure 3.16

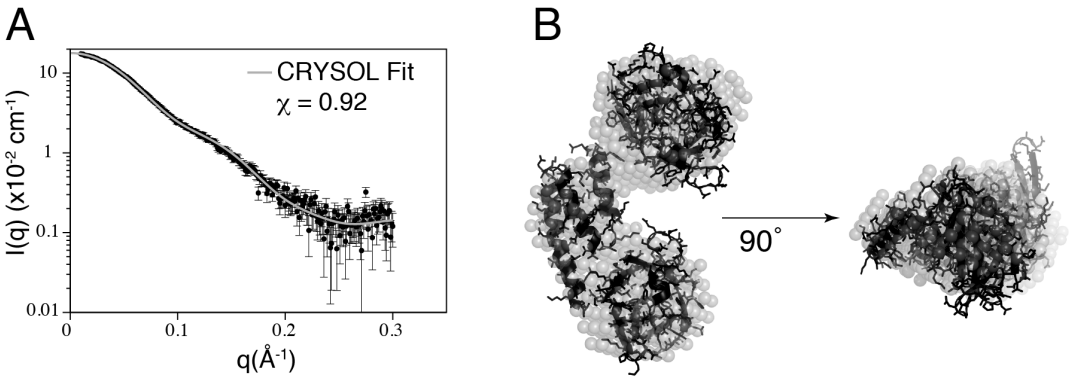

3.6 The IsdH:Hb interaction is compatible with the Hb:Hp interaction however, IsdH does not interact directly with Hp.

Under normal physiological conditions, small amounts of Hb are continually released into the serum by low levels of haemolysis, which occurs as part of the natural turn over of red blood cells. Extracellular Hb is bound by the serum scavenger protein haptoglobin (Hp), which inhibits globin denaturation and targets Hb to the scavenger receptor CD163 on macrophages, resident in the liver and spleen. It is of interest to examine the interactions of IsdB/H with Hb:Hp complexes because[83,145,147,205] access to this pool of Hb iron could be a significant factor in the early stages of *S. aureus* infection. IsdB/H can bind to Hb:Hp complexes[83,145,147,205]. Recently the structure of a porcine dimeric Hb:Hp complex was solved[250]. Superposition with the $IsdH^{N2N3}$:Hb complex indicates that Hp does not present a steric impediment to $IsdH^{N2N3}$:globin interactions (Fig. 3.17), suggesting that Hb:Hp is available as an iron source for *S. aureus.* In addition, binding of $IsdH^{N2N3}$ might block the interaction of Hb:Hb with CD163 impacting on clearance of Hb from serum.

IsdH has also been reported to bind directly to Hp[83,145,147]. Several functions for binding to Hp have been proposed. Direct capture of haptoglobin may function to enhance the Hb binding activity of the bacterial protein[147]. The Hb:Hp interaction is extremely high affinity (estimated to be $> K_d = 10^{-15}$ M) and despite being non-covalent, it is considered to be irreversible[250-253]. Hence an interaction with Hp that retains the Hb binding interface could produce a very efficient Hb receptor tethered to the cell wall. Alternatively, decoration the bacterial surface with the host Hp, may allow *S. aureus* to escape detection by the host immune system[147] or perform anti-inflammatory functions by inhibiting phagocytosis and oxidative killing[83]. Mutagenesis studies have suggested that $IsdH^{N1}$ uses the same interface to bind to Hb or Hp[147]. Hb and Hp have distinct folds and a specific interaction with both proteins would imply that the NEAT domain fold is highly flexible in its capacity to recognise ligands. It is already known that the haem binding and Hb binding NEAT domains have evolved to use the same protein face to bind to their highly dissimilar ligands. Together with high stability and solubility, these properties would make the NEAT domain fold an interesting candidate for protein engineering for biotechnology applications.

There are three allelic forms of the Hp gene: *Hp1F, Hp1S* and *Hp2*. Proteins expressed from the *Hp1* genes form simple dimers. However, the Hp2 protein can form a range of higher molecular weight homo or hetero oligomers[253]. IsdH was shown to interact with Hp from pooled human serum, which contains a range of Hp oligomers, and a construct containing $IsdH^{N1}$ accounted for the majority of the Hp binding activity in ELISA and SPR experiments[83,145,147].

To investigate the proposed interaction between $IsdH^{N1}$ and Hp, SEC and static light scattering experiments were performed with Hp1-1, which is the simplest oligomer of Hp. The data shown in Figure 3.18 A&B were provided by D. Gell. In Figure 3.18 A, $IsdH^{N1}$ eluted as a single mono-dispersed peak with a M_W of 18.6 kDa. The Hp1-1 protein gave rise to a major peak (M_W: 92.2 kDa) corresponding to Hp1-1 dimers and a second peak of contaminating higher molecular weight species (Fig. 3.18 A, upper panel; blue). A mixture of $IsdH^{N1}$ and Hp1-1 did not show any evidence of an interaction as both the elution profile and M_W measurements remained unchanged from those of the free proteins (Fig.3.18 A, lower panel; dashed line). Under the same conditions, Hp1-1 formed a complex with Hb (Fig. 3.18 B, lower panel; orange) with the expected molecular weight for a Hp1-1 dimer bound to two Hb dimers (M_W: 152 kDa) indicating that the Hp protein was functional. $IsdH^{N1}$ was able to bind to the Hb:Hp 1-1 complex, presumably through a site on α/β Hb, as indicated by a shift in elution volume and an increase in M_W to 172 kDa (Fig. 3.18 B, lower panel; dashed line).

To test whether IsdH contains a binding site for any of the allelic forms of Hp, I performed SEC and static light scattering experiments with Hp purified from pooled human serum and an IsdH construct covering all three NEAT domains ($IsdH^{N1N2N3}$). Details of the expression and purification of $IsdH^{N1N2N3}$ can be found in Section 4.3.1. The pooled Hp protein produced several overlapping peaks arising from the different oligomers, with a measured M_W range of 133 kDa – 1 MDa (Fig. 3.18 C, upper panel). $IsdH^{N1N2N3}$ eluted as a single peak with a M_W of 70.5 kDa (Fig. 3.18 C, upper panel). When $IsdH^{N1N2N3}$ was mixed with the pooled Hp, the elution profile was identical to those of the free proteins and the measured M_W's remained unchanged (Fig. 3.18 C, lower panel). Hence no interaction between $IsdH^{N1N2N3}$ and any of the Hp oligomers could be detected. In contrast, addition of Hb to the pooled Hp led to a change in the shape of the

elution profile with a shift to an earlier elution time, indicating that the Hp oligomers were bound to Hb (Fig. 3.18 D, lower panel, dashed line). When $IsdH^{N1N2N3}$ was added to the mixture of Hp:Hb complexes, no free $IsdH^{N1N2N3}$ peak was observed suggesting that $IsdH^{N1N2N3}$ was bound to the Hb:Hp complexes. Hence, under the conditions tested, IsdH does not bind directly to purified Hp but can bind to Hb:Hp complexes, consistent with the model depicted in Figure 3.17.

Figure 3.17 The Hb:Hp interaction is compatible with $IsdH^{N2N3}$:Hb interaction. The crystal structure of porcine Hp 1-1 (green and yellow) bound to two Hb dimers (red and pink) (PDB 4F4O). Overlaid is a Hb dimer (orange) with two $IsdH^{N2N3}$ molecules bound (blue and cyan).

Figure 3.18 IsdH does not bind directly to Hp but can bind to Hb:Hp complexes. (A) *Upper panel*: SEC traces of free Hp 1-1 (blue) and $IsdH^{N1}$ (grey). *Lower panel*: a mixture of Hp 1-1 and $IsdH^{N1}$ (dashed line) indicates that $IsdH^{N1}$ does not bind to Hp 1-1. **(B)** *Upper panel*: SEC traces of free Hp 1-1 (blue) and Hb (grey). *Lower panel*: A Hb:Hp complex (orange) will bind to $IsdH^{N1}$ (dashed line). **(C)** *Upper panel*: SEC traces of free pooled Hp (blue) and $IsdH^{N1N2N3}$ (grey). *Lower panel*: a mixture of pooled Hp and $IsdH^{N1N2N3}$ (dashed line) indicates that IsdH does not bind to Hp. **(D)** *Upper panel*: SEC traces of free pooled Hp 1-1 (blue). *Lower panel*: A pooled Hp will bind to Hb (orange) and form a larger complex with IsdH (dashed line).

Figure 3.17

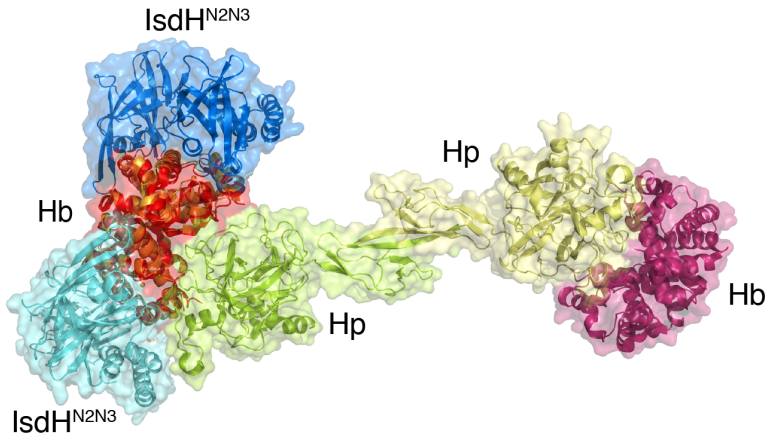

Figure 3.18

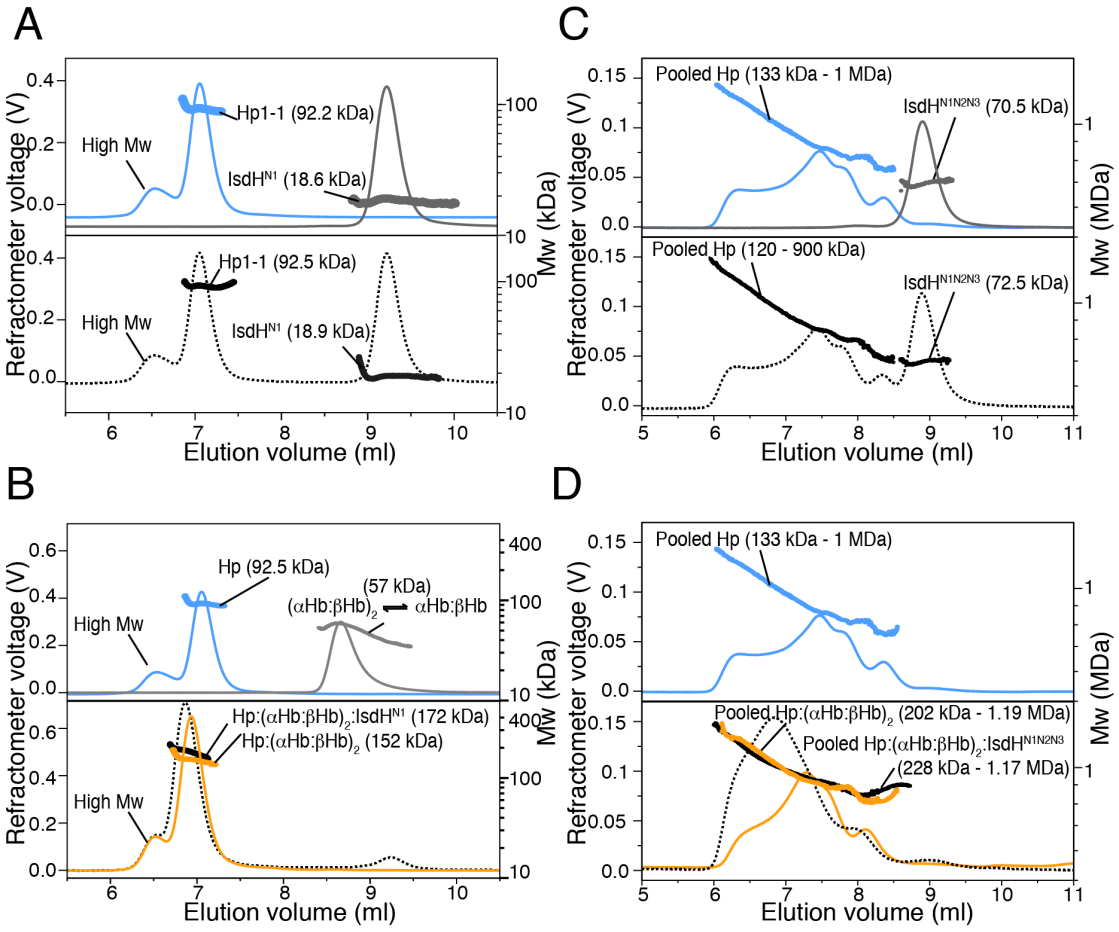

3.7 Discussion.

The structural studies presented in this chapter indicate that haem capture from Hb involves direct positioning of the haem capture domain adjacent to the globin haem pocket. The three domains work together by anchoring the receptor to Hb through the $IsdH^{N2}$ domain and precisely placing the haem binding $IsdH^{N3}$ domain via the scaffolding linker domain. $IsdH^{N2N3}$ is ~ 60% sequence-identical to IsdB and ~ 50% sequence-identical to the IsdB homolog of *S. lugdunensis*, suggesting that the mechanism of haem capture proposed here is applicable to the three known Hb receptors found in pathogenic staphylococcal species.

SAXS studies indicate that the receptor does not undergo any major conformation changes upon binding to Hb suggesting that the domain architecture is pre-organised to strip haem from Hb. This does not rule out small inter-domain motions that do not change the radius of gyration of the protein, as these motions would not be detected by SAXS. The $IsdH^{N3}$ and linker domains make contacts across a substantial interface consistent with the two domains behaving as a single entity, however minimal contacts are evident between the linker and $IsdH^{N2}$ domain suggesting some flexibility here. Recent NMR relaxation measurements of the free $IsdH^{N2N3}$ protein, confirm that the three domains predominantly behave as a single unit but that the $IsdH^{N2}$ domain also undergoes limited motions in isolation from the rest of the $IsdH^{N2N3}$ receptor (R. Clubb, unpublished results).

Separation of the Hb binding and haem removal functions to distinct interfaces of IsdH may be necessary to achieve the task of haem capture from Hb. Release of haem from Hb is predicted to require unfolding of the globin haem pocket, hence recognition of a distant surface of Hb for specific binding might allow for localised changes in the globin haem pocket while maintaining the integrity of the receptor-binding site. Consistent with this idea, mutagenesis studies of the Hb receptor A (HgbA) from Gram-negative *Haemophilus ducreyi* and HmbR from *Neisseria meningitidis* indicate that there is likewise a physical separation of the Hb-binding and haem uptake interfaces[134,135,139]. This similarity suggests that an architecture involving multiple interaction interfaces might have a functional advantage for haem extraction from Hb in a range of systems. Multiple interaction

surfaces also increase the potential for targeted design of inhibitors. Haem capture by the haem binding domains was dependent upon interactions mediated by the $IsdH^{N2}$/$IsdB^{N1}$ domains and hence blocking Hb binding or haem binding are viable avenues for inhibiting haem uptake.

IsdH bound to α and β Hb chains using the same interaction 'mode' and was able to capture haem from all four globin subunits. These structural and functional data suggest that the same mechanism of haem removal may operate for α and β Hb. Consistent with this idea, Zhu *et al.,* showed that haem is almost completely transferred from Hb to IsdB in under 2 min at 22 °C with a single rate constant[149]. The data presented in this chapter suggests that the receptors can access iron from Hb regardless of the Hb chain encountered or the oligomeric status of the protein. This versatility would enhance the likelihood of successful encounters with Hb as dissociation of the Hb tetramer is known to occur *in vivo* following erythrocyte lysis, due to dilution effects and autooxidation processes. In addition, removal of haem from one or more globin chains is expected to destabilize Hb, leading to increased formation of monomers[167,169].

Both Hb and Hb:Hp complexes have been shown to support *S. aureus* growth in the absence of other sources of iron[83]. While uptake of haem from Hb:Hp complexes by IsdH or IsdB has not been demonstrated, IsdH was able to bind to Hb:Hp complexes in gel filtration assays. In addition, the crystal structure of the $IsdH^{N2N3}$:Hb complex indicates that concurrent binding to Hp would not disrupt the Hb targeting or haem capture interactions of the bacterial receptor. In contrast to previous reports, direct binding of IsdH to Hp was not observed. A discussion of why these results might differ form previous findings in given in Section 4.8.

In conclusion, Chapter 3 has addressed the first aim of this thesis: to determine the molecular mechanism used by the multi-domain receptors, IsdH and IsdB, to capture haem from Hb. The experiments presented in this chapter have shown how the three domains of the receptors work synergistically to position the haem capture machinery at the globin haem pocket and bring about haem transfer. The molecular contacts that occur at this interface are investigated further in Chapter 6.

Chapter 4. Haem relay function of IsdB and IsdH is linked to Hb binding affinity.

4.1 Introduction

IsdH and IsdB possess a number of physical and functional similarities, including high sequence homology and similar rates of haem capture from Hb (see Sections 1.5.4.4 and 3.1). The results presented in Chapter 3 show that the homologous regions of IsdH and IsdB, $IsdH^{N2N3}$ and $IsdB^{N1N2}$, are both able to quantitatively capture haem from α and β Hb chains. In addition, SAXS showed that $IsdB^{N1N2}$ and $IsdH^{N2N3}$ adopt a similar shape, suggesting that the $IsdH^{N2N3}$:Hb structure provides a good model for $IsdB^{N1N2}$:Hb interactions. These similarities might predict that $IsdB^{N1N2}$ and $IsdH^{N2N3}$ perform similar functions in haem uptake *in vivo*. However, *S. aureus* strains with deletions of *isdB* have a much more pronounced growth deficit in media where Hb is the sole iron source, compared to *ΔisdH* strains (see Section 1.6.1). In addition, *ΔisdB* strains are more disabled than *ΔisdH* strains in most animal models of infection (see Section 1.6.1). I therefore hypothesised that differences exist in the way that IsdB and IsdH interact with Hb and/or transport haem.

IsdB can transfer haem from Hb to IsdA or IsdC in a purified system[149,230], providing a mechanism for haem relay to the IsdEF complex in the cytoplasmic membrane. The same haem relay function has not been demonstrated for IsdH. Conversely, Hb-binding attributes of $IsdH^{N1}$ and $IsdH^{N2}$, and $IsdH^{N2N3}$ have been determined (Chapter 3 and Section 1.5.4.4), whereas the IsdB:Hb interaction is less well-characterised. Hence the aims of this chapter were (1) to determine whether both IsdB and IsdH function as haem transfer catalysts *in vitro*, and (2) to investigate the Hb binding properties of IsdB, and isolated NEAT domains of IsdB, in order to directly compare the Hb binding functions of IsdB and IsdH.

4.2 IsdB is more efficient than IsdH^{N2N3} and IsdH at catalysing haem transfer to downstream acceptors IsdA and IsdC.

To investigate haem relay from IsdH^{N2N3} and IsdB^{N1N2} to IsdA and IsdC, the full-length sequences of IsdA and IsdC, lacking the N-terminal secretion signal and C-terminal sortase anchor, were cloned into pET-15b (see Section 2.3 and Appendix A). The constructs carried an N-terminal histidine tag and were purified by Ni-affinity chromatography, followed by gel-filtration. SDS-PAGE analysis of the purification process is shown in Figure 4.1. A–D. Apo-IsdC could be separated from partially haem bound preparations by ion exchange over DEAE resin or by acid acetone haem removal. The holo-IsdC and apo-IsdC spectra are shown in Figure 4.1, E. Titration of haem into apo-IsdC was monitored by UV-visible spectroscopy, as described in Section 3.2.1. The Apo-IsdC protein bound haem at a stoichiometry of ~1:1.2, close to the expected 1:1 ratio (Fig. 4.1 F).

Figure 4.1. SDS-PAGE analysis of expression and purification of IsdC and IsdA. (A) Purification of IsdC by Ni-affinity chromatography: *lane 1*, Mark 12 protein standards; *lane 2*, bacterial lysate; *lane 3*, flow through; *lane 4*, 30 mM imidazole wash; *lanes 5–9*, 100 mM imidazole elution fractions. **(B)** Purification of IsdC by gel filtration over a Superose 12 column (GE healthcare): *lane 1*, Kaleidoscope protein standards (Bio-Rad); *lanes 2–10*, elution fractions from gel filtration. **(C)** Purification of IsdA by Ni-affinity chromatography: *lane 1*, bacterial lysate; *lanes 2–3*, flow through; *lane 4*, 10 mM imidazole wash; *lanes 5–9*, 30 mM imidazole elution fractions; lane 10, Kaleidoscope protein standards. **(D)** Purification of IsdA by gel filtration over a Superose 12 column (GE healthcare): *lane 1*, Kaleidoscope protein standards; *lanes 2–10*, elution fractions from gel filtration. Arrows indicate overexpressed recombinant proteins. Stars indicate fractions collected for use from the final purification step. **(E)** The UV-visible absorption spectra of holo- (black) and apo- (grey) IsdC. **(F)** Titration of haem into apo-IsdC. Data points were fit, by linear regression, in two groups. A 1:1 binding stoichiometry (assuming accurate concentration determination and K_d << working concentration) would see the linear fits intersect at the vertical dashed line.

Figure 4.1

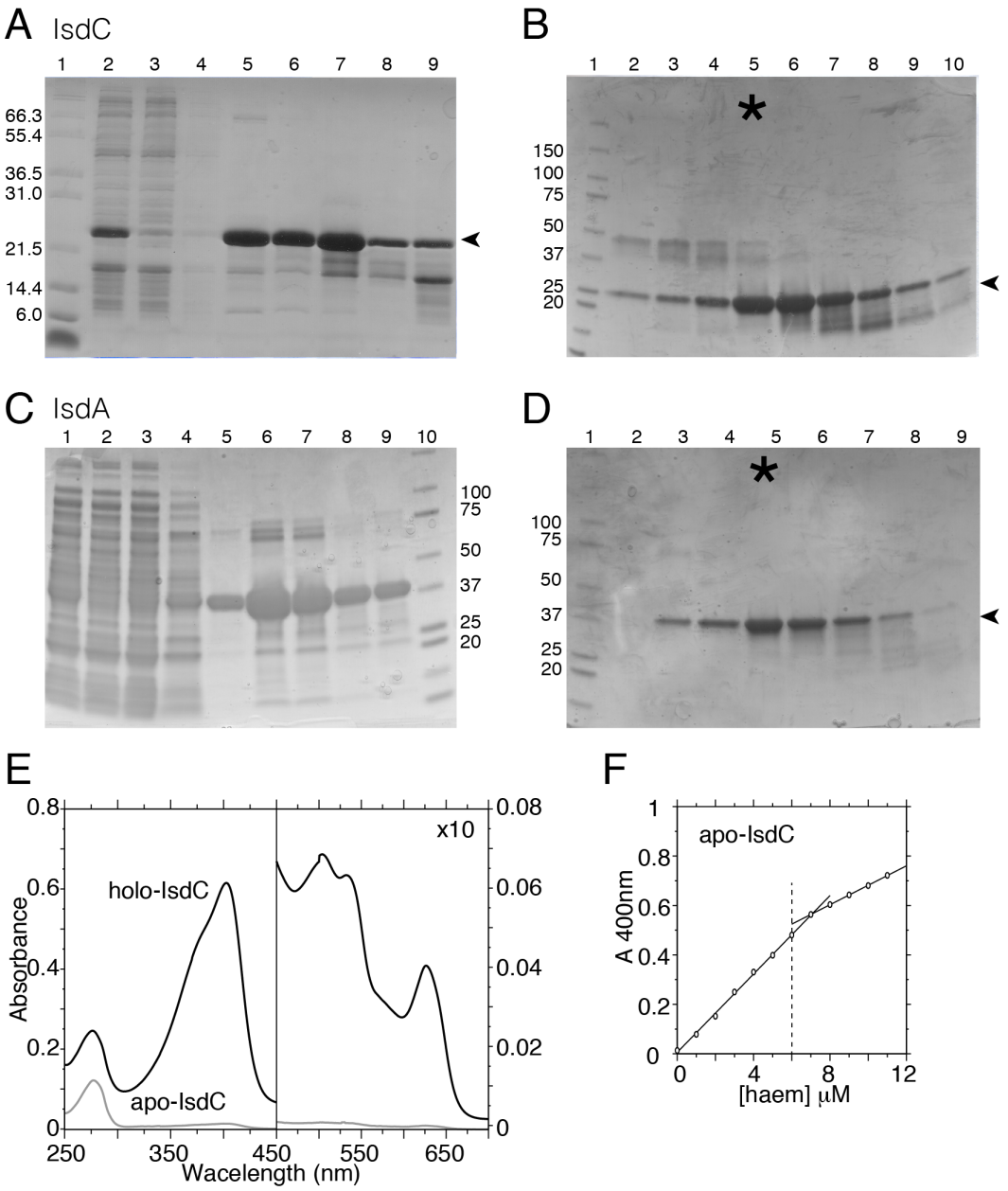
A IsdC
1 2 3 4 5 6 7 8 9
66.3
55.4
36.5
31.0
21.5
14.4
6.0
B
1 2 3 4 5 6 7 8 9 10
*
150
100
75
50
37
25
20
C IsdA
1 2 3 4 5 6 7 8 9 10
100
75
50
37
25
20
D
1 2 3 4 5 6 7 8 9
*
100
75
50
37
25
20
E
0.8
0.6
0.4
0.2
0
Absorbance
holo-IsdC
apo-IsdC
x10
0.08
0.06
0.04
0.02
0
250 350 450 550 650
Wacelength (nm)
F
1
0.8
0.6
0.4
0.2
0
A 400nm
apo-IsdC
0 4 8 12
[haem] μM

The relay of haem from Fe(III)-Hb to apo-IsdC was measured in the presence of small quantities (2–13% of the total haem concentration) of $IsdB^{N1N2}$ or $IsdH^{N2N3}$ (Fig. 4.2). When Fe(III)-Hb was mixed with 125% (measured as a % of the number of Hb haem-binding sites in the reaction) apo-IsdC alone, the haem transfer was negligible (Fig.4.2 B, D, dashed lines). However, 13% $IsdB^{N1N2}$ achieved complete haem transfer from Fe(III)-Hb to IsdC in under 10 min at 4˚C (Fig. 4.2 A, B). In comparison 13% $IsdH^{N2N3}$ resulted in slow relay of haem from Fe(III)-Hb to IsdC and the reaction did not reach completion within 35 min (Fig. 4.2 C, D).

Figure 4.2. Haem transfer from Fe(III)-Hb to IsdC in the presence of $IsdB^{N1N2}$ or $IsdH^{N2N3}$. (A) Spectral recorded at 40-s intervals for a mixture of 1.5 mM Fe(III)-Hb tetramer in the presence of 125% apo-IsdC (measured as a % of the number of Hb haem sites in the reaction) and 13% apo-$IsdB^{N1N2}$. **(B)** Normalised change in absorbance at 406 nm for mixtures of Fe(III)-Hb with 125% apo-IsdC (per Hb haem) and 2–13% apo-$IsdB^{N1N2}$ (per Hb haem). **(C)** Spectra recorded at 40-s intervals for a mixture of Fe(III)-Hb with 125% apo-IsdC (per Hb haem) and 13.3% apo-$IsdH^{N2N3}$ (per Hb haem). **(D)** Normalised change in absorbance at 406 nm for mixtures of 1.5 mM Fe(III)-Hb with 125% apo-IsdC (per Hb haem) and 2–13% apo-$IsdH^{N2N3}$ (per Hb haem). These data are from single measurements.

Figure 4.2

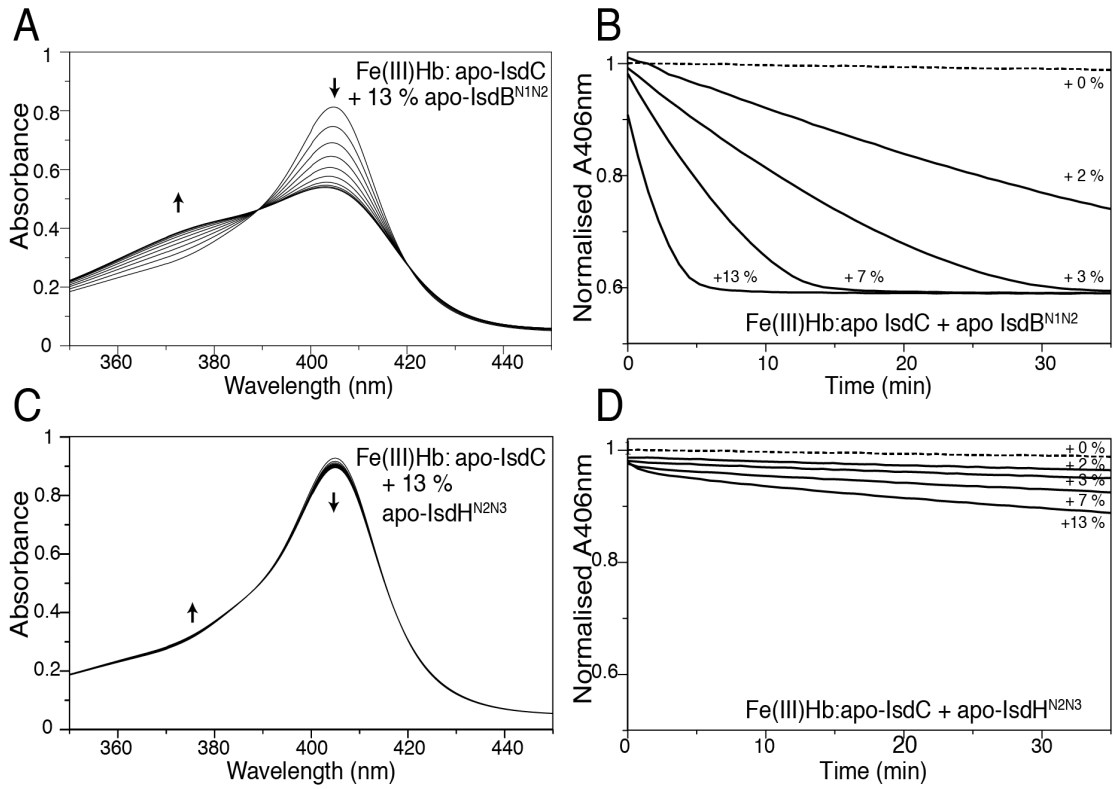
A
Fe(III)Hb: apo-IsdC
+ 13 % apo-IsdB^{N1N2}
Absorbance
Wavelength (nm)
B
Normalised A406nm
+ 0 %
+ 2 %
+ 3 %
+ 7 %
+13 %
Fe(III)Hb:apo IsdC + apo IsdB^{N1N2}
Time (min)
C
Fe(III)Hb: apo-IsdC
+ 13 %
apo-IsdH^{N2N3}
Absorbance
Wavelength (nm)
D
Normalised A406nm
+ 0 %
+ 2 %
+ 3 %
+ 7 %
+13 %
Fe(III)Hb:apo-IsdC + apo-IsdH^{N2N3}
Time (min)

An attempt was also made to measure haem relay from Fe(III)-Hb to IsdA in the presence of $IsdH^{N2N3}$ and $IsdB^{N1N2}$; however, apo-IsdA preparations produced by acid acetone haem removal appeared to have a large proportion of non-functional protein and underwent time-dependent precipitation. IsdA is a larger protein than IsdC (265 residues in mature IsdA vs 160 residues in mature IsdC), and contains an extensive region of unknown structure between the NEAT domain and the C-terminal sortase-recognition motif. It is possible that the larger IsdA protein did not refold properly after solvent extraction of the haem ligand and further optimisation of haem removal and protein refolding is required.

Preliminary experiments were performed with apo-IsdA, immediately after refolding and before the protein had begun to precipitate. Fe(III)-Hb-tetramer was mixed 125% apo-IsdA alone, or in the presence of 7% apo-$IsdB^{N1N2}$, or apo-$IsdH^{N2N3}$ (Fig. 4.3). Like IsdC, apo-IsdA alone did not capture haem from Hb (Fig. 4.3 C, dashed line). When IsdB was present an initial rapid change in the spectrum was observed that was faster than IsdB-catalysed transfer from Hb to IsdC. However, this was followed by a slower phase and the reaction did not go to completion within the time course (Fig. 4.3 A, C), as judged by inspection of the final spectrum, which indicated the presence of Fe(III)-Hb and IsdB/A. $IsdH^{N2N3}$ also transferred haem to IsdA (Fig. 4.3 B, C) more efficiently than to IsdC. In summary, $IsdB^{N1N2}$ was more effective than the homologous region of IsdH ($IsdH^{N2N3}$) at relaying haem from Hb to IsdA, or from Hb to IsdC. In addition, whereas $IsdB^{N1N2}$ transferred haem to IsdA or IsdC, $IsdH^{N2N3}$ showed very limited ability to transfer haem to IsdC.

Figure 4.3. Haem transfer from Fe(III)-Hb to IsdA in the presence of $IsdB^{N1N2}$ or $IsdH^{N2N3}$. (A) Spectral recorded at 40-s intervals for a mixture of 1.5 mM Fe(III)-Hb tetramer in the presence of 125% apo-IsdA (measured as a % of the number of Hb haem sites in the reaction) and 7% apo-$IsdB^{N1N2}$ (per Hb haem). **(B) S**pectra recorded at 40-s intervals for a mixture of Fe(III)-Hb with 125% apo-IsdA (per Hb haem) and 7% apo-$IsdH^{N2N3}$ (per Hb haem). **(C)** Normalised change in absorbance at 406 nm for mixtures of Fe(III)-Hb with 125% apo-IsdA (per Hb haem) and 7% apo-$IsdB^{N1N2}$ or 7% apo-$IsdH^{N2N3}$ (per Hb haem). These data are from single measurements.

Figure 4.3

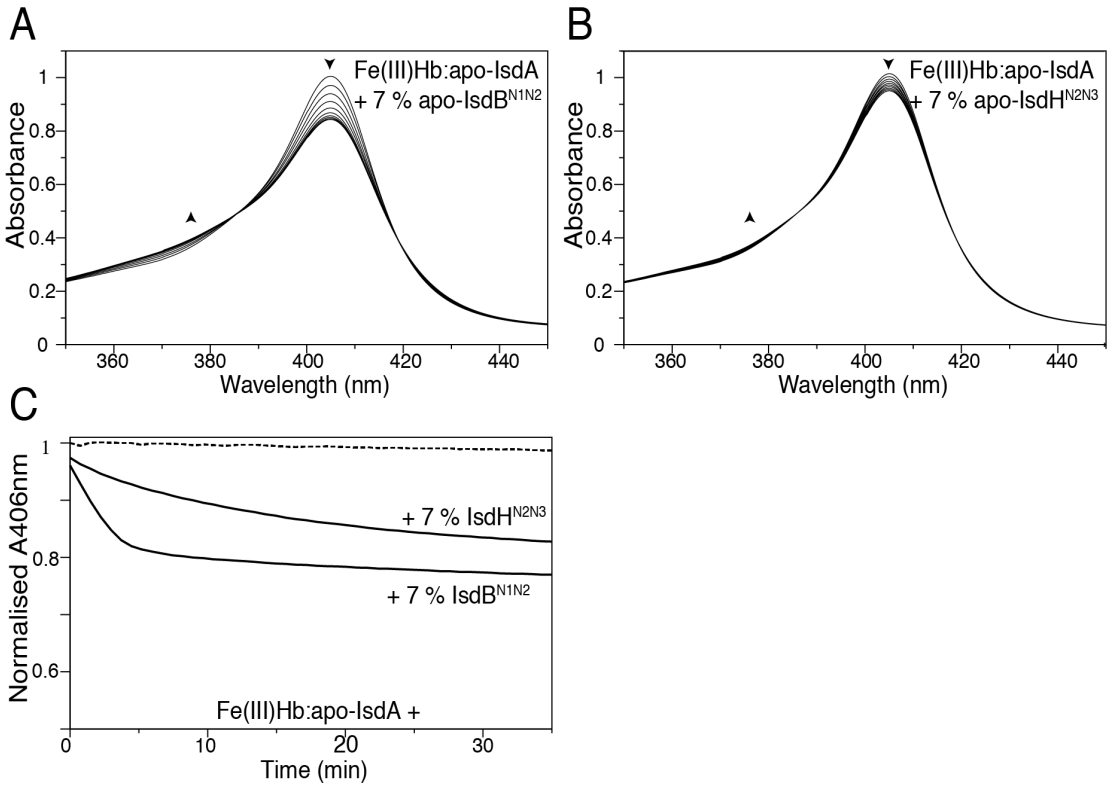
A
Fe(III)Hb:apo-IsdA
+ 7 % apo-IsdB^{N1N2}
Absorbance
Wavelength (nm)
B
Fe(III)Hb:apo-IsdA
+ 7 % apo-IsdH^{N2N3}
Absorbance
Wavelength (nm)
C
+ 7 % IsdH^{N2N3}
+ 7 % IsdB^{N1N2}
Fe(III)Hb:apo-IsdA +
Normalised A406nm
Time (min)

4.3 IsdH^{N1} appears to hinder haem removal from Hb and transfer to IsdA/C

In addition to the IsdB-homologous region, IsdH contains a further N-terminal NEAT domain (IsdH^{N1}), which interacts with the α chain of Hb[146]. The role of the IsdH^{N1} domain in haem capture and transfer is unknown and it is possible that this domain is important for IsdH haem-transfer function. To investigate this, IsdH^{N1N2N3} was expressed and purified as for IsdH^{N2N3}, yielding ~90% pure protein by SDS-PAGE analysis (Fig. 4.4 A, B; cloning, expression and purification described in Sections 2.3 and 2.5). The apo-IsdH protein was produced by acid-acetone haem-extraction and, following refolding, apo-IsdH bound haem in a 1:1 stoichiometry (Fig.4.4 C).

Fe(III)-Hb was incubated with excess apo-IsdH^{N1N2N3} and the spectral changes were recorded. Interestingly, after a 10-min incubation the spectrum had not completely converted to that of holo-IsdH, suggesting that, unlike IsdH^{N2N3}, IsdH^{N1N2N3} took only a fraction of the haem groups (Fig.4.4 D, solid black line). A time course suggested an initial rapid uptake of ~50% of haem groups in ~60 s, which was similar to the activity seen for IsdH^{N2N3} (Fig. 4.4 E, F). However, removal of the remaining ~50% haem was dramatically slowed. The data suggest that IsdH^{N1} significantly inhibits haem transfer from ~50% of the globin chains.

Figure 4.4. Expression, purification, haem binding and haem capture properties of IsdH^{N1N2N3}. (A) Purification of IsdH^{N1N2N3} by Ni-affinity chromatography: *lane 1*, Kaleidoscope protein standards; *lane 2*, bacterial lysate; *lane 3*, flow through; *lanes 4–5*, 10 mM imidazole wash; *lanes 6–7*, 100 mM imidazole elution fractions; *lane 1*, Kaleidoscope protein standards. **(B)** Purification of IsdH^{N1N2N3} by anion exchange chromatography: *lane 1*, Mark 12 protein standards; *lane 2*, load condition; *lanes 3*, flow through; *lanes 4–9*, eluted fractions over a 50–300 mM NaCl gradient. **(C)** Titration of haem into apo-IsdH^{N1N2N3}. Data points were fit, by linear regression, in two groups. A 1:1 binding stoichiometry (assuming accurate concentration determination and K_d << working concentration) would see the linear fits intersect at the vertical dashed line. **(D)** UV-visible absorption spectra of Fe(III)-Hb (6 μM haem, corresponding to 1.5 μM tetramer), holo-IsdH^{N1N2N3} (6 μM) and apo-IsdH^{N1N2N3} (7.5 μM), showing that they are distinct. The spectrum of a mixture of Fe(III)-Hb (1.5 μM) and apo-IsdH^{N1N2N3} (7.5 μM) after a 10 min incubation at 4 °C is shown as a thicker solid line. **(E)** Spectra (taken at 40-s intervals) of a mixture of Fe(III)-Hb (1.5 μM) and apo-IsdH^{N1N2N3} (7.5 μM), which was incubated at 4 °C. The spectrum of Fe(III)-Hb (1.5 μM) is overlaid for comparison. Arrows indicate the direction of spectral change. **(F)** A time course over 200 min showing the percentage of haem remaining bound to Fe(III)-Hb (1.5 μM) after mixing with apo-IsdH^{N1N2N3} (7.5 μM). Time courses for Fe(III)-Hb mixed with apo-IsdH^{N2N3}, apo-IsdB^{N1N2} or IsdH^{N2N3}(Y642A) are shown for comparison. These data are representative of two measurements.

Figure 4.4

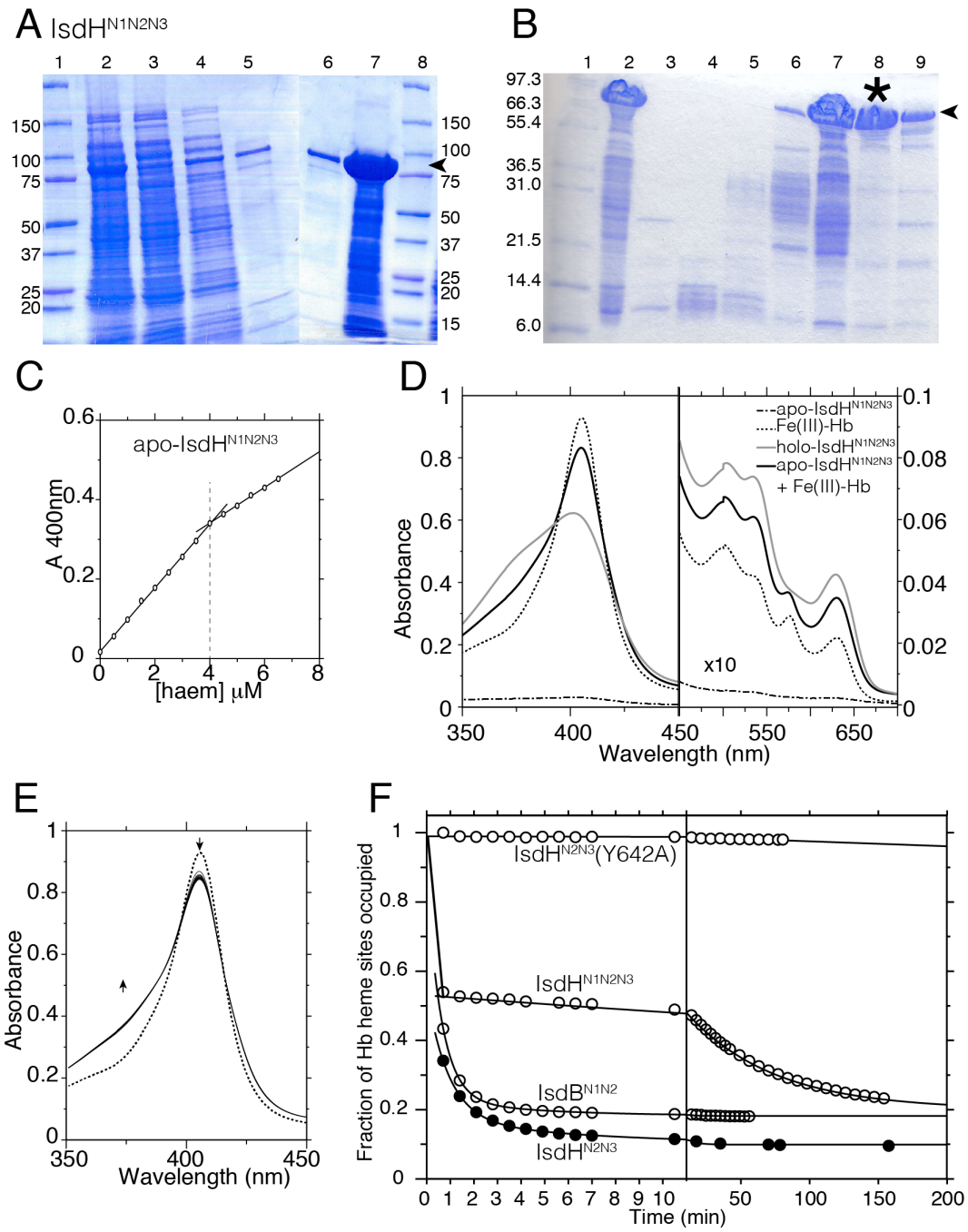
A IsdH^N1N2N3
1 2 3 4 5 6 7 8
150
100
75
50
37
25
20
150
100
75
50
37
25
20
15
B
1 2 3 4 5 6 7 8 9
97.3
66.3
55.4
36.5
31.0
21.5
14.4
6.0
*
C
apo-IsdH^N1N2N3
A 400nm
0.6
0.4
0.2
0
0 2 4 6 8
[haem] μM
D
---apo-IsdH^N1N2N3
.....Fe(III)-Hb
holo-IsdH^N1N2N3
apo-IsdH^N1N2N3
+ Fe(III)-Hb
x10
Absorbance
1
0.8
0.6
0.4
0.2
0
0.1
0.08
0.06
0.04
0.02
0
350 400 450 550 650
Wavelength (nm)
E
Absorbance
1
0.8
0.6
0.4
0.2
0
350 400 450
Wavelength (nm)
F
IsdH^N2N3(Y642A)
IsdH^N1N2N3
IsdB^N1N2
IsdH^N2N3
Fraction of Hb heme sites occupied
1
0.8
0.6
0.4
0.2
0
0 1 2 3 4 5 6 7 8 9 10 50 100 150 200
Time (min)

Next the role of IsdH^{N1} domain in haem relay was assessed. Fe(III)-Hb to was mixed with 125% apo-IsdC (measured as a % of the number of Hb haem sites in the reaction) and 13% apo-IsdH^{N1N2N3}. Strikingly, IsdH^{N1N2N3} did not transfer haem from Fe(III)-Hb to IsdC, indicating that the presence of the IsdH^{N1} domain strongly inhibits haem relay to downstream IsdC (Fig. 4.5 A, B). To explore the possibility that haem relay function was lost because IsdH^{N1N2N3} did not refold correctly during purification of the apo protein, the experiment was repeated using holo-IsdH^{N1N2N3} that was purified directly from *E. coli* without unfolding. The amount of haem contamination introduced by holo-IsdH^{N1N2N3} was small (only ~10% of the available IsdC binding capacity) and so should not prevent haem relay from Hb being observed. Similar to apo-IsdH^{N1N2N3}, holo-IsdH^{N1N2N3} was unable to enhance transfer of haem from Fe(III)-Hb to IsdC (Fig. 4.5 B, long-dashed line). In addition, IsdH^{N1N2N3} did not transfer haem from Fe(III)-Hb to IsdA (Fig. 4.5 C, D). Hence the IsdH^{N1} domain inhibits both haem capture and relay activity.

Taken together, the results presented in Sections 4.2 and 4.3 show that IsdB is a more efficient haem relay protein than IsdH *in vitro* and predict distinct roles for these proteins in *S. aureus* haem capture *in vivo*.

Figure 4.5. Haem transfer from Fe(III)-Hb to IsdC and IsdA in the presence of IsdH^{N1N2N3}. (A) Spectra recorded at 40-s intervals for a mixture of Fe(III)-Hb with 125% apo-IsdC (measured as a % of the number of Hb haem sites in the reaction) and 13.3% (per Hb haem) apo-IsdH^{N1N2N3}. **(B)** Normalised change in absorbance at 406 nm for mixtures of 1.5 mM Fe(III)-Hb with a 125% apo-IsdC (per Hb haem) and 13.3% apo-IsdH^{N1N2N3} (solid line) or holo-IsdH^{N1N2N3} (long dashed line). **(C)** Spectra recorded at 40 s intervals for a mixture of Fe(III)-Hb with 125% apo-IsdA (per Hb haem) and 7% (per Hb haem) apo-IsdH^{N1N2N3}. **(D)** Normalised change in absorbance at 406 nm for mixtures of 1.5 mM Fe(III)-Hb with a 125% apo-IsdA (per Hb haem) and 20% apo-IsdH^{N1N2N3} (solid line).

Figure 4.5

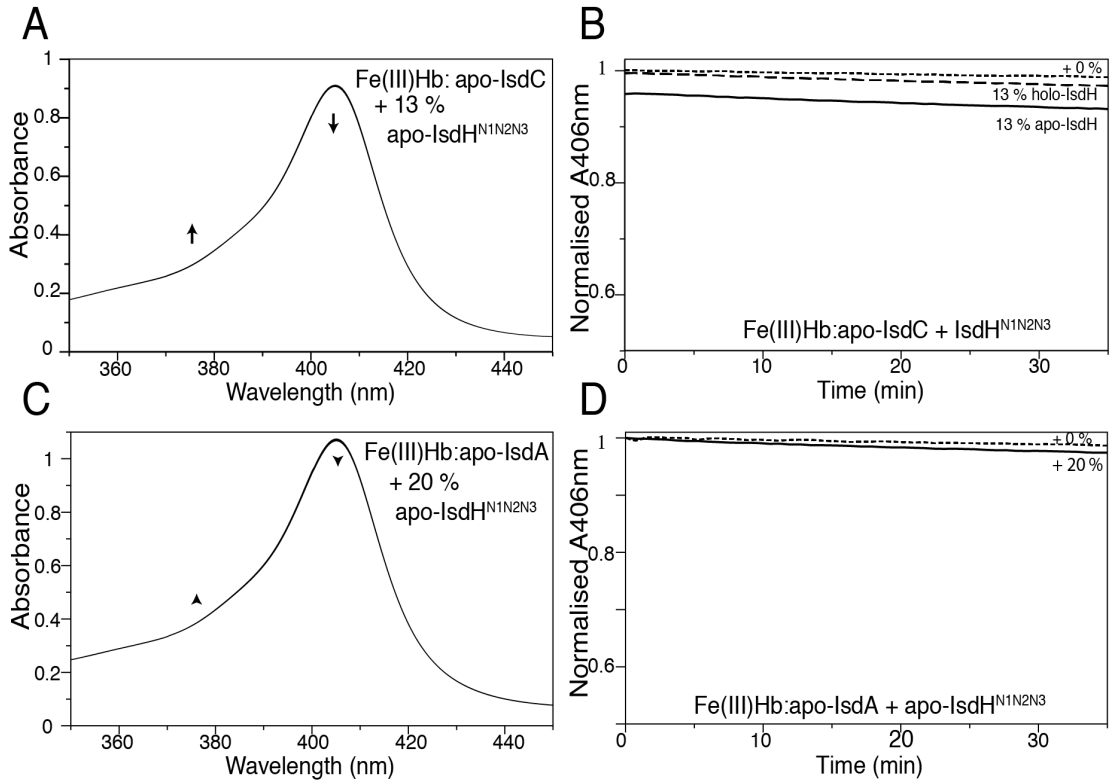
A
Absorbance
Wavelength (nm)
Fe(III)Hb: apo-IsdC
+ 13 %
apo-IsdH^N1N2N3
B
Normalised A406nm
Time (min)
+ 0 %
13 % holo-IsdH
13 % apo-IsdH
Fe(III)Hb:apo-IsdC + IsdH^N1N2N3
C
Absorbance
Wavelength (nm)
Fe(III)Hb:apo-IsdA
+ 20 %
apo-IsdH^N1N2N3
D
Normalised A406nm
Time (min)
+ 0 %
+ 20 %
Fe(III)Hb:apo-IsdA + apo-IsdH^N1N2N3

4.4 IsdH and IsdB interact differently with Hb.

To investigate interactions between IsdB/IsdH and Hb, SEC-RALLS experiments were performed. IsdH^{N1N2N3} eluted as a single peak and had a M_W of 72.5±0.9 kDa determined by RALLS – close to the expected value based on sequence (68 kDa, Fig.4.6 Ai, Table 4.1). The M_W of HbCO was 55.2±2.0 kDa, consistent with the dimer-tetramer equilibrium constant (K_d = 1.5 μM, expressed in units of molar haem and measured at ~20°C in 50–100 mM Na phosphate, pH 7.0[254,255]) and the working concentration; samples were loaded onto the column at ~136 μM haem (or 34 μM Hb tetramer), which is >10x K_d and therefore even with dilution on the column, Hb is expected to be predominantly tetrameric. A mixture containing one IsdH^{N1N2N3} per HbCO tetramer led to complete depletion of the Hb peak and a single broad peak eluting at an earlier time point (Fig.4.6 Aii). RALLS analysis indicated that this peak contained a mixture of species with M_W in the range 130–170 kDa. The smallest and the largest species in this peak are bigger than the expected M_W of one IsdH molecule bound to one Hb dimer (100 kDa) or one Hb tetramer (132 kDa). Each IsdH^{N1N2N3} molecule contains two Hb binding NEAT domains that are separated by an unstructured linker and have the potential to independently bind to Hb chains from the same Hb molecule, or different Hb molecules, potentially leading to extended chains of IsdH-linked Hb. I did not investigate these interaction models further and the primary conclusion was that IsdH forms stable complexes with Hb.

The full-length IsdB protein (residues 41–609) eluted as a single peak with a measured M_W of 70.6 kDa, close to the expected value of 66.4 kDa (Fig.4.6 Bi, Table 4.1). When IsdB was mixed at a 1:1 molar ratio with HbCO (per Hb tetramer), two peaks were observed with M_W practically the same as the M_W of the free proteins (Fig.4.6 Bii, black dashed line; Table 4.1). Slight peak broadening and shift to an earlier elution volume provided some evidence of an interaction. At a 2:1 mixing ratio (Fig. 4.6 Bii, grey dashed line) the Hb peak was substantially broadened and the IsdB peak showed a change in mobility suggesting a very weak interaction (M_W 80–90 kDa across peak). This behaviour contrasts with the stable binding observed for a 1:1 mixture of IsdH^{N1N2N3} and Hb (which has an equivalent number of Hb binding sites to the 2:1 IsdB:Hb mixture), indicating that IsdB and IsdH interact differently with Hb.

The presence of an additional domain in IsdH^{N1N2N3}, or unstructured N- and C-terminal regions in IsdB, may modify the Hb-interaction functions of the conserved region. Therefore, to investigate if sequence differences in the homologous regions of IsdB and IsdH result in different interactions with Hb, a similar analysis to that described above was performed with the IsdH^{N2N3} and IsdB^{N1N2} constructs. The free IsdH^{N2N3} protein eluted as a single peak (Fig. 4.7 Ai), however had a M_W of 57.7±0.5 kDa, which is larger than expected based upon the primary sequence (41.4 kDa) suggesting some aggregation of the protein. The molecular weight was reduced upon dilution (51.5±0.5 kDa), possibly indicating a concentration-dependent self-association. To determine whether the IsdH^{N2N3} protein undergoes reversible or irreversible aggregation, a dilution series should be performed and M_W measurements made over a 10-fold change in concentration. This was not investigated further as the small amount of aggregation did not prevent an interaction with Hb; a 2:1 mixture of IsdH^{N2N3} with HbCO produced a single SEC peak corresponding to a protein complex with a molecular weight of 124 kDa (Fig. 4.7 Aii). The M_W measured for Hb (55.2±2.0 kDa) indicates that ~70% of mass is distributed as tetramers. Assuming one IsdH^{N2N3} bound to each αβ dimer, and assuming the dimer-tetramer equilibrium to be unaltered by the binding of IsdH^{N2N3}, the expected M_W would be 126 kDa, which is similar to the measured value.

The free IsdB^{N1N2} protein eluted as a single SEC peak (Fig. 4.7 Bi), however also had a M_W slightly larger than expected (48.8±0.2 kDa vs 42.3 kDa), again proving some evidence of aggregation. A 2:1 mixture of IsdB^{N1N2} with HbCO gave rise to a much smaller shift in peak elution time, compared to IsdH^{N2N3}, and the M_W measured across this peak (68 kDa) was only marginally greater than the M_W of the free proteins (Fig. 4.7 Bii, Table 4.1). Assuming that IsdB does not dramatically alter the dimer-tetramer equilibrium of Hb, these data suggest that interactions between IsdB and Hb are considerably weaker that interactions between IsdH^{N2N3} and Hb.

Table 4.1. M_W measurements of IsdB and IsdH and their complexes with HbCO by SEC-RALLS.

Protein	Concentration mg/ml (μM)	M_W Peak 1**† (kDa)	M_W Peak 2 (kDa)
HbCO	2.2 (34)*	55.2±2.0	-
$IsdH^{N1N2N3}$	2.6 (38)	72.5±0.9 (68)	-
$IsdH^{N1N2N3}$:HbCO 1:1	4.6	130–170	-
HbCO	2.2 (34)	46.4	-
IsdB	2.5 (38)	70.6 (66.4)	-
IsdB:HbCO 1:1	4.5	71.5	48.4
IsdB:HbCO 2:1	6.7	80–90	52.8
HbCO	2.2 (34)	55.2±2.0	-
Holo-$IsdH^{N2N3}$	1 (24)	51.5±0.5 (41.4)	-
Holo-$IsdH^{N2N3}$	2.9 (69)	57.7±0.5 (41.4)	-
Holo-$IsdH^{N2N3}$:HbCO 2:1	5	123.8	-
Holo-$IsdB^{N1N2}$	2.7 (65)	48.8±0.2 (42.3)	-
Holo-$IsdB^{N1N2}$	5.6 (132)	51.0±0.5 (42.3)	-
Holo-$IsdB^{N1N2}$:HbCO 2:1	4.9	67.7	-

*Calculated as Hb tetramer
**Where given, errors are ± S.E. for two or three repeat measurements
†Values in parentheses are the molecular weights calculated from primary sequence

Figure 4.6. SEC of mixtures of Hb with $IsdH^{N1N2N3}$ and IsdB. (Ai) SEC elution traces of free Hb (black) and $IsdH^{N1N2N3}$ (blue). (ii) A 1:1 mixture $IsdH^{N1N2N3}$ with Hb tetramer (black dotted line) and a 2:1 mixture of $IsdH^{N1N2N3}$ with Hb tetramer (grey dashed line). **(Bi)** SEC elution traces of free Hb (black) and IsdB (orange). (ii) A 1:1 mixture IsdB with Hb tetramer (black dotted line) and a 2:1 mixture of IsdB with Hb tetramer (grey dashed line).

Figure 4.7. SEC of mixtures of Hb with $IsdH^{N2N3}$ and $IsdB^{N1N2}$. (Ai) Upper panel: SEC elution traces of free Hb (black) and $IsdH^{N2N3}$ (green). (ii) A 2:1 mixture of $IsdH^{N2N3}$ with Hb tetramer (grey dashed line). **(Bi)** Upper panel: SEC elution traces of free Hb (black) and $IsdB^{N1N2}$ (purple). (ii) A 2:1 mixture of $IsdB^{N1N2}$ with Hb tetramer (grey dashed line).

Figure 4.6

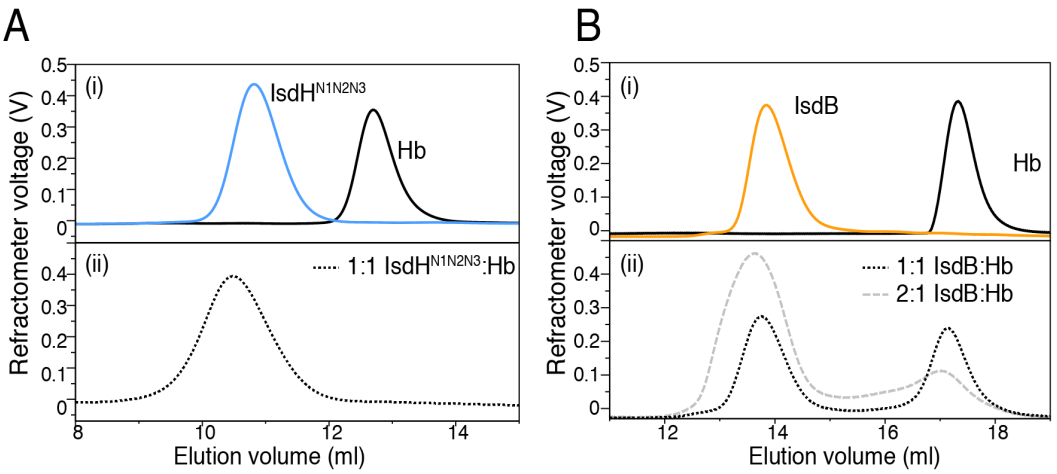

Figure 4.7

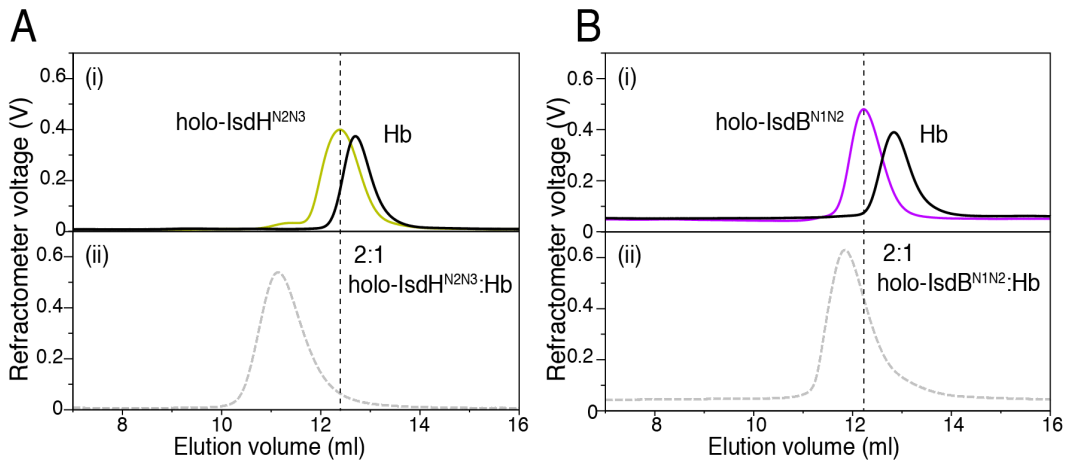

4.5 IsdH binds stably to α Hb and transiently to β Hb, while IsdB binds transiently to both α and β Hb

To determine which globin chain forms the primary binding site for IsdH and IsdB, Hb was separated into isolated α and β chains using *p*-hydroxymercuribenzoate (PMB), which modifies cysteine side chains at the $\alpha_1\beta_1$ interface and prevents the formation of αβ dimers[256]. The cysteine modification was reversed following chromatographic separation of the α^{PMB} and β^{PMB} chains, by the addition of excess DTT. The separated Hb chains used in this thesis were prepared by D. Gell and K. Krishna Kumar.

The $IsdH^{N1N2N3}$ protein, which is well resolved from the free globin chains (Fig. 4.8 Ai), generated a stable complex with α Hb (Fig. 4.8 Aii). As α Hb was added in increasing concentrations (0–2.5 molar equivalents) to $IsdH^{N1N2N3}$ the M_W increased to reach a plateau at 99 kDa (Table 4.2), close to the M_W expected for a 2:1 complex of $IsdH^{N1N2N3}$:α Hb of 98.2 kDa. The conclusion is that the $IsdH^{N1}$ and $IsdH^{N2}$ domains each bind to one α Hb chain. The elution profile for a 1:1 mixture of $IsdH^{N1N2N3}$ and β Hb is shown in Figure 4.8 Aiii, where a residual peak of unbound free β Hb suggests weaker binding to β Hb.

Table 4.2. M_W measurements IsdH and IsdH:CO-αHb complexes by SEC-RALLS.

Protein	Concentration mg/ml (μM)	M_W Peak 1 kDa (expected)	M_W Peak 2 kDa
αHbCO	0.48 (32)	15.4 (15.1)	-
IsdH	1 (15)	71 (68)	-
IsdH:αHbCO 1:0.8	1.13	88	-
IsdH:αHbCO 1:1.6	1.27	95	-
IsdH:αHbCO 1:2.2	1.58	96	-
IsdH:αHbCO 1:2.5	1.72	99	19

Similar SEC analyses showed that holo-$IsdH^{N2N3}$ and $IsdH^{N2N3}$(Y642A) formed stable complexes with α Hb and displayed weaker binding to β Hb (Fig. 4.8 B, C), as seen for the full-length protein. The overall similarity in SEC traces for haem-bound $IsdH^{N2N3}$ and the Tyr642-to-Ala mutant, which is unable to bind haem, indicate that the presence of haem did not prevent interaction with Hb, and therefore it is unlikely that uptake of haem causes a structural change in the receptor that triggers Hb to be released.

When IsdB was mixed with either α or β Hb, only a small change in mobility of the free globin peak was observed, suggesting that IsdB interacts weakly with both globin chains (Fig. 4.8 D). By the same criteria, the haem bound $IsdB^{N1N2}$ and $IsdB^{N1N2}$(Y440A) constructs also formed a weak interaction with α Hb (Fig. 4.8 E, F). Significant peak overlap made it difficult to determine the interaction with β Hb (Fig. 4.8 Eiii, Fiii). By analogy with IsdH, it was predicted that interactions between IsdB and Hb would be mediated through the $IsdB^{N1}$ domain. To test this, the isolated $IsdB^{N1}$ domain was produced. A small change in the mobility of α Hb in the presence of $IsdB^{N1}$ was evidence of weak interaction (Fig. 4.9 ii). No interaction with β Hb was detected (Fig. 4.9 iii). A comparison of β Hb peak mobility in Figure 4.8 Eiii, Fiii and Figure 4.9 iii suggested that binding to β Hb was stronger for $IsdB^{N1N2}$ than for the isolated $IsdB^{N1}$ domain. Thus, regions outside of the N-terminal NEAT domain, for example in the Linker domain and/or $IsdH^{N3}$ domain, may contribute significantly to the binding affinity for β Hb. In a very recent publication, Bowden *et al.* measured Hb binding affinity of 422 nM for $IsdB^{N1N2}$ by ITC and no interaction was detected between Hb and the isolated $IsdB^{N1}$ domain[230]. Taken together with the data of Bowden *et al.*, the data presented in Figures 4.8 and 4.9 support the conclusion that weak interactions, mediated by multiple IsdB domains, contribute to α and β Hb binding in a cooperative fashion, and, that the Linker and $IsdB^{N2}$ domains contribute a greater part of the overall binding affinity for the β Hb chain. In summary, IsdH makes stable interactions with α Hb through both the $IsdH^{N1}$ and $IsdH^{N2}$ domains and binds weakly to β Hb, while IsdB shows weak interactions with both globin chains.

Figure 4.8. SEC analysis of IsdH and IsdB binding to the isolated α and β chains of Hb. (A–F) SEC elution traces of $IsdH^{N1N2N3}$ (A), holo-$IsdH^{N2N3}$ (B), or $IsdH^{N2N3}$(Y642A) (C)**,** IsdB (D), holo-$IsdB^{N1N2}$ (E) or $IsdB^{N1N2}$(Y440A) (F) with, or without, addition of isolated α and β Hb. In each of A–F, SEC traces are shown for (i) free α Hb (red), β Hb (pink) and IsdH (blue) or IsdB protein (orange), (ii) a 1:1 molar mixture of IsdH/IsdB with α Hb, and (iii) a 1:1 molar mixture of IsdB with β Hb.

Figure 4.8

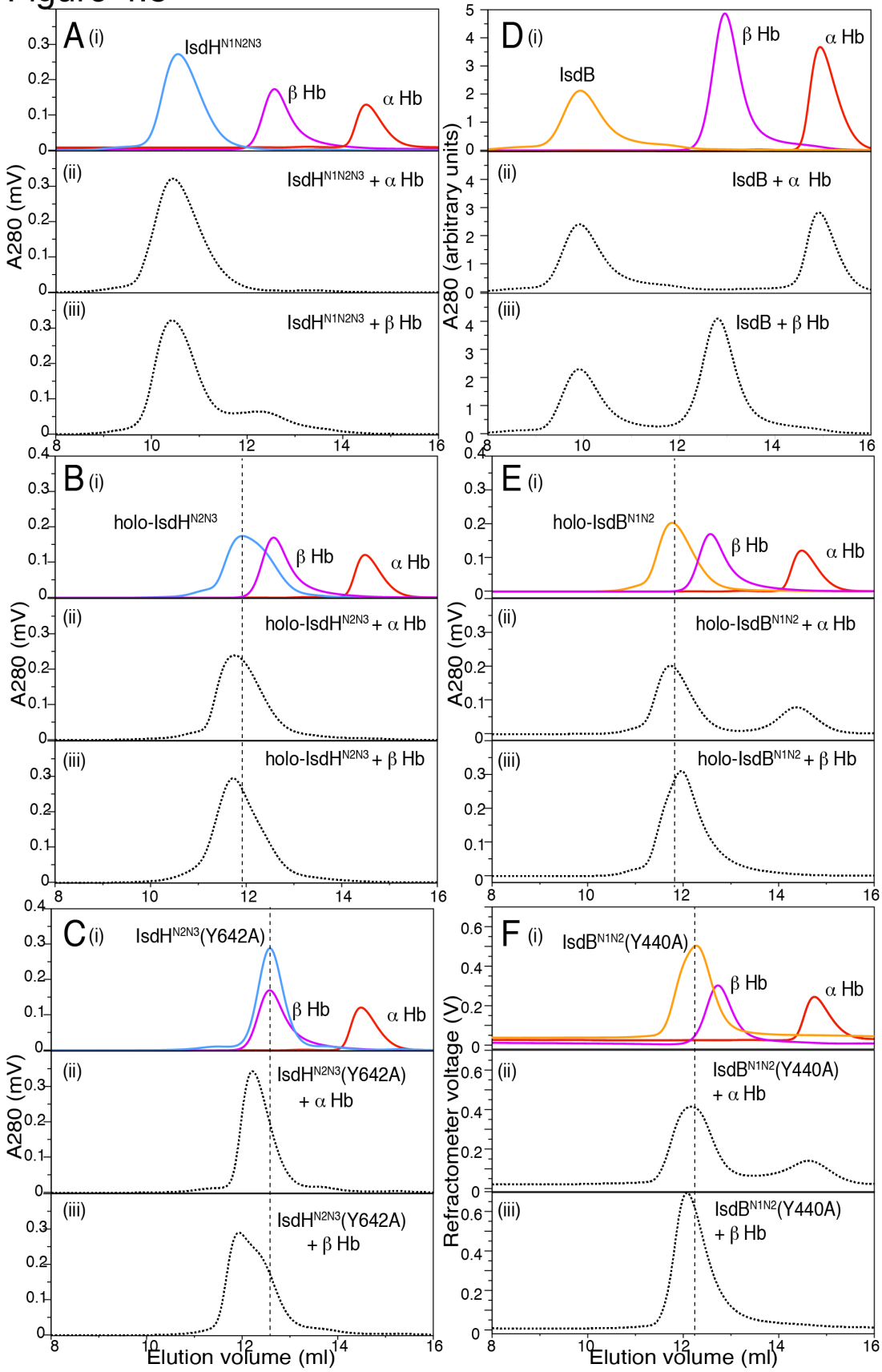
A (i)
IsdH^N1N2N3
β Hb
α Hb
(ii)
IsdH^N1N2N3 + α Hb
(iii)
IsdH^N1N2N3 + β Hb
A280 (mV)
D (i)
IsdB
β Hb
α Hb
(ii)
IsdB + α Hb
(iii)
IsdB + β Hb
A280 (arbitrary units)
B (i)
holo-IsdH^N2N3
β Hb
α Hb
(ii)
holo-IsdH^N2N3 + α Hb
(iii)
holo-IsdH^N2N3 + β Hb
A280 (mV)
E (i)
holo-IsdB^N1N2
β Hb
α Hb
(ii)
holo-IsdB^N1N2 + α Hb
(iii)
holo-IsdB^N1N2 + β Hb
A280 (mV)
C (i)
IsdH^N2N3(Y642A)
β Hb
α Hb
(ii)
IsdH^N2N3(Y642A)
+ α Hb
(iii)
IsdH^N2N3(Y642A)
+ β Hb
A280 (mV)
Elution volume (ml)
F (i)
IsdB^N1N2(Y440A)
β Hb
α Hb
(ii)
IsdB^N1N2(Y440A)
+ α Hb
(iii)
IsdB^N1N2(Y440A)
+ β Hb
Refractometer voltage (V)
Elution volume (ml)

Figure 4.9. SEC analysis of IsdB^{N1} binding to the isolated α and β chains of Hb. (i) SEC elution trace of free IsdB^{N1} (orange). (ii) SEC elution traces of free α Hb (black) overlaid with a 1:1 mixture of IsdB^{N1} and α Hb (grey dashed line). (iii) SEC elution traces of free β Hb (black) overlaid with a 1:1 mixture of IsdB^{N1} and β Hb (grey dashed line).

Figure 4.9

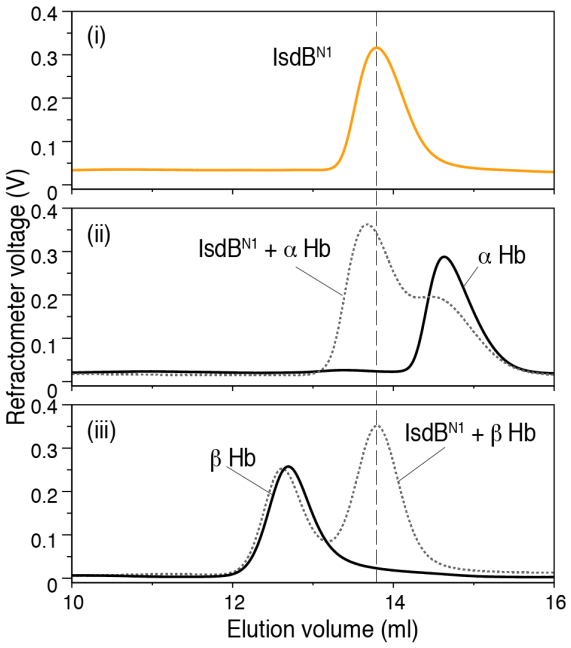
(i)
IsdB^{N1}
(ii)
IsdB^{N1} + α Hb
α Hb
(iii)
β Hb
IsdB^{N1} + β Hb
Refractometer voltage (V)
0.4
0.3
0.2
0.1
0
10
12
14
16
Elution volume (ml)

4.6 Haem relay activity of IsdB and IsdH correlates with Hb binding affinity

It was hypothesised that the differences in Hb binding affinity between IsdH and IsdB may be responsible for the differences in haem relay activity by influencing the rate at which the receptor is recycled between consecutive Hb chains and IsdA/C. In order to rank the Hb binding affinities of IsdB, IsdH, and their isolated NEAT domains, SEC was used to detect the quantity of unbound Hb at a range of IsdB/H concentrations. To investigate binding to the α chain, increasing concentrations of Isd protein were mixed with a fixed concentration of α Hb (12.6 μM) and subject to SEC analysis. In Figure 4.10 A–G the α Hb peak alone is shown in black. The curves for mixtures containing α Hb and 2.5–50 μM Isd protein (corresponding to 0.2–4 fold molar excess over α Hb) are overlaid and coloured in a spectrum from blue to red. In Figure 4.10 A, C, E the single NEAT domains eluted at the same time as the free α Hb peak and so elution traces were recorded at 410 nm; at this wavelength α Hb can be detected by virtue of the constituent haem group, whereas $IsdH^{N1}$, $IsdH^{N2}$ and $IsdB^{N1}$ do not absorb visible light. The full-length Isd proteins were well resolved from α Hb and mixtures of these proteins were monitored at 280 nm (Fig. 4.10 D, F, G). To compare the α binding behaviours the change in height of the free α Hb peak was plotted against Isd:αHb mixing ratio (Fig. 4.10 H).

Upon addition of increasing concentrations of $IsdH^{N1}$ the free αHb peak was reduced to zero (a relative reduction in α Hb peak height of '1' in Figure 4.10 H) and the change in α Hb peak height with increasing $IsdH^{N1}$ concentration was linear (Fig. 4.10 H, solid black line), indicating complete complex formation with each addition of $IsdH^{N1}$. Hence the equilibrium dissociation constant for this interaction is presumed to be well below the working protein concentrations (~μM on the column). In this case, the [NEAT]/[αHb] ratio at which the free α Hb peak is depleted gives the stoichiometry, which for $IsdH^{N1}$, occurs at a 1:1 molar stoichiometry (Fig. 4.10 A, H, filled circles, solid black line). For comparison, the same experiment was performed with α Hb stabilising protein (AHSP), which forms a heterodimer with α Hb with K_d = 20 nM[257]. AHSP caused the same quantitative depletion of α Hb (Fig. 4.10 B, H) as seen with $IsdH^{N1}$, indicating 1:1 stoichiometry with sub-micromolar affinity. In contrast to $IsdH^{N1}$, 2–4 molar-equivalents

of IsdH^{N2} (Fig. 4 C, H) or IsdH^{N2N3}(Y642A) (Fig. 4.10 D, H) were required in order to reduce the free α Hb peak to undetectable levels, indicative of weaker α Hb binding compared to IsdH^{N1}. Note, an additional peak eluting after α Hb in Figure 4.10 D is a contaminating species that was present in the IsdH^{N2N3}(Y642A) sample used in this experiment.

The addition of up to 4 molar equivalents of IsdB^{N1}, IsdB^{N1N2} or IsdB^{N1N2}(Y440A) did not deplete the free α Hb peak but caused peak broadening consistent with a very weak interaction (Fig. 4.10 E–G). An alternative explanation for changes in peak shape/mobility might be that Isd proteins are inducing haem loss from α Hb leading to globin aggregation. However IsdH^{N2}, IsdH^{N2N3}(Y642A), IsdB^{N1} and IsdB^{N1N2}(Y440A) did not induce changes in the UV-visible spectrum of Hb (see Section 3.3.1)[167,230] suggesting that this is unlikely.

Based on the curves shown in Figure 4.10, Isd domains were ranked in order of decreasing affinity for αHb as follows: IsdH^{N1} > IsdH^{N2} ≈ IsdH^{N2N3} >> IsdB^{N1} ≈ IsdB. A comparison with the independently determined binding affinity of α Hb for IsdH^{N1} (K_d = 20–100 nM)[145-147] suggests that the K_d > 100 nM for all other interactions tested here. Peak overlap between Isd:β Hb complexes and free β Hb prevented a similar analysis of β Hb interactions. Unlike native β Hb chains which are in equilibrium between monomeric, dimeric and tetrameric species, modified β^{PMB} chains are predominantly monomeric[258] and so are predicted to be well separated from Isd:β^{PMB} complexes. Therefore, the PMB modified β chains could be used in future studies to compare the strength of Isd:β Hb interactions. As the PMB modification is on the α1β1 interface, away from the Isd interaction surface, it is not expected to prevent Isd:β Hb interactions.

Figure 4.10. Relative affinities of IsdH and IsdB constructs for isolated α Hb by SEC titration experiments. (A–G) The UV trace of 12.6 μM α Hb (black) overlaid with traces of 12.6 μM α Hb mixed with 0.2 (blue), 0.4 (cyan), 0.8 (green), 1.2 (yellow), 2 (orange) or 4 (red) molar equivalents of: $IsdH^{N1}$ (A), AHSP (B), $IsdH^{N2}$ (C), $IsdH^{N2N3}$(Y642A) (D), $IsdB^{N1}$ (E), IsdB (F), or $IsdB^{N1N2}$(Y440A) (G). Traces were recorded at 280 nm or 410 nm (arbitrary units) with the wavelength remaining the same for each titration series. **(H)** The fraction changes in α Hb peak height at different mixing ratios with Isd protein.

Figure 4.10

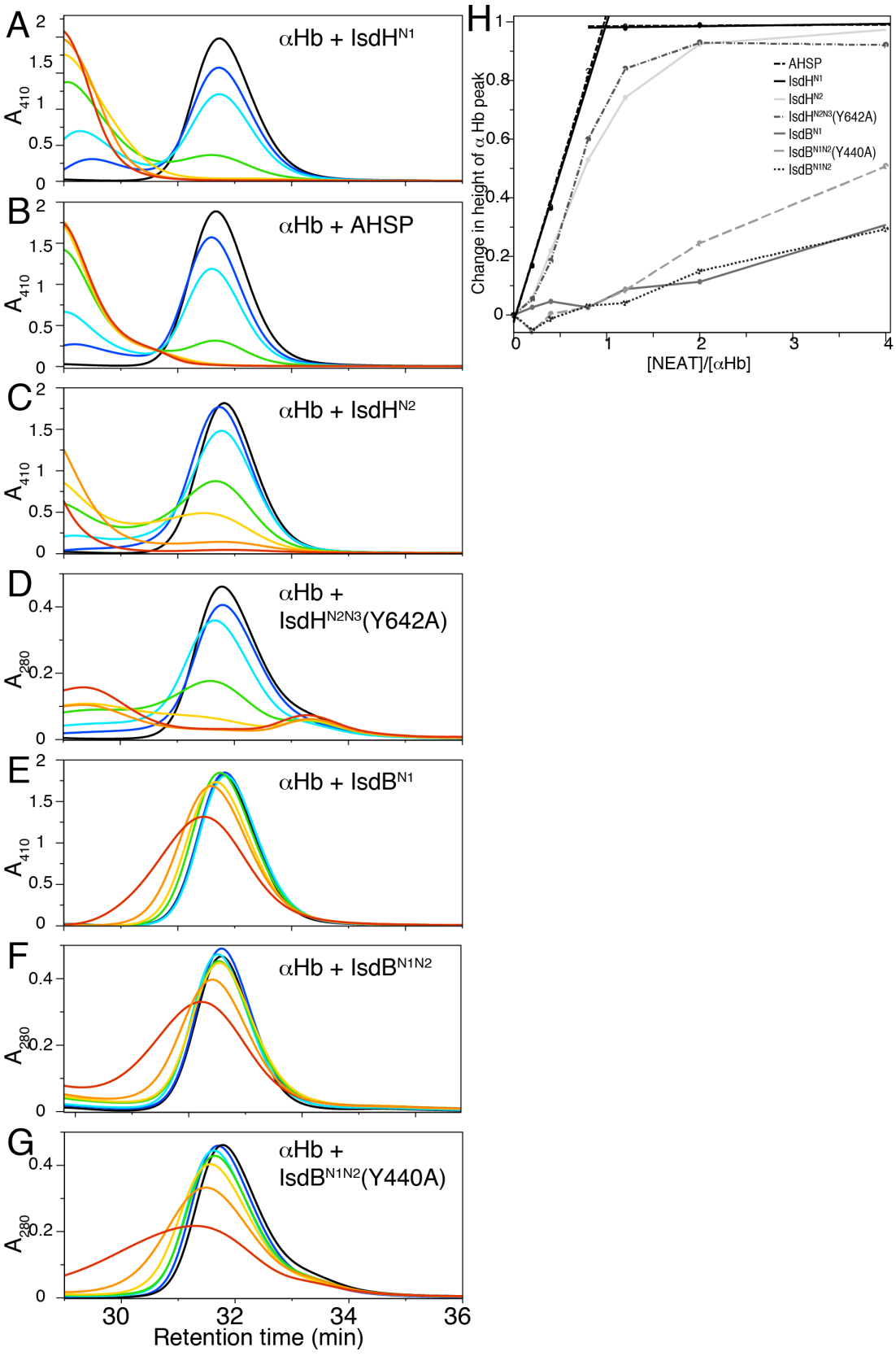
A
αHb + IsdH^N1
B
αHb + AHSP
C
αHb + IsdH^N2
D
αHb + IsdH^N2N3(Y642A)
E
αHb + IsdB^N1
F
αHb + IsdB^N1N2
G
αHb + IsdB^N1N2(Y440A)
A410
A280
Retention time (min)
H
Change in height of α Hb peak
[NEAT]/[αHb]
AHSP
IsdH^N1
IsdH^N2
IsdH^N2N3(Y642A)
IsdB^N1
IsdB^N1N2(Y440A)
IsdB^N1N2

4.7 Haem transfer in the IsdH^{N2N3}:Hb complex does not trigger disassembly of the complex

To explore the possibility that haem transfer from Hb might lead to unfolding of the globin chain and subsequent dissociation of the IsdH:Hb complex, mixtures of apo-IsdH^{N2N3} and Fe(III)-Hb were assessed by SEC. To demonstrate that the refolded apo protein was competent to bind Hb, it was first mixed with HbCO and the elution profiles and measured molecular weights were compared to those of holo-IsdH^{N2N3}:Hb complexes (Fig. 4.11 A, Table 4.3). Figure 4.11 Aii shows that apo-IsdH^{N2N3} formed a complex with Hb at both 1:1 and 2:1 mixing ratios and that the elution profiles were similar to those of the holo-IsdH^{N2N3}:Hb complexes. In addition, the average molecular weights for the holo and apo complexes were unchanged (Table 4.3), indicating that the apo-protein is fully functional to bind to Hb.

Next, apo-IsdH^{N2N3} or the control, holo-IsdH^{N2N3}, was mixed with Fe(III)-Hb. The protein mixtures were incubated overnight and then separated by gel filtration. A 5:1 molar excess (per Hb tetramer) was used to ensure that all of the haem could be transferred to the apo-receptor. Haem content was determined by UV-visible absorption spectra using an inline UV-detector, or by collecting the peaks as they eluted off the column and then recording spectra. The elution profiles of Fe(III)-Hb mixed with apo-IsdH^{N2N3} or holo-IsdH^{N2N3} are overlaid in Figure 4.11 B; each profile contains two peaks. The UV-visible absorption spectrum of Peak 1 derived from the holo-IsdH^{N2N3}:Fe(III)-Hb mixture contained contributions from both IsdH and Hb (Fig. 4.11 C, green trace) and the molecular species eluting in Peak 1 had a M_W of 130 kDa, indicating that an holo-IsdH^{N2N3}:Fe(III)-Hb complex was formed. The UV-visible spectrum of Peak 1 of the apo-IsdH^{N2N3}:Fe(III)-Hb mixture resembled haem-bound IsdH only (Fig. 4.11 C, blue trace), and the M_W of species in this peak was 110 kDa. These data suggest the presence of a holo-IsdH^{N2N3}:apo-Hb complex, and therefore that, despite haem transfer, the IsdH and Hb proteins remained in a complex. To confirm identity and stoichiometry of the polypeptides in each peak, elution fractions should be collected across the two peaks for the holo and apo complexes, and analysed by SDS-PAGE. In both samples, Peak 2 had a UV-visible spectrum characteristic of haem-bound IsdH^{N2N3} (Fig. 4.11 D) and the M_W measured across the peak was consistent with IsdH^{N2N3} monomer (Table 4.3), thus Peak 2

corresponded to the excess unbound receptor. Hence, haem transfer to IsdH does not appear to trigger disassembly of the complex.

Table 4.3. M_W measurements apo-IsdH and apo-IsdH:Hb complexes by SEC-RALLS.

Protein	Concentration mg/ml (μM)	M_W Peak 1 kDa (expected)	M_W Peak 2 kDa
HbCO	0.5 (8)	32.1±0.1*	-
Holo-IsdH^{N2N3}	0.65 (16)	51 (41.4)	-
Holo-IsdH^{N2N3}:HbCO 1:1	0.82	98	40
Holo-IsdH^{N2N3}:HbCO 2:1	1.15	116	-
Apo-IsdH^{N2N3}	0.65 (16)	61 (41.4)	-
Apo-IsdH^{N2N3}:HbCO 1:1	0.82	95	39
Apo-IsdH^{N2N3}:HbCO 2:1	1.15	120	-
Holo-IsdH^{N2N3}:Fe(III)-Hb 5:1	2.1	132	62
Apo-IsdH^{N2N3}:Fe(III)-Hb 5:1	2.1	110	64
Holo-IsdH^{N2N3}:HbCO 5:1	2.1	130	62

*Error is given as ± SE for two measurements

Figure 4.11. SEC analysis of the interaction of apo-IsdH^{N2N3} with Hb. (Ai**)** SEC elution traces of free CO-Hb (black), holo-IsdH^{N2N3} (green) and apo-IsdH^{N2N3} (blue). (ii) A 1:1 molar mixture of holo-IsdH^{N2N3} with CO-Hb tetramer (black solid line) overlaid with a 2:1 molar mixture of holo-IsdH^{N2N3} with CO-Hb tetramer (grey solid line), a 1:1 molar mixture of apo-IsdH^{N2N3} with CO-Hb tetramer (black dashed line) and a 2:1 molar mixture of holo-IsdH^{N2N3} with CO-Hb tetramer (grey dashed line). **(B)** A 5:1 molar mixture of holo-IsdH^{N2N3} (green) or apo-IsdH^{N2N3} (blue) with Fe(III)-Hb. Mixing ratios are per Hb tetramer. **(C)** The UV-visible absorption spectra of Peak 1 collected from the SEC runs shown in B. **(D)** The UV-visible absorption spectra of Peak 2 collected from the SEC run shown in B. The holo-IsdH^{N2N3}:Hb complex is coloured green while the apo-IsdH^{N2N3}:Hb complex is coloured blue.

Figure 4.11

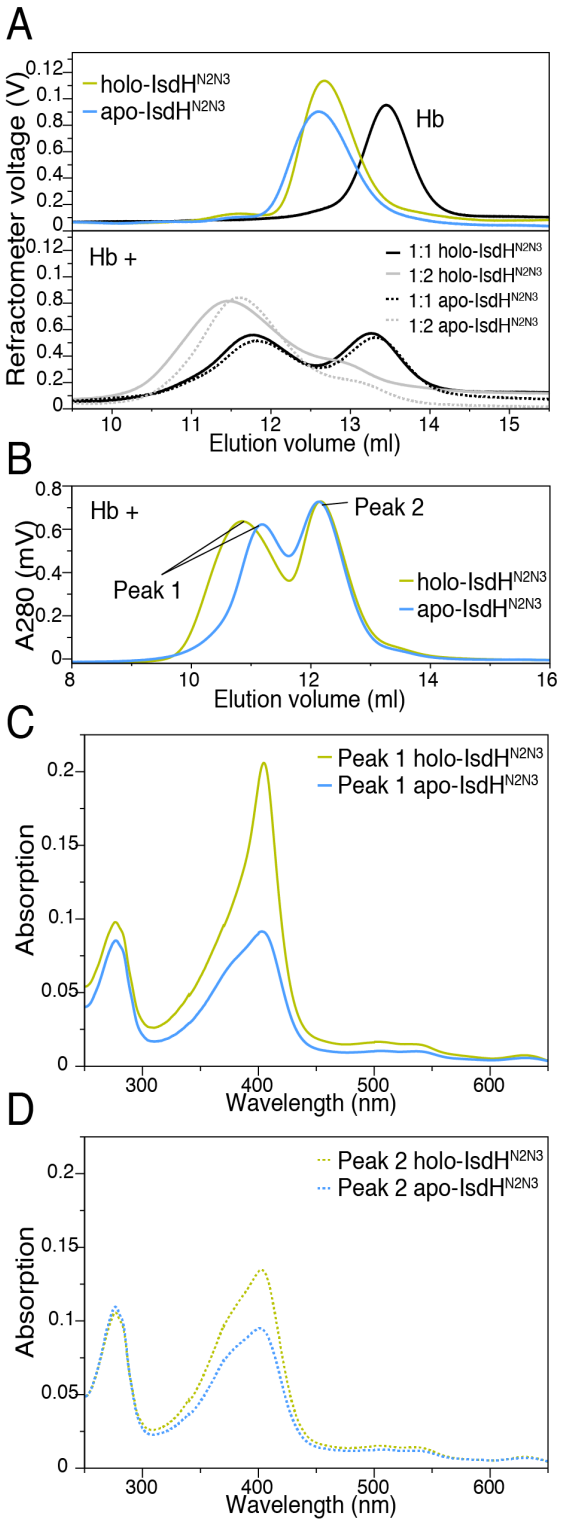
A
Refractometer voltage (V)
holo-IsdH^N2N3
apo-IsdH^N2N3
Hb
Hb +
1:1 holo-IsdH^N2N3
1:2 holo-IsdH^N2N3
1:1 apo-IsdH^N2N3
1:2 apo-IsdH^N2N3
Elution volume (ml)
B
A280 (mV)
Hb +
Peak 2
Peak 1
holo-IsdH^N2N3
apo-IsdH^N2N3
Elution volume (ml)
C
Absorption
Peak 1 holo-IsdH^N2N3
Peak 1 apo-IsdH^N2N3
Wavelength (nm)
D
Absorption
Peak 2 holo-IsdH^N2N3
Peak 2 apo-IsdH^N2N3
Wavelength (nm)

4.8 Discussion

IsdB but not IsdH was able to rapidly and quantitatively capture haem from Hb and catalyse its transfer to the downstream haem binding proteins IsdA and IsdC *in vitro*. This is the first biochemical study to identify a difference in activity between IsdH and IsdB and provides a rationale for the observation that IsdB but not IsdH is required for *S. aureus* growth using Hb as an iron source in *in vitro* growth assays[8,84]. This difference in function predicts that IsdB and IsdH will have distinct roles in haem uptake during infection, and is consistent with a different requirement for IsdB or IsdH during colonisation of different organs in *in vivo* infection models[84,174,203].

The work in this chapter has established an inverse correlation between haem relay activity and Hb binding affinity. It is possible that a weak interaction with Hb may be an important part of the haem relay mechanism, because a weak interaction would allow for rapid recycling of the receptor. The 'handclasp mechanism' of haem transfer between IsdA and IsdC involves an interaction between the haem pockets of donor and acceptor proteins[170,171]. Based on the structure of $IsdH^{N2N3}$ bound to Hb (Chapter 3) such an interaction could not occur without large conformational changes in the IsdB/H receptors or dissociation of the complex. The hypothesis that a weak interaction with Hb is important for catalysis of haem relay by IsdB is explored further in Chapter 5.

Previous measurements of IsdB:Hb affinity have ranged from 55 nM (obtained by SPR)[8,145] to 422 nM (obtained by ITC)[230], however, the SEC experiments performed here suggest that the interaction is much weaker – in the mM–μM range[259]. The reasons for this discrepancy are unclear; however, the preparations of IsdB used in this thesis are clearly competent to capture haem from Hb and rapidly transfer this haem to IsdA/C with much higher activity than IsdH constructs, hence it is presumed that IsdB preparations are correctly folded and active. A systematic analysis of all Hb binding NEAT domains via multiple biophysical methods is required to provide accurate measurements of Hb binding affinities and to allow further comparisons of Hb binding activity.

It has been suggested that IsdB is the protein that is primarily responsible for binding Hb to the surface of *S. aureus,* as Hb binding is largely abolished in *ΔisdB* strains[208,260]. This is at odds with the higher affinity binding to Hb demonstrated by IsdH compared to IsdB.

Part of the answer might be that IsdB is more highly abundant than IsdH on the cell surface under low iron conditions[5,6,98,202] and therefore the contribution from IsdH may be masked. Fluorescence imaging studies performed by Pishchany *et al.,* indicated that, while Hb and IsdB colocalise on surface, Hb fluorescence is punctate and IsdB fluorescence is diffuse[260]. They concluded that either multiple IsdB molecules are required to bind Hb (avidity effect) or that an additional factor may be involved in Hb binding by IsdB.

Interestingly, the relative Hb binding affinities of $IsdH^{N1}$, $IsdH^{N2}$ and $IsdB^{N1}$ determined in Section 4.6 correlate with the reported binding activities for Hp. $IsdH^{N1}$ binds to Hp with higher affinity (K_d 5–35 μM)[145,146] than $IsdH^{N2}$ (binding observed but affinity not determined), and no binding has been observed for IsdB[83,145]. Pilpa *et al.,* showed that mutagenesis of the Hb binding interface of $IsdH^{N1}$ removes interaction with Hp[147]. These findings have suggested that the same interface of NEAT domain can interact with the unrelated folds of Hb and Hp. However, the SEC experiments in Chapter 3 failed to detect an interaction with Hp and an alternative explanation is that apparent IsdH:Hp interactions are a result of binding though contaminating Hb. Hp has exceptionally high affinity for Hb, making it is possible that preparations of Hp from human serum contain small amounts of contaminating Hb. The presence of contaminating Hb may not be seen in a gel filtration experiment, which observes the bulk response, while SPR or ELISA, are expected to be more sensitive to a less abundant species.

IsdH showed impeded haem capture and almost no haem relay activity compared to $IsdH^{N2N3}$; hence, the additional N-terminal domain inhibits both of these functions. $IsdH^{N1}$ and $IsdH^{N2}$ interact with the same interface of α Hb[146,175], and thus the higher affinity of $IsdH^{N1}$ could prevent binding of $IsdH^{N2}$. Because $IsdH^{N2}$ is critical for positioning the $IsdH^{N3}$ haem capture domain (Chapter 3) this competition for α Hb binding could potentially interfere with haem uptake from this Hb subunit. Indeed, rapid capture of 50% of the globin haems by $IsdH^{N1N2N3}$ is consistent with only the β haems being accessible. To investigate whether IsdH is limited to accessing the β haem pockets, Hb carrying differently labelled haem in the α and β chains could be used to track haem transfer. One such potential experiment is presented in schematic form in Figure 4.12, and is outlined below. Hb that is chain-selectively labelled so that either the α or β haem

pockets carried ^{15}N labelled haem groups could be produced according to the protocol of Simplaceanu *e. al.,*[261]. In Figure 4.12 A, Hb is selectively labelled so that the β chains only cary ^{15}N labelled haem. Isotopic labelling could be confirmed by mass spectrometry (Fig. 4.12 B). The selectively labelled Hb could then be mixed with sub-stoichiometric amounts of IsdH to allow haem transfer (Fig. 4.12 C), and the mixture separated using Ni-affinity chromatography (native Hb binds to the column and IsdH is collected in the flow-through). Mass spectrometry could then be used to identify whether an excess of labelled or unlabelled haem was transferred to IsdH and hence whether IsdH accesses one or both of the α and β haems (Fig. 4.12 D).

The requirement for IsdH in haem uptake has not been established and the high affinity binding to Hb, compared to IsdB, suggests that IsdH may have a function that relies on a stable interaction with Hb, as opposed to haem relay by IsdB, which is facilitated by weak interactions with Hb. One possibility is that the high affinity binding to Hb by the $IsdH^{N1}$ domain will provide an advantage in Hb capture under conditions where Hb availability is low. Alternatively, IsdH may have a role that is independent of nutrient haem acquisition, such as a role in immune evasion. Visai *et al.,* showed that expression of IsdH was involved in evasion of phagocytosis by neutrophils and in bacterial survival in human blood[205]. It is also possible that peroxidase activity of Hb and Hb:Hp complexes[262] bound to IsdH on the bacterial cell is harnessed in order to escape oxidative damage by reactive oxygen species generated and released by immune cells. A similar activity has been suggested for the *S. pyogenes* Hb receptor, Shr[263].

In conclusion, the experiments presented in Chapter 4 have addressed the second broad aim of this thesis: to investigate how haem is relayed by IsdB/H from Hb to IsdA/C. Towards this goal, the haem relay activity and Hb binding properties of IsdB and IsdH were compared. Differences in haem relay activity were correlated with Hb binding affinity. The superior haem relay activity of IsdB, together with a weaker binding to Hb, suggest that short-lived interactions with Hb are a feature of efficient haem relay. This hypothesis is explored further in Chapter 5.

Figure 4.12

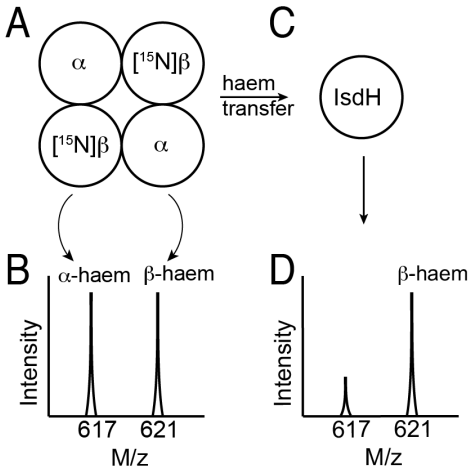

Figure 4.12. Schematic diagram of an experiment to determine which Hb haem pocket is accessible to IsdH. (A) Hb carrying 15N-labelled haem at the β Hb subunits only. **(B)** The mass spectrum of the selectively labelled Hb in **(A)** would show a singly charged species with a mass of ~617 Da, corresponding to the native (^{14}N) haem from α Hb subunits and a species with mass of ~621 Da corresponding to the ^{15}N-labelled haem from the β Hb subunits (porphyrin contains 4 pyrrole nitrogens). **(C)** Following haem transfer, a mixture of IsdH and the selectively labelled Hb could be separated by Ni chromatography and the isolated IsdH subject to mass spectrometry. **(D)** An enrichment in ^{15}N-labelled haem over unlabelled haem, in the mass spectrum of the separated IsdH would indicate that haem was preferentially removed from β Hb subunits. The Figure was provided by D. Gell.

Chapter 5. Engineering Hb-targeting NEAT domains for functional and crystallographic studies.

5.1 Introduction

The goal of the experiments in this section was to identify residues in the Hb-targeting NEAT domains that determine binding affinity for α and β Hb, and to engineer Isd variants with altered Hb-binding properties. These IsdB and IsdH variants were then used to investigate the mechanism of haem relay to IsdA/C, and to obtain new stable complexes for crystallographic studies aimed at understanding the mechanism of haem release from Hb.

The 'rigid' structure of the conserved three-domain region in IsdB and IsdH (as described in Section 3.5) predicts that the receptor:Hb complex must dissociate in order for the receptor to dock with downstream IsdA/C. Hence the receptor must strike a compromise bewteen binding to Hb tightly enough to promote haem release, but weakly enough to release the globin on a time-scale that is useful for transport through IsdA/C. The results in Section 4.6 provide evidence that the Hb binding affinity of IsdB is tuned to achieve efficient haem relay, whereas IsdH has high affinity interactions with Hb and does not efficiently relay haem. To further investigate this model of haem relay I set out to test the hypothesis: IsdB mutants with increased Hb binding affinity will have reduced rates of haem transfer to IsdA/C.

The crystal structure of the $IsdH^{N2N3}$:Hb complex presented in Chapter 3 revealed that the haem pocket of IsdH sits directly adjacent to the globin haem coordination site. The haem transfer kinetics discussed in Section 3.1 show that interactions must occur on this interface to destabilise the Hb fold and promote haem release. However, because this interface was not well defined at a data resolution of 4.2 Å it was not possible to determine the molecular contacts across the interface or to identify changes in the globin fold. Hence improved data resolution is required in order to probe the mechanism of induced haem release. Attempts to improve crystal quality by traditional approaches such as changing the Isd:Hb mixing ratio, seeding, optimising cryoprotection, and crystal annealing were unsuccessful. The findings of Chapter 3 indicate that the Hb capture and haem transfer functions are separated between two spatially distinct interfaces (involving

the N- and C-terminal NEAT domains, respectively). Based on these findings, I devised a strategy to introduce mutations that alter receptor:Hb stoichiometry and stability (with aim of obtaining more ordered crystals) without altering the haem transfer interface of interest.

The first step was to identify potential causes of disorder in crystals of the original complex. The positioning of the four receptors is such that the $IsdH^{N3}$ domains butt up against each other. The electron density at these interfaces was weak and the haem binding β-hairpins were poorly defined or absent. Attempts to model the haem binding β-hairpins based upon structures of the free $IsdH^{N3}$ domain indicated that these structures might clash in two adjacent domains. In addition, one whole $IsdH^{N3}$ domain, belonging to one of the four $IsdH^{N2N3}$ molecules, could not be built into the $IsdH^{N2N3}$:Hb structure, presumably because the position of this domain was not consistent throughout the crystal lattice. Together these observations provide evidence that four receptors do not fit on the surface of one Hb tetramer without steric interference between the $IsdH^{N3}$ domains. The receptor for which the $IsdH^{N3}$ domain could not be modelled was bound to a β Hb subunit. As $IsdH^{N2N3}$ binds with much lower affinity to the β Hb chains than to α Hb chains it was reasoned that engineering $IsdH^{N2N3}$ to remove the interaction with β Hb (and retain or enhance the interaction with α Hb) would lead to a more "crystallisable" complex.

Section 5.2 describes point mutations in IsdB that cause diminished binding to Hb, which were introduced into *S. aureus* to investigate the role of Hb binding *in vivo*. The remaining sections detail the approach taken to rationally engineer IsdB and IsdH receptors to enhance Hb binding, primarily in order to facilitate crystallisation of high-resolution receptor:Hb complexes, with the secondary aim of identifying the determinants of Hb affinity and testing the role of 'weak' protein-protein interactions in haem relay. Analysis of the resulting crystal structures is presented in Chapter 6.

5.2 Conserved aromatic residues on the IsdB:Hb binding interface are essential for Hb binding and haem capture

In collaboration with the laboratory of Dr Eric Skaar (Vanderbilt University School of Medicine) we set out to investigate the importance of Hb-targeting interactions for the survival of *S. aureus* in a mouse model of infection. The strategy was to make *S. aureus* strains carrying point mutations that knock out Hb binding. Because IsdB appears to play a greater role than IsdH in Hb utilisation[84,260] it seemed necessary to make the mutants in IsdB; however, the molecular contacts that determine binding of IsdB to Hb were unknown. Residues of IsdB that might be involved in Hb binding were identified based upon conservation with the Hb binding interface of $IsdH^{N1}$ and $IsdH^{N2}$. The α Hb-targeting faces of the $IsdH^{N1}$ and $IsdH^{N2}$ domains comprise a short aromatic helix in loop 2 and loops 4, 6 and 8 (Fig. 5.1 A; residues known to make direct contacts with α Hb are coloured red). The primary sequence of $IsdB^{N1}$ is 67% identical to $IsdH^{N2}$ and so is predicted to adopt the same fold and use the same interface to contact Hb (Fig. 5.1 A; residues in $IsdH^{N2}$ predicted to make contact with α Hb are bold). Few residues on the α Hb binding interface are conserved between the all three Hb binding NEAT domains (Fig. 5.1 A; conserved residues are underlined). One highly conserved feature is the aromatic motif on loop 2 of $IsdH^{N1}$, $IsdH^{N2}$ and $IsdB^{N1}$. The role of this motif in $IsdH^{N1}$ has previously been investigated by alanine scanning mutation. This study observed a 40–150-fold reduction in Hb binding affinity when residues 125–129 (YYHFF) were individually replaced with Ala, indicating that the aromatic motif is indispensible for binding to Hb[147]. The primary sequence of this motif is conserved in $IsdH^{N2}$ and $IsdB^{N1}$ (QFYHYF), and varies in $IsdH^{N1}$ (QYYHFF). To investigate the role of this motif in Hb binding by IsdB, and in *S. aureus* virulence, single Ala substitutions were introduced into IsdB to replace Gln, Tyr or His residue at positions 1, 3 and 4 of the QFYHYF motif. In the crystal structures of $IsdH^{N1}$:Hb and $IsdH^{N2}$:Hb, the equivalent Tyr is involved in contacts with Hb, while Glu163 and His166 make intra-molecular interactions that are expected to stabilise the conformation of loop 2 when bound to Hb[146,175]. Hence mutations in Glu163, Try165 and His166 were predicted to abrogate the interaction with Hb and produce observable effects *in vivo*. An additional mutation, in which the FYHYA motif of IsdB was substituted with the YYHFF sequence, was made to investigate whether the two aromatic motifs are interchangeable. *isdB* genes carrying the loop 2

mutations were introduced into *S. aureus* by allelic replacement in the Skaar laboratory and the strains harbouring these mutations were tested for their ability to bind Hb to the cell-surface[208]. Recombinant mutant IsdB proteins carrying the same substitutions (residues 41–609 of IsdB with a intact N-terminal histidine affinity tag), together with ferric Hb, were produced by Dr Skaar's laboratory and shipped as lyophilised proteins.

Gel filtration was used to assess the interaction of purified IsdB mutants with ferric Hb. Hb was first reacted with CN to minimise precipitation of unstable Fe(III)-Hb on the column. IsdB or IsdB mutants were mixed in a 2:1 molar ratio (per Hb tetramer) with CN-Fe(III)-Hb and subject to SEC analysis. Wild-type IsdB showed evidence of weak interaction with Hb (Fig. 5.1 Bi), as expected based on results of Section 4.4. As both the Hb and IsdB protein used here were produced by the Skaar laboratory this is good corroboration of the findings in Chapter 4 that weak binding to Hb is a functional property of IsdB. Substitution of Gln163, Tyr166 or His166 attenuated the interaction (Fig. 5.1 Bii–iv). In particular, The Tyr165Ala mutation removed any indication of an interaction (Fig. 5.1 Biv). This mutation also dramatically reduced the binding of Hb to the surface of *S. aureus*[208]. In $IsdH^{N1}$ and $IsdH^{N2}$ this tyrosine packs against the A-helix of the globin at the centre of the interface and so is likely to play a key role in stabilising the interaction between Hb and IsdB. To determine whether the aromatic motifs are interchangeable the motif of IsdB was substituted with the $IsdH^{N1}$ sequence. The loop FYHYA→YYHFF substitution also attenuated binding to Hb indicating that in the context of IsdB the YYHFF motif of $IsdH^{N1}$ cannot effectively bind to Hb (Fig. 5.1 Bv).

It was predicted that disrupting interactions through the $IsdB^{N1}$ domain would reduce or block haem uptake by the $IsdB^{N2}$ domain. To investigate this, the IsdB proteins carrying mutations in $IsdB^{N1}$ loop 2 were mixed in a 4:1 ratio with Fe(III)-Hb and haem transfer was monitored using UV-visible absorption spectroscopy (as described in Section 2.7). The change in peak height at 406 nm over time, normalised to the starting absorbance (spectrum of Fe(III)-Hb), is shown in Figure 5.1 C. All of the $IsdB^{N1}$ loop 2 mutations had a substantial effect on haem capture from Hb. The spectral change was fitted to single- or double-exponential expressions and the calculated rates are shown in Table 5.1. The Gln163Ala, His166Ala, and FYHYA164→168YYHFF mutations result in 15–20-fold reductions in haem transfer rate compared to wild-type IsdB. Transfer rates to IsdB

carrying the Tyr165Ala are ~50-fold slower than for wild-type IsdB. Hence the conserved aromatic residues of loop 2 of IsdB are vital for both Hb binding and haem transfer activity of IsdB. These residues likely play a role in stabilising the fold of loop 2 as well contributing to the Hb binding surface.

Using a mouse model of systemic infection, Pishchany *et al*., demonstrated that an *S. aureus* strain expressing IsdB(Y165A) had significantly reduced ability to colonise the kidneys and hearts of infected animals[208]. *S. aureus* carrying the Tyr165-to-Ala mutation had similar virulence to an *isdB* deletion strain, with close to a 100-fold decrease in colony forming units isolated from infected tissues when compared to the wild type strain. Hence interactions between IsdB and Hb are necessary for haem capture from Hb *in vitro* and contribute to the virulence of *S. aureus in vivo*.

Table 5.1. Rates of haem transfer from Hb to IsdB at 4°C.

IsdB construct	k_1 min^{-1}	k_2 min^{-1}
IsdB	1.08 ± 0.24	0.114 ± 0.024
IsdB(FYHYA→YYHYF)	0.066 ± 0.001	-
IsdB(H166A)	0.042 ± 0.001	-
IsdB(Q163A)	0.051 ± 0.002	-
IsdB(Y165A)	0.020 ± 0.004	-

UV-vis data were fitted to single or double-exponential expressions. Rate measurements are average ± 1SD from 2–3 experiments.

Figure 5.1. Hb binding and haem capture properties of IsdB proteins carrying mutations in conserved residues in the Hb binding domain. (A) Sequence alignment of selected regions of $IsdH^{N1}$, $IsdH^{N2}$ and $IsdB^{N1}$. Residues that contact α Hb are coloured red. Residues that are predicted to contact α Hb in $IsdB^{N1}$ are bold. Residues conserved in all three sequences are underlined. **(B)** Gel filtration analysis of Hb (brown) overlaid with traces acquired for samples of Hb mixed with wild type IsdB, or IsdB carrying mutations in the Hb binding domain. Traces for wild-type IsdB and IsdB(Y165A) alone are shown as dashed lines. These data were recorded by D. Gell. **(C)** The absorbance at 406 nm measured over a 35-min time period for Fe(III)-Hb alone (brown) or Fe(III)-Hb mixed with IsdB proteins. The absorbance was normalised to the starting condition (spectrum of Fe(III)-Hb). These data are representative of two-three measurements.

Figure 5.1

A

	Helix2/Loop2		Loop4		Loop6		Loop8	
121	NETQYYHFFSIKDP	… 149	DINTASTWK	… 176	SPVPEDHAY	… 203	QIDDGEETNY	IsdH^{N1}
361	GERQFYHYASTVEP	… 389	GLKTASTWK	… 416	DSDK–DYAY	… 263	EYGENIHEDY	IsdH^{N2}
160	GTQQ**FY**HY**AS**SVKP	… 188	GL**QS**GQ**F**WR	… 215	DTV**K–DY**AY	… 62	HFN–NKEEKY	IsdB^{N1}

B

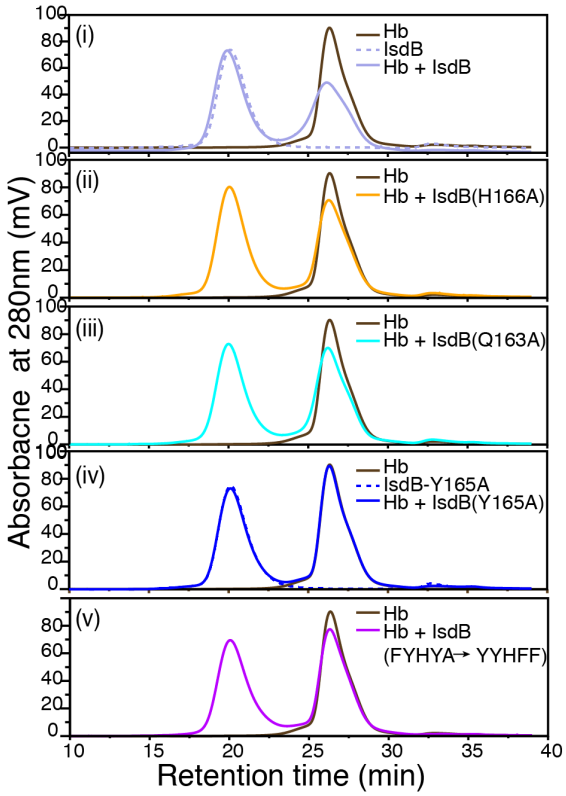

C

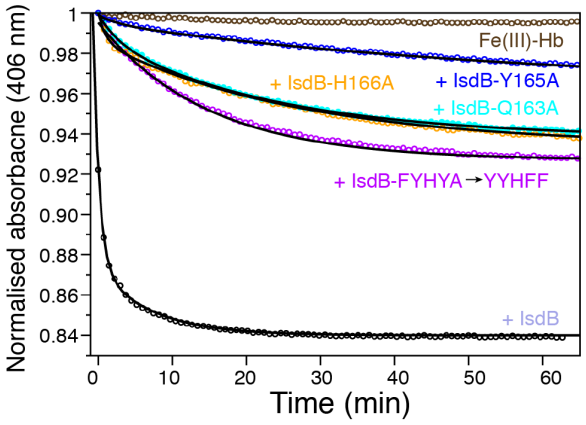

5.3 A TxxT motif in loop 4 of IsdB confers high affinity binding to α Hb

Section 5.2 showed that mutating residues in loop 2 of $IsdB^{N1}$, that are conserved in $IsdH^{N1}$ and $IsdH^{N2}$, led to a loss of Hb binding and reduced haem transfer. This enabled the Skaar lab to demonstrate the importance of Hb binding in *S. aureus* pathogenesis, but does not contribute to the main goal of this chapter, which was to understand how differences in NEAT domain sequences lead to differences in Hb-binding and haem relay, and engineer IsdB/H variants with altered Hb binding properties. Side chains that might confer differences in α/β binding affinity and selectivity were identified based on comparison of the native $IsdH^{N1}$, $IsdH^{N2}$ and $IsdB^{N1}$ sequences. Sequence features common to $IsdH^{N1}$ and $IsdH^{N2}$ (which share similar α binding properties) but not shared by $IsdB^{N1}$ (which has much lower affinity for α Hb), were identified as potential determinants of high-affinity binding to α Hb. Thus, $IsdH^{N1}$ and $IsdH^{N2}$ share a common sequence in loop 4 that is not present in IsdB (Fig. 5.2 A). Site directed mutagenesis was used to replace Gln190, Ser191 and Phe194 in loop 4 of $IsdB^{N1}$, or Lys391 in loop 4 of $IsdH^{N2}$, with the corresponding sequence of $IsdH^{N1}$ (Fig. 5.2 B). The mutations were introduced into $IsdB^{N1N2}$, comprising residues 120–459, and $IsdH^{N2N3}$, comprising residues 326–660. Primer sequences used for mutagenesis, and protein sequences of the templates can be found in Appendices B and C. Substitution of Lys391 in $IsdH^{N2N3}$ with Asn (Fig. 5.2 C, compare panels i and ii) or substitution of Gln190 in $IsdB^{N1N2}$ with Asn (Fig. 5.2 D, compare panels i and ii) had minimal effect on α Hb binding. These results are consistent with a previous study, which showed that replacing Asn151 of $IsdH^{N1}$ with Ala caused only a 1.4-fold decrease in Hb binding affinity[147]. Substitution of IsdB Phe194 with Thr ($IsdB^{N1N2}$(F194T)) abolished binding to α Hb (Fig. 5.2 Diii). However, when all three interfacial loop 4 residues in IsdB were replaced with their counterparts in $IsdH^{N1}$ ($IsdB^{N1N2}$(QSF→NTT)) there was a dramatic increase in α Hb binding affinity (Fig. 5.2 Div). Overall, the binding properties of $IsdB^{N1N2}$(QSF→NTT) were comparable to $IsdH^{N2N3}$ (Fig. 5.2, compare Div, with Ci). Together, these results suggest that a TxxT motif in loop 4 is an important determinant of high-affinity α Hb binding.

In $IsdH^{N1}$, Thr152 makes hydrogen-bonding interactions with Lys11 of α Hb, while Thr155 forms a hydrogen bond with Thr8 of α Hb (Fig. 5.2 E)[146,175]. Pilpa *et al,* showed

that substitution of Thr155 in $IsdH^{N1}$ led to a 10-fold decrease in Hb binding affinity, supporting a role for this residue in high affinity binding to α Hb[147]. Asn151 of $IsdH^{N1}$ makes hydrogen-bonding interactions with αLys11 through both the side chain amide and backbone carbonyl group (Fig. 5.2 E)[146]. In $IsdH^{N2}$ the backbone carbonyl of Lys391 makes intra-molecular hydrogen bonds and the ε-amino group is within hydrogen bonding distance of the αAla71 backbone carbonyl. However, these residues do not contribute significantly to α Hb binding according to results in Figure 5.2 C and from Pilpa *et al.*[147].

Figure 5.2. α Hb binding properties of IsdH and IsdB proteins carrying mutations in loop 4 of their Hb binding NEAT domains. (A) Sequence alignment of selected regions of $IsdH^{N1}$, $IsdH^{N2}$ and $IsdB^{N1}$. Residues that contact α Hb are coloured red. Residues that are predicted to contact α Hb in $IsdB^{N1}$ are bold. **(B)** Mutations introduced into loop 4 of NEAT2 of $IsdH^{N2N3}$ or NEAT1 of $IsdB^{N1N2}$ are indicated in green. **(C)** SEC analysis of 12.6 μM αHb (black) overlaid with traces acquired for samples of 12.6 μM αHb mixed with 0.2 (blue), 0.4 (cyan), 0.8 (green), 1.2 (yellow), 2 (orange) or 4 (red) molar equivalents of: (i) $IsdH^{N2N3}$Y642A, or (ii) $IsdH^{N2N3}$K391N. **(D)** As for C with IsdB proteins. For IsdB constructs carrying the Q109N (ii) and F194T (iii) mutations, additions of 0.4 (cyan), 0.8 (green) and 2 (orange) molar equivalents of IsdB protein are shown. **(E)** The α Hb binding interface of $IsdH^{N1}$ (blue) bound to α Hb (orange). Thr152 and Thr155 of the TxxT motif are shown in green and interact with residues of α Hb coloured cyan.

Figure 5.2

A

	Helix2/Loop2		Loop4		Loop6		Loop8	
121	NETQYYHFFSIKDP	…	149 DINTASTWK	…	176 SPVPEDHAY	…	203 QIDDGEETNY	$IsdH^{N1}$
361	GERQFYHYASTVEP	…	389 GLKTASTWK	…	416 DSDK-DYAY	…	263 EYGENIHEDY	$IsdH^{N2}$
160	GTQQFYHYASSVKP	…	188 GLQSGQFWR	…	215 DTVK-DYAY	…	62 HFN-NKEEKY	$IsdB^{N1}$

B

361	GERQFYHYASTVEP	…	389 GLNTASTWK	…	416 DSDK-DYAY	…	$IsdH^{N2N3}$(K391N)
160	GTQQFYHYASSVKP	…	188 GLNSGQFWR	…	215 DTVK-DYAY	…	$IsdB^{N1N2}$(Q190N)
160	GTQQFYHYASSVKP	…	188 GLQSGQTWR	…	215 DTVK-DYAY	…	$IsdB^{N1N2}$(F194T)
160	GTQQFYHYASSVKP	…	188 GLNTGQTWR	…	215 DTVK-DYAY	…	$IsdB^{N1N2}$(QSF→NTT)

C

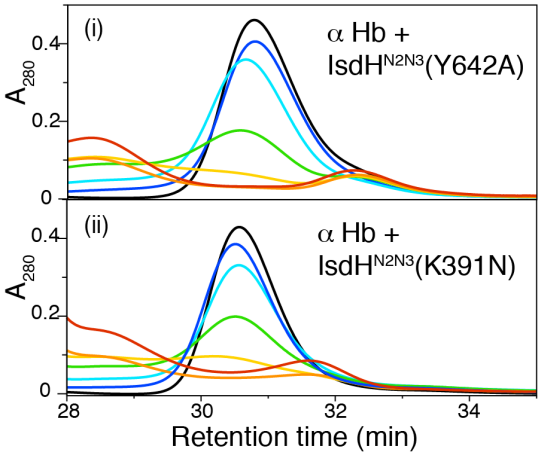

D

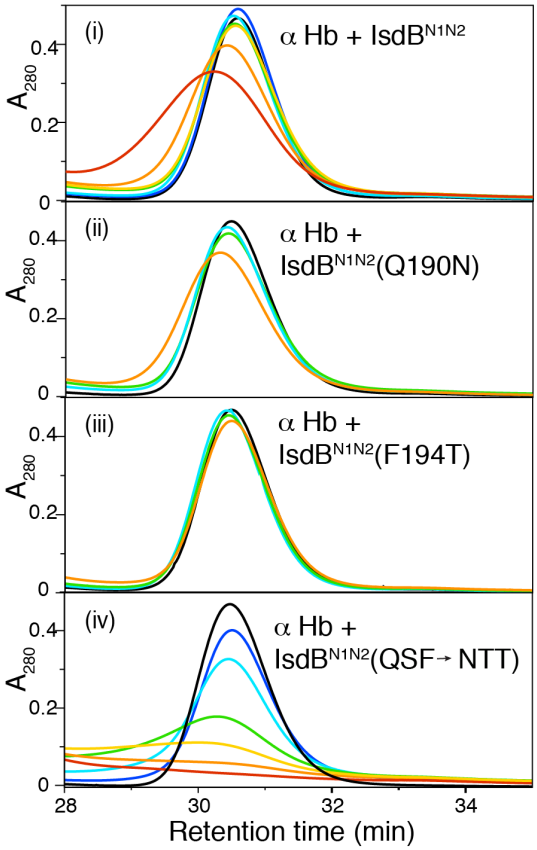

E

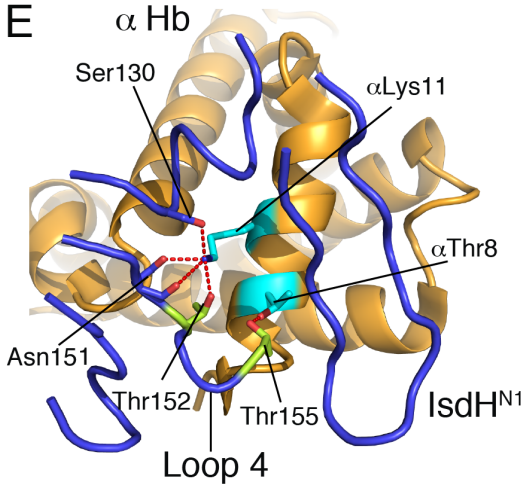

Having established the effect of mutations in loop 4 of the NEAT domain on α Hb binding, I next investigated interactions with β Hb. The monomer-tetramer self-association of β Hb resulted in extensive peak overlap with the Isd proteins making titration experiments similar to those shown in Figure 5.2 impractical. However, as shown in Figure 5.3 Ai, interaction between wild type $IsdH^{N2N3}$ and β Hb was clearly detectible. By a similar measure, all loop 4 mutations in $IsdB^{N1N2}$ or $IsdH^{N2N3}$ (except $IsdB^{N1N2}$(Q190N), which was not tested) resulted in diminished, or loss of, β binding (Fig. 5.3 Aii, Bii, Biii). Thus the main conclusion from these experiments was that the TxxT sequence motif is important for high affinity α binding.

Loss of binding of $IsdB^{N1N2}$(F194T) to α and β Hb indicates that loop 4 of IsdB forms part of the binding site for both α and β Hb. Interestingly, multiple substitutions in loop 4 were required to enhance α Hb binding affinity, while single mutations had no effect or reduced the interaction. One hypothesis is that a single Phe194Thr mutation does not allow the Thr hydroxyl to approach closely enough to the α or β Hb surface to hydrogen bond, leaving a cavity, whereas substitution of QSF→NTT (replacing both of the large Gln and Phe residues) allows loop 4 to move closer to α Hb and satisfy multiple hydrogen bonds with αLys11 and αThr8 as seen in the $IsdH^{N1}$:α Hb crystal structure (Fig. 5.2 E). The most obvious difference between α Hb and β Hb at this face is the position of αLys11, which is occupied by Thr12 in β Hb. It has previously been shown that substitution of αLys11 with Thr abrogates the interaction between $IsdH^{N1}$ and α Hb, demonstrating the importance of interactions in this region[146]. Further structural characterisation is required to determine how loop 4 of IsdB allows for binding to the distinct surfaces of α Hb and β Hb.

Figure 5.3

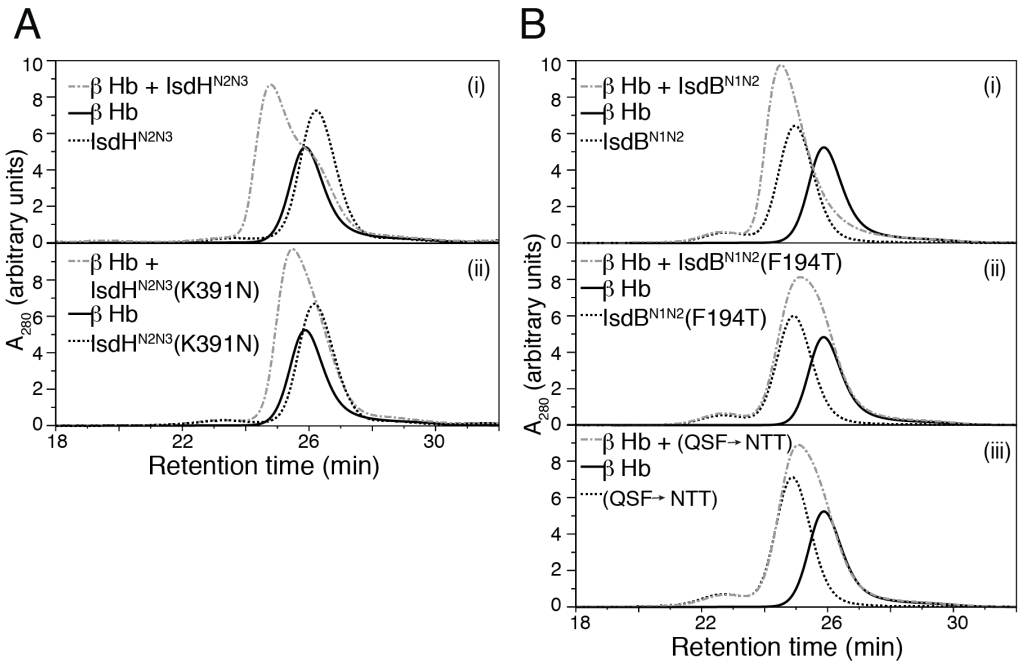

Figure 5.3. β Hb binding properties of IsdH and IsdB proteins carrying mutations in loop 4 of their Hb binding NEAT domains. (A) SEC traces of β Hb mixed with equimolar amounts of: (i) $IsdH^{N2N3}$, or (ii) $IsdH^{N2N3}$K391N. **(B)** SEC traces of β Hb mixed with equimolar amounts of: (i) $IsdB^{N1N2}$, (ii) $IsdB^{N1N2}$F194T, or (iii) $IsdB^{N1N2}$ carrying the QSF→NTT mutation.

5.4 The FxxxA, but not YxxxF, motif in loop 2 allows NEAT binding to β Hb

Sequence features that are common to $IsdH^{N2}$ and $IsdB^{N1}$ (which share ability to bind β Hb), but not $IsdH^{N1}$ (which does not bind β Hb), were identified as potential determinants of β Hb interactions. This identified an FxxYA motif in the loop 2 helix and a KxY motif in loop 6 (Fig. 5.4 A). Considering first the aromatic sequence in loop2, crystal structures of the $IsdH^{N1}$:Hb and $IsdH^{N2}$:Hb complexes both show a Phe side chain buried at the interface with α Hb (Fig. 5.4 B). These Phe side chains are separated in the sequence alignment by the equivalent of one helical turn (YxxxF vs FxxxA); nevertheless, they are oriented to make similar interactions with α Hb (Fig. 5.4 B). To determine whether differences in the two aromatic motif sequences confer Hb chain selectivity, Phe164 and Ala168 of IsdB, and Phe365 and Ala369 of $IsdH^{N2N3}$, were replaced with Tyr and Phe residues (Fig. 5.4 C). Tyr167 and Tyr368, of IsdB and IsdH, respectively, were left unchanged because this position is solvent exposed on the periphery of the Hb binding interface and, therefore, was not expected to play a major role in binding.

The IsdB and $IsdH^{N2N3}$ proteins carrying the loop 2 mutations were assessed for their ability to bind to α and β Hb using the SEC-titration assay. The FYHYA→YYHYF mutation caused little or no change in α Hb binding affinity compared to native IsdB or $IsdH^{N2N3}$ (Fig. 5.4 D, compare panel ii with panel i, and compare panel iv with panel iii). However, the FYHYA→YYHYF mutation caused $IsdH^{N2N3}$ to lose binding to β Hb (Fig. 5.4 E, compare grey dot-dashed lines in panels i and ii). The interaction of IsdB carrying the FYHYA→YYHYF mutation with β Hb was not tested. These results suggests that FxxxA and YxxxF sequences are similarly compatible with α Hb binding, but that only the Phe side chain positioned as FxxxA is compatible with β Hb binding. The most likely explanation for loss of β Hb binding is that a small hydrophobic side chain, like Ala, is needed at position 5 to avoid steric clash with the β Hb surface. In complex with β Hb, the aromatic side chain at position 1 could potentially be oriented as seen for Tyr125 of $IsdH^{N1}$ or Phe365 of $IsdH^{N2}$ on α Hb (Fig. 5.4 B, F). Single substitutions of Phe⇔Tyr (position 1) and Phe⇔Ala (position 5) could be made in both $IsdH^{N1}$ and $IsdH^{N2}$ to investigate this further.

In summary, selectivity for α Hb was successfully engineered into the IsdH^{N2N3}. More extensive mutagenesis studies that target residues in the globin chains as well as single point mutations of NEAT loop 2 and structural studies of NEAT:β Hb complexes are necessary to explain why the YYHFF motif is not compatible with binding to β Hb and to understand how the FYHYA motif is more versatile in its ability to recognise the surfaces of both α Hb and β Hb.

Figure 5.4. Mutagenesis of loop 2 on the Hb binding interface of IsdH and IsdB. (A) Sequence alignment of selected regions of $IsdH^{N1}$, $IsdH^{N2}$ and $IsdB^{N1}$. Residues that contact α Hb are coloured red. Residues that are predicted to contact α Hb in $IsdB^{N1}$ are bold. **(B)** A ribbon diagram of the loop 2 sequence of $IsdH^{N1}$ (green) and $IsdH^{N2}$ (orange) and its interactions with the A and E helices of α Hb (PDB 4F3C and 3SZK). Phe129 of $IsdH^{N1}$ and Phe365 $IsdH^{N2}$ adopt conformations that allow the side chains to occupy the same position at the interface. **(C)** Mutations introduced into loop 2 of NEAT2 of $IsdH^{N2N3}$ or NEAT1 of $IsdB^{N1N2}$ are indicated in green. **(D)** SEC analysis of 12.6 μM α Hb (black) overlaid with traces of 12.6 μM α Hb mixed with 0.2 (blue), 0.4 (cyan), 0.8 (green), 1.2 (yellow), 2 (orange) or 4 (red) molar equivalents of: (i) $IsdH^{N2N3}$Y642A, (ii) $IsdH^{N2N3}$ carrying the FYHYA→YYHYF mutation, or (iii) $IsdB^{N1N2}$. (iv) SEC analysis of 12.6 μM α Hb (black) overlaid with traces of 12.6 μM α Hb mixed with 0.8 (green) or 2 (orange) molar equivalents of $IsdB^{N1N2}$ carrying the FYHYA→YYHYF mutation. **(E)** SEC traces of β Hb mixed with equimolar amounts of: (i) $IsdH^{N2N3}$, or (ii) $IsdH^{N2N3}$ carrying the FYHYA→YYHYF mutation. **(F)** The α Hb binding interface of $IsdH^{N1}$ (blue) bound to α Hb (orange). Phe129 and Tyr125 of loop2 are shown in green and interact with residues of α Hb coloured cyan.

Figure 5.4

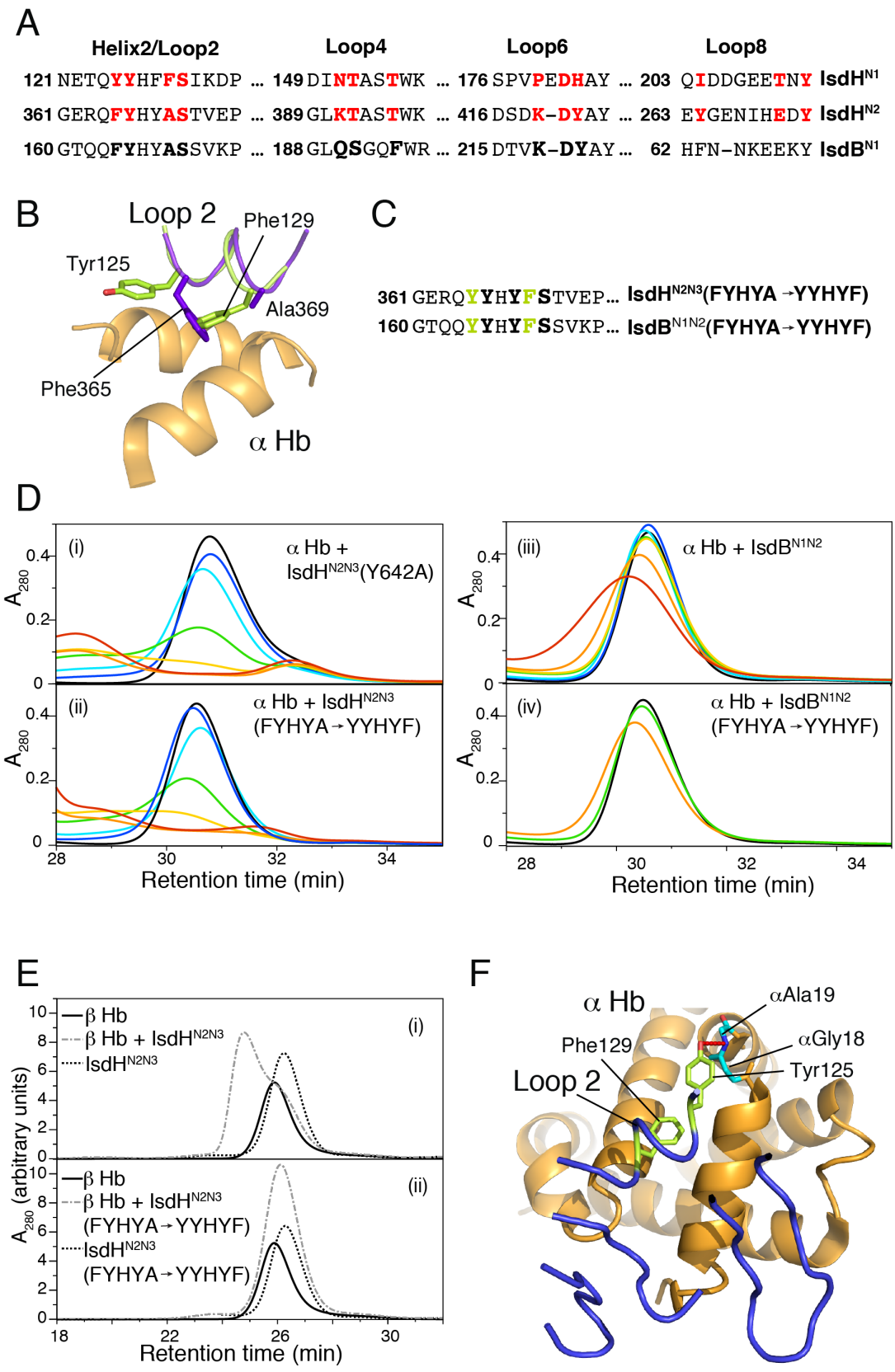
A
Helix2/Loop2
Loop4
Loop6
Loop8
121 NETQYYHFFSIKDP ... 149 DINTASTWK ... 176 SPVPEDHAY ... 203 QIDDGEETNY IsdH^N1
361 GERQFYHYASTVEP ... 389 GLKTASTWK ... 416 DSDK-DYAY ... 263 EYGENIHEDY IsdH^N2
160 GTQQFYHYASSVKP ... 188 GLQSGQFWR ... 215 DTVK-DYAY ... 62 HFN-NKEEKY IsdB^N1
B
Loop 2
Phe129
Tyr125
Ala369
Phe365
α Hb
C
361 GERQYYHYFSTVEP... IsdH^N2N3(FYHYA→YYHYF)
160 GTQQYYHYFSSVKP... IsdB^N1N2(FYHYA→YYHYF)
D
(i)
α Hb + IsdH^N2N3(Y642A)
(ii)
α Hb + IsdH^N2N3 (FYHYA→YYHYF)
(iii)
α Hb + IsdB^N1N2
(iv)
α Hb + IsdB^N1N2 (FYHYA→YYHYF)
A280
Retention time (min)
E
β Hb
β Hb + IsdH^N2N3
IsdH^N2N3
(i)
β Hb
β Hb + IsdH^N2N3 (FYHYA→YYHYF)
IsdH^N2N3 (FYHYA→YYHYF)
(ii)
A280 (arbitrary units)
Retention time (min)
F
α Hb
αAla19
Phe129
αGly18
Loop 2
Tyr125

5.5 Mutations in multiple loops to improve selectivity for α

To improve the selectivity of $IsdB^{N1N2}$ and $IsdH^{N2N3}$ for binding to α Hb over β Hb, I combined mutations in multiple interfacial loops (Fig. 5.5 A, B). IsdB carrying both the QSF→NTT (loop 4) and FYHYA→YYHYF (loop 2) substitutions bound to α Hb with higher affinity than wild type IsdB, and showed no measurable binding to β Hb (Fig. 5.5 D, F). α Hb binding by this mutant was indistinguishable from IsdB carrying the QSF→NTT mutation alone (Table, 5.2), consistent with the earlier conclusion that the aromatic loop 2 sequences are similarly compatible with α Hb. In the same way, $IsdH^{N2N3}$ carrying K391N and FYHYA→YYHYF mutations showed features that could be predicted based on the activities of the single-loop mutants: α binding was only marginally affected and binding to β was abrogated (Fig. 5.5 C, E; Table 5.2).

Figure 5.5. Hb interactions of IsdH and IsdB constructs carrying mutations on loop 2 and loop 4 of the Hb targeting domains. (A) Sequence alignment of selected regions of $IsdH^{N1}$, $IsdH^{N2}$ and $IsdB^{N1}$. Residues that contact α Hb are coloured red. Residues that are predicted contact α Hb in $IsdB^{N1}$ are bold. **(B)** Mutations introduced into loops 2 and 4 of NEAT2 of $IsdH^{N2N3}$ or NEAT1 of $IsdB^{N1N2}$ are indicated in green. **(C)** SEC analysis of 12.6 μM αHb (black) overlaid with traces of 12.6 μM α Hb mixed with 0.2 (blue), 0.4 (cyan), 0.8 (green), 1.2 (yellow), 2 (orange) or 4 (red) molar equivalents of $IsdH^{N2N3}$Y642A (i) or $IsdH^{N2N3}$ carrying the K391N and FYHYA→YYHYF mutations (ii). **(D)** SEC analysis of 12.6 μM α Hb (black) overlaid with traces of 12.6 μM α Hb mixed with 0.2 (blue), 0.4 (cyan), 0.8 (green), 1.2 (yellow), 2 (orange) or 4 (red) molar equivalents of $IsdB^{N1N2}$ (i) or $IsdB^{N1N2}$ carrying the QSF→NTT and FYHYA→YYHYF mutations (ii). **(D)** SEC traces of β Hb mixed with equimolar amounts of $IsdH^{N2N3}$ (i) or $IsdH^{N2N3}$ carrying the K391N and FYHYA→YYHYF mutations (ii). **(E)** SEC traces of β Hb mixed with equimolar amounts of $IsdB^{N2N3}$ (i) or $IsdB^{N1N2}$ carrying the QSF→NTT and FYHYA→YYHYF mutations (ii).

Figure 5.5

A

	Helix2/Loop2		Loop4		Loop6		Loop8	
121	NETQYYHFFSIKDP	…	149 DINTASTWK	…	176 SPVPEDHAY	…	203 QIDDGEETNY	$IsdH^{N1}$
361	GERQFYHYASTVEP	…	389 GLKTASTWK	…	416 DSDK-DYAY	…	263 EYGENIHEDY	$IsdH^{N2}$
160	GTQQFYHYASSVKP	…	188 GLQSGQFWR	…	215 DTVK-DYAY	…	62 HFN-NKEEKY	$IsdB^{N1}$

B

361	GERQYYHYFSTVEP	389	GLNTASTWK …	416	DSDK-DYAY…
160	GTQQYYHYFSSVKP…	188	GLNTGQTWR …	215	DSDK-DYAY…

$IsdH^{N2N3}$(K391N FYHYA→YYHYF)

$IsdB^{N1N2}$(QSF→NTT, FYHYA→YYHYF)

C

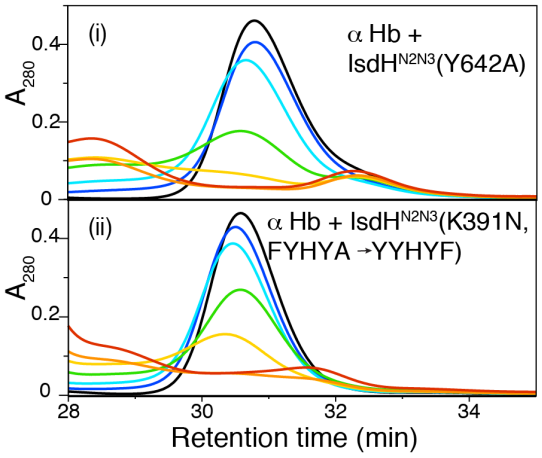

D

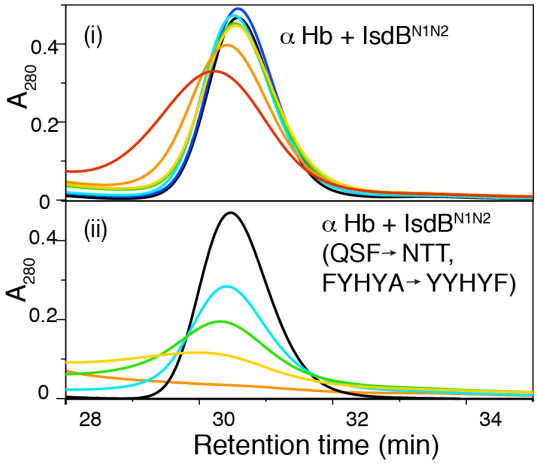

E

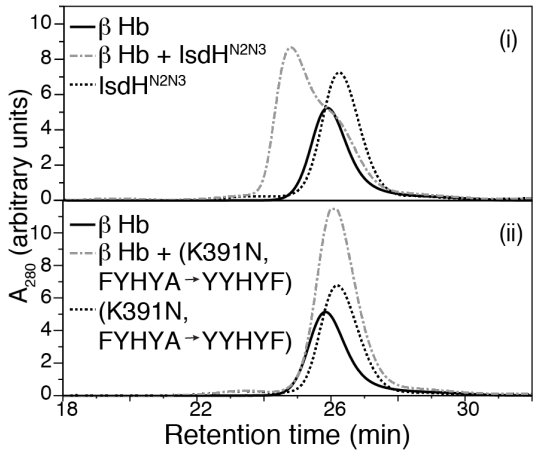

F

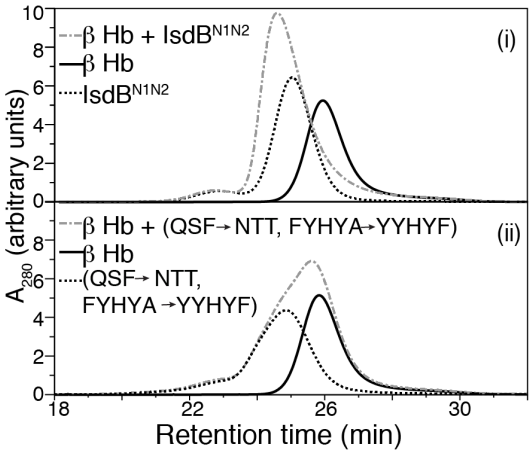

For further crystallographic studies, my aim was to generate mutations with increased binding to α Hb and decreased (or abrogated) binding to β Hb. Although increased α Hb binding was achieved for IsdB, none of the $IsdH^{N2N3}$ mutations that were tested showed enhanced binding to α Hb. This suggests that residues outside of helix 2 and loop 4 are responsible for the stronger interaction with α Hb observed for $IsdH^{N1}$, compared to $IsdH^{N2}$. Two other loops, which contribute to the α Hb binding interface, show primary sequence differences between $IsdH^{N1}$ and $IsdH^{N2}$ (Fig. 5.6 A). To investigate the role of loop 6 and loop 8 in α Hb binding affinity, 5 residues in loop 6 of $IsdH^{N2}$ were replaced with their counterparts in $IsdH^{N1}$ and two residues (Tyr443 and Glu449) were replaced on loop 8 (Fig. 5.6 A–C). All mutations in loop 6 and 8, in combination with the loop 2 and loop 4 changes, led to dramatic reductions in α binding (Fig. 5.6 D). Thus, although all residues at the $IsdH^{N2}$:α interface were changed to match residues of $IsdH^{N1}$, the α binding function of $IsdH^{N1}$ was not transplanted. It is possible that the mutations caused changes in the folding of the protein, which should be investigated by recording NMR and CD spectra; note that Isd^{N2N3} is a large (>40 kDa) protein and signal overlap, together with line broadening, might make NMR unsuitable. An alternative explanation is that regions outside of the direct binding interface are important for α Hb binding affinity, for example the β-sheet adjacent to and contacting loop 2, which has different sequence in IsdB and IsdH, may influence the loop 2 conformation when bound to Hb.

Figure 5.6. Mutations outside of loops 2 and 4 did not enhance the α Hb binding affinity of IsdH^{N2N3}. (A) Sequence alignment of selected regions of IsdH^{N1}, IsdH^{N2} and IsdB^{N1}. Residues that contact α Hb are coloured red. Residues that are predicted contact α Hb in IsdB^{N1} are bold. **(B)** Mutations introduced into multiple loops of IsdH^{N2N3} are indicated in green; '1' denotes IsdH^{N2N3}(K391N,FYHYA→YYHYF,Y264I,E270T), '2' denotes IsdH^{N2N3}(K391N,FYHYA→YYHYF,loop6), '3' denotes IsdH^{N2N3}(K391N,FYHYA→YYHYF,loop6,Y264I,E270T). **(C)** The α Hb binding interface of IsdH^{N1} (blue) bound to α Hb (orange). The position of residues on loops 6 and 8 that were substituted in IsdH^{N2N3} are shown in green. Residues of α Hb that are involved in hydrogen bonding with loop 6 are coloured cyan. **(D)** SEC analysis of 12.6 μM α Hb (black) overlaid with traces of 12.6 μM α Hb mixed with 0.2 (blue), 0.4 (cyan), 0.8 (green), 1.2 (yellow), 2 (orange) or 4 (red) molar equivalents of IsdH^{N2N3}Y642A (i); panels (ii-iv) show mixtures with IsdH^{N2N3}Y642A proteins carrying multiple mutations (proteins '1', '2' and '3'as indicated in (B)).

Figure 5.6

A

	Helix2/Loop2		Loop4		Loop6		Loop8	
121	NETQYYHFFSIKDP	…	149 DINTASTWK	…	176 SPVPEDHAY	…	203 QIDDGEETNY	$IsdH^{N1}$
361	GERQFYHYASTVEP	…	389 GLKTASTWK	…	416 DSDK-DYAY	…	263 EYGENIHEDY	$IsdH^{N2}$

B

361	GERQYYHYFSTVEP	389	GLNTASTWK	…	416	DSDK-DYAY	…	263 EIGENIHTD	1
361	GERQYYHYFSTVEP	389	GLNTASTWK	…	416	SPSPEDHAY	…	263 EYGENIHED	2
361	GERQYYHYFSTVEP	389	GLNTASTWK	…	416	SPSPEDHAY	…	263 EIGENIHTD	3

C

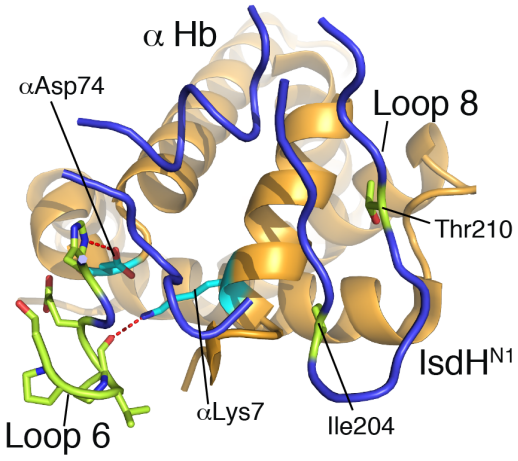

D

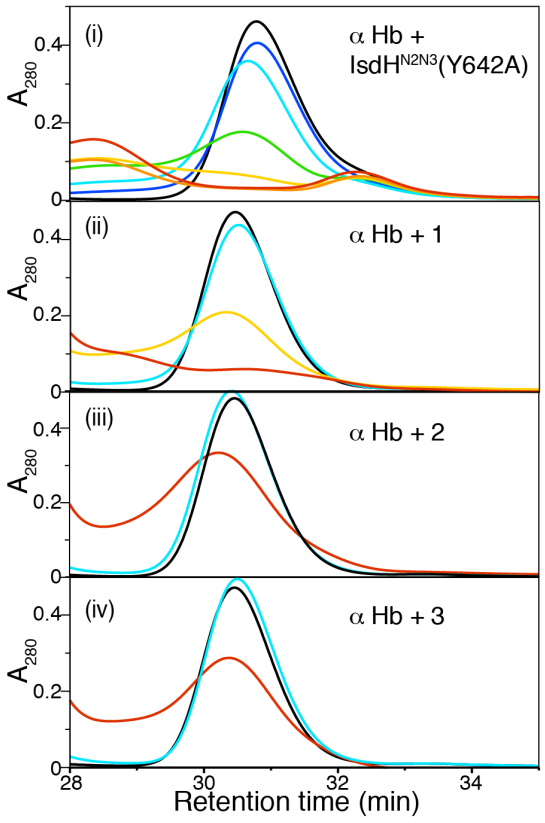

From the SEC experimetents described above, a qualitative measure of the relative α and β Hb binding affinities for each of the IsdH and IsdB mutants was made, and is provided in Table 5.2.

Table 5.2. Summary of the α and β Hb interactions of IsdH and IsdB proteins carrying mutations in the Hb binding domains, detected by SEC

Protein	α Hb	β Hb
$IsdH^{N2N3}$(Y642A)	+++	+
$IsdH^{N2N3}$(K391N)	+++	+/-
$IsdH^{N2N3}$(FYHYA→YYHYF)	+++	–
$IsdH^{N2N3}$(K391N,FYHYA→YYHYF)	+++	–
$IsdH^{N2N3}$(1) †	++	**NA**
$IsdH^{N2N3}$(2) ††	+	**NA**
$IsdH^{N2N3}$(3) †††	+	**NA**
$IsdB^{N1N2}$	+	+
$IsdB^{N1N2}$(Q190N)	+	**NA**
$IsdB^{N1N2}$(F194T)	–	–
$IsdB^{N1N2}$(QSF→NTT)	+++	–
$IsdB^{N1N2}$(FYHYA→YYHYF)	+	**NA**
$IsdB^{N1N2}$(QSF→NTT,FYHYA→YYHYF)	+++	–

† (1) $IsdH^{N2N3}$($IsdH^{N2N3}$(K391N,FYHYA→YYHYF,Y264I,E270T)
†† (2) $IsdH^{N2N3}$($IsdH^{N2N3}$(K391N,FYHYA→YYHYF,loop6)
††† (3) $IsdH^{N2N3}$($IsdH^{N2N3}$(K391N,FYHYA→YYHYF,loop6,Y264I,E270T)
– indicates no detectable binding
NA, not tested
+/- indicates a possible interaction which could not be clearly detected using the SEC assay

5.6 Weak binding to Hb is required for effective haem relay

The work in Chapter 4 revealed an inverse correlation between haem relay activity and Hb binding affinity for IsdH, $IsdH^{N2N3}$ and IsdB. The mutants of IsdB with altered Hb binding properties, described above, provided the opportunity to further explore the relationship between Hb binding affinity and haem relay activity. $IsdB^{N1N2}$(F194T) or $IsdB^{N1N2}$(QSF→NTT) were first tested to see whether the changes in Hb binding affected haem capture from Hb. $IsdB^{N1N2}$(F194T) or $IsdB^{N1N2}$(QSF→NTT) were mixed at different molar ratios with Fe(III)-Hb and the change in the visible absorption spectrum recorded over time. The change in spectra was converted to the fraction of haem remaining in Hb over time, as described in Section 3.2.3, and is shown in Figure 5.7 A. A 2:1 mixture of $IsdB^{N1N2}$(QSF→NTT) or $IsdB^{N1N2}$(F194T) with Hb (where the mixing ratio was per Hb tetramer) resulted in the depletion of ~41% and ~45% of haems from Hb

respectively, after 10 min (Fig. 5.7 A). Note that some difference in the haem transfer curve for a 2:1 molar ratio of $IsdB^{N1N2}$(QSF→NTT):Hb and the wild-type mixture was observed (Fig. 5.7 A). This may indicate a defect in haem capture from Hb, evident at low mixing ratios, however the experiment will need to be repeated to have confidence in this difference (limitations are discussed in Section 5.7 below). At a 5:1 molar ratio, $IsdB^{N1N2}$(QSF→NTT) and $IsdB^{N1N2}$(F194T) captured ~90% and ~94% of haem groups from Hb after 10 min (Fig. 5.7 A). This is similar to the amount of haem captured by wild-type $IsdB^{N1N2}$ reported in Chapter 3 (45±0.5% and 89±0.3%, for 2:1 and 5:1 mixtures respectively; errors are given as ± S.E. from three-to-four experiments). As haem was quantitatively depleted by the IsdB proteins, the haem transfer curves are the result of transfer out of *both* Hb chains, despite undetectable binding to one or both Hb chains, by $IsdB^{N1N2}$(QSF→NTT) and $IsdB^{N1N2}$(F194T) respectively, in the SEC assay (see Table 5.2). Although the former interactions were not detected by SEC, interactions mediated by the $IsdB^{N1}$ domain are required for haem capture from all four globin chains, as the isolated $IsdB^{N2}$ domain was unable to capture haem from Hb (see Section 3.2.4). Hence both $IsdB^{N1N2}$(F194T) and $IsdB^{N1N2}$(QSF→NTT) must retain some level of specific binding to both globin chains albeit with greatly reduced affinity. Therefore, haem transfer within the complex occurs more rapidly than dissociation of even the ultra-weak complexes.

By contrast, $IsdB^{N1N2}$ carrying the QSF→NTT and FYHYA→YYHYF substitutions, showed substantially reduced rates of haem capture from Hb (Fig. 5.7 A). After 10 min, 37% and 75% of globin haem groups were transferred in the 2:1 and 5:1 mixtures with $IsdB^{N1N2}$(QSF→NTT,FYHYA→YYHYF); ~ 80% of the haem transferred to the wild-type protein. Since the FYHYA→YYHYF mutation did not affect binding to α Hb in the SEC experiments but removed binding to β Hb (Table 5.2), these results suggest that the defect in haem capture from Hb results from dramatic loss of binding at β sites. Hence the FYHYA motif contributes to recognition of and haem capture from β Hb.

To measure the effect of altered Hb binding affinity on haem relay to IsdC, Fe(III)-Hb was mixed with excess apo-IsdC and catalytic amounts of the IsdB mutants, and the change in absorbance at 406 nm was measured over time (Fig. 5.7 B). Small amounts of $IsdB^{N1N2}$(F194T) (7 or 13% of the haem concentration) transferred haem from Fe(III)-Hb

to IsdC at wild-type rates (Fig. 5.7 B, compare red and orange curves), indicating that the reduced affinity of $IsdB^{N1N2}$(F194T) for α and β Hb did not affect haem relay. In contrast, the $IsdB^{N1N2}$(QSF→NTT) protein showed considerably lower haem relay activity (Fig. 5.7 B, cyan). Based on the similar haem capture by $IsdB^{N1N2}$(QSF→NTT) compared to wild-type IsdB and $IsdB^{N1N2}$(F194T) (Fig. 5.7 A), the slower transfer to IsdC might be, at least partly, due to tighter binding to α Hb and a consequent slower release of haem-bound IsdB.

The haem relay function of IsdB with the combined QSF→NTT and FYHYA→YYHYF changes was even more attenuated (Fig. 5.7 B). Catalytic amounts (7 or 13% of the IsdC concentration) of IsdB carrying the QSF→NTT and FYHYA→YYHYF mutations initially produced similar spectral changes to IsdB carrying QSF→NTT alone (Fig. 5.7 B, compare cyan and blue curves); however, a second slower phase was evident for the double mutant. It is tempting to speculate that the bi-phasic nature of haem relay to IsdC by IsdB(QSF→NTT,FYHYA→YYHYF) (Fig. 5.7 B) is related to different rates of haem uptake from the α and β Hb subunits. As mentioned above, α Hb binding is insensitive to the loop 2 mutation suggesting that the slower phase corresponds to relay from the β subunits. In summary, the weak binding of IsdB to α and β Hb is sufficient to achieve effective haem capture and haem relay. The activity of the IsdB proteins carrying mutations in the Hb targeting domain indicates that substantially weaker binding prevents haem uptake and much stronger binding prevents efficient haem relay.

Figure 5.7. Haem capture and relay properties of IsdB proteins with altered Hb binding affinity. (A) The figure shows the fraction of haem remaining in Fe(III)-Hb (1.5 μM Hb or 6 μM haem) after mixing with a 2-fold (3 μM) or 5-fold (7.5 μM) excess of apo-IsdB (red), apo-IsdB(QSF→NTT) (cyan), apo-IsdB(F194T) (yellow) or apo-IsdB(QSF→NTT,FYHYA→YYHYF) (blue). Error bars are shown for the wild-type IsdB protein and represent S.E. from three-to-five experiments. **(B)** Haem relay from Fe(III)-Hb (1.5 μM Hb or 6 μM haem) to excess apo-IsdC (7.5 μM or 125% measured as a % of the number of Hb haem sites in the reaction) in the presence of 7% or 13% apo-IsdB (red), apo-IsdB(QSF→NTT) (cyan), apo-IsdB(F194T) (yellow) or apo-IsdB(QSF→NTT,FYHYA→YYHYF) (blue). These data are from single measurements.

Figure 5.7

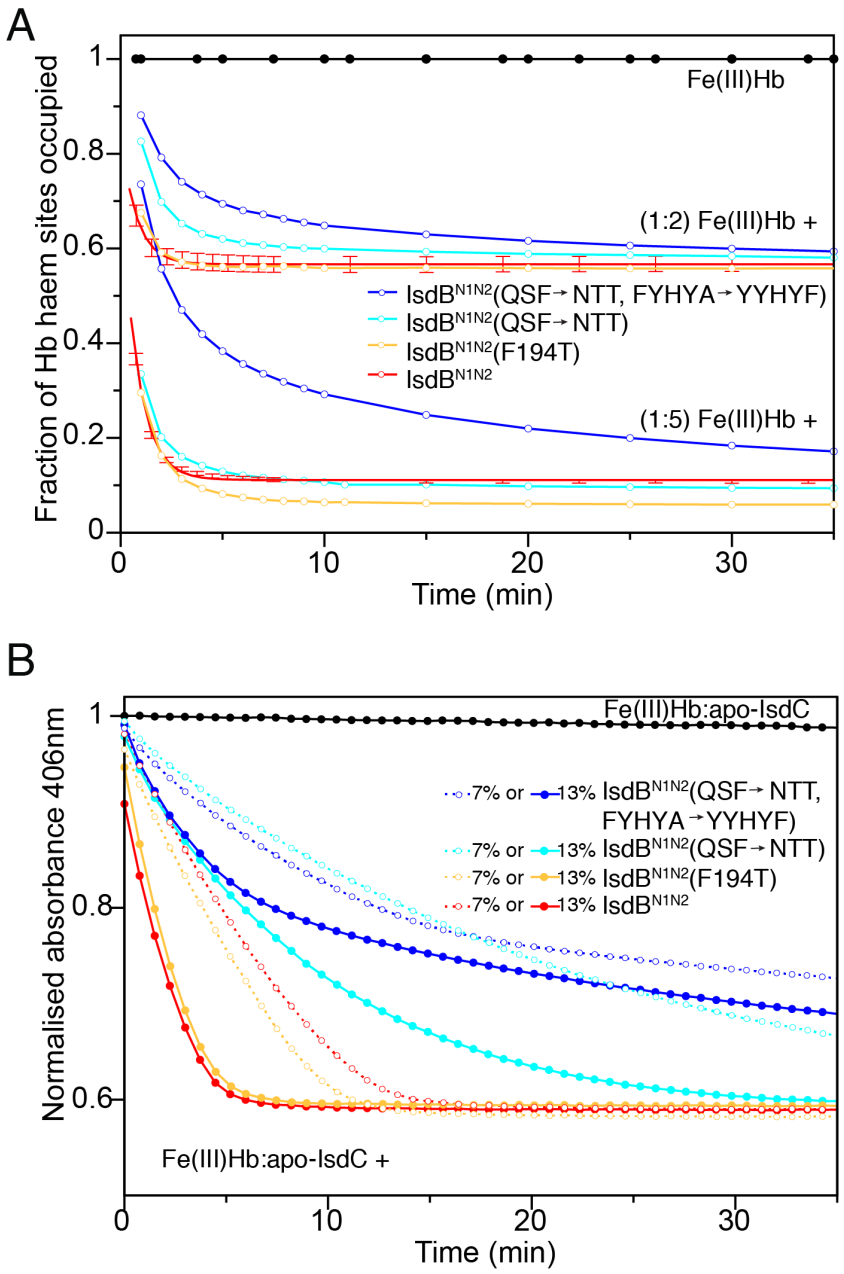
A
Fraction of Hb haem sites occupied
Time (min)
Fe(III)Hb
(1:2) Fe(III)Hb +
(1:5) Fe(III)Hb +
IsdB^N1N2(QSF→NTT, FYHYA→YYHYF)
IsdB^N1N2(QSF→NTT)
IsdB^N1N2(F194T)
IsdB^N1N2
B
Normalised absorbance 406nm
Time (min)
Fe(III)Hb:apo-IsdC
Fe(III)Hb:apo-IsdC +
7% or 13% IsdB^N1N2(QSF→NTT, FYHYA→YYHYF)
7% or 13% IsdB^N1N2(QSF→NTT)
7% or 13% IsdB^N1N2(F194T)
7% or 13% IsdB^N1N2

5.7 Future directions and discussion

The experiments described above provide evidence that weak binding between IsdB and Hb is necessary for rapid haem capture and haem relay. However, there are some limitations to this work.

First, the correct folding of each of the mutant constructs should be demonstrated by CD or NMR spectroscopy. In addition a quantitative measure of Hb binding by IsdB, IsdH and their mutants is required in order to effectively rank their relative binding affinities and interpret haem relay activity. For example, the $IsdB^{N1N2}$(QSF→NTT) protein showed reduced haem relay activity (Fig. 5.7 B), however, it was not possible to say with confidence whether this reduced activity was due to a higher affinity interaction with α Hb or substantially reduced binding to β Hb. Although an interaction between $IsdB^{N1N2}$(F194T) and β Hb could not be detected here, $IsdB^{N1N2}$(F194T) relayed haem with wild-type activity implying an interaction. If the defect in binding to β Hb by $IsdB^{N1N2}$(QSF→NTT) was of greater magnitude than that of $IsdB^{N1N2}$(F194T), it may fall below the threshold required for haem capture from Hb, in turn affecting haem relay. In addition, kinetic measurements of complex formation and dissociation should be made for comparison with the rates of haem transfer.

Second, the rapid haem capture from Hb means that the start of the haem transfer curve cannot be effectively captured on a conventional spectrometer, preventing accurate measurements of the haem transfer rates. To study and compare the transfer kinetics for the different IsdB/H proteins, the experiments should be repeated with stopped-flow equipment.

Third, interpretation of haem capture and relay measurements are complicated by reactions occurring at both α and β haem pockets. Future studies could aim to simplify the measurements by blocking haem transfer from one globin haem site by using a non-iron porphyrin. Alternatively, haem transfer from the isolated α and β Hb chains could be measured. Finally, to support the argument that a difference in Hb binding affinity between IsdB and IsdH is responsible for the difference in haem relay activity, it is important to produce an IsdH protein with reduced affinity for Hb and to demonstrate a

gain of function for haem relay speed. One possibility would be to introduce the loop 4 sequence of IsdB into $IsdH^{N2N3}$ to reduce α Hb binding affinity.

Recently, Bowden *et al.,* demonstrated that IsdB can catalyse haem transfer from Hb to $IsdA^{230}$. The rate of IsdB-catalysed haem relay of from Fe(III)-Hb to IsdA was shown to be ~400 times slower than haem transfer from IsdB to IsdA and similar to the rate of haem extraction from Hb^{230}, suggesting that haem capture from Hb is the rate-limiting step in the haem relay process. The work presented in this chapter may add to this model by providing evidence that dissociation of the Isd:Hb complex is rate-limiting in haem relay reaction; the relationship between Hb binding and haem relay should now be investigated further. In addition, Bowden *et al.,* proposed an alternative mechanism for haem relay that involves the formation of a ternary complex between Hb, IsdB and $IsdA^{230}$. The formation of a ternary complex may be compatible with a mechanism that requires weak binding to Hb as catalysis of haem transfer from consecutive globin haem pockets will still require rapid release of Hb. However, in the absence of a large conformational change in the receptor, the buried haem transfer interface of IsdB and IsdH in X-ray crystallography structures of the IsdH:Hb and IsdB:Hb complexes (see Chapters 3 and 5) argue against haem relay in a ternary complex. No evidence for a large conformational change was detected by SAXS (Chapter 3).

The related Hb receptor of *Staphylococcus lugdunensis* (slIsdB) was identified as a homologue of IsdB and contains the three-domain architecture involved in Hb receptor function[264]. However, sequence alignment reveals that slIsdB contains the TxxT motif in loop 4, suggesting that the receptor has similar α Hb binding properties and haem transfer function to $IsdH^{N2N3}$. Hb binding studies conducted by D. Gell and E. Devenish indicate that slIsdB does bind to α Hb with an affinity more similar to $IsdH^{N2N3}$ than to $IsdB^{N1N2}$ (unpublished data). It will be interesting and informative to see whether the haem relay activity of slIsdB also correlates with Hb binding affinity. The higher affinity binding to Hb by slIsdB compared to IsdB, also makes this homologue a good candidate for crystallisation trials. Preliminary screening with the slIsdB protein, containing the Tyr491-to-Ala mutation in the haem binding domain, did not lead to any hit conditions, and it was not possible to optimise the screening strategy within the time-frame of this PhD.

In summary, Chapter 5 has investigated residues that determine the Hb binding affinity of IsdB and IsdH with the goal of addressing both of the main aims of this thesis: to investigate the mechanism of haem capture from Hb and to investigate the process of haem relay. The relationship between Hb binding affinity and haem relay suggests that the weak IsdB:Hb interaction is optimised to allow for both haem transfer and haem relay. Crystallisation of IsdH and IsdB constructs with altered Hb binding properties is described in the following chapter.

Chapter 6. Haem release from Hb involves perturbation of the Hb haem pocket.

6.1 Molecular details of the IsdH^{N2N3}:Hb haem pocket interface

6.1.1 Crystallisation of IsdH^{N2N3} carrying the FYHYA→YYHYF and Y642A mutations in complex with Hb

The aim of this Chapter was to determine the structure of the IsdH:Hb haem transfer interface with the goal of understanding the mechanism of haem release from Hb. In Chapter 5, Isd receptors with altered Hb binding properties were generated and characterised and receptors that bound only to the α chain of Hb were carried forward for structural studies on the premise that these might form more ordered crystals. IsdH^{N2N3} carrying the FYHYA→YYHYF mutation was selected for crystallisation trials because this mutation effectively removed the interaction with β Hb, yet had minimal impact on the interaction with α Hb. In addition, the Y642A mutation that inhibits haem binding was introduced into the IsdH^{N3} domain with the aim of trapping a pre haem-transfer complex. The resulting IsdH^{N2N3} mutant protein was mixed with Hb at a 2:1 molar ratio and subject to sparse-matrix crystallisation screening at 21 °C. Beautiful hexagonal crystals (Fig. 6.1 A) grew reproducibly in 0.2 M K/Na tartrate, 0.1 M tri-sodium citrate pH 5.6, 2 M ammonium sulfate. In a fine screen, crystals of identical morphology were obtained over a pH range of 5.4–5.8 and a precipitant concentration of 2–2.2 M ammonium sulfate. Ethylene glycol, glycerol and MPD were tested as cryoprotectants. The crystals cracked in well solution containing ethylene glycol or MPD, but survived soaking for 10–30 s in well solution containing 10, 20 or 30% glycerol before being flash cooled in liquid nitrogen. Because UTas does not posses a home x-ray source, the cryo-conditions could not be screened to determine effects on diffraction quality before taking the crystals to the synchrotron.

An initial diffraction data set was collected at the Australian Synchrotron on the MX1 beam line to a resolution of 2.96 Å and was used for molecular replacement. A subsequent data set that was used for refinement was collected to a resolution of 2.45 Å on the MX2 beam line after using the micro-focus beam to screen for the best regions

within the crystals. The asymmetric unit of the crystals had one very long axis (Table 6.1). To accommodate this long axis, a longer sample-to-detector distance was selected to limit spot overlap at the expense of resolution. The beam-line set up did not allow for changes to the goniometer κ angle to realign the long axis of the crystal parallel with the rotation axis. The diffraction data were indexed with XDS[265] and scaled with AIMLESS[266]; see Table 6.1 for collection and refinement statistics.

6.1.2 Molecular replacement and refinement

The structure of IsdH^{N2N3}Y642A carrying the FYHYA→YYHYF bound to Hb was solved by molecular replacement. The search models included: one α Hb and one β Hb monomer derived from a 2-Å resolution crystal structure of human Fe(III)-Hb (PDB 3P5Q); IsdH^{N2} (PDB 4FC3); IsdH^{N3} with the haem binding β-hairpin removed (PDB 2Z6F); and the helical linker (PDB 4IJ2). Molecular replacement, performed with PHASER[243], gave rise to a single solution. Multiple rounds of restrained refinement were performed with REFMAC 5.7[267] and model building was completed with Coot[268]. In later rounds of refinement, translation/liberation/screw refinement was introduced, with groups defined as single domains (where the linker-N3 unit was considered to be a single group). The PDB_REDO server[269] was used periodically to validate and bench-mark the refinement process. PDB_REDO performs an automated iterative refinement strategy that aims to optimise TLS parameters, B-factor refinement, and weighting of geometry, amongst other parameters. The models generated by REFMAC were validated using MolProbity[247]. Ramachandran statistics for the final model are as follows: 96.6 % of residues were found in favoured regions; 100 % in allowed regions; 0% in disallowed regions. A final check of geometry will be performed before the structure factors and coordinates are submitted to the PDB.

Table 6.1. **Data collection and refinement statistics (molecular replacement)**

IsdH^{N2N3}Y642A-FYHYA→YYHYF:Hb		
	Molecular replacement	Refinement
Data collection		
Wavelength (Å)	0.96580	0.95370
Space group	P 6_5 2 2	P 6_5 2 2
Cell dimensions		
a, *b*, *c* (Å)	92.475, 92.475, 365.296	92.29, 92.29, 365.34
α, β, γ (°)	90, 90, 120	90, 90, 120
Resolution (Å)	182.65–2.96 (3.14-2.96)	79.93–2.45 (2.51-2.45)
R_{merge} (%)	7.1 (35)	9.9 (79.6)
I / σI	20.6 (4.7)	12.3 (1.6)
Completeness (%)	99.8 (99.3)	99.62 (97.85)
Redundancy	12.4 (12.2)	8.9 (6.4)
Refinement		
Resolution (Å)		79.93 -2.45 (2.51-2.45)
No. reflections		33226
R_{work} / R_{free}		2.41/2.74 (3.95/4.38)
No. atoms		
Protein		4748
Ligand/ion		94
Water		9
B-factors		
Protein		75.1
Ligand/ion		84.1
Water		54.2
R.m.s. deviations		
Bond lengths (Å)		0.004
Bond angles (°)		0.780

Values in parentheses are for the highest resolution shell.

6.1.3 The IsdH^{N2N3}Y642A-FYHYA→YYHYF:Hb complex

The asymmetric unit contained a single IsdH^{N2N3}(Y642A,FYHYA→YYHYF) receptor bound to the α chain of an αβ Hb dimer (Fig., 6.1 B). Two αβ Hb dimers make contacts across the α1β2 and α2β1 interfaces; however, the tetramers do not adopt any of the well-known Hb quaternary structures. Residues 384–389 (comprising loop 3 which is away from the α Hb binding interface) and 467–472 (which connect IsdH^{N2} and the Linker domain and are located adjacent to loop 3) are absent from the model as the electron density in these regions was weak. The structure of the receptor overlayed with each of the three receptors in the previously solved IsdH:Hb complex (4IJ2, see Chapter 3) with backbone r.m.s.d.'s of 0.92, 1.13 and 1.78 Å; the closest match was to one of the α bound receptors in 4IJ2 (chain G, Fig. 6.1 C). The three domains assembled in the expected positions on the surface of α Hb, with close alignment of the IsdH^{N2} domain

(r.m.s.d of 1.22 Å over 128 Cα atoms), indicating that the introduced mutations do not interfere with how the receptor assembles on Hb (Fig. 6.1 C). Molecular contacts at the interface between α Hb and $IsdH^{N2}$ are the same as observed for the 2.3-Å resolution $IsdH^{N2:}$Hb crystal structure (PDB 4F3C, Fig. 6.1 D) with the exception of contacts made by the introduced Tyr365 and Phe369 side chains in Loop 2 of $IsdH^{N2}$. The conformation of the loop 2 helix of $IsdH^{N2}$ in the mutant receptor (Fig. 6.1 E and Fig. 6.1 F, purple) is essentially identical to the loop 2 helix in $IsdH^{N1}$:Hb (Fig. 6.1 F, cyan, PDB 3S48), showing that the α Hb-interaction face of $IsdH^{N1}$ was successfully transplanted onto $IsdH^{N2}$.

Figure 6.1. Crystal structure of $IsdH^{N2N3}$Y642A, carrying the FYHYA→YYHYF mutation, bound through the α chain of Hb. (A) Crystals of the engineered complex. **(B)** The crystal structure of the engineered $IsdH^{N2N3}$ complex was determined at a resolution of 2.5 Å. The crystallographic asymmetric unit contained one $IsdH^{N2N3}$ receptor (purple) bound though the α chain (orange) of an αβ Hb dimer. **(C)** The structure of the engineered $IsdH^{N2N3}$ complex (purple) is shown overlaid with an $IsdH^{N2N3}$(Y642A):α Hb dimer (red, PDB 4IJ2). **(D)** The figure shows a comparison of the α Hb binding faces of engineered $IsdH^{N2N3}$ (purple) and wild-type $IsdH^{N2}$ (PDB 4F3C; red). Interfacial contacts are the same in both complexes, with the exception of residues in the mutated aromatic helix in loop 2. **(E)** The introduced Phe369 on aromatic helix in loop 2 (purple) is buried between the A and E helices of α Hb (orange). The $2F_O$-F_C density is shown contoured at 1.5 σ. **(F)** The side chains of Phe369 and Try365 in the mutated receptor (purple) adopt the same conformation as in $IsdH^{N1}$ (cyan). The wild type $IsdH^{N2}$ domain is also shown for comparison (red). Only the residues of the mutated receptor are labelled.

Figure 6.1

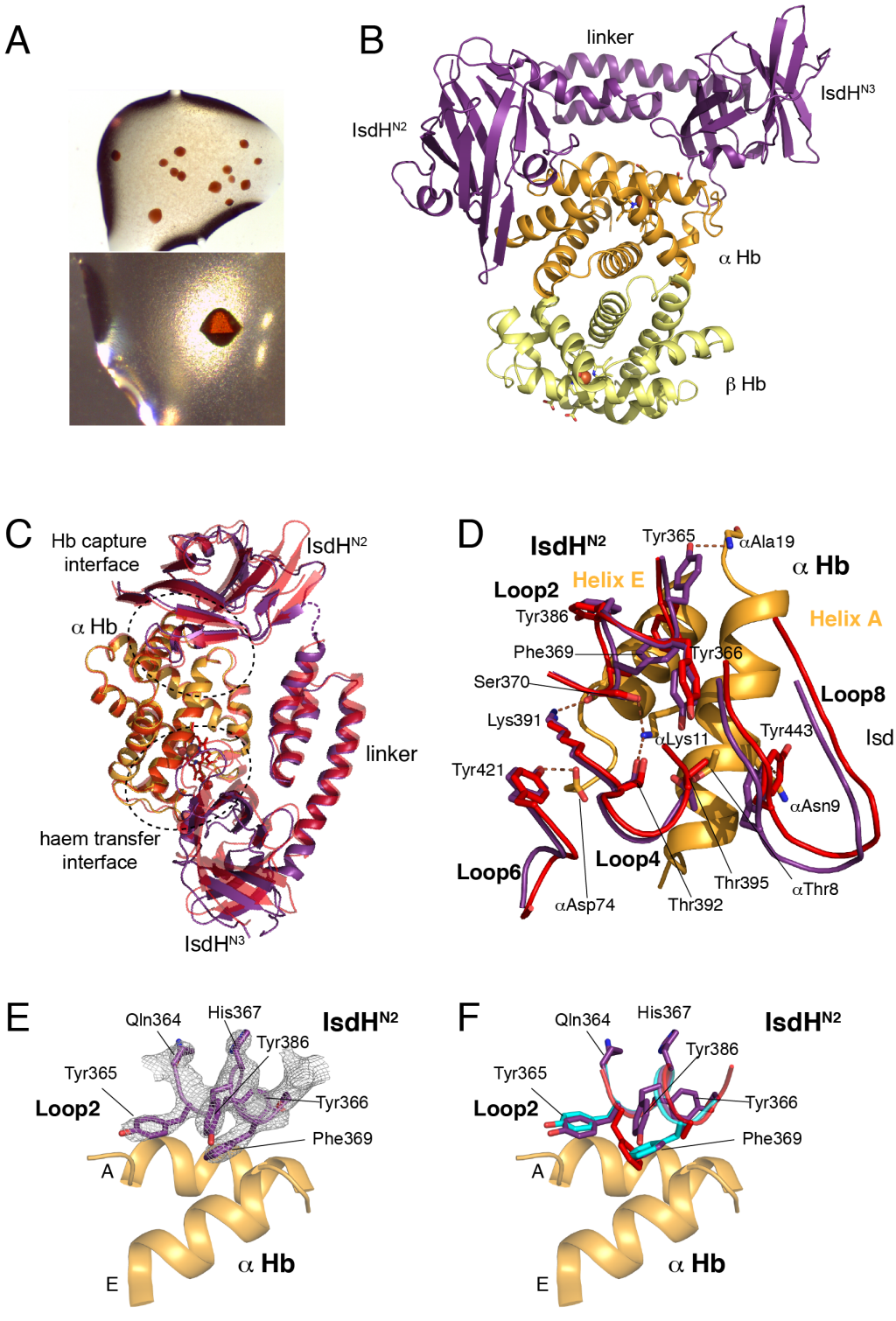
A
B
linker
IsdH^N3
IsdH^N2
α Hb
β Hb
C
Hb capture interface
IsdH^N2
α Hb
linker
haem transfer interface
IsdH^N3
D
IsdH^N2
Tyr365
αAla19
α Hb
Loop2
Helix E
Tyr386
Helix A
Phe369
Tyr366
Ser370
Loop8
Lys391
αLys11
Tyr443
IsdH^N2
Tyr421
αAsn9
Loop6
Loop4
Thr395
αThr8
αAsp74
Thr392
E
Qln364
His367
IsdH^N2
Tyr386
Tyr365
Loop2
Tyr366
Phe369
A
α Hb
E
F
Qln364
His367
IsdH^N2
Tyr386
Tyr365
Loop2
Tyr366
Phe369
A
α Hb
E

In the IsdH^{N2N3}(Y642A,FYHYA→YYHYF) receptor, the haem binding β-strands of the IsdH^{N3} domain adopt a conformation that is different from both the holo- and apo-structures of the free IsdH^{N3} domain. In the IsdH^{N2N3}(Y642A,FYHYA→YYHYF) receptor the β7–8 turn projects towards, and makes contact with, the CD loop and F-helix of α Hb (Fig. 6.2 A). Three hydrophobic residues in the β7–8 turn – Val637, Ala638 and Leu640 – pack against side chains of α Hb – Tyr42, Pro44, His45, His89 and Leu91 – forming one wall of the haem transfer chamber. Anomalous signal was detected at the globin haem iron sites but not in the receptor haem pockets (Fig. 6.2 B), indicating that haem transfer did not occur, presumably due to the Y642A mutation. In addition, the absence of difference electron density indicates that the receptor haem pocket is not occupied by a ligand that might block haem transfer (e.g., Mack *et. al.,* observed that IsdC was recovered from *E. coli* expression with non-metallated protoporphyrin-IX bound[229]). These results reinforce the view that difference density seen in the receptor haem binding sites in the 4.2-Å resolution structure (Chapter 3) may have been due to haem from denatured Hb in the crystallization drop, or an uncharacterized ligand picked up during purification or crystallisation. Crystallization conditions for IsdH^{N2N3}(Y642A,FYHYA→YYHYF) did not produce large amounts of Hb precipitate, as was the case for the 4.2-Å resolution structure.

Figure 6.2. (A) Hydrophobic residues on the IsdH^{N3} β7–β8 hairpin (purple spheres) pack against the α Hb CE and FG loops (green spheres) in the IsdH^{N2N3}(Y642A,FYHYA→YYHYF):Hb complex. The structures of isolated holo-IsdH^{N3} (PDB 2Z6F, blue) and apoIsdH^{N3} (PDB 2E7D, red) are overlaid, to show the different conformations of the haem binding beta strands. **(B)** Anomalous signal (green) contoured at 3 σ and 2Fo-Fc density contoured at 1.5 σ (grey) are seen in the α Hb haem pocket (orange) but not in the IsdH^{N3} haem pocket.

Figure 6.2

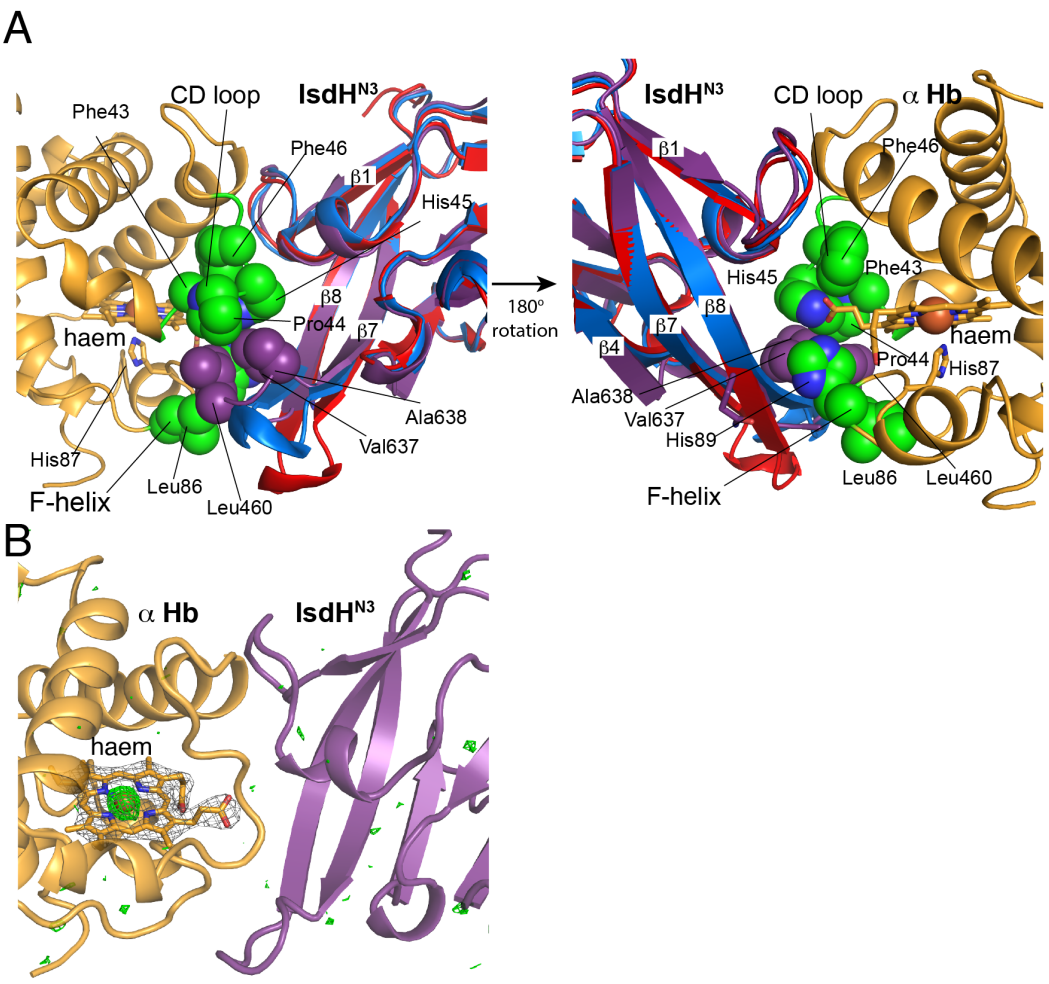
A
Phe43
CD loop
IsdH^N3
Phe46
β1
His45
β8
Pro44
β7
haem
Ala638
Val637
His87
Leu86
F-helix
Leu460
180°
rotation
IsdH^N3
CD loop
α Hb
β1
Phe46
His45
Phe43
β8
β7
haem
β4
Pro44
His87
Ala638
Val637
His89
F-helix
Leu86
Leu460
B
α Hb
IsdH^N3
haem

Overall, the backbone conformation of α Hb in IsdH^{N2N3}(Y642A,FYHYA→YYHYF):Hb is unchanged from native Fe(III)-α Hb (r.m.s.d. of 0.32 Å over 105 Cα atom pairs, excluding Val73–Arg92, with PDB 3P5Q). However, localised conformational changes occur across a contiguous region of residues (Val73–Arg92) that comprise the F-helix and the FG loop (Fig. 6.3 A, coloured red). The largest changes are seen for residues Leu86–Leu91 (Fig. 6.3 B, residues coloured red or pink). A number of salt bridges and hydrogen bonding interactions are evident between IsdH (Linker and IsdH^{N3} domains) and the E and F helices and haem group of α Hb, (Fig. 6.3 C, green and cyan side chains). For example, Tyr495 and Lys499 of IsdH^{N3} form a hydrogen bond and salt bridge with αAsp85. αAsp85 marks the boundary between segments of the F-helix with native and non-native conformation. At the opposite side of the interface, Glu562 of IsdH^{N3} hydrogen bonds to Gln54 on the E-helix of α Hb. Interestingly, the side chain of Tyr646 (Fig.. 6.3 D, cyan), which in holo-IsdH^{N3} interacts with the haem coordinating tyrosine to stabilize haem binding, makes hydrogen bonding interactions with one of the haem propionates. Due to the change in the conformation of the F-helix upon IsdH binding, the side chain of αHis89 is moved ~11 Å to a new position adjacent to the haem pocket entrance and, together with the imidazole side chain of αHis45, makes hydrogen bonding interactions with the same haem propionate that contacts IsdH Tyr646 (Fig. 6.3 D).

His and Tyr side chains are suitable ligands for haem iron and it is tempting to speculate that one or more of His89, His85 and Tyr646 might act as an intermediate haem ligand during haem transfer process. However, it is important to recognise that mutation of Tyr642-to-Ala in this structure may have influenced the positions and interactions of other side chains at the interface. In Figure 6.3 D the wild-type holo-IsdH^{N3} domain is overlaid to show the location of Try642 (yellow) in the native IsdH^{N3} domain. In the presence of the Tyr642-to-Ala mutation, the side chain of Val637 partially occupies this location, indicating some compensatory local adjustments in the structure in the Tyr642-to-Ala mutant. It is clear that a steric clash would prevent αHis89 and IsdH Tyr642 from both adopting the positions shown in Figure 6.3 D. Thus, in the native structure, Tyr642 might displace His89 from its position in the current structure. Even if the Tyr642-to-Ala mutation causes minimal perturbation of the interface, it is a limitation of the study that the position of Tyr642, a key residue, cannot be determined. One way to address this limitation would be to introduce a Try642-to-Phe mutation; the Phe side chain occupies a

similar volume to Tyr but is unable to bind haem. Alternatively, a previously described Tyr646-to-Ala mutation, which is unable to bind specifically to haem or capture haem from Hb[155,160] but retains the haem coordinating Tyr642, could be trialled. Other possible ways to block haem transfer, but retain the native Tyr642 and Tyr646 side chains, would be to introduce amino acids with large side chains that protrude into the haem binding cavity and present a steric impediment to haem binding. In the β subunit, αHis45 and αHis89 are replaced by βSer44 and βAsp94, neither of which can act as ligands for the haem iron. Hence, if intermediate iron ligands do prove to be involved in haem transfer from α Hb to IsdH, different mechanisms would be expected for transfer from β Hb chains.

Notwithstanding the caveats above, the haem transfer interface provides a potential explanation for receptor-induced haem loss from the globin. In native Hb, the haem pocket residues limit the rate of haem loss from the globin haem pocket in several ways. The F-helix of native α Hb contains the haem-coordinating His residue (His87) and also contributes three residues, Leu83, Leu86 and Leu91, which together with Val93, Phe98 and Leu136 form a hydrophobic surface of the proximal haem pocket that interacts with the hydrophobic porphyrin ring (Fig. 6.3 E). These six hydrophobic residues enclose His87 and protect and stabilise the interaction between the imidazole side chain and the haem iron. These interactions are critical for the stability of the globin:haem interaction because histidine can be readily displaced by water. The proximal haem pocket residues act to prevent water from competing with His87 for the haem iron coordination[270,271]. The six hydrophobic residues are conserved in β Hb (Fig. 6.3 F) and their function is also conserved in myoglobin (Mb). In complex with $IsdH^{N2N3}$(Y642A,FYHYA→YYHYF) two hydrophobic residues, Leu86 and Leu91, are displaced from their native positions and are peeled away from the haem pocket (Fig. 6.3 G). In this complex the side chain and Cα of Ala88 move into the position occupied by Leu91 in native α Hb, under haem pyrrol II; however, the smaller methyl side chain is unlikely to compensate for loss of the larger Leu91 and Leu86 residues. Numerous studies with both Hb and Mb have shown that disrupting the hydrophobic barrier through mutagenesis both removes favourable hydrophobic contacts with the haem group and introduces water into the proximal haem pocket leading to greatly increased rates of haem loss[270-272]. In addition, a range of unstable Hb variants arise from single amino acid substitutions to hydrophobic residues in

the F-helix and FG loop. These include (but are not limited to): Hb Boras, β Leu88Arg[273]; Hb Les Andelys, α Leu83Pro[274]; Hb Santa Ana, β Leu88Pro[275]; and Hb Köln, β Val98Met[272,276]. All of the aforementioned show increased haem loss and instability attributed to increased solvation of the distal haem pocket and disruption to the F-helix conformation. Hence, by unravelling the F-helix, the receptor undermines measures that the globin has evolved in order to protect and stabilise the globin-haem interaction.

Conformational flexibility of the F-helix is necessary for haem insertion during globin chain synthesis[277,278]. The F-helix is also an important component of the allosteric mechanism that achieves cooperative oxygen binding[279]. In addition, the chaperone α Hb stabilizing protein (AHSP) causes conformational changes in the α Hb haem pocket, to regulate metal oxidation, by introducing strain into the globin F-helix[280-283]. Removal of the haem group must also require unfolding of the globin haem pocket and the results shown here suggest that the IsdH receptor targets the F-helix, a region of the protein in which conformation plasticity is required for function.

Figure 6.3. The haem transfer interface. (A) The α Hb subunit from the IsdH^{N2N3}(Y642A,FYHYA→YYHYF):Hb complex (orange and red) overlaid with native Fe(III)-Hb (PDB 3P5Q, cyan). A localized change in backbone conformation occurs across the F-helix (red). **(B)** Close up of the haem pocket E and F helices. Residues of the F-helix that have altered conformation are shown as sticks (red, pink and green) and the corresponding $2F_O$-F_C electron density is shown at 1.5 σ. **(C)** The haem transfer interface. The IsdH^{N2N3} receptor (purple) makes hydrogen bonds and one salt bridge with the α Hb polypeptide and haem propionates through four side chains (cyan). The Tyr642Ala mutation is shown as a yellow sphere. Residues of α Hb that are involved in hydrogen bonds with the receptor are coloured green while the two His of α that interact with the haem propionate are coloured pink. The rest of the F-helix of α Hb that has altered conformation is coloured red. **(D)** The IsdH^{N2N3}(Y642A,FYHYA→YYHYF):Hb interface, with holo-IsdH^{N3} (PDB 2Z6F) overlaid. The position of Tyr642 in PDB 2Z6F is shown as yellow sticks. **(E-F)** The haem pocket of native Fe(III)-α Hb (E), and native Fe(III)-β Hb (F). Hydrophobic residues of the proximal haem pocket (spheres) contact the haem group and protect the haem coordinating histidine (red) against hydration. **(G)** At the IsdH^{N2N3}(Y642A,FYHYA→YYHYF):Hb interface some of the proximal haem pocket residues (spheres) are displaced from their native positions.

Figure 6.3

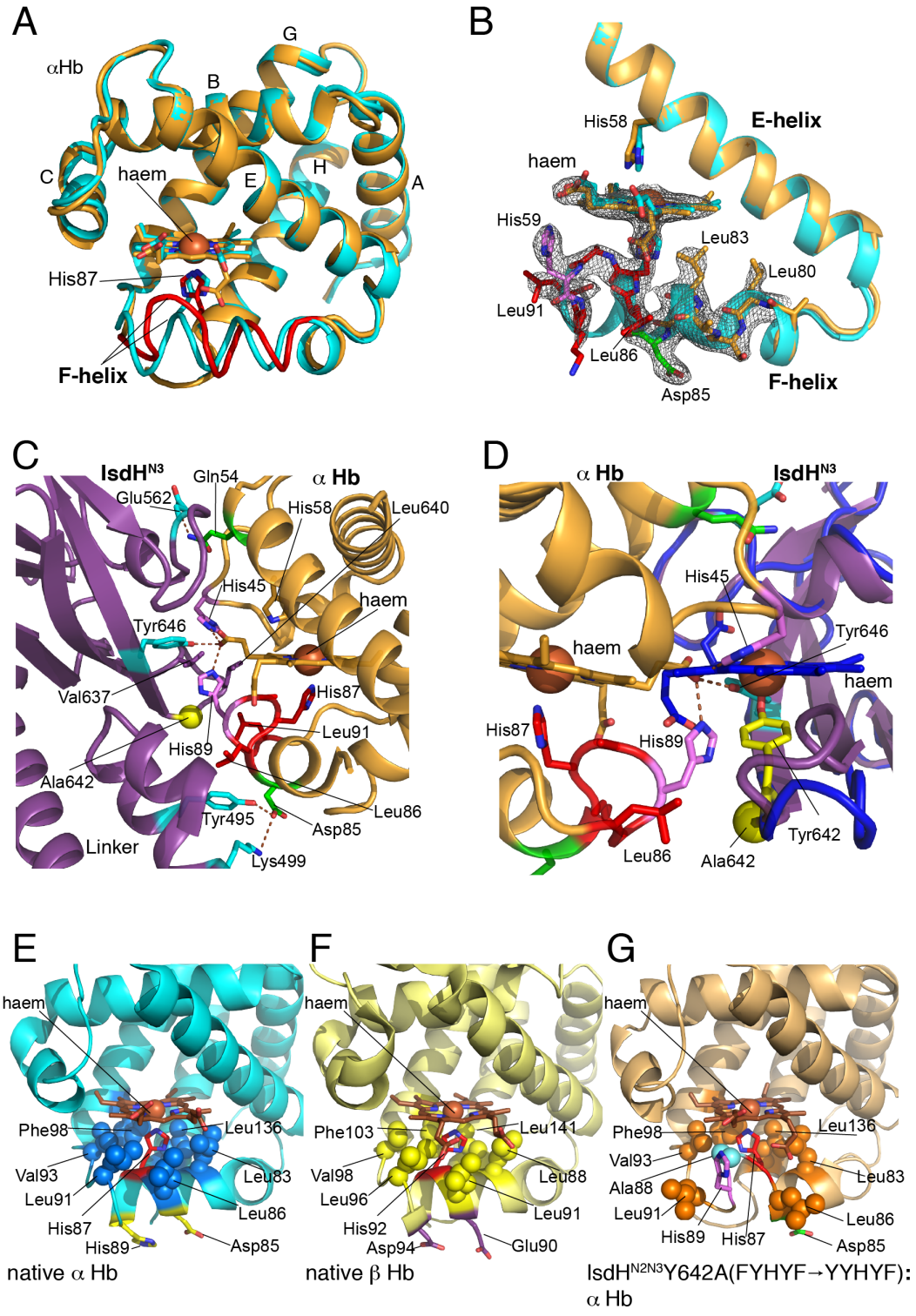
A
αHb
G
B
C
haem
E
H
A
His87
F-helix
B
His58
E-helix
haem
His59
Leu83
Leu80
Leu91
Leu86
Asp85
F-helix
C
IsdH^N3
Gln54
α Hb
Glu562
His58
Leu640
His45
haem
Tyr646
Val637
His87
Leu91
His89
Ala642
Tyr495
Asp85
Leu86
Linker
Lys499
D
α Hb
IsdH^N3
His45
Tyr646
haem
haem
His87
His89
Tyr642
Leu86
Ala642
E
haem
Phe98
Leu136
Val93
Leu83
Leu91
Leu86
His87
His89
Asp85
native α Hb
F
haem
Phe103
Leu141
Val98
Leu88
Leu96
Leu91
His92
Asp94
Glu90
native β Hb
G
haem
Phe98
Leu136
Val93
Leu83
Ala88
Leu91
Leu86
His89
His87
Asp85
IsdH^N2N3Y642A(FYHYF→YYHYF):
α Hb

Two, symmetry-related, αβ dimers make α1β2 and α2β1 interfaces; however, the quaternary interactions do not represent either R or T state Hb. The positioning of the two dimers is more similar to T state Hb, but involves a greater rotation of the α2β2 unit relative to the α1β1 unit. Table 6.2 lists Hb subunit interactions that are characteristic of R state and T state Hb, respectively, and the Hb subunit interactions seen in the $IsdH^{N2N3}$:Hb complex. Three of the salt-bridge and hydrogen-bonding interactions which are characteristic of T state Hb are present in $IsdH^{N2N3}$(Y642A,FYHYA→YYHYF):Hb. On the whole, far fewer specific contacts are seen when the receptor is present than in either native Hb conformations, suggesting that the Hb tetramer is held together more loosely. The altered quaternary structure does not appear to be the result of changes in the α or β Hb monomer structure, or changes in the α1β1 (or α2β2) interfaces: αβ dimers align with an r.m.s.d. of 0.43 Å over 233 Cα atom pairs. Interestingly, the crystal structure provides some evidence that receptor binding induces strain in the native Hb tetramer conformation. The β-hairpin of an $IsdH^{N3}$ molecule that is bound to an α Hb subunit in the α1β1 dimer, projects across to contact the C-helix of a β Hb subunit in the neighbouring α2β2 dimer (Fig. 6.4 A). If the Hb tetramer were to adopt either the R or the T state quaternary conformation then the C-helix would sterically clash with the Leu640 and Gly641 of the receptor (Fig. 6.4 A, B). Using ESI-mass spectrometry, Spirig *et al.*, observed dissociation of Hb tetramers into dimers in the presence of the $IsdH^{N2N3}$ receptor independent of haem removal from the globin haem pocket[167]. Based on these findings they proposed a mechanism whereby binding of the receptor induced dissociation of Hb into dimers in order to accelerate haem release from Hb. The steric interaction between $IsdH^{N3}$ and the β Hb subunit across the α1β2 interface provides a molecular basis for such a mechanism.

Table 6.2. **Quaternary state interactions**

Region	Interactions		
	R-state	T-state	$IsdH^{N2N3}$:Hb
Switch region αC:βFG Side chain positioning	His97 positioned between Thr38 and Thr41	Asp99 positioned between aTyr41 and aTyr42	Asp99 positioned between aTyr41 and aTyr42
Terminal salt bridges*	β1His146 – β1Val1	α1Arg141 – α2Asp126 α1Arg141 – α2Lys127 β1His146 – α2Lys40 β1His146 – β1Asp94	β1His146 – α2Lys40
Hydrogen-bonding interactions characteristic of quaternary state	α1Asn97 – α1Tyr42 β2Trp37 – β2Asn102 β2Asn102 – α1Asp94 α1Val1 – α2Ser138	α1Asn97 – β2Asp99 α1Tyr42 – β2Asp99 β2Trp37 – α2Asp94 β1Val1 – β1Leu78 α1Lys127 – α1Val1	α1Asn97 – β2Asp99 α1Tyr42 – β2Asp99

*Functional groups involved are: βHis146 α-carboxyl; βVal1 α-amino; αArg141 α-carboxyl; αArg141 guanidinium; αAsp126 β-carboxyl; βHis146 imidazolium; αLys40 ε-amino; βAsp94 β-carboxyl.

Figure 6.4. Steric interactions between the receptor and the β_2 subunit across the $\alpha_1\beta_2$ interface. (A) The $IsdH^{N2N3}$ receptor (purple) is shown bound through the α chain of the Hb tetramer. The α1β1 and α2β2 dimers are coloured yellow and orange, respectively. The β-hairpin of $IsdH^{N3}$ sits between the C and F helices (red) of the β2 subunit. The T state Hb tetramer (2ND2; α1β1 and α2β2 dimers coloured grey and blue, respectively) is overlayed with $IsdH^{N2N3}$(Y642A,FYHYA→YYHYF):Hb, by superposition of the α1β1 dimers in both complexes. Residues of the receptor and T state Hb that would clash are shown are spheres. **(B)** An enlarged image of the boxed region in (A). Hydrogen bonding between the β-hairpin of $IsdH^{N3}$ and β2 Hb is represented by red dashed lines. Predicted steric clashes that would occur if IsdH bound to T state Hb are represented by black dashed lines.

Figure 6.4

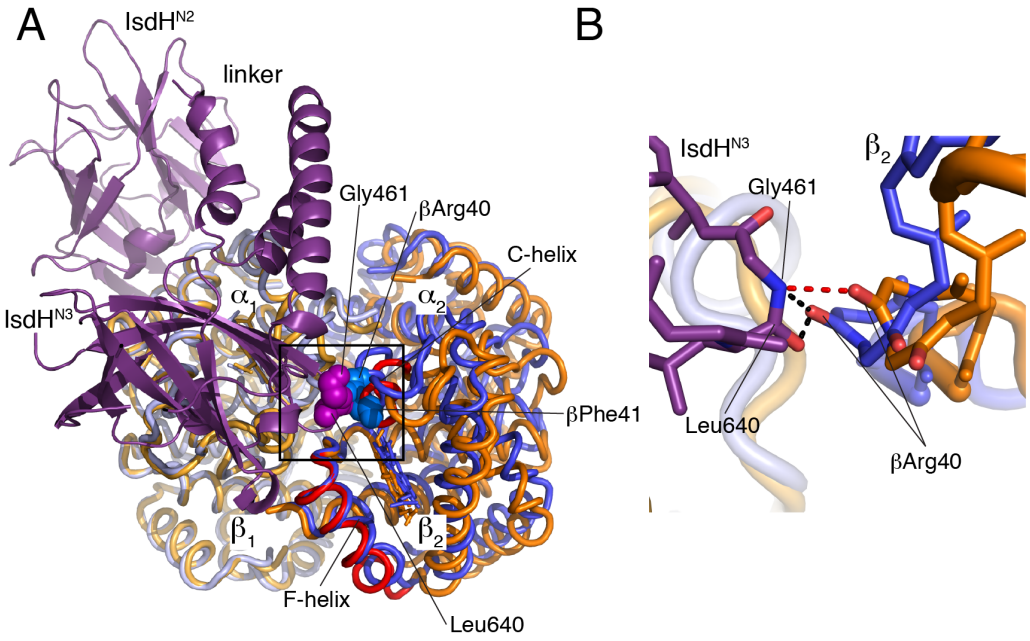
A
IsdH^N2
linker
Gly461
βArg40
C-helix
α1
α2
IsdH^N3
βPhe41
β1
β2
F-helix
Leu640
B
IsdH^N3
β2
Gly461
Leu640
βArg40

6.2 IsdH^{N3}/IsdB^{N2} perturb the haem pocket of Hb in solution

During the course of performing UV-Vis experiments described in Section 3.3.1 it was noticed that the spectrum of Fe(III)-Hb mixed with IsdH^{N2N3}(Y642A) was not identical to that of Fe(III)-Hb alone. Immediately after mixing at 4 °C a small red-shift in the Soret band (~400 nm) and changes in the Q band region (peaks at ~500–580 nm) were observed (Fig. 6.5 A). Importantly, after the first spectrum (~40 s) no further changes were observed over the next 30 min of incubation at 4 °C (Fig. 3.9 B). Two possible explanations for the observed spectral change are: (i) a change in the structure of the globin haem pocket upon IsdH^{N2N3}(Y642A) binding in the absence of haem transfer or (ii) a minor proportion of haem groups transfer to reach a point of equilibrium in <40 s. There is no obvious physical mechanism that would lead to rapid transfer of such a small proportion of haem groups. Therefore, small changes in the spectrum of IsdH^{N2N3}(Y642A):Hb may may be evidence of structural changes in solution, similar to those seen in IsdH^{N2N3}(Y642A,FYHYA→YYHYF):Hb crystal structure. Spectral changes were also observed immediately upon mixing Hb with IsdB^{N1N2}Y440A (Fig. 6.5 B), suggesting that IsdB may also induce conformational changes in the globin haem pocket. In summary, the spectroscopic studies provide some evidence that the structural changes observed in the crystal structure also occur in solution.

Figure 6.5. (A) The spectrum of Fe(III)-Hb alone and in the presence of excess IsdH^{N2N3}(Y642A). The spectrum of the complex is shown immediately after mixing and after 7.5 min, indicating that no change occurs over time. **(A)** The spectrum of Fe(III)-Hb alone, and in the presence of excess IsdB^{N1N2}Y440A. Minimal changes occur in the spectrum over 7.5 min.

Figure 6.5

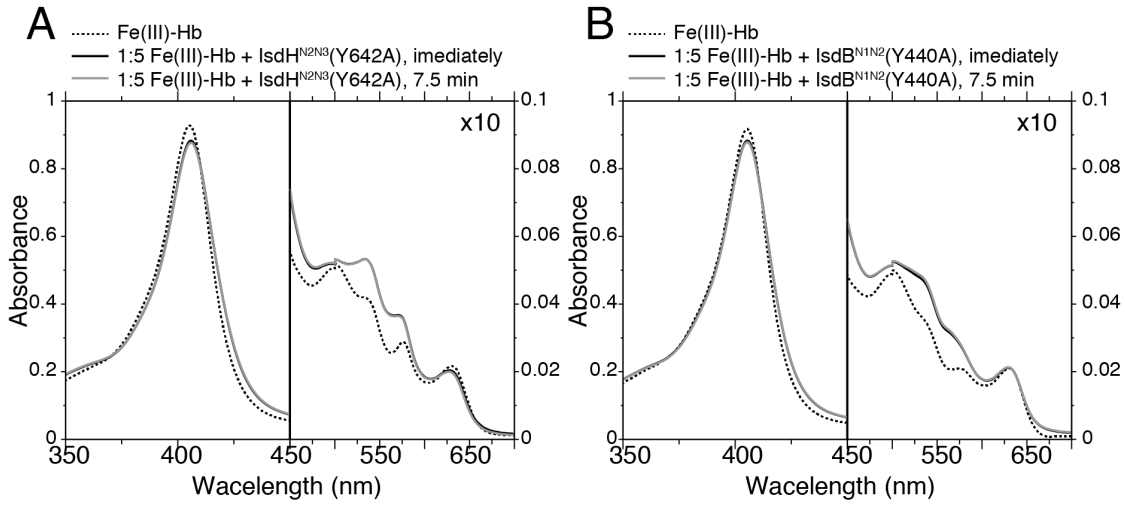
A
Fe(III)-Hb
1:5 Fe(III)-Hb + IsdH^{N2N3}(Y642A), imediately
1:5 Fe(III)-Hb + IsdH^{N2N3}(Y642A), 7.5 min
x10
Absorbance
Wacelength (nm)
B
Fe(III)-Hb
1:5 Fe(III)-Hb + IsdB^{N1N2}(Y440A), imediately
1:5 Fe(III)-Hb + IsdB^{N1N2}(Y440A), 7.5 min
x10
Absorbance
Wacelength (nm)

6.3 Towards a haem transfer mechanism

To build a more comprehensive picture of the haem transfer reaction, crystallisation screening was performed with complexes of the receptor that had a wild type haem pocket. The aim was to capture a complex after haem had been transferred out of the globin haem pocket to visualise the final step in the haem capture process. Crystallisation trials were performed with two different complexes that were competent to undergo haem transfer. First, a 2:1 complex of apo-IsdH^{N2N3}(FYHYA→YYHYF) with Fe(III)-Hb, and second, a 2:1 complex of apo-IsdB^{N1N2} (carrying the QSF→NTT and FYHYA→YYHYF mutations as described in Chapter 5) with Fe(III)-Hb was prepared. Finally, because the structure of IsdB in complex with Hb has not been determined in the pre- or post-transfer state, IsdB^{N1N2}(QSF→NTT,FYHYA→YYHYF) was prepared with an addition Tyr440Ala mutation which inhibits haem binding and combined 2:1 with Fe(III)-Hb. All three complexes produced crystals or crystalline formations in the initial trials. Optimisation of crystal growth was attempted for each of the complexes; however, during the timeframe of this PhD only the apo-IsdB^{N1N2}:Hb complex produced diffraction quality crystals.

6.3.1 Crystallisation of apo-IsdB^{N1N2} carrying the QSF→NTT and FYHYA→YYHYF mutations, in complex with Hb

Crystalline formations grew in 0.15 M DL-malic acid, pH 7.0, 20% (w/v) PEG 3350. Addition of isopropanol or ethanol to 10–20% (v/v) led to small, layered crystals. Larger crystals were grown in 16–17% PEG 3350 at pH 7.2–7.4. Finally, multiple rounds of streak seeding produced large crystals in 0.1 M DL-malic acid, pH 7.2, 16% (w/v) PEG 3350, 15% isopropanol (Fig. 6.6 A). Although the crystals appeared single they had an unusual morphology with a slot in one side, suggesting that they were in fact clusters. The crystals dissolved in well solution containing glycerol and so were cryo-protected in well solution containing 25% ethylene glycol. Diffraction data were collected on the Australian Synchrotron MX2 beam line to 3.7 Å. The crystal contained multiple lattices, but a single lattice could be indexed with XDS[265] and scaled with AIMLESS[266]; see Table 6.3 for collection and refinement statistics.

6.3.2 Molecular replacement and refinement

Molecular replacement was performed with PHASER[243] using αβ Hb dimers (PDB 3P5Q), the holo-IsdB^{N3} domain (PDB 3RTL) and a poly-alanine model of IsdH^{N2} (PDB 4FC3), which was produced by removing all the side chains from the PDB file using CHAINSAW[242]. The volume of the asymmetric unit was consistent with two Hb tetramers and four IsdH receptors – a total of 20 domains! The initial solution contained four αβ Hb dimers, two IsdB^{N2} domains and two IsdH^{N2} domains. REFMAC[267] was used to perform an initial round of rigid body refinement after which MOLREP was able to place another IsdB^{N2} domain, followed by an IsdH^{N2} domain. Helical density was present in the F_O–F_C electron density map between each of the NEAT domain pairs, allowing the three-helix linkers to be built using Coot[268] (Fig.. 6.6 B). Model building and refinement is incomplete, however, the statistics for the model at time of writing are given in table 6.3.

Table 6.3. **Data collection and refinement statistics (molecular replacement)**

IsdB^{N1N2} (QSF→NTT, FYHYA→YYHYF):Hb	
Data collection	
Wavelength (Å)	0.95370
Space group	C 2 2 2
Cell dimensions	
a, *b*, *c* (Å)	154.07, 268.695, 153.74
α, β, γ (°)	90, 90, 90
Resolution (Å)	48.14–3.701 (3.88-3.70)
R_{merge} (%)	11.0 (63.0)
I / σI	9.7 (1.9)
Completeness (%)	99.2 (96.0)
Redundancy	3.7 (3.7)
Refinement	
Resolution (Å)	44.59–3.70 (3.797-3.701)
No. reflections	32378
R_{work} / R_{free}	0.32/0.33 (0.38/0.36)
No. atoms	
Protein	17117
Ligand/ion	301
Water	-
B-factors	
Protein	63.77
Ligand/ion	75.28
Water	-
R.m.s. deviations	
Bond lengths (Å)	0.004
Bond angles (°)	0.74

Values in parentheses are for the highest resolution shell.

6.3.3 The IsdB^{N1N2}(QSF→NTT,FYHYA→YYHYF):Hb complex

Although the structure is not fully refined, inspection of the preliminary model reveals some interesting features. The four IsdB^{N1N2}(QSF→NTT,FYHYA→YYHYF) receptors are bound through the α Hb chains (Fig. 6.6 C–D). The three domains of a single IsdB receptor bind to a single α Hb chain, to generate separate Hb-capture and haem-transfer interfaces as seen for IsdH^{N2N3}:Hb interactions (compare Figure 6.6 D with Figure 3.15 B). The IsdB^{N2} domain anchors the receptor to the A and E helices of α Hb. The helical linker domain contacts the globin F-helix and an interaction between αAsp85 and Tyr293 is evident in the electron density as seen for IsdH (Fig. 6.3C). The haem binding domain, IsdB^{N2}, is positioned next to the globin haem pocket. With the exception of a small difference in the arrangement of the three helices of the IsdB^{N1N2} Linker, the overall architecture of IsdB^{N1N2} and IsdH^{N2N3} is the same (Fig. 6.6 E). Thus the two homologous regions of the *S. aureus* Hb receptors, IsdB and IsdH, have a conserved structure and are likely to extract haem from Hb via a conserved mechanism.

At the haem transfer interface, clear electron density is seen in the haem pocket of the IsdB^{N2} domain while the α Hb pockets are empty, indicating that haem has been transferred to the receptor (Fig. 6.6 B and F). The low resolution, and the fact that the structure is not yet fully refined, makes any comment on the conformation of the α Hb pockets speculative; however, the F-helix appears more similar to native α Hb than to the "pre-transfer" complex of IsdH^{N2N3}(Y642A,FYHYA→YYHYF). This would suggest that contacts that impart the initial strain on the globin haem pocket are removed after haem transfer has occurred.

Figure 6.6. Crystal structure of IsdB^{N1N2} (carrying the QSF→NTT and FYHYA→YYHYF mutations) bound through the a chain of Hb. (A) Photos of the hanging drop experiments showing multiple rounds of streak seeding. **(B)** The IsdB receptor (blue) with $2F_O$-F_C electron density shown at 1.5 σ (grey mesh) and F_O-F_C density shown at 3 σ (green mesh), generated from a model without the helical Linker domains or haem groups. Difference electron density is present for three α-helices of the Linker domain, the haem group, and the missing side chains in the IsdB^{N1} domains. **(C)** The two IsdB^{N1N2}:Hb complexes in the asymmetric unit. The four receptors (grey, blue, purple and green) are bound through the α subunits of Hb (orange). The β subunits are coloured yellow. **(D)** The three domains of IsdB^{N1N2} bind to one α Hb chain to create separate Hb capture and haem transfer interfaces as seen in the IsdH^{N2N3}:α Hb complex (Fig. 3.15 B). **(E)** The two complete IsdB^{N1N2} molecules (yellow and lavender) overlaid with the 2.5 Å structure of IsdH^{N2N3} (purple). **(F)** The haem transfer interface of IsdB^{N1N2} and α Hb. $2F_O$-F_C electron density is shown at 1.5 σ (grey mesh).

Figure 6.6

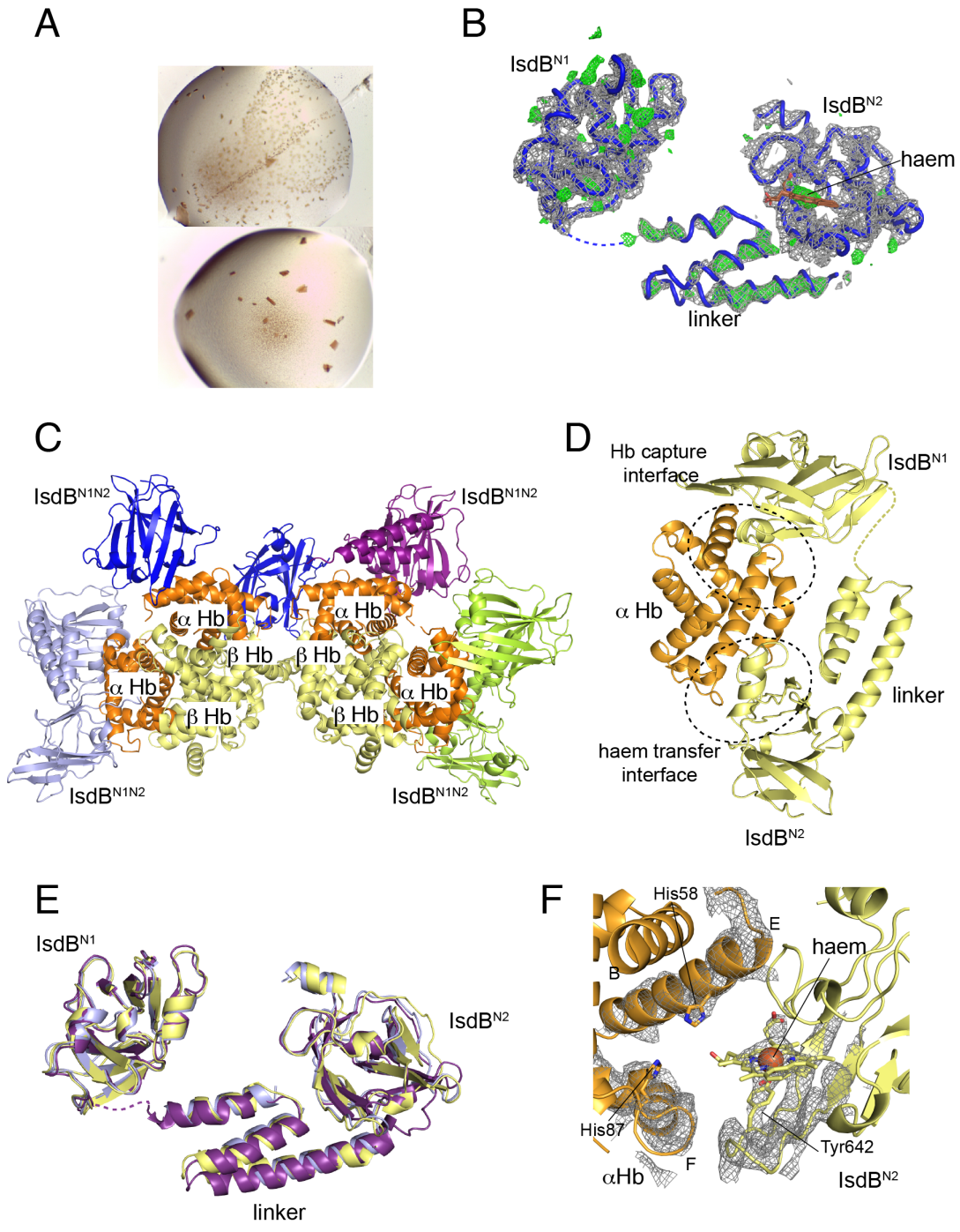
A
B
IsdB^N1
IsdB^N2
haem
linker
C
IsdB^N1N2
IsdB^N1N2
α Hb
β Hb
α Hb
β Hb
α Hb
β Hb
α Hb
β Hb
IsdB^N1N2
IsdB^N1N2
D
Hb capture interface
IsdB^N1
α Hb
linker
haem transfer interface
IsdB^N2
E
IsdB^N1
IsdB^N2
linker
F
His58
E
haem
B
His87
Tyr642
αHb
F
IsdB^N2

6.3.4 Future directions

The structures of engineered $IsdH^{N2N3}$ and $IsdB^{N1N2}$ suggest that the haem binding NEAT domain ($IsdH^{N3}$ or $IsdB^{N2}$) and the Linker domain both contribute to the haem transfer interface. The structure of the "pre-transfer" complex could now be used as a starting point for molecular dynamics (MD) simulations to investigate the haem transfer reaction. The IsdB:Hb "post-transfer" complex provides means to validate the outcomes of MD simulations. To confirm the involvement of specific residues in haem transfer, mutations could be introduced into the Isd receptors or the globin chain. For example, Tyr495 and Lys499 on the IsdH linker domain interact with αAsp85, which marks the boundary between sections of the F-helix that have native and non-native conformations in the pre-transfer $IsdH^{N2N3}$ complex. These interactions also appear to be conserved in IsdB:Hb interactions. This interaction, along with contacts at the haem pockets, could be targeted through mutagenesis, and haem capture and relay activity could be assessed *in vitro* as was done for the mutations disabling Hb binding in Chapter 5. Pishchany *et al.*, introduced IsdB genes carrying mutations in the Hb binding domain into the staphylococcal genome and demonstrated inhibited binding of Hb to *S. aureus* cells, reduced bacterial growth using Hb as an iron source, and reduced bacterial virulence[208]. If mutations at the interface between the haem binding NEAT domains and Hb, or the Linker domain and Hb, inhibit IsdB/H function *in vitro* and *S. aureus* growth *in vivo*, this opens up the possibility that inhibitors of these interactions might have utility against *S. aureus* infection.

The approach taken to rationally engineer the $IsdH^{N2N3}$ receptor, successfully produced crystals with better diffraction properties than those grown from the wild type complex. A comparison of the 2.5-Å $IsdH^{N2N3}$(Y642A,FYHYA→YYHYF):Hb structure and the 4.2-Å $IsdH^{N2N3}$Y642A:Hb structure reveals a slight repositioning of the Linker and $IsdH^{N3}$ domains. The whole Linker-$IsdH^{N3}$ unit appears to have pivoted from the start of helix 1, close to the attachment point of the linker with the $IsdH^{N2}$ domain. The result is that the β7–8 turn and the helical lip have moved ~ 7 Å in the direction of the α Hb haem pocket. In addition, the haem binding β-hairpin of $IsdH^{N3}$ is clearly defined in the electron density map, supporting the hypothesis that in the 4.2 Å structure, the $IsdH^{N3}$ domains were hindered in their binding to α Hb due to steric interference. Hence the strategy to selectively remove low-affinity interactions between IsdH and β Hb to capture

the IsdH:α Hb haem pocket interactions has been successful. The IsdB/H:β Hb interface has not yet been characterised and a similar approach to enhance β Hb interactions and remove α Hb interactions may allow for the crystallisation of an IsdB/H:β Hb complex. One possible target for mutagenesis is loop 4 of $IsdB^{N1}$ or $IsdH^{N2}$. In Chapter 5, the primary sequence of loop 4 was shown in to be a determinant of high affinity binding to α Hb. In IsdH, residues of loop 4 interact with Lys11 of α Hb. Thr12 occupies the same position of β Hb and it may be possible to tailor loop4 to be more complementary to the size and charge of βThr12. An alternative strategy may be to introduce mutations into the β Hb sequence; a Thr12-to-Lys mutation in the β chain of Hb was previously shown to enhance the binding of $IsdH^{N2}$ to Hb^{146}. In addition, it may be possible to block the α Hb sites with the isolated $IsdH^{N1}$ domain by virtue of the higher affinity binding of the $IsdH^{N1}$ domain to α Hb detected in Chapter 4. Structural information on the haem transfer interface at the β Hb haem pockets will confirm whether a similar or distinct haem-transfer mechanism operates at the two globin haem pockets. This may be relevant for the design of inhibitors that aim to prevent uptake of haem from both Hb chains.

In conclusion, the structural studies performed in Chapter 6 have addressed the aim of determining the molecular mechanism used by IsdB and IsdH to liberate haem from Hb. The structure of the engineered $IsdH^{N2N3}$ protein bound to Hb has revealed direct contacts at the Hb haem pocket, and an altered Hb haem pocket conformation, providing a potential mechanism for facilitated haem release from Hb. The contribution of these molecular contacts to haem transfer can now be tested through mutagenesis studies that target the haem transfer interface.

Chapter 7. Discussion

7.1 The mechanism of haem capture from Hb

Haem is relayed through the bacterial cell wall, a distance of up to ~90 nm, via an energy-independent mechanism that involves the formation of protein-protein complexes between Isd proteins to transfer the haem ligand[149,167,168,170,171]. Haem transport across the membrane is achieved by an ABC transporter (of which two components are IsdE and IsdF), and, is therefore presumed to be ATP-dependent. At the onset of this project it was known that interactions between Hb and the Hb receptors, IsdH and IsdB, facilitate the release of haem from Hb, leading to rapid haem capture[149,167]. The nature of these key interactions and the molecular mechanism of facilitated haem release were unknown.

Towards understanding this mechanism, the structures of the intact homologous regions of the Hb receptors were investigated, free and in complex with Hb. $IsdB^{N1N2}$ and $IsdH^{N2N3}$ adopt a conserved supra-domain structure that is preserved upon binding to Hb. The three domains of a receptor are arranged to contact a single globin chain such that two interfaces are formed: a Hb targeting interface and a haem transfer interface. The use of multiple interaction surfaces may allow for localised conformational changes in the globin fold, which are necessary for haem release, without disrupting the receptor:Hb complex. The engineered pre-transfer complex of $IsdH^{N2N3}$ bound to Hb revealed that the Linker and $IsdH^{N3}$ domains contribute a limited number of specific molecular contacts at the haem transfer interface that could not be identified in the lower resolution $IsdH^{N2N3}$(Y642A):Hb complex. These contacts promote unfolding of the globin F-helix. The proposed mechanism of haem release is that unfolding of the F-helix disrupts the hydrophobic seal that protects the iron-histidine bond and destabilises the globin-haem interaction, and also widens the entrance through which haem can move out of the globin.

Besides IsdH and IsdB, only two other interactions with Hb have been structurally characterised. These are Hb complexes with the mammalian proteins AHSP[281-283] and Hp[250]. AHSP binds the free α chain of Hb while Hp binds to an αβ dimer. In each case the binding site is distant from the haem pocket and distinct from the surface contacted by the Isd proteins. Hp binds to αβ Hb dimers (blocking tetramer formation) and stabilises the native globin fold, preventing haem loss and autooxidation[250]. Binding of AHSP

introduces structural changes into the α Hb haem pocket to induce a bishistidyl haem ligation that is protective against oxidative damage by limiting redox cycling of the haem iron[281,282]. To bring about these structural changes in the haem pocket, AHSP introduces strain into the α Hb structure that is transmitted though the globin F-helix and proximal His to weaken the Fe–O_2 bond in oxygenated α Hb[280,283]. Interestingly, AHSP binding accelerates haem loss from Fe(III)-α Hb by a factor of 2, presumably though increased hydration of the haem pocket (the physiological significance of this effect, if any, is unknown)[284]. In conclusion, it is likely that any disturbance of the native haem pocket structure will result in increased autooxidation and haem dissociation, and this is exploited by the IsdB/H receptors to promote haem release.

The three-domain architecture necessary for direct haem capture is specific to $IsdB^{N1N2}$ and $IsdH^{N2N3}$ and the related protein slIsdB, implying that the putative Hb receptors in Gram-positive *S. pyogens*, *B. cereus*, *B. anthracis* and *L. monocotogenes*[69,163,183,187], which have different domain architectures, may function via a distinct mechanism. The putative Hb receptors, Shr, IlsA, IsdX1, Hal and Hbp2 (see Section 1.5.4.5) are multi-domain proteins, and it is hypothesised that some of these domains might bind to Hb, whilst the conserved NEAT domain(s) capture haem, in a fashion analogous to the two-interface mechanism of IsdB/H.

While the Hb interactions of the putative Hb receptors are yet to be characterised, the structure of the IsdH:Hb complex may help to interpret some of the available data. Structures are available for the isolated IsdX1-NEAT and IsdX2-NEAT5 of *B. anthracis*[154,184]. In both cases residues of 3_{10} helix were implicated in Hb binding and haem capture. In the IsdH:Hb structure, the helical lip is adjacent to the globin C-E loop and the E-helix, where Glu562 of $IsdH^{N3}$ hydrogen bonds to αGln54. Assuming that the IsdX NEAT domains dock to the globin haem pocket in the same orientation as $IsdH^{N3}$ then Gln29 of IsdX-NEAT2, which was shown to be required for haem scavenging from Hb[157], is in a position to interact with αGln54 (Fig. 7.1). Interactions between the 3_{10} helix of the IsdX proteins and the globin E-helix may act to tether the receptor to the haem pocket surface, although the interaction is expected to be weak without an additional Hb targeting domain. The two haem binding tyrosines are also present in conserved positions with Tyr642 and Tyr646 of $IsdH^{N3}$. In contrast, the rest of the haem

binding β-hairpin is dissimilar to $IsdH^{N3}$ and it is difficult to predict whether interactions will occur with this surface and the globin F-helix. The rate of haem capture by IsdX1 or IsdX2 from Hb has not been determined, so it is not known if this is limited by passive dissociation from Hb chains, or if IsdX1/2 facilitates haem release as is the case for IsdB/H. If the latter is true, additional contacts that destabilise the haem pocket are expected. The five NEAT domains of IsdX2 could potentially perform multiple roles in binding/destabilising Hb and binding to haem. To determine whether the Gram-positive Hb receptors function through similar mechanisms to IsdH and IsdB, kinetic measurements of haem transfer together with structural studies of the intact receptors in complex with Hb are required.

Figure 7.1. Possible interactions of IsdX2-NEAT5 with the haem pocket of α Hb. The isolated NEAT5 domain of IsdX2 (blue; PDB 4H8P) is shown overlaid with $IsdH^{N3}$ (purple) at the haem transfer interface of α Hb (orange). A hydrogen bond between Glu562 of $IsdH^{N3}$ (cyan) and Gln54 of α Hb (green), present in the crystal structure of $IsdH^{N2N3}$(Y642A,FYHYA→YYHYF) is shown. Gln29 (red) of IsdX2-NEAT5 is positioned such that it could possibly interact with Gln54 of α Hb. Side chain rotamers of IsdX2-NEAT5 have not been optimised for hydrogen bonding with α Hb.

Figure 7.1

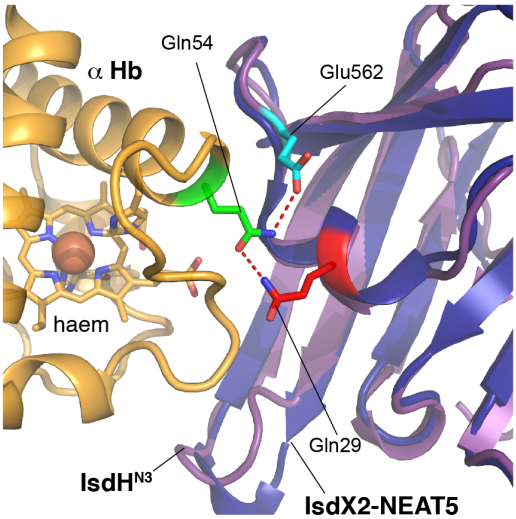

7.2 The mechanism of haem relay from Hb

Despite a conserved mechanism of haem capture, IsdB and IsdH show differences in haem relay function, with IsdB but not IsdH catalysing haem transfer from Hb to IsdA/C. Higher haem relay activity was found to correlate with lower Hb binding affinity. Thus, IsdB showed considerably weaker affinity for α Hb and β Hb than IsdH or $IsdH^{N2N3}$ but showed much greater haem relay activity. To investigate the relationship between Hb affinity and haem relay further, I introduced mutations into the Hb targeting domain of IsdB that enhanced or reduced the interaction with Hb. The haem relay activity of IsdB proteins with altered Hb binding affinity was consistent with the hypothesis that Hb binding affinity is optimised to allow for both a specific interaction and rapid haem relay (discussed in Section 5.6). A mechanism in which rapid dissociation of the Isd:Hb complex is necessary for efficient haem relay is consistent with the $IsdH^{N2N3}$ and $IsdB^{N1N2}$ structures presented in Chapters 3 and 6, because the haem pockets of IsdB and IsdH are not accessible to IsdA/C when bound to Hb. No large conformational changes were observed between the free and the bound forms of the receptor; hence, the structure studies predict that the complex must dissociate for haem relay to occur.

Ligand-transfer pathways, which involve relay of a ligand though a network of proteins, often rely on transient or weak associations between protein partners. These interactions, with typical dissociation constants in the range of mM–μM, allow for rapid and repeated interactions between the donor and acceptor proteins to convey the ligand[172,173,285]. Weak or transient interactions occur at multiple stages in the Isd pathway as transfer of haem between IsdA and IsdC involves an 'ultra-weak' interaction (K_d ~5 mM)[171]. Hence low affinity protein-protein interactions are likely to be a general feature of bacterial haem relay pathways.

7.3 Potential roles for IsdB and IsdH in haem uptake from Hb

The superior haem relay activity of IsdB identified in this project provides a biochemical basis to understand why IsdB is the primary receptor involved in haem import from Hb *in vivo*[8,84]. This raises the question, if IsdB is more efficient at haem uptake from Hb than IsdH, why does *S. aureus* produce IsdH? IsdH may have alternative roles in infection (as discussed in section 4.8); however, the high-affinity Hb binding and haem extraction functions presumably play some role. One possibility is that IsdH and IsdB play

complementary roles under different conditions of Hb abundance (Fig. 7.2). In environments where the concentration of Hb is high, encounters between IsdB and Hb will occur frequently and rapid association and dissociation of complexes is expected to allow for efficient haem relay to IsdA/C. In contrast, IsdH provides two higher affinity α Hb binding domains and may provide an advantage in Hb capture under conditions where Hb concentration is low. The $IsdH^{N1}$ domain was shown to be connected to the protein via an unstructured linker domain of ~ 100 residues (K. Krishna Kumar and D. Gell, unpublished), which may further increase the chances of binding Hb through a 'fly-casting' mechanism. In addition, when haem is in excess, IsdH may act as a reservoir for haem, buffering against a change in conditions. A buffering role has been proposed for the second NEAT domain of Shr, which binds to haem but does not rapidly transfer this haem to Shp[178,179], and for the multiple NEAT domains of IsdX2[184]. IsdB and IsdH may have diverged in their Hb capture and haem relay activities in order to optimise haem uptake at different sites of infection within the host that offer different Hb availability. *Bacillus anthracis* also produces numerous Hb/haem receptors, IsdX1, IsdX2, Blsk and Hal[86,157,183,186,286]. Indeed, the expression of multiple factors that play complementary functions in iron import is common amongst bacterial pathogens. Recently, it has been shown that the siderophores, pyoverdine and pyrochelin, produced by *Pseudomonas aeruginosa,* operate in iron uptake under different conditions of iron availability[287]. Pyoverdine has a high affinity for iron but is metabolically more expensive to produce than the lower-affinity iron chelator, pyrochelin. Varying the relative abundance of these two siderophores was shown to provide a competitive advantage in an environment fluctuating in iron availability.

Future work should investigate the model that IsdH and IsdB play distinct roles in haem uptake. One possibility would be to measure growth of genetically engineered *S. aureus* strains that are deficient in either IsdB or IsdH production under a range of conditions with different Hb availability. Competition assays with deletion vs wild type strains may determine whether expression of both proteins provides a growth advantage across different Hb concentrations. An alternative possibility is that IsdH may contribute to haem capture from Hb:Hp complexes. Hp may stabilise the Hb fold and prevent haem loss[250] and IsdB/H may differ in their ability to extract haem from Hb in the presence of Hp. The role Hp in haem uptake by IsdB/IsdH should now be investigated.

Figure 7.2. A schematic model describing potential complementary roles for IsdB and IsdH in environments with different concentrations of available Hb. Under conditions where Hb is highly abundant, weak interactions between IsdB and Hb will allow for efficient relay of haem from Hb to the haem carrier proteins IsdA/C (black). Under conditions where Hb is scarce, the high affinity Hb binding domain of IsdH (white), attached to a freely diffusing linker, may provide an advantage in Hb capture. Hb that is bound by this domain may be delivered to the haem extraction domains of IsdH or IsdB (light grey). Slow haem relay from IsdH may provide a haem reservoir to buffer against fluctuations in Hb availability.

Figure 7.2

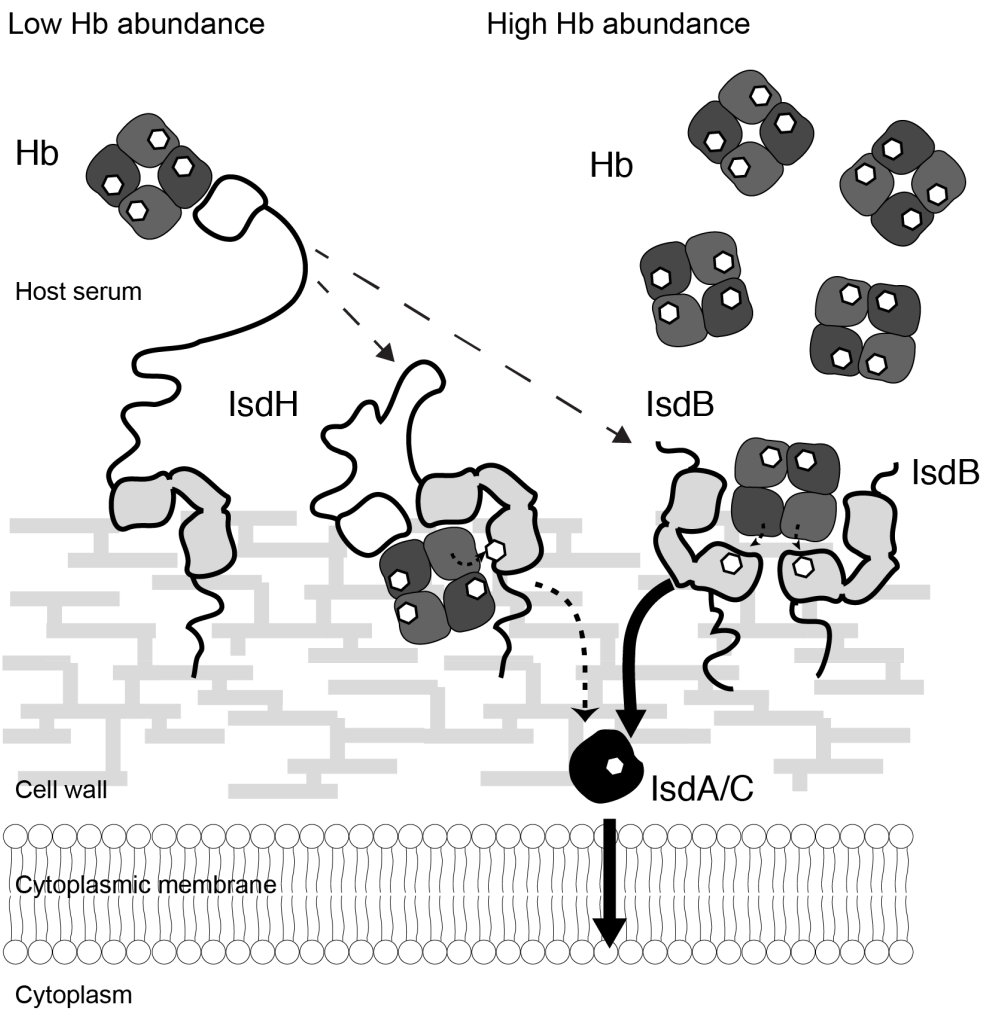
Low Hb abundance
High Hb abundance
Hb
Hb
Host serum
IsdH
IsdB
IsdB
Cell wall
IsdA/C
Cytoplasmic membrane
Cytoplasm

7.4 The Hb receptors as targets for antimicrobial therapies

Iron is an essential nutrient for *S. aureus* growth and inhibiting iron uptake is a possible target for antibiotic development. *S. aureus* employs multiple iron uptake systems during infection, including the Isd system. Inactivating elements of the Isd pathway significantly reduces *S. aureus* growth and infectivity however does not render *S. aureus* avirulent. While inhibiting the Isd system in isolation is unlikely to be effective in curing *S. aureus* infection, a combinatorial approach that targets each of the redundant iron import systems, including the Isd system, may be highly effective. In addition, the Isd system may be exploited as a route to import antibacterial agents that have been liked to porphyrin mimetics. Since the Isd system is specific to *S. aureus*, a drug that is imported by Isd system may have the advantage of not killing commensal and beneficial bacteria.

The Isd system has received considerable interest as a target for antimicrobial therapies. Current avenues being explored include the development of porphyrin inhibitors that bind to Isd proteins but cannot be relayed through the pathway[288], non-iron metalloporphyrin complexes that hijack the haem uptake pathways to import bactericidal metals[176,221,289], and vaccine design using Isd proteins as antigens[290-293].

A new possibility, based on the work from this thesis and elsewhere, may be to develop molecules to inhibit the Isd:Hb, protein-protein interactions. Haem transfer experiments in Chapters 3 and 5, together with previous studies[167,208], indicate that specific interactions at both the Hb binding interface and the haem transfer interface are required for haem uptake from Hb. Blocking Hb:Isd interactions through mutagenesis of Hb or the IsdB receptor, reduces (in the case of Hb mutants)[146] or largely abolishes (in the case of IsdB mutants)[208] *S. aureus* growth using Hb as an iron source. In infection models, an *S. aureus* strain expressing an IsdB mutant that cannot bind to Hb shows reduced colonisation of kidneys and hearts[208]. Hence disrupting the Isd:Hb interactions may be of therapeutic benefit for infections of these organs. *S. aureus* is an important cause of infective endocarditis, and is associated with high mortality, meaning that new treatments are certainly required. If used in combined therapies, inhibitors of Isd:Hb interactions may enhance the action of porphyrin based inhibitors, by favouring uptake of the antibiotic molecule rather than Hb-derived haem. Since the antimicrobial porphyrin compounds identified to date have a lower affinity for the Isd proteins than haem, this

effect may be significant[166,221]. The Isd:Hb structures indicate that both NEAT domains and the linker contribute to the Hb binding surface, providing several potential faces to target. IsdH and IsdB use the same surfaces to contact Hb and many of the interactions are conserved and so it might be possible design an inhibitor to knock out both interactions with Hb. Compounds that target any of these sites may be identified through fragment screening or *in silico* methods (computer aided drug design), followed by structure determination and lead optimisation[294-297].

An alternative anti-microbial therapy is vaccine development. The Isd proteins are expressed in *S. aureus* strains isolated from infected tissues[260] and are highly immunogenic[290,298,299]. Preliminary vaccination trials and passive transfer of antibodies against IsdA, IsdB and IsdH show protective effects in mouse and bovine models[174,290,291,300]. However, preliminary vaccination trials using recombinant IsdB have failed to provide significant protection in humans[299]. More recently fusion proteins combining several fragments of immunogenic proteins, including IsdB, have shown greater efficacy in mouse models[292,293]. From the IsdH/B:Hb structures it may be possible to identify functional regions and regions that are conserved between IsdB/H which could improve fusion vaccine design.

7.5 Conclusion

The ability to import iron from host proteins is an important aspect of bacterial virulence. Many pathogenic bacteria utilise the abundant protein Hb as a source of nutrient iron during colonisation of a mammalian host. This thesis presents structural and functional data that provide insights on how the Hb receptors of *S. aureus* function to capture haem from human Hb. This is the first structural characterisation of an intact Gram-positive Hb receptor in complex with Hb and may inform our understanding of Hb receptor function in other Gram-positive species.

References

1. Braun, V. & Killmann, H. Bacterial solutions to the iron-supply problem. *Trends Biochem Sci* **24**, 104-9 (1999).

2. Weinberg, E.D. Iron loading and disease surveillance. *Emerg Infect Dis* **5**, 346-52 (1999).

3. Weinberg, E.D. Iron availability and infection. *Biochim Biophys Acta* **1790**, 600-5 (2009).

4. Weinberg, E.D. Microbial pathogens with impaired ability to acquire host iron. *Biometals* **13**, 85-9 (2000).

5. Allard, M. et al. Transcriptional modulation of some *Staphylococcus aureus* iron-regulated genes during growth *in vitro* and in a tissue cage model *in vivo. Microbes Infect* **8**, 1679-90 (2006).

6. Malachowa, N. et al. Global changes in *Staphylococcus aureus* gene expression in human blood. *PLoS One* **6**, e18617 (2011).

7. Mazmanian, S.K. et al. Passage of heme-iron across the envelope of *Staphylococcus aureus*. *Science* **299**, 906-9 (2003).

8. Pishchany, G. et al. Specificity for human hemoglobin enhances *Staphylococcus aureus* infection. *Cell Host Microbe* **8**, 544-50 (2010).

9. Ogston, A. Micrococcus Poisoning. *J Anat Physiol* **17**, 24-58 (1882).

10. Ogston, A. Report upon Micro-Organisms in Surgical Diseases. *Br Med J* **1**, 369.b2-375 (1881).

11. Rosenbach, F.J. Microorganismen bei den Wund-Infections-Krankheiten des Menschen. *J.F. Bergmann, Wiesbaden*, 1-122 (1884).

12. Klevens, R.M. et al. Invasive methicillin-resistant *Staphylococcus aureus* infections in the United States. *Jama* **298**, 1763-71 (2007).

13. Kluytmans, J., van Belkum, A. & Verbrugh, H. Nasal carriage of S*taphylococcus aureus:* epidemiology, underlying mechanisms, and associated risks. *Clin Microbiol Rev* **10**, 505-20 (1997).

14. Deurenberg, R.H. & Stobberingh, E.E. The evolution of *Staphylococcus aureus. Infect Genet Evol* **8**, 747-63 (2008).

15. Chambers, H.F. & Deleo, F.R. Waves of resistance: *Staphylococcus aureus* in the antibiotic era. *Nat Rev Microbiol* **7**, 629-41 (2009).

16. Jevons, M.P. Celbenin-resistant Staphylococci. *Br Med J* **1**, 124-125 (1961).

17. Dukic, V.M., Lauderdale, D.S., Wilder, J., Daum, R.S. & David, M.Z. Epidemics of community-associated methicillin-resistant *Staphylococcus aureus* in the United States: a meta-analysis. *PLoS One* **8**, e52722 (2013).

18. Klein, E., Smith, D.L. & Laxminarayan, R. Hospitalizations and deaths caused by methicillin-resistant *Staphylococcus aureus*, United States, 1999-2005. *Emerg Infect Dis* **13**, 1840-6 (2007).

19. Song, M.D., Wachi, M., Doi, M., Ishino, F. & Matsuhashi, M. Evolution of an inducible penicillin-target protein in methicillin-resistant *Staphylococcus aureus* by gene fusion. *FEBS Lett* **221**, 167-71 (1987).

20. Ubukata, K., Yamashita, N. & Konno, M. Occurrence of a beta-lactam-inducible penicillin-binding protein in methicillin-resistant staphylococci. *Antimicrob Agents Chemother* **27**, 851-7 (1985).

21. Wielders, C.L. et al. In-vivo transfer of mecA DNA to *Staphylococcus aureus* [corrected]. *Lancet* **357**, 1674-5 (2001).

22. Hiramatsu, K. et al. Genomic Basis for Methicillin Resistance in *Staphylococcus aureus*. *Infect Chemother* **45**, 117-36 (2013).

23. Tsubakishita, S., Kuwahara-Arai, K., Sasaki, T. & Hiramatsu, K. Origin and molecular evolution of the determinant of methicillin resistance in staphylococci. *Antimicrob Agents Chemother* **54**, 4352-9 (2010).

24. Ito, T. et al. Structural comparison of three types of staphylococcal cassette chromosome mec integrated in the chromosome in methicillin-resistant *Staphylococcus aureus*. *Antimicrob Agents Chemother* **45**, 1323-36 (2001).

25. Hiramatsu, K., Katayama, Y., Yuzawa, H. & Ito, T. Molecular genetics of methicillin-resistant *Staphylococcus aureus*. *Int J Med Microbiol* **292**, 67-74 (2002).

26. David, M.Z. & Daum, R.S. Community-associated methicillin-resistant *Staphylococcus aureus*: epidemiology and clinical consequences of an emerging epidemic. *Clin Microbiol Rev* **23**, 616-87 (2010).

27. Lee, S.M. et al. Fitness cost of staphylococcal cassette chromosome mec in methicillin-resistant *Staphylococcus aureus* by way of continuous culture. *Antimicrob Agents Chemother* **51**, 1497-9 (2007).

28. Bocchini, C.E. et al. Panton-Valentine leukocidin genes are associated with enhanced inflammatory response and local disease in acute hematogenous *Staphylococcus aureus* osteomyelitis in children. *Pediatrics* **117**, 433-40 (2006).

29. Tristan, A. et al. Global distribution of Panton-Valentine leukocidin-positive methicillin-resistant *Staphylococcus aureus*, 2006. *Emerg Infect Dis* **13**, 594-600 (2007).

30. Udo, E.E., Pearman, J.W. & Grubb, W.B. Genetic analysis of community isolates of methicillin-resistant *Staphylococcus aureus* in Western Australia. *J Hosp Infect* **25**, 97-108 (1993).

31. Collignon, P., Nimmo, G.R., Gottlieb, T. & Gosbell, I.B. *Staphylococcus aureus* bacteremia, Australia. *Emerg Infect Dis* **11**, 554-61 (2005).

32. Townell, N.J. et al. Community-associated methicillin-resistant *Staphylococcus aureus* endocarditis 'down under': case series and literature review. *Scand J Infect Dis* **44**, 536-40 (2012).

33. Turnidge, J.D. et al. *Staphylococcus aureus* bacteraemia: a major cause of mortality in Australia and New Zealand. *Med J Aust* **191**, 368-73 (2009).

34. Fridkin, S.K. et al. Epidemiological and microbiological characterization of infections caused by *Staphylococcus aureus* with reduced susceptibility to vancomycin, United States, 1997-2001. *Clin Infect Dis* **36**, 429-39 (2003).

35. Hiramatsu, K. et al. Dissemination in Japanese hospitals of strains of *Staphylococcus aureus* heterogeneously resistant to vancomycin. *Lancet* **350**, 1670-3 (1997).

36. Projan, S.J. Why is big Pharma getting out of antibacterial drug discovery? *Curr Opin Microbiol* **6**, 427-30 (2003).

37. Projan, S.J. Whither antibacterial drug discovery? *Drug Discov Today* **13**, 279-80 (2008).

38. Raymond, K.N., Dertz, E.A. & Kim, S.S. Enterobactin: an archetype for microbial iron transport. *Proc Natl Acad Sci U S A* **100**, 3584-8 (2003).

39. Pierre, J.L. & Fontecave, M. Iron and activated oxygen species in biology: the basic chemistry. *Biometals* **12**, 195-9 (1999).

40. Beinert, H., Holm, R.H. & Munck, E. Iron-sulfur clusters: nature's modular, multipurpose structures. *Science* **277**, 653-9 (1997).

41. Johnson, D.C., Dean, D.R., Smith, A.D. & Johnson, M.K. Structure, function, and formation of biological iron-sulfur clusters. *Annu Rev Biochem* **74**, 247-81 (2005).

42. McKie, A.T. et al. An iron-regulated ferric reductase associated with the absorption of dietary iron. *Science* **291**, 1755-9 (2001).

43. Fleming, M.D. et al. Microcytic anaemia mice have a mutation in Nramp2, a candidate iron transporter gene. *Nat Genet* **16**, 383-6 (1997).

44. Kuo, Y.M. et al. Mislocalisation of hephaestin, a multicopper ferroxidase involved in basolateral intestinal iron transport, in the sex linked anaemia mouse. *Gut* **53**, 201-6 (2004).

45. Vulpe, C.D. et al. Hephaestin, a ceruloplasmin homologue implicated in intestinal iron transport, is defective in the sla mouse. *Nat Genet* **21**, 195-9 (1999).

46. Canonne-Hergaux, F., Donovan, A., Delaby, C., Wang, H.J. & Gros, P. Comparative studies of duodenal and macrophage ferroportin proteins. *Am J Physiol Gastrointest Liver Physiol* **290**, G156-63 (2006).

47. Delaby, C., Pilard, N., Goncalves, A.S., Beaumont, C. & Canonne-Hergaux, F. Presence of the iron exporter ferroportin at the plasma membrane of macrophages is enhanced by iron loading and down-regulated by hepcidin. *Blood* **106**, 3979-84 (2005).

48. Mizutani, K., Toyoda, M. & Mikami, B. X-ray structures of transferrins and related proteins. *Biochim Biophys Acta* **1820**, 203-11 (2012).

49. Aisen, P. & Leibman, A. Lactoferrin and transferrin: a comparative study. *Biochim Biophys Acta* **257**, 314-23 (1972).

50. Pakdaman, R., Petitjean, M. & El Hage Chahine, J.M. Transferrins - a mechanism for iron uptake by lactoferrin. *Eur J Biochem* **254**, 144-53 (1998).

51. Cheng, Y., Zak, O., Aisen, P., Harrison, S.C. & Walz, T. Structure of the human transferrin receptor-transferrin complex. *Cell* **116**, 565-76 (2004).

52. Mayle, K.M., Le, A.M. & Kamei, D.T. The intracellular trafficking pathway of transferrin. *Biochim Biophys Acta* **1820**, 264-81 (2012).

53. Halbrooks, P.J. et al. Investigation of the mechanism of iron release from the C-lobe of human serum transferrin: mutational analysis of the role of a pH sensitive triad. *Biochemistry* **42**, 3701-7 (2003).

54. Princiotto, J.V. & Zapolski, E.J. Functional heterogeneity and pH-dependent dissociation properties of human transferrin. *Biochim Biophys Acta* **428**, 766-71 (1976).

55. Legrand, D. & Mazurier, J. A critical review of the roles of host lactoferrin in immunity. *Biometals* **23**, 365-76 (2010).

56. Andrews, S.C., Robinson, A.K. & Rodriguez-Quinones, F. Bacterial iron homeostasis. *FEMS Microbiol Rev* **27**, 215-37 (2003).

57. Clarke, S.R. & Foster, S.J. IsdA protects *Staphylococcus aureus* against the bactericidal protease activity of apolactoferrin. *Infect Immun* **76**, 1518-26 (2008).

58. Hoffbrand, A.V. & Moss, P.A.H. *Essential Haematology*, (Wiley-Blackwell, Oxford, 2011).

59. Collins, H.L. Withholding iron as a cellular defence mechanism - friend or foe? *Eur J Immunol* **38**, 1803-6 (2008).

60. Nairz, M., Schroll, A., Sonnweber, T. & Weiss, G. The struggle for iron - a metal at the host-pathogen interface. *Cell Microbiol* **12**, 1691-702 (2010).

61. Andrews, N.C. Iron homeostasis: insights from genetics and animal models. *Nat Rev Genet* **1**, 208-17 (2000).

62. Pishchany, G. & Skaar, E.P. Taste for blood: hemoglobin as a nutrient source for pathogens. *PLoS Pathog* **8**, e1002535 (2012).

63. Higgins, M.K. et al. Structure of the trypanosome haptoglobin-hemoglobin receptor and implications for nutrient uptake and innate immunity. *Proc Natl Acad Sci U S A* **110**, 1905-10 (2013).

64. Almeida, R.S., Wilson, D. & Hube, B. *Candida albicans* iron acquisition within the host. *FEMS Yeast Res* **9**, 1000-12 (2009).

65. Moors, M.A., Stull, T.L., Blank, K.J., Buckley, H.R. & Mosser, D.M. A role for complement receptor-like molecules in iron acquisition by Candida albicans. *J Exp Med* **175**, 1643-51 (1992).

66. Arosio, P., Adelman, T.G. & Drysdale, J.W. On ferritin heterogeneity. Further evidence for heteropolymers. *J Biol Chem* **253**, 4451-8 (1978).

67. Chasteen, N.D. & Harrison, P.M. Mineralization in ferritin: an efficient means of iron storage. *J Struct Biol* **126**, 182-94 (1999).

68. Harrison, P.M., Fischbach, F.A., Hoy, T.G. & Haggis, G.H. Ferric oxyhydroxide core of ferritin. *Nature* **216**, 1188-90 (1967).

69. Daou, N. et al. IlsA, a unique surface protein of *Bacillus cereus* required for iron acquisition from heme, hemoglobin and ferritin. *PLoS Pathog* **5**, e1000675 (2009).

70. Segond, D. et al. Iron acquisition in *Bacillus cereus*: the roles of IlsA and bacillibactin in exogenous ferritin iron mobilization. *PLoS Pathog* **10**, e1003935 (2014).

71. Nairz, M. et al. Interferon-gamma limits the availability of iron for intramacrophage *Salmonella typhimurium. Eur J Immunol* **38**, 1923-36 (2008).

72. Expert, D. WITHHOLDING AND EXCHANGING IRON: Interactions Between Erwinia spp. and Their Plant Hosts. *Annu Rev Phytopathol* **37**, 307-334 (1999).

73. Geiser, D.L. & Winzerling, J.J. Insect transferrins: multifunctional proteins. *Biochim Biophys Acta* **1820**, 437-51 (2012).

74. Giansanti, F. et al. Antiviral activity of ovotransferrin discloses an evolutionary strategy for the defensive activities of lactoferrin. *Biochem Cell Biol* **80**, 125-30 (2002).

75. Merchant, M., Sanders, P., Dronette, J., Mills, K. & Berken, J. Iron withholding as an innate immune mechanism in the American alligator (Alligator mississippiensis). *J Exp Zool A Ecol Genet Physiol* **307**, 406-10 (2007).

76. Nemeth, E. et al. Hepcidin regulates cellular iron efflux by binding to ferroportin and inducing its internalization. *Science* **306**, 2090-3 (2004).

77. Paradkar, P.N. et al. Iron depletion limits intracellular bacterial growth in macrophages. *Blood* **112**, 866-74 (2008).

78. Kristiansen, M. et al. Identification of the haemoglobin scavenger receptor. *Nature* **409**, 198-201 (2001).

79. Paoli, M. et al. Crystal structure of hemopexin reveals a novel high-affinity heme site formed between two beta-propeller domains. *Nat Struct Biol* **6**, 926-31 (1999).

80. Tolosano, E. & Altruda, F. Hemopexin: structure, function, and regulation. *DNA Cell Biol* **21**, 297-306 (2002).

81. Fournier, C., Smith, A. & Delepelaire, P. Haem release from haemopexin by HxuA allows *Haemophilus influenzae* to escape host nutritional immunity. *Mol Microbiol* **80**, 133-48 (2011).

82. Skaar, E.P., Humayun, M., Bae, T., DeBord, K.L. & Schneewind, O. Iron-source preference of *Staphylococcus aureus* infections. *Science* **305**, 1626-8 (2004).

83. Dryla, A., Gelbmann, D., von Gabain, A. & Nagy, E. Identification of a novel iron regulated staphylococcal surface protein with haptoglobin-haemoglobin binding activity. *Mol Microbiol* **49**, 37-53 (2003).

84. Torres, V.J., Pishchany, G., Humayun, M., Schneewind, O. & Skaar, E.P. *Staphylococcus aureus* IsdB is a hemoglobin receptor required for heme iron utilization. *J Bacteriol* **188**, 8421-9 (2006).

85. Jin, B. et al. Iron acquisition systems for ferric hydroxamates, haemin and haemoglobin in *Listeria monocytogenes. Mol Microbiol* **59**, 1185-98 (2006).

86. Tarlovsky, Y. et al. A Bacillus anthracis S-layer homology protein that binds heme and mediates heme delivery to IsdC. *J Bacteriol* **192**, 3503-11 (2010).

87. Ochsner, U.A., Johnson, Z. & Vasil, M.L. Genetics and regulation of two distinct haem-uptake systems, phu and has, in *Pseudomonas aeruginosa*. *Microbiology* **146 (Pt 1)**, 185-98 (2000).

88. Bullen, J.J., Leigh, L.C. & Rogers, H.J. The effect of iron compounds on the virulence of *Escherichia coli* for guinea-pigs. *Immunology* **15**, 581-8 (1968).

89. Burrows, T.W. & Jackson, S. The virulence-enhancing effect of iron on nonpigmented mutants of virulent strains of *Pasteurella pestis*. *Br J Exp Pathol* **37**, 577-83 (1956).

90. Sword, C.P. Mechanisms of pathogenesis in *Listeria monocytogenes* infection. I. Influence of iron. *J Bacteriol* **92**, 536-42 (1966).

91. Wright, A.C., Simpson, L.M. & Oliver, J.D. Role of iron in the pathogenesis of *Vibrio vulnificus* infections. *Infect Immun* **34**, 503-7 (1981).

92. Weinberg, E.D. The role of iron in protozoan and fungal infectious diseases. *J Eukaryot Microbiol* **46**, 231-8 (1999).

93. Khan, F.A., Fisher, M.A. & Khakoo, R.A. Association of hemochromatosis with infectious diseases: expanding spectrum. *Int J Infect Dis* **11**, 482-7 (2007).

94. Quenee, L.E. et al. Hereditary hemochromatosis restores the virulence of plague vaccine strains. *J Infect Dis* **206**, 1050-8 (2012).

95. Boelaert, J.R., Vandecasteele, S.J., Appelberg, R. & Gordeuk, V.R. The effect of the host's iron status on tuberculosis. *J Infect Dis* **195**, 1745-53 (2007).

96. Brune, I. et al. The DtxR protein acting as dual transcriptional regulator directs a global regulatory network involved in iron metabolism of *Corynebacterium glutamicum*. *BMC Genomics* **7**, 21 (2006).

97. Ernst, J.F., Bennett, R.L. & Rothfield, L.I. Constitutive expression of the iron-enterochelin and ferrichrome uptake systems in a mutant strain of *Salmonella typhimurium*. *J Bacteriol* **135**, 928-34 (1978).

98. Torres, V.J. et al. *Staphylococcus aureus* fur regulates the expression of virulence factors that contribute to the pathogenesis of pneumonia. *Infect Immun* **78**, 1618-28 (2010).

99. Wennerhold, J. & Bott, M. The DtxR regulon of *Corynebacterium glutamicum*. *J Bacteriol* **188**, 2907-18 (2006).

100. Bagg, A. & Neilands, J.B. Ferric uptake regulation protein acts as a repressor, employing iron (II) as a cofactor to bind the operator of an iron transport operon in *Escherichia coli*. *Biochemistry* **26**, 5471-7 (1987).

101. Boyd, J., Oza, M.N. & Murphy, J.R. Molecular cloning and DNA sequence analysis of a diphtheria tox iron-dependent regulatory element (dtxR) from *Corynebacterium diphtheriae. Proc Natl Acad Sci U S A* **87**, 5968-72 (1990).

102. Calderwood, S.B. & Mekalanos, J.J. Iron regulation of Shiga-like toxin expression in *Escherichia coli* is mediated by the fur locus. *J Bacteriol* **169**, 4759-64 (1987).

103. Friedman, D.B. et al. *Staphylococcus aureus* redirects central metabolism to increase iron availability. *PLoS Pathog* **2**, e87 (2006).

104. Campagnari, A.A., Shanks, K.L. & Dyer, D.W. Growth of *Moraxella catarrhalis* with human transferrin and lactoferrin: expression of iron-repressible proteins without siderophore production. *Infect Immun* **62**, 4909-14 (1994).

105. Schryvers, A.B. & Gray-Owen, S. Iron acquisition in *Haemophilus influenzae*: receptors for human transferrin. *J Infect Dis* **165 Suppl 1**, S103-4 (1992).

106. West, S.E. & Sparling, P.F. Response of *Neisseria gonorrhoeae* to iron limitation: alterations in expression of membrane proteins without apparent siderophore production. *Infect Immun* **47**, 388-94 (1985).

107. Lee, B.C. & Schryvers, A.B. Specificity of the lactoferrin and transferrin receptors in *Neisseria gonorrhoeae. Mol Microbiol* **2**, 827-9 (1988).

108. Matias, V.R. & Beveridge, T.J. Native cell wall organization shown by cryo-electron microscopy confirms the existence of a periplasmic space in *Staphylococcus aureus*. *J Bacteriol* **188**, 1011-21 (2006).

109. Kammler, M., Schon, C. & Hantke, K. Characterization of the ferrous iron uptake system of *Escherichia coli. J Bacteriol* **175**, 6212-9 (1993).

110. Ash, M.R. et al. Potassium-activated GTPase reaction in the G Protein-coupled ferrous iron transporter B. *J Biol Chem* **285**, 14594-602 (2010).

111. Hantke, K. Is the bacterial ferrous iron transporter FeoB a living fossil? *Trends Microbiol* **11**, 192-5 (2003).

112. Schroder, I., Johnson, E. & de Vries, S. Microbial ferric iron reductases. *FEMS Microbiol Rev* **27**, 427-47 (2003).

113. Velayudhan, J. et al. Iron acquisition and virulence in *Helicobacter pylori:* a major role for FeoB, a high-affinity ferrous iron transporter. *Mol Microbiol* **37**, 274-86 (2000).

114. Stojiljkovic, I., Cobeljic, M. & Hantke, K. *Escherichia coli* K-12 ferrous iron uptake mutants are impaired in their ability to colonize the mouse intestine. *FEMS Microbiol Lett* **108**, 111-5 (1993).

115. Tsolis, R.M., Baumler, A.J., Heffron, F. & Stojiljkovic, I. Contribution of TonB- and Feo-mediated iron uptake to growth of *Salmonella typhimurium* in the mouse. *Infect Immun* **64**, 4549-56 (1996).

116. Sandy, M. & Butler, A. Microbial iron acquisition: marine and terrestrial siderophores. *Chem Rev* **109**, 4580-95 (2009).

117. Harris, W.R. et al. Coordination chemistry of microbial iron transport compounds. 19. Stability constants and electrochemical behavior of ferric enterobactin and model complexes. *J Am Chem Soc* **101**, 6097-104 (1979).

118. Noinaj, N., Guillier, M., Barnard, T.J. & Buchanan, S.K. TonB-dependent transporters: regulation, structure, and function. *Annu Rev Microbiol* **64**, 43-60 (2010).

119. Wandersman, C. & Delepelaire, P. Bacterial iron sources: from siderophores to hemophores. *Annu Rev Microbiol* **58**, 611-47 (2004).

120. Funahashi, T. et al. Identification and characterization of an outer membrane receptor gene in *Acinetobacter baumannii* required for utilization of desferricoprogen, rhodotorulic acid, and desferrioxamine B as xenosiderophores. *Biol Pharm Bull* **35**, 753-60 (2012).

121. Tanabe, T. et al. Characterization of *Vibrio parahaemolyticus* genes encoding the systems for utilization of enterobactin as a xenosiderophore. *Microbiology* **158**, 2039-49 (2012).

122. Beasley, F.C. & Heinrichs, D.E. Siderophore-mediated iron acquisition in the staphylococci. *J Inorg Biochem* **104**, 282-8 (2010).

123. Sebulsky, M.T., Hohnstein, D., Hunter, M.D. & Heinrichs, D.E. Identification and characterization of a membrane permease involved in iron-hydroxamate transport in *Staphylococcus aureus*. *J Bacteriol* **182**, 4394-400 (2000).

124. Theodore, T.S. & Schade, A.L. Carbohydrate metabolism of iron-rich and iron-poor *Staphylococcus aureus*. *J Gen Microbiol* **40**, 385-95 (1965).

125. Letoffe, S., Ghigo, J.M. & Wandersman, C. Secretion of the *Serratia marcescens* HasA protein by an ABC transporter. *J Bacteriol* **176**, 5372-7 (1994).

126. Rossi, M.S. et al. Identification and characterization of the hemophore-dependent heme acquisition system of *Yersinia pestis*. *Infect Immun* **69**, 6707-17 (2001).

127. Yukl, E.T. et al. Kinetic and spectroscopic studies of hemin acquisition in the hemophore HasAp from *Pseudomonas aeruginosa*. *Biochemistry* **49**, 6646-54 (2010).

128. Wandersman, C. & Delepelaire, P. Haemophore functions revisited. *Mol Microbiol* **85**, 618-31 (2012).

129. Izadi, N. et al. Purification and characterization of an extracellular heme-binding protein, HasA, involved in heme iron acquisition. *Biochemistry* **36**, 7050-7 (1997).

130. Arnoux, P. et al. The crystal structure of HasA, a hemophore secreted by *Serratia marcescens*. *Nat Struct Biol* **6**, 516-20 (1999).

131. Krieg, S. et al. Heme uptake across the outer membrane as revealed by crystal structures of the receptor-hemophore complex. *Proc Natl Acad Sci U S A* **106**, 1045-50 (2009).

132. Izadi-Pruneyre, N. et al. The heme transfer from the soluble HasA hemophore to its membrane-bound receptor HasR is driven by protein-protein interaction from a high to a lower affinity binding site. *J Biol Chem* **281**, 25541-50 (2006).

133. Burkhard, K.A. & Wilks, A. Characterization of the outer membrane receptor ShuA from the heme uptake system of *Shigella dysenteriae*. Substrate specificity and identification of the heme protein ligands. *J Biol Chem* **282**, 15126-36 (2007).

134. Fusco, W.G., Choudhary, N.R., Council, S.E., Collins, E.J. & Leduc, I. Mutational analysis of hemoglobin binding and heme utilization by a bacterial hemoglobin receptor. *J Bacteriol* **195**, 3115-23 (2013).

135. Perkins-Balding, D., Baer, M.T. & Stojiljkovic, I. Identification of functionally important regions of a haemoglobin receptor from *Neisseria meningitidis*. *Microbiology* **149**, 3423-35 (2003).

136. Buchanan, S.K. et al. Crystal structure of the outer membrane active transporter FepA from *Escherichia coli*. *Nat Struct Biol* **6**, 56-63 (1999).

137. Bracken, C.S., Baer, M.T., Abdur-Rashid, A., Helms, W. & Stojiljkovic, I. Use of heme-protein complexes by the *Yersinia enterocolitica* HemR receptor: histidine residues are essential for receptor function. *J Bacteriol* **181**, 6063-72 (1999).

138. Liu, X., Olczak, T., Guo, H.C., Dixon, D.W. & Genco, C.A. Identification of amino acid residues involved in heme binding and hemoprotein utilization in the *Porphyromonas gingivalis* heme receptor HmuR. *Infect Immun* **74**, 1222-32 (2006).

139. Nepluev, I. et al. An immunogenic, surface-exposed domain of *Haemophilus ducreyi* outer membrane protein HgbA is involved in hemoglobin binding. *Infect Immun* **77**, 3065-74 (2009).

140. Noinaj, N., Buchanan, S.K. & Cornelissen, C.N. The transferrin-iron import system from pathogenic *Neisseria* species. *Mol Microbiol* **86**, 246-57 (2012).

141. Cornelissen, C.N., Biswas, G.D. & Sparling, P.F. Expression of gonococcal transferrin-binding protein 1 causes Escherichia coli to bind human transferrin. *J Bacteriol* **175**, 2448-50 (1993).

142. Noinaj, N. et al. Structural basis for iron piracy by pathogenic *Neisseria. Nature* **483**, 53-8 (2012).

143. Andrade, M.A., Ciccarelli, F.D., Perez-Iratxeta, C. & Bork, P. NEAT: a domain duplicated in genes near the components of a putative Fe3+ siderophore transporter from Gram-positive pathogenic bacteria. *Genome Biol* **3**, research0047.1–0047.5 (2002).

144. Skaar, E.P. & Schneewind, O. Iron-regulated surface determinants (Isd) of *Staphylococcus aureus*: stealing iron from heme. *Microbes Infect* **6**, 390-7 (2004).

145. Dryla, A. et al. High-affinity binding of the staphylococcal HarA protein to haptoglobin and hemoglobin involves a domain with an antiparallel eight-stranded beta-barrel fold. *J Bacteriol* **189**, 254-64 (2007).

146. Krishna Kumar, K. et al. Structural Basis for Hemoglobin Capture by *Staphylococcus aureus* Cell-surface Protein, IsdH. *J Biol Chem* **286**, 38439-47 (2011).

147. Pilpa, R.M. et al. Functionally distinct NEAT (NEAr Transporter) domains within the *Staphylococcus aureus* IsdH/HarA protein extract heme from methemoglobin. *J Biol Chem* **284**, 1166-76 (2009).

148. Muryoi, N. et al. Demonstration of the iron-regulated surface determinant (Isd) heme transfer pathway in *Staphylococcus aureus*. *J Biol Chem* **283**, 28125-36 (2008).

149. Zhu, H. et al. Pathway for heme uptake from human methemoglobin by the iron-regulated surface determinants system of *Staphylococcus aureus*. *J Biol Chem* **283**, 18450-60 (2008).

150. Spirig, T., Weiner, E.M. & Clubb, R.T. Sortase enzymes in Gram-positive bacteria. *Mol Microbiol* **82**, 1044-59 (2011).

151. Mazmanian, S.K., Ton-That, H., Su, K. & Schneewind, O. An iron-regulated sortase anchors a class of surface protein during *Staphylococcus aureus* pathogenesis. *Proc Natl Acad Sci U S A* **99**, 2293-8 (2002).

152. Maresso, A.W. & Schneewind, O. Iron acquisition and transport in *Staphylococcus aureus*. *Biometals* **19**, 193-203 (2006).

153. Marraffini, L.A. & Schneewind, O. Anchor structure of staphylococcal surface proteins. V. Anchor structure of the sortase B substrate IsdC. *J Biol Chem* **280**, 16263-71 (2005).

154. Ekworomadu, M.T. et al. Differential Function of Lip Residues in the Mechanism and Biology of an Anthrax Hemophore. *PLoS Pathog* **8**, e1002559 (2012).

155. Gaudin, C.F.M., Grigg, J.C., Arrieta, A.L. & Murphy, M.E.P. Unique Heme-Iron Coordination by the Hemoglobin Receptor IsdB of *Staphylococcus aureus.* *Biochemistry* **50**, 5443-52 (2011).

156. Grigg, J.C., Vermeiren, C.L., Heinrichs, D.E. & Murphy, M.E. Haem recognition by a *Staphylococcus aureus* NEAT domain. *Mol Microbiol* **63**, 139-49 (2007).

157. Honsa, E.S., Owens, C.P., Goulding, C.W. & Maresso, A.W. The Near-Iron Transporter (NEAT) domains of the anthrax hemophore IsdX2 require a critical glutamine to extract heme from methemoglobin. *J Biol Chem* **288**, 8479-90 (2013).

158. Pilpa, R.M. et al. Solution structure of the NEAT (NEAr Transporter) domain from IsdH/HarA: the human hemoglobin receptor in *Staphylococcus aureus*. *J Mol Biol* **360**, 435-47 (2006).

159. Sharp, K.H., Schneider, S., Cockayne, A. & Paoli, M. Crystal structure of the heme-IsdC complex, the central conduit of the Isd iron/heme uptake system in *Staphylococcus aureus*. *J Biol Chem* **282**, 10625-31 (2007).

160. Watanabe, M. et al. Structural basis for multimeric heme complexation through a specific protein-heme interaction: the case of the third neat domain of IsdH from *Staphylococcus aureus*. *J Biol Chem* **283**, 28649-59 (2008).

161. Clarke, S.R. et al. Iron-regulated surface determinant protein A mediates adhesion of *Staphylococcus aureus* to human corneocyte envelope proteins. *Infect Immun* **77**, 2408-16 (2009).

162. Clarke, S.R., Wiltshire, M.D. & Foster, S.J. IsdA of *Staphylococcus aureus* is a broad spectrum, iron-regulated adhesin. *Mol Microbiol* **51**, 1509-19 (2004).

163. Ouattara, M. et al. Shr of Group A Streptococcus is a new type of composite NEAT protein involved in sequestering heme from methemoglobin. *Mol Microbiol* **78**, 739-56 (2010).

164. Vermeiren, C.L., Pluym, M., Mack, J., Heinrichs, D.E. & Stillman, M.J. Characterization of the heme binding properties of *Staphylococcus aureus* IsdA. *Biochemistry* **45**, 12867-75 (2006).

165. Liu, M. et al. Direct hemin transfer from IsdA to IsdC in the iron-regulated surface determinant (Isd) heme acquisition system of *Staphylococcus aureus*. *J Biol Chem* **283**, 6668-76 (2008).

166. Moriwaki, Y. et al. Heme binding mechanism of structurally similar iron-regulated surface determinant near transporter domains of *Staphylococcus aureus* exhibiting different affinities for heme. *Biochemistry* **52**, 8866-77 (2013).

167. Spirig, T. et al. *Staphylococcus aureus* uses a novel multi-domain receptor to break apart human hemoglobin and steal its heme. *J Biol Chem* **288**, 1065-78 (2012).

168. Tiedemann, M.T. & Stillman, M.J. Heme binding to the IsdE(M78A; H229A) double mutant: challenging unidirectional heme transfer in the iron-regulated surface determinant protein heme transfer pathway of *Staphylococcus aureus*. *J Biol Inorg Chem* **23**, 23 (2012).

169. Hargrove, M.S., Whitaker, T., Olson, J.S., Vali, R.J. & Mathews, A.J. Quaternary structure regulates hemin dissociation from human hemoglobin. *J Biol Chem* **272**, 17385-9 (1997).

170. Abe, R., Caaveiro, J.M., Kozuka-Hata, H., Oyama, M. & Tsumoto, K. Mapping ultra-weak protein-protein interactions between heme transporters of *Staphylococcus aureus*. *J Biol Chem* **287**, 16477-87 (2012).

171. Villareal, V.A. et al. Transient weak protein-protein complexes transfer heme across the cell wall of *Staphylococcus aureus*. *J Am Chem Soc* **133**, 14176-9 (2011).

172. Crowley, P.B. & Ubbink, M. Close encounters of the transient kind: protein interactions in the photosynthetic redox chain investigated by NMR spectroscopy. *Acc Chem Res* **36**, 723-30 (2003).

173. Cruz-Gallardo, I., Diaz-Moreno, I., Diaz-Quintana, A. & De la Rosa, M.A. The cytochrome f-plastocyanin complex as a model to study transient interactions between redox proteins. *FEBS Lett* **586**, 646-52 (2012).

174. Kim, H.K. et al. IsdA and IsdB antibodies protect mice against *Staphylococcus aureus* abscess formation and lethal challenge. *Vaccine* **28**, 6382-92 (2010).

175. Dickson, C.F. et al. Structure of the hemoglobin-IsdH complex reveals the molecular basis of iron capture by *Staphylococcus aureus*. *J Biol Chem* (2014).

176. Moriwaki, Y. et al. Molecular basis of recognition of antibacterial porphyrins by heme-transporter IsdH-NEAT3 of *Staphylococcus aureus*. *Biochemistry* **50**, 7311-20 (2011).

177. Fisher, M. et al. Shr is a broad-spectrum surface receptor that contributes to adherence and virulence in group A streptococcus. *Infect Immun* **76**, 5006-15 (2008).

178. Ouattara, M. et al. Kinetics of heme transfer by the Shr NEAT domains of Group A Streptococcus. *Arch Biochem Biophys* **538**, 71-9 (2013).

179. Lu, C., Xie, G., Liu, M., Zhu, H. & Lei, B. Direct heme transfer reactions in the Group A Streptococcus heme acquisition pathway. *PLoS One* **7**, e37556 (2012).

180. Aranda, R.t. et al. Bis-methionyl coordination in the crystal structure of the heme-binding domain of the streptococcal cell surface protein Shp. *J Mol Biol* **374**, 374-83 (2007).

181. Liu, M. & Lei, B. Heme transfer from streptococcal cell surface protein Shp to HtsA of transporter HtsABC. *Infect Immun* **73**, 5086-92 (2005).

182. Kobe, B. & Kajava, A.V. The leucine-rich repeat as a protein recognition motif. *Curr Opin Struct Biol* **11**, 725-32 (2001).

183. Maresso, A.W., Garufi, G. & Schneewind, O. *Bacillus anthracis* secretes proteins that mediate heme acquisition from hemoglobin. *PLoS Pathog* **4**, e1000132 (2008).

184. Honsa, E.S., Fabian, M., Cardenas, A.M., Olson, J.S. & Maresso, A.W. The five near-iron transporter (NEAT) domain anthrax hemophore, IsdX2, scavenges heme from hemoglobin and transfers heme to the surface protein IsdC. *J Biol Chem* **286**, 33652-60 (2011).

185. Fabian, M., Solomaha, E., Olson, J.S. & Maresso, A.W. Heme transfer to the bacterial cell envelope occurs via a secreted hemophore in the Gram-positive pathogen *Bacillus anthracis*. *J Biol Chem* **284**, 32138-46 (2009).

186. Balderas, M.A., Nobles, C.L., Honsa, E.S., Alicki, E.R. & Maresso, A.W. Hal Is a *Bacillus anthracis* heme acquisition protein. *J Bacteriol* **194**, 5513-21 (2012).

187. Newton, S.M. et al. The svpA-srtB locus of *Listeria monocytogenes:* fur-mediated iron regulation and effect on virulence. *Mol Microbiol* **55**, 927-40 (2005).

188. Xiao, Q. et al. Sortase independent and dependent systems for acquisition of haem and haemoglobin in *Listeria monocytogenes*. *Mol Microbiol* **80**, 1581-97 (2011).

189. Grigg, J.C., Cheung, J., Heinrichs, D.E. & Murphy, M.E. Specificity of Staphyloferrin B recognition by the SirA receptor from *Staphylococcus aureus*. *J Biol Chem* **285**, 34579-88 (2010).

190. Grigg, J.C., Cooper, J.D., Cheung, J., Heinrichs, D.E. & Murphy, M.E.P. The *Staphylococcus aureus* Siderophore Receptor HtsA Undergoes Localized Conformational Changes to Enclose Staphyloferrin A in an Arginine-rich Binding Pocket. *Journal of Biological Chemistry* **285**, 11162-11171 (2010).

191. Grigg, J.C., Vermeiren, C.L., Heinrichs, D.E. & Murphy, M.E. Heme coordination by *Staphylococcus aureus* IsdE. *J Biol Chem* **282**, 28815-22 (2007).

192. Beasley, F.C. et al. Characterization of staphyloferrin A biosynthetic and transport mutants in *Staphylococcus aureus*. *Mol Microbiol* **72**, 947-63 (2009).

193. Morrissey, J.A., Cockayne, A., Hill, P.J. & Williams, P. Molecular cloning and analysis of a putative siderophore ABC transporter from *Staphylococcus aureus*. *Infect Immun* **68**, 6281-8 (2000).

194. Speziali, C.D., Dale, S.E., Henderson, J.A., Vines, E.D. & Heinrichs, D.E. Requirement of *Staphylococcus aureus* ATP-binding cassette-ATPase FhuC for

iron-restricted growth and evidence that it functions with more than one iron transporter. *J Bacteriol* **188**, 2048-55 (2006).

195. Grigg, J.C., Ukpabi, G., Gaudin, C.F. & Murphy, M.E. Structural biology of heme binding in the *Staphylococcus aureus* Isd system. *J Inorg Biochem* **104**, 341-48 (2010).

196. Schuller, D.J., Zhu, W., Stojiljkovic, I., Wilks, A. & Poulos, T.L. Crystal structure of heme oxygenase from the gram-negative pathogen *Neisseria meningitidis* and a comparison with mammalian heme oxygenase-1. *Biochemistry* **40**, 11552-8 (2001).

197. Unno, M. et al. Crystal structure of the dioxygen-bound heme oxygenase from *Corynebacterium diphtheriae:* implications for heme oxygenase function. *J Biol Chem* **279**, 21055-61 (2004).

198. Duong, T. et al. Structural and functional characterization of an Isd-type haem-degradation enzyme from *Listeria monocytogenes*. *Acta Crystallogr D Biol Crystallogr* **70**, 615-26 (2014).

199. Lee, W.C., Reniere, M.L., Skaar, E.P. & Murphy, M.E. Ruffling of metalloporphyrins bound to IsdG and IsdI, two heme-degrading enzymes in *Staphylococcus aureus*. *J Biol Chem* **283**, 30957-63 (2008).

200. Reniere, M.L. et al. The IsdG-family of haem oxygenases degrades haem to a novel chromophore. *Mol Microbiol* **75**, 1529-38 (2010).

201. Matsui, T. et al. Heme degradation by *Staphylococcus aureus* IsdG and IsdI liberates formaldehyde rather than carbon monoxide. *Biochemistry* **52**, 3025-7 (2013).

202. Hempel, K., Herbst, F.A., Moche, M., Hecker, M. & Becher, D. Quantitative proteomic view on secreted, cell surface-associated, and cytoplasmic proteins of the methicillin-resistant human pathogen *Staphylococcus aureus* under iron-limited conditions. *J Proteome Res* **10**, 1657-66 (2011).

203. Cheng, A.G. et al. Genetic requirements for *Staphylococcus aureus* abscess formation and persistence in host tissues. *Faseb J* **23**, 3393-404 (2009).

204. Reniere, M.L. & Skaar, E.P. *Staphylococcus aureus* haem oxygenases are differentially regulated by iron and haem. *Mol Microbiol* **69**, 1304-15 (2008).

205. Visai, L. et al. Immune evasion by *Staphylococcus aureus* conferred by iron-regulated surface determinant protein IsdH. *Microbiology* **155**, 667-79 (2009).

206. Hurd, A.F. et al. The iron-regulated surface proteins IsdA, IsdB, and IsdH are not required for heme iron utilization in *Staphylococcus aureus. FEMS Microbiol Lett* **329**, 93-100 (2012).

207. Pishchany, G., Haley, K.P. & Skaar, E.P. *Staphylococcus aureus* Growth using Human Hemoglobin as an Iron Source. *J Vis Exp* (2013).

208. Pishchany, G. et al. IsdB-dependent Hemoglobin Binding Is Required for Acquisition of Heme by *Staphylococcus aureus*. *J Infect Dis* (2014).

209. Clarke, S.R. et al. The *Staphylococcus aureus* surface protein IsdA mediates resistance to innate defenses of human skin. *Cell Host Microbe* **1**, 199-212 (2007).

210. Miajlovic, H. et al. Direct interaction of iron-regulated surface determinant IsdB of *Staphylococcus aureus* with the GPIIb/IIIa receptor on platelets. *Microbiology* **156**, 920-8 (2010).

211. Zapotoczna, M., Jevnikar, Z., Miajlovic, H., Kos, J. & Foster, T.J. Iron-regulated surface determinant B (IsdB) promotes *Staphylococcus aureus* adherence to and internalization by non-phagocytic human cells. *Cell Microbiol* **15**, 1026-41 (2013).

212. Smith, E.J., Visai, L., Kerrigan, S.W., Speziale, P. & Foster, T.J. The Sbi protein is a multifunctional immune evasion factor of *Staphylococcus aureus*. *Infect Immun* **79**, 3801-9 (2011).

213. Sambrook, J., Fritsch, E. & Maniatis, T. Lysis by alkali in *Molecular cloning a laboratory manual* 1.38-1.40 (Cold Spring Harbour Laboratory Press, 1989).

214. Liu, H. & Naismith, J.H. An efficient one-step site-directed deletion, insertion, single and multiple-site plasmid mutagenesis protocol. *BMC Biotechnol* **8**, 91 (2008).

215. Ascoli, F., Fanelli, M.R. & Antonini, E. Preparation and properties of apohemoglobin and reconstituted hemoglobins. *Methods Enzymol* **76**, 72-87 (1981).

216. Gell, D., Kong, Y., Eaton, S.A., Weiss, M.J. & Mackay, J.P. Biophysical characterization of the alpha-globin binding protein alpha-hemoglobin stabilizing protein. *J Biol Chem* **277**, 40602-9 (2002).

217. Brantley, R.E., Jr., Smerdon, S.J., Wilkinson, A.J., Singleton, E.W. & Olson, J.S. The mechanism of autooxidation of myoglobin. *J Biol Chem* **268**, 6995-7010 (1993).

218. Sadrzadeh, S.M., Graf, E., Panter, S.S., Hallaway, P.E. & Eaton, J.W. Hemoglobin. A biologic fenton reagent. *J Biol Chem* **259**, 14354-6 (1984).

219. Rodkey, F.L., O'Neal, J.D., Collison, H.A. & Uddin, D.E. Relative affinity of hemoglobin S and hemoglobin A for carbon monoxide and oxygen. *Clin Chem* **20**, 83-4 (1974).

220. Eaton, W.A. & Hofrichter, J. Polarized absorption and linear dichroism spectroscopy of hemoglobin. *Methods Enzymol* **76**, 175-261 (1981).

221. Vu, N.T. et al. Selective binding of antimicrobial porphyrins to the heme-receptor IsdH-NEAT3 of *Staphylococcus aureus*. *Protein Sci* **22**, 942-53 (2013).

222. Jeffries, C.M., Whitten, A.E., Harris, S.P. & Trewhella, J. Small-angle X-ray scattering reveals the N-terminal domain organization of cardiac myosin binding protein C. *J Mol Biol* **377**, 1186-99 (2008).

223. Konarev, P.V., Volkov, V.V., Sokolova, A.V., Koch, M.H. & Svergun, D.I. PRIMUS: a windows PC-based system for small-angle scattering data analysis. *J Appl Crystallogr* **36**, 1277-82 (2000).

224. Jacques, D.A. & Trewhella, J. Small-angle scattering for structural biology - expanding the frontier while avoiding the pitfalls. *Protein Sci* **19**, 642-57 (2010).

225. Bernado, P., Mylonas, E., Petoukhov, M.V., Blackledge, M. & Svergun, D.I. Structural characterization of flexible proteins using small-angle X-ray scattering. *J Am Chem Soc* **129**, 5656-64 (2007).

226. Rupp, B. *Biomolecular Crystallography: Principles, Practice, and Application to Structural Biology*, (Garland Science, New York, 2010).

227. Tiedemann, M.T., Muryoi, N., Heinrichs, D.E. & Stillman, M.J. Iron acquisition by the haem-binding Isd proteins in *Staphylococcus aureus:* studies of the mechanism using magnetic circular dichroism. *Biochem Soc Trans* **36**, 1138-43 (2008).

228. Geoghegan, K.F. et al. Spontaneous alpha-N-6-phosphogluconoylation of a "His tag" in Escherichia coli: the cause of extra mass of 258 or 178 Da in fusion proteins. *Anal Biochem* **267**, 169-84 (1999).

229. Mack, J., Vermeiren, C., Heinrichs, D.E. & Stillman, M.J. In vivo heme scavenging by *Staphylococcus aureus* IsdC and IsdE proteins. *Biochem Biophys Res Commun* **320**, 781-8 (2004).

230. Bowden, C.F., Verstraete, M.M., Eltis, L.D. & Murphy, M.E. Hemoglobin binding and catalytic heme extraction by IsdB near iron transporter domains. *Biochemistry* **53**, 2286-94 (2014).

231. Hemdan, E.S., Zhao, Y.J., Sulkowski, E. & Porath, J. Surface topography of histidine residues: a facile probe by immobilized metal ion affinity chromatography. *Proc Natl Acad Sci U S A* **86**, 1811-5 (1989).

232. Nienhaus, K. & Nienhaus, G.U. Probing heme protein-ligand interactions by UV/visible absorption spectroscopy. *Methods Mol Biol* **305**, 215-42 (2005).

233. Yip, Y.K., Waks, M. & Beychok, S. Influence of prosthetic groups on protein folding and subunit assembly. I. Conformational differences between separated human alpha- and beta- globins. *J. Biol. Chem.* **247**, 7237-44 (1972).

234. Benesch, R.E. & Kwong, S. The stability of the heme-globin linkage in some normal, mutant, and chemically modified hemoglobins. *J Biol Chem* **265**, 14881-5 (1990).

235. Volkov, V.V. & Svergun, D.I. Uniqueness of ab-initio shape determination in small-angle scattering. *J. Appl. Cryst.* **36**, 860-64 (2003).

236. Franke, D. & Svergun, D.I. DAMMIF, a program for rapid ab-initio shape determination in small-angle scattering. *J. Appl. Cryst.* **42**, 343-6 (2009).

237. Beckham, S.A. et al. Conformational rearrangements of RIG-I receptor on formation of a multiprotein:dsRNA assembly. *Nucleic Acids Res* **41**, 3436-45 (2013).

238. Durand, D. et al. NADPH oxidase activator p67(phox) behaves in solution as a multidomain protein with semi-flexible linkers. *J Struct Biol* **169**, 45-53 (2010).

239. Receveur-Brechot, V. & Durand, D. How random are intrinsically disordered proteins? A small angle scattering perspective. *Curr Protein Pept Sci* **13**, 55-75 (2012).

240. Bernado, P. et al. Structure and dynamics of ribosomal protein L12: An ensemble model based on SAXS and NMR relaxation. *Biophys J* **98**, 2374-82 (2010).

241. Otwinowski, Z. & Minor, W. Processing of X-ray diffraction data collected in oscillation mode. *Methods Enzymol* **276**, 307-26 (1997).

242. Stein, N. CHAINSAW: a program for mutating pdb files used as templates in molecular replacement. *J Appl Crystallogr* **41**, 641-43 (2008).

243. McCoy, A.J. et al. Phaser crystallographic software. *J Appl Crystallogr* **40**, 658-674 (2007).

244. Vagin, A. & Teplyakov, A. An approach to multi-copy search in molecular replacement. *Acta Crystallogr D Biol Crystallogr* **56**, 1622-4 (2000).

245. Bricogne, G. et al. BUSTER version 2.10.0. *Cambridge, United Kingdom: Global Phasing Ltd* (2011).

246. Smart, O.S. et al. Exploiting structure similarity in refinement: automated NCS and target-structure restraints in BUSTER. *Acta Crystallogr D Biol Crystallogr* **68**, 368-80 (2012).

247. Chen, V.B. et al. MolProbity: all-atom structure validation for macromolecular crystallography. *Acta Crystallogr D Biol Crystallogr* **66**, 12-21 (2010).

248. Svergun, D.I., Barberato, C. & Koch, M.H.J. CRYSOL - a program to evaluate X-ray solution scattering of biological macromolecules from atomic coordinates. *J Appl Crystallogr*, 768-773 (1995).

249. Kozin, M. & Svergun, D.I. Automated matching of high- and low-resolution structural models. *J Appl Crystallogr* **34**, 33-41 (2001).

250. Andersen, C.B. et al. Structure of the haptoglobin-haemoglobin complex. *Nature* (2012).

251. Chiancone, E. et al. Studies on the reaction of haptoglobin with haemoglobin and haemoglobin chains. I. Stoichiometry and affinity. *J Mol Biol* **34**, 347-56 (1968).

252. Hwang, P.K. & Greer, J. Interaction between hemoglobin subunits in the hemoglobin . haptoglobin complex. *J Biol Chem* **255**, 3038-41 (1980).

253. Polticelli, F., Bocedi, A., Minervini, G. & Ascenzi, P. Human haptoglobin structure and function - a molecular modelling study. *Febs J* **275**, 5648-56 (2008).

254. Antonini, E. & Brunori, M. Hemoglobin. *Annu Rev Biochem* **39**, 977-1042 (1970).

255. Arisaka, F., Nagai, Y. & Nagai, M. Dimer-tetramer association equilibria of human adult hemoglobin and its mutants as observed by analytical ultracentrifugation. *Methods* **54**, 175-80 (2011).

256. Bucci, E. Preparation of isolated chains of human hemoglobin. *Methods Enzymol* **76**, 97-106 (1981).

257. Mollan, T.L., Khandros, E., Weiss, M.J. & Olson, J.S. The kinetics of alpha-globin binding to alpha hemoglobin stabilizing protein (AHSP) indicate preferential stabilization of a hemichrome folding intermediate. *J Biol Chem* **287**, 11338-11350 (2012).

258. Antonini, E. et al. The properties and interactions of the isolated alpha- and beta-chains of human haemoglobin. V. The reaction of alpha- and beta-chains. *J Mol Biol* **17**, 29-46 (1966).

259. Stevens, F.J. & Schiffer, M. Computer simulation of protein self-association during small-zone gel filtration. Estimation of equilibrium constants. *Biochem J* **195**, 213-9 (1981).

260. Pishchany, G., Dickey, S.E. & Skaar, E.P. Subcellular localization of the *Staphylococcus aureus* heme iron transport components IsdA and IsdB. *Infect Immun* **77**, 2624-34 (2009).

261. Simplaceanu, V. et al. Chain-selective isotopic labeling for NMR studies of large multimeric proteins: application to hemoglobin. *Biophys J* **79**, 1146-54 (2000).

262. Kapralov, A. et al. Peroxidase activity of hemoglobin-haptoglobin complexes: covalent aggregation and oxidative stress in plasma and macrophages. *J Biol Chem* **284**, 30395-407 (2009).

263. Bates, C.S., Montanez, G.E., Woods, C.R., Vincent, R.M. & Eichenbaum, Z. Identification and characterization of a *Streptococcus pyogenes* operon involved

in binding of hemoproteins and acquisition of iron. *Infect Immun* **71**, 1042-55 (2003).

264. Zapotoczna, M., Heilbronner, S., Speziale, P. & Foster, T.J. Iron regulated surface determinant (Isd) proteins of *Staphylococcus lugdunensis*. *J Bacteriol* **194**, 6453-67 (2012).

265. Kabsch, W. XDS. *Acta Crystallogr D Biol Crystallogr* **66**, 125-32 (2010).

266. Collaborative Computational Project, N. The CCP4 suite: programs for protein crystallography. *Acta Crystallogr D Biol Crystallogr* **50**, 760-3 (1994).

267. Murshudov, G.N., Vagin, A.A. & Dodson, E.J. Refinement of macromolecular structures by the maximum-likelihood method. *Acta Crystallogr D Biol Crystallogr* **53**, 240-55 (1997).

268. Emsley, P. & Cowtan, K. Coot: model-building tools for molecular graphics. *Acta Crystallogr D Biol Crystallogr* **60**, 2126-32 (2004).

269. Joosten, R.P., Joosten, K., Murshudov, G.N. & Perrakis, A. PDB_REDO: constructive validation, more than just looking for errors. *Acta Crystallogr D Biol Crystallogr* **68**, 484-96 (2012).

270. Hargrove, M.S., Wilkinson, A.J. & Olson, J.S. Structural factors governing hemin dissociation from metmyoglobin. *Biochemistry* **35**, 11300-9 (1996).

271. Liong, E.C., Dou, Y., Scott, E.E., Olson, J.S. & Phillips, G.N., Jr. Waterproofing the heme pocket. Role of proximal amino acid side chains in preventing hemin loss from myoglobin. *J Biol Chem* **276**, 9093-100 (2001).

272. Smith, M.L., Hjortsberg, K., Romeo, P.H., Rosa, J. & Paul, K.G. Mutant hemoglobin stability depends upon location and nature of single point mutation. *FEBS Lett* **169**, 147-50 (1984).

273. Bird, A.R. et al. Hb Boras or alpha 2 beta 2(88)(F4)Leu-Arg in a South African female. *Hemoglobin* **11**, 157-60 (1987).

274. Wajcman, H. et al. HB Les Andelys [alpha83(F4)LEU-PRO]: a new moderately unstable variant. *Hemoglobin* **22**, 129-40 (1998).

275. Tanaka, Y. et al. Oxygen binding and stability properties of Hb Santa Ana (beta 88 Leu-Pro). *Hemoglobin* **9**, 157-69 (1985).

276. Jacob, H.S. & Winterhalter, K.H. The role of hemoglobin heme loss in Heinz body formation: studies with a partially heme-deficient hemoglobin and with genetically unstable hemoglobins. *J Clin Invest* **49**, 2008-16 (1970).

277. Eliezer, D. & Wright, P.E. Is apomyoglobin a molten globule? Structural characterization by NMR. *J Mol Biol* **263**, 531-8 (1996).

278. Krishna Kumar, K., Dickson, C.F., Weiss, M.J., Mackay, J.P. & Gell, D.A. Alpha-haemoglobin stabilizing protein (AHSP) stabilizes apo-alpha-haemoglobin in a partially folded state. *Biochem J* **432**, 275-282 (2010).

279. Baldwin, J. & Chothia, C. Haemoglobin: the structural changes related to ligand binding and its allosteric mechanism. *J Mol Biol* **129**, 175-220 (1979).

280. Dickson, C.F. et al. alpha-Hemoglobin-stabilizing protein (AHSP) perturbs the proximal heme pocket of oxy-alpha-hemoglobin and weakens the iron-oxygen bond. *J Biol Chem* **288**, 19986-20001 (2013).

281. Feng, L. et al. Molecular mechanism of AHSP-mediated stabilization of alpha-hemoglobin. *Cell* **119**, 629-40 (2004).

282. Feng, L. et al. Structure of oxidized alpha-haemoglobin bound to AHSP reveals a protective mechanism for haem. *Nature* **435**, 697-701 (2005).

283. Gell, D.A. et al. A cis-proline in alpha-hemoglobin stabilizing protein directs the structural reorganization of alpha-hemoglobin. *J Biol Chem* **284**, 29462-9 (2009).

284. Khandros, E. et al. Insights into hemoglobin assembly through in vivo mutagenesis of alpha-hemoglobin stabilizing protein. *J Biol Chem* **287**, 11325–11337 (2012).

285. Banci, L. et al. The Atx1-Ccc2 complex is a metal-mediated protein-protein interaction. *Nat Chem Biol* **2**, 367-368 (2006).

286. Honsa, E.S. & Maresso, A.W. Mechanisms of iron import in anthrax. *Biometals* **22**, 22 (2011).

287. Dumas, Z., Ross-Gillespie, A. & Kummerli, R. Switching between apparently redundant iron-uptake mechanisms benefits bacteria in changeable environments. *Proc Biol Sci* **280**, 20131055 (2013).

288. Tiedemann, M.T., Pinter, T.B. & Stillman, M.J. Insight into blocking heme transfer by exploiting molecular interactions in the core Isd heme transporters IsdA-NEAT, IsdC-NEAT, and IsdE of *Staphylococcus aureus*. *Metallomics* **4**, 751-60 (2012).

289. Stojiljkovic, I., Kumar, V. & Srinivasan, N. Non-iron metalloporphyrins: potent antibacterial compounds that exploit haem/Hb uptake systems of pathogenic bacteria. *Mol Microbiol* **31**, 429-42 (1999).

290. Kuklin, N.A. et al. A novel *Staphylococcus aureus* vaccine: iron surface determinant B induces rapid antibody responses in rhesus macaques and specific increased survival in a murine S. aureus sepsis model. *Infect Immun* **74**, 2215-23 (2006).

291. Stranger-Jones, Y.K., Bae, T. & Schneewind, O. Vaccine assembly from surface proteins of *Staphylococcus aureus*. *Proc Natl Acad Sci U S A* **103**, 16942-7 (2006).

292. Yu, L. et al. Improved protective efficacy of a chimeric *Staphylococcus aureus* vaccine candidate iron-regulated surface determinant B (N 126- P 361) -target of RNAIII activating protein in mice. *Microbiol Immunol* **57**, 857-64 (2013).

293. Zuo, Q.F. et al. Evaluation of the protective immunity of a novel subunit fusion vaccine in a murine model of systemic MRSA infection. *PLoS One* **8**, e81212 (2013).

294. Coutard, B. et al. Assessment of Dengue virus helicase and methyltransferase as targets for fragment-based drug discovery. *Antiviral Res* **106C**, 61-70 (2014).

295. Furci, L.M. et al. Inhibition of the bacterial heme oxygenases from Pseudomonas aeruginosa and *Neisseria meningitidis*: novel antimicrobial targets. *J Med Chem* **50**, 3804-13 (2007).

296. Hom, K. et al. Small molecule antivirulents targeting the iron-regulated heme oxygenase (HemO) of *P. aeruginosa*. *J Med Chem* **56**, 2097-109 (2013).

297. Li, H., Kasam, V., Tautermann, C.S., Seeliger, D. & Vaidehi, N. A computational method to identify druggable binding sites that target protein-protein interactions. *J Chem Inf Model* (2014).

298. Harro, C. et al. Safety and immunogenicity of a novel *Staphylococcus aureus* vaccine: results from the first study of the vaccine dose range in humans. *Clin Vaccine Immunol* **17**, 1868-74 (2010).

299. Moustafa, M. et al. Phase IIa study of the immunogenicity and safety of the novel *Staphylococcus aureus* vaccine V710 in adults with end-stage renal disease receiving hemodialysis. *Clin Vaccine Immunol* **19**, 1509-16 (2012).

300. Ster, C. et al. Evaluation of some *Staphylococcus aureus* iron-regulated proteins as vaccine targets. *Vet Immunol Immunopathol* **136**, 311-8 (2010).

Appendices

Appendix A. Recombinant protein constructs

Name	Residue range	Vector	F-primer sequence	R-primer sequence	*Mw* (Da)	ε_{280nm} ($M^{-1}\cdot cm^{-1}$)
IsdA	47-312	pET-15b	aagcgCTCGAGgcaacagaagctacgaacgca	attcgGGATCCttattctttagctttagatgcttg	32186.6	17420
IsdB	41-609	pET-15b	tggcgCTCGAGgcagctgaagaaacaggtggt	aggttGGATCCttatgattttgctttattttcttg	66405.1	43780
$IsdB^{N1N2}$	120-459	pET-15b	gagtCTCGAGaatacatatcctattttgaat	agataGGATCCttaggtattggcttttgtaaatgc	42306.0	42780
$IsdB^{N1}$*	120-265	pET-15b	gagtCTCGAGaatacatatcctattttgaat	tgtacGGATCCttaatctgcactgttataaattgg	16942.1	20400
$IsdB^{N2}$*	341-459	pET-15b	-N-terminal residue changed by MQC see Appendix B	agataGGATCCttaggtattggcttttgtaaatgc	16496.7	17420
IsdC	29-188	pET-15b	caagtCTCGAGgcagatagcggtactttgaat	tttcaGGATCCttattctactttgtctttattcgaact	20248.0	20400
$IsdH^{N1N2N3}$	82-655	pET-15b	ttgcgCTCGAGgcagaaaatacaaatacttcagat	aagctGGATCCttacattttagattgactaagttt	68006.9	72660
$IsdH^{N2N3}$	321-655	pET-15b	gatcgcCTCGAGcaacagtatccaccagcagat	tttaGGATCCttagatatcctgatttataattct	41370.3	50770
$IsdH^{N1}$**	86–229		-	-	18876.8	20400
$IsdH^{N2}$***	321–467	pET-15b	gatcgcCTCGAGcaacagtatccaccagcagat	gacaGGATCCttagtctgggttattagtaatagg	19459.9	25900
$IsdH^{N3}$	542-655	pET-15b	actagtCTCGAGgatcaattaacagatttacaa	tttaGGATCCttagatatcctgatttataattct	15640.5	15930
208**	326–660	pHis-SUMO	-	-	38880.5 (sumo-cleaved)	49280
216**	326–660 Carries Y642A mutation	pHis-SUMO	-	-	38788 (sumo-cleaved)	47790

*Cloning was assisted by Dr Fiona Stennard and Ee-Jon Yeoh
**Provided by Prof R.Clubb. Details can be found in Spirig *et. al.*[142]
***Cloned by K. Krishna Kumar[121]

Appendix B. Recombinant protein constructs produced by modified quick change mutagenesis

Name and mutation	Parent vector	Residue range	F-primer sequence	R-primer sequence	*Mw* (Da)	ε_{280nm} ($M^{-1}\cdot cm^{-1}$)	Altered haem binding
$IsdB^{N2}$	$IsdB^{N2}$	341-459	catatgctcgagaaaatgactgatttacaagatacaaaatatgtt	cattttctcgagcatatggctgccgcgcgg	16496.7	17420	No
IsdBY440A	IsdB	120-459	gattgatgccgatggacaataccatgtcagaatcgttgat	gtccatcggcatcaatcgtttttacgtgaacttaacgat	42214	42290	Yes
$IsdH^{N2N3}$Y642A	$IsdH^{N2N3}$	321-655	cattggtgcggaaggtcaatatcatgtcagaattataaatcagg	accttccgcaccaatgtttgccacaacgacttaacaat	41278.2	49280	Yes
IsdHY642A	IsdH	82-655	cattggtgcggaaggtcaatatcatgtcagaattataaatcagg	accttccgcaccaatgtttgccacaacgacttaacaat	67914.8	71170	Yes
IsdB-Q190N	IsdB	120-459	attaaattcaggtcaattttggagaaaatttgaagtttatga	aaattgacctgaatttaatcctaattcaatttctggttttga	42292	43780	No
IsdB-F194T	IsdB	120-459	attaaatacaggtcaaacttggagaaaatttgaagttatatga	agtttgacctgtatttaatcctaattcaatttctggttttga	42259.9	43780	No
IsdB-QSF→NTT	IsdB	120-459	attaaatacaggtcaaacttggagaaaatttgaagttatatga	agtttgacctgtatttaatcctaattcaatttctggttttga	42259.9	43780	No
IsdB-FYHYA→YYHYF	IsdB	120-459	tcaacagtattatcattatttcagttctgttaaacctgctaga	gaaataatgataatactgttgagttccatctttcttttttcatttca	42398.1	45270	No
IsdB-QSF-FYHYA→NTT-YYHYF	IsdB-QSF→NTT	120-459	tcaacagtattatcattatttcagttctgttaaacctgctaga	gaaataatgataatactgttgagttccatctttcttttttcatttca	42352	45270	No
IsdB-QSF-FYHYA→NTT-YYHYF-Y440A	IsdB-QSF-FYHYA→NTT-YYHYF	120-459	gattgatgccgatggacaataccatgtcagaatcgttgat	gtccatcggcatcaatcgtttttacgtgaacttaacgat	42259.9	43780	Yes
$IsdH^{N2N3}$–K391N	208	326–660	attaggtttaaatacagcttcaacatggaagaaatttgaa	gctgtatttaaacctaattcaattattggtcctgtttttg	3866.4	49280	No
$IsdH^{N2N3}$–FYHYA→YYH	208	326–660	cagtattatcattatttcagtactgttgaaccagcaact	actgaaataatgataatactgtctttcacctttatcatttttca	38972.6	50770	No

YF							
IsdH^{N2N3} – K391N FYHYA→YYH YF	IsdH^{N2N3} –K391N	326–660	cagtattatcattatttcagtactgttgaaccagcaact	actgaaataatgataatactgtctttcacctttatcatttttca	38958.5	50770	No
IsdH^{N2N3} – K391N FYHYA→YYH YF-IT	IsdH^{N2N3} – FYHYA→YYHYF	326–660	aattggtgagaacatccatacagactatgattatacgct	ggatgttctcaccaatttcaatagatgacacaatttaact	38880.5	49280	No
IsdH^{N2N3} – K391N FYHYA→YYH YF-PH*	IsdH^{N2N3} – K391N FYHYA→YYHYF	326–660	catgcttacattcgcttctctgtatcaaacggaa	gcgaatgtaagcatgatctttaggagtatcgtatga	38914.5	49280	No
IsdH^{N2N3} – K391N FYHYA→YYH YF-PH-IT**	IsdH^{N2N3} – K391N FYHYA→YYHYF -PH	326–660	aattggtgagaacatccatacagactatgattatacgct	ggatgttctcaccaatttcaatagatgacacaatttaact	38836.5	47790	No
IsdH^{N2N3} – K391N FYHYA→YYH YF-loop6	IsdH^{N2N3} – K391N FYHYA→YYHYF -PH	326–660	agtcgaattagtatcatattcaccttctcctgaagatcatgcct	tgaatatgatactaattcgactggtaacttttgtcaccttcataaa	38984.6	49280	No
IsdH^{N2N3} – K391N FYHYA→YYH YF-IT-loop6	IsdH^{N2N3} – K391N FYHYA→YYHYF -PH-IT	326–660	agtcgaattagtatcatattcaccttctcctgaagatcatgcct	tgaatatgatactaattcgactggtaacttttgtcaccttcataaa	38906.5	47790	No
IsdH^{N2N3} – FYHYA→YYH YF-Y642A	IsdH^{N2N3} – FYHYA→YYHYF	326–660	cattggtgcggaaggtcaatatcatgtcagaattataatcagg	accttccgcaccaatgtttgccacaacgacttaacaat	38880.5	49280	Yes

* Intermediate step for cloning of loop6 mutation

** Intermediate step for cloning of loop6-IT mutation

Appendix C. Recombinant protein sequences

IsdA

MGSSHHHHHHSSGLVPRGSHMLEATEATNATNNQSTQVSQATSQPINFQVQKDGSSEKSHMDDYMQHPGKVIKQNNKYYFQTVLNNASFWKEYKFY
NANNQELATTVVNDNKKADTRTINVAVEPGYKSLTTKVHIVVPQINYNHRYTTHLEFEKAIPTLADAAKPNNVKPVQPKPAQPKTPTEQTKPVQPK
VEKVKPTVTTTSKVEDNHSTKVVSTDTTKDQTKTQTAHTVKTAQTAQEQNKVQTPVKDVATAKSESNNQAVSDNKSQQTNKVTKHNETPKQASKAK
E

IsdB$^{41\text{-}609}$

MGSSHHHHHHSSGLVPRGSHMLEAAEETGGTNTEAQPKTEAVASPTTTSEKAPETKPVANAVSVSNKEVEAPTSETKEAKEVKEVKAPKETKEVKP
AAKATNNTYPILNQELREAIKNPAIKDKDHSAPNSRPIDFEMKKKDGTQQFYHYASSVKPARVIFTDSKPEIELGLQSGQFWRKFEVYEGDKKLPI
KLVSYDTVKDYAYIRFSVSNGTKAVKIVSSTHFNNKEEKYDYTLMEFAQPIYNSADKFKTEEDYKAEKLLAPYKKAKTLERQVYELNKIQDKLPEK
LKAEYKKKLEDTKKALDEQVKSAITEFQNVQPTNEKMTDLQDTKYVVYESVENNESMMDTFVKHPIKTGMLNGKKYMVMETTNDDYWKDFMVEGQR
VRTISKDAKNNTRTIIFPYVEGKTLYDAIVKVHVKTIDYDGQYHVRIVDKEAFTKANTDKSNKKEQQDNSAKKEATPATPSKPTPSPVEKESQKQD
SQKDDNKQLPSVEKENDASSESGKDKTPATKPTKGEVESSSTTPTKVVSTTQNVAKPTTASSKTTKDVVQTSAGSSEAKDSAPLQKANIKNTNDGH
TQSQNNKNTQENKAKS

IsdB

MGSSHHHHHHSSGLVPRGSHMLENTYPILNQELREAIKNPAIKDKDHSAPNSRPIDFEMKKKDGTQQFYHYASSVKPARVIFTDSKPEIELGLQSG
QFWRKFEVYEGDKKLPIKLVSYDTVKDYAYIRFSVSNGTKAVKIVSSTHFNNKEEKYDYTLMEFAQPIYNSADKFKTEEDYKAEKLLAPYKKAKTL
ERQVYELNKIQDKLPEKLKAEYKKKLEDTKKALDEQVKSAITEFQNVQPTNEKMTDLQDTKYVVYESVENNESMMDTFVKHPIKTGMLNGKKYMVM
ETTNDDYWKDFMVEGQRVRTISKDAKNNTRTIIFPYVEGKTLYDAIVKVHVKTIDYDGQYHVRIVDKEAFTKANT

IsdB^{N1}

MGSSHHHHHHSSGLVPRGSHMLENTYPILNQELREAIKNPAIKDKDHSAPNSRPIDFEMKKKDGTQQFYHYASSVKPARVIFTDSKPEIELGLQSG
QFWRKFEVYEGDKKLPIKLVSYDTVKDYAYIRFSVSNGTKAVKIVSSTHFNNKEEKYDYTLMEFAQPIYNSAD

IsdB^{N2}

MGSSHHHHHHSSGLVPRGSHMLEKMTDLQDTKYVVYESVENNESMMDTFVKHPIKTGMLNGKKYMVMETTNDDYWKDFMVEGQRVRTISKDAKNNT
RTIIFPYVEGKTLYDAIVKVHVKTIDYDGQYHVRIVDKEAFTKANT

IsdC

MGSSHHHHHHSSGLVPRGSHMLEADSGTLNYEVYKYNTNDTSIANDYFNKPAKYIKKNGKLYVQITVNHSHWITGMSIEGHKENIISKNTAKDERT
SEFEVSKLNGKIDGKIDVYIDEKVNGKPFKYDHHYNITYKFNGPTDVAGANAPGKDDKNSASGSDKGSDGTTTGQSESNSSNKDKVE

IsdH^{N1N2N3}

MGSSHHHHHHSSGLVPRGSHMLENYPAADESLKDAIKDPALENKEHDIGPREQVNFQLLDKNNETQYYHFFSIKDPADVYYTKKKAEVELDINTAS
TWKKFEVYENNQKLPVRLVSYSPVPEDHAYIRFPVSDGTQELKIVSSTQIDDGEETNYDYTKLVFAKPIYNDPSLVKSDTNDAVVTNDQSSSVASN
QTNTNTSNQNTSTINNANNQPQATTNMSQPAQPKSSTNADQASSQPAHETNSNGNTNDKTNESSNQSDVNQQYPPADESLQDAIKNPAIIDKEHTA
DNWRPIDFQMKNDKGERQFYHYASTVEPATVIFTKTGPIIELGLKTASTWKKFEVYEGDKKLPVELVSYDSDKDYAYIRFPVSNGTREVKIVSSIE
YGENIHEDYDYTLMVFAQPITNNPDDYVDEETYNLQKLLAPYHKAKTLERQVYELEKLQEKLPEKYKAEYKKKLDQTRVELADQVKSAVTEFENVT
PTNDQLTDLQEAHFVVFESEENSESVMDGFVEHPFYTATLNGQKYVVMKTKDDSYWKDLIVEGKRVTTVSKDPKNNSRTLIFPYIPDKAVYNAIVK
VVVANIGYEGQYHVRIINQDI

IsdH^{N2N3}

MGSSHHHHHHSSGLVPRGSHMLEQQYPPADESLQDAIKNPAIIDKEHTADNWRPIDFQMKNDKGERQFYHYASTVEPATVIFTKTGPIIELGLKTA
STWKKFEVYEGDKKLPVELVSYDSDKDYAYIRFPVSNGTREVKIVSSIEYGENIHEDYDYTLMVFAQPITNNPDDYVDEETYNLQKLLAPYHKAKT
LERQVYELEKLQEKLPEKYKAEYKKKLDQTRVELADQVKSAVTEFENVTPTNDQLTDLQEAHFVVFESEENSESVMDGFVEHPFYTATLNGQKYVV
MKTKDDSYWKDLIVEGKRVTTVSKDPKNNSRTLIFPYIPDKAVYNAIVKVVVANIGYEGQYHVRIINQDI

IsdH^{N1}

MGSSHHHHHHSSGLVPRGSHMADESLKDAIKDPALENKEHDIGPREQVNFQLLDKNNETQYYHFFSIKDPADVYYTKKKAEVELDINTASTWKKFE
VYENNQKLPVRLVSYSPVPEDHAYIRFPVSDGTQELKIVSSTQIDDGEETNYDYTKLVFAKPIYNDPSL

IsdH^{N2}

MGSSHHHHHHSSGLVPRGSHMLEQQYPPADESLQDAIKNPAIIDKEHTADNWRPIDFQMKNDKGERQFYHYASTVEPATVIFTKTGPIIELGLKTA
STWKKFEVYEGDKKLPVELVSYDSDKDYAYIRFPVSNGTREVKIVSSIEYGENIHEDYDYTLMVFAQPITNNPDD

IsdH^{N3}

MGSSHHHHHHSSGLVPRGSHMLEDQLTDLQEAHFVVFESEENSESVMDGFVEHPFYTATLNGQKYVVMKTKDDSYWKDLIVEGKRVTTVSKDPKNN
SRTLIFPYIPDKAVYNAIVKVVVANIGYEGQYHVRIINQDI

208

SADESLQDAIKNPAIIDKEHTADNWRPIDFQMKNDKGERQFYHYASTVEPATVIFTKTGPIIELGLKTASTWKKFEVYEGDKKLPVELVSYDSDKD
YAYIRFPVSNGTREVKIVSSIEYGENIHEDYDYTLMVFAQPITNNPDDYVDEETYNLQKLLAPYHKAKTLERQVYELEKLQEKLPEKYKAEYKKKL
DQTRVELADQVKSAVTEFENVTPTNDQLTDLQEAHFVVFESEENSESVMDGFVEHPFYTATLNGQKYVVMKTKDDSYWKDLIVEGKRVTTVSKDPK
NNSRTLIFPYIPDKAVYNAIVKVVVANIGYEGQYHVRIINQDINTKDD

216

SADESLQDAIKNPAIIDKEHTADNWRPIDFQMKNDKGERQFYHYASTVEPATVIFTKTGPIIELGLKTASTWKKFEVYEGDKKLPVELVSYDSDKD
YAYIRFPVSNGTREVKIVSSIEYGENIHEDYDYTLMVFAQPITNNPDDYVDEETYNLQKLLAPYHKAKTLERQVYELEKLQEKLPEKYKAEYKKKL
DQTRVELADQVKSAVTEFENVTPTNDQLTDLQEAHFVVFESEENSESVMDGFVEHPFYTATLNGQKYVVMKTKDDSYWKDLIVEGKRVTTVSKDPK
NNSRTLIFPYIPDKAVYNAIVKVVVANIGAEGQYHVRIINQDINTKDD

Appendix D. Recombinant protein sequences produced by site directed mutagenesis

IsdB-Y440A

MGSSHHHHHHSSGLVPRGSHMLENTYPILNQELREAIKNPAIKDKDHSAPNSRPIDFEMKKKDGTQQFYHYASSVKPARVIFTDSKPEIELGLQSG
QFWRKFEVYEGDKKLPIKLVSYDTVKDYAYIRFSVSNGTKAVKIVSSTHFNNKEEKYDYTLMEFAQPIYNSADKFKTEEDYKAEKLLAPYKKAKTL
ERQVYELNKIQDKLPEKLKAEYKKKLEDTKKALDEQVKSAITEFQNVQPTNEKMTDLQDTKYVVYESVENNESMMDTFVKHPIKTGMLNGKKYMVM
ETTNDDYWKDFMVEGQRVRTISKDAKNNTRTIIFPYVEGKTLYDAIVKVHVKTIDADGQYHVRIVDKEAFTKANT

IsdB-Q190N

MGSSHHHHHHSSGLVPRGSHMLENTYPILNQELREAIKNPAIKDKDHSAPNSRPIDFEMKKKDGTQQFYHYASSVKPARVIFTDSKPEIELGLNSG
QFWRKFEVYEGDKKLPIKLVSYDTVKDYAYIRFSVSNGTKAVKIVSSTHFNNKEEKYDYTLMEFAQPIYNSADKFKTEEDYKAEKLLAPYKKAKTL
ERQVYELNKIQDKLPEKLKAEYKKKLEDTKKALDEQVKSAITEFQNVQPTNEKMTDLQDTKYVVYESVENNESMMDTFVKHPIKTGMLNGKKYMVM
ETTNDDYWKDFMVEGQRVRTISKDAKNNTRTIIFPYVEGKTLYDAIVKVHVKTIDYDGQYHVRIVDKEAFTKANT

IsdB-F194T

MGSSHHHHHHSSGLVPRGSHMLENTYPILNQELREAIKNPAIKDKDHSAPNSRPIDFEMKKKDGTQQFYHYASSVKPARVIFTDSKPEIELGLQSG
QTWRKFEVYEGDKKLPIKLVSYDTVKDYAYIRFSVSNGTKAVKIVSSTHFNNKEEKYDYTLMEFAQPIYNSADKFKTEEDYKAEKLLAPYKKAKTL
ERQVYELNKIQDKLPEKLKAEYKKKLEDTKKALDEQVKSAITEFQNVQPTNEKMTDLQDTKYVVYESVENNESMMDTFVKHPIKTGMLNGKKYMVM
ETTNDDYWKDFMVEGQRVRTISKDAKNNTRTIIFPYVEGKTLYDAIVKVHVKTIDYDGQYHVRIVDKEAFTKANT

IsdB-QSF→NTT

MGSSHHHHHHSSGLVPRGSHMLENTYPILNQELREAIKNPAIKDKDHSAPNSRPIDFEMKKKDGTQQFYHYASSVKPARVIFTDSKPEIELGLNTG
QTWRKFEVYEGDKKLPIKLVSYDTVKDYAYIRFSVSNGTKAVKIVSSTHFNNKEEKYDYTLMEFAQPIYNSADKFKTEEDYKAEKLLAPYKKAKTL
ERQVYELNKIQDKLPEKLKAEYKKKLEDTKKALDEQVKSAITEFQNVQPTNEKMTDLQDTKYVVYESVENNESMMDTFVKHPIKTGMLNGKKYMVM
ETTNDDYWKDFMVEGQRVRTISKDAKNNTRTIIFPYVEGKTLYDAIVKVHVKTIDYDGQYHVRIVDKEAFTKANT

IsdB-FYHYA→YYHYF

MGSSHHHHHHSSGLVPRGSHMLENTYPILNQELREAIKNPAIKDKDHSAPNSRPIDFEMKKKDGTQQYYHYFSSVKPARVIFTDSKPEIELGLQSG
QFWRKFEVYEGDKKLPIKLVSYDTVKDYAYIRFSVSNGTKAVKIVSSTHFNNKEEKYDYTLMEFAQPIYNSADKFKTEEDYKAEKLLAPYKKAKTL
ERQVYELNKIQDKLPEKLKAEYKKKLEDTKKALDEQVKSAITEFQNVQPTNEKMTDLQDTKYVVYESVENNESMMDTFVKHPIKTGMLNGKKYMVM
ETTNDDYWKDFMVEGQRVRTISKDAKNNTRTIIFPYVEGKTLYDAIVKVHVKTIDYDGQYHVRIVDKEAFTKANT

IsdB-QSF-FYHYA→NTT-YYHYF

MGSSHHHHHHSSGLVPRGSHMLENTYPILNQELREAIKNPAIKDKDHSAPNSRPIDFEMKKKDGTQQYYHYFSSVKPARVIFTDSKPEIELGLNTG
QTWRKFEVYEGDKKLPIKLVSYDTVKDYAYIRFSVSNGTKAVKIVSSTHFNNKEEKYDYTLMEFAQPIYNSADKFKTEEDYKAEKLLAPYKKAKTL
ERQVYELNKIQDKLPEKLKAEYKKKLEDTKKALDEQVKSAITEFQNVQPTNEKMTDLQDTKYVVYESVENNESMMDTFVKHPIKTGMLNGKKYMVM
ETTNDDYWKDFMVEGQRVRTISKDAKNNTRTIIFPYVEGKTLYDAIVKVHVKTIDYDGQYHVRIVDKEAFTKANT

IsdB-QSF-FYHYA→NTT-YYHYF-PH

MGSSHHHHHHSSGLVPRGSHMLENTYPILNQELREAIKNPAIKDKDHSAPNSRPIDFEMKKKDGTQQYYHYFSSVKPARVIFTDSKPEIELGLNTG
QTWRKFEVYEGDKKLPIKLVSYDTPKDHAYIRFSVSNGTKAVKIVSSTHFNNKEEKYDYTLMEFAQPIYNSADKFKTEEDYKAEKLLAPYKKAKTL
ERQVYELNKIQDKLPEKLKAEYKKKLEDTKKALDEQVKSAITEFQNVQPTNEKMTDLQDTKYVVYESVENNESMMDTFVKHPIKTGMLNGKKYMVM
ETTNDDYWKDFMVEGQRVRTISKDAKNNTRTIIFPYVEGKTLYDAIVKVHVKTIDYDGQYHVRIVDKEAFTKANT

IsdB-QSF-FYHYA→NTT-YYHYF-Y440A

MGSSHHHHHHSSGLVPRGSHMLENTYPILNQELREAIKNPAIKDKDHSAPNSRPIDFEMKKKDGTQQYYHYFSSVKPARVIFTDSKPEIELGLNTG
QTWRKFEVYEGDKKLPIKLVSYDTVKDYAYIRFSVSNGTKAVKIVSSTHFNNKEEKYDYTLMEFAQPIYNSADKFKTEEDYKAEKLLAPYKKAKTL
ERQVYELNKIQDKLPEKLKAEYKKKLEDTKKALDEQVKSAITEFQNVQPTNEKMTDLQDTKYVVYESVENNESMMDTFVKHPIKTGMLNGKKYMVM
ETTNDDYWKDFMVEGQRVRTISKDAKNNTRTIIFPYVEGKTLYDAIVKVHVKTIDADGQYHVRIVDKEAFTKANT

IsdH^{N2N3}-K391N

SADESLQDAIKNPAIIDKEHTADNWRPIDFQMKNDKGERQFYHYASTVEPATVIFTKTGPIIELGLNTASTWKKFEVYEGDKKLPVELVSYDSDKD
YAYIRFPVSNGTREVKIVSSIEYGENIHEDYDYTLMVFAQPITNNPDDYVDEETYNLQKLLAPYHKAKTLERQVYELEKLQEKLPEKYKAEYKKKL
DQTRVELADQVKSAVTEFENVTPTNDQLTDLQEAHFVVFESEENSESVMDGFVEHPFYTATLNGQKYVVMKTKDDSYWKDLIVEGKRVTTVSKDPK
NNSRTLIFPYIPDKAVYNAIVKVVVANIGAEGQYHVRIINQDINTKDD

IsdH^{N2N3}-FYHYA→YYHYF

SADESLQDAIKNPAIIDKEHTADNWRPIDFQMKNDKGERQYYHYFSTVEPATVIFTKTGPIIELGLKTASTWKKFEVYEGDKKLPVELVSYDSDKD
YAYIRFPVSNGTREVKIVSSIEYGENIHEDYDYTLMVFAQPITNNPDDYVDEETYNLQKLLAPYHKAKTLERQVYELEKLQEKLPEKYKAEYKKKL
DQTRVELADQVKSAVTEFENVTPTNDQLTDLQEAHFVVFESEENSESVMDGFVEHPFYTATLNGQKYVVMKTKDDSYWKDLIVEGKRVTTVSKDPK
NNSRTLIFPYIPDKAVYNAIVKVVVANIGYEGQYHVRIINQDINTKDD

IsdH^{N2N3}-K391N-FYHYA→YYHYF

SADESLQDAIKNPAIIDKEHTADNWRPIDFQMKNDKGERQYYHYFSTVEPATVIFTKTGPIIELGLNTASTWKKFEVYEGDKKLPVELVSYDSDKD
YAYIRFPVSNGTREVKIVSSIEYGENIHEDYDYTLMVFAQPITNNPDDYVDEETYNLQKLLAPYHKAKTLERQVYELEKLQEKLPEKYKAEYKKKL
DQTRVELADQVKSAVTEFENVTPTNDQLTDLQEAHFVVFESEENSESVMDGFVEHPFYTATLNGQKYVVMKTKDDSYWKDLIVEGKRVTTVSKDPK
NNSRTLIFPYIPDKAVYNAIVKVVVANIGYEGQYHVRIINQDINTKDD

IsdH^{N2N3}-K391N-FYHYA→YYHYF-IT

SADESLQDAIKNPAIIDKEHTADNWRPIDFQMKNDKGERQYYHYFSTVEPATVIFTKTGPIIELGLNTASTWKKFEVYEGDKKLPVELVSYDSDKD
YAYIRFPVSNGTREVKIVSSIEIGENIHTDYDYTLMVFAQPITNNPDDYVDEETYNLQKLLAPYHKAKTLERQVYELEKLQEKLPEKYKAEYKKKL
DQTRVELADQVKSAVTEFENVTPTNDQLTDLQEAHFVVFESEENSESVMDGFVEHPFYTATLNGQKYVVMKTKDDSYWKDLIVEGKRVTTVSKDPK
NNSRTLIFPYIPDKAVYNAIVKVVVANIGYEGQYHVRIINQDINTKDD

IsdH^{N2N3}-K391N-FYHYA→YYHYF-PH

SADESLQDAIKNPAIIDKEHTADNWRPIDFQMKNDKGERQYYHYFSTVEPATVIFTKTGPIIELGLNTASTWKKFEVYEGDKKLPVELVSYDSPKD
HAYIRFPVSNGTREVKIVSSIEYGENIHEDYDYTLMVFAQPITNNPDDYVDEETYNLQKLLAPYHKAKTLERQVYELEKLQEKLPEKYKAEYKKKL
DQTRVELADQVKSAVTEFENVTPTNDQLTDLQEAHFVVFESEENSESVMDGFVEHPFYTATLNGQKYVVMKTKDDSYWKDLIVEGKRVTTVSKDPK
NNSRTLIFPYIPDKAVYNAIVKVVVANIGYEGQYHVRIINQDINTKDD

IsdH^{N2N3}-K391N-FYHYA→YYHYF-PH-IT

SADESLQDAIKNPAIIDKEHTADNWRPIDFQMKNDKGERQYYHYFSTVEPATVIFTKTGPIIELGLNTASTWKKFEVYEGDKKLPVELVSYDSPKD
HAYIRFPVSNGTREVKIVSSIEIGENIHTDYDYTLMVFAQPITNNPDDYVDEETYNLQKLLAPYHKAKTLERQVYELEKLQEKLPEKYKAEYKKKL
DQTRVELADQVKSAVTEFENVTPTNDQLTDLQEAHFVVFESEENSESVMDGFVEHPFYTATLNGQKYVVMKTKDDSYWKDLIVEGKRVTTVSKDPK
NNSRTLIFPYIPDKAVYNAIVKVVVANIGYEGQYHVRIINQDINTKDD

IsdH^{N2N3}-K391N-FYHYA→YYHYF-loop6

SADESLQDAIKNPAIIDKEHTADNWRPIDFQMKNDKGERQYYHYFSTVEPATVIFTKTGPIIELGLNTASTWKKFEVYEGDKKLPVELVSYSPSPE
DHAYIRFPVSNGTREVKIVSSIEYGENIHEDYDYTLMVFAQPITNNPDDYVDEETYNLQKLLAPYHKAKTLERQVYELEKLQEKLPEKYKAEYKKK
LDQTRVELADQVKSAVTEFENVTPTNDQLTDLQEAHFVVFESEENSESVMDGFVEHPFYTATLNGQKYVVMKTKDDSYWKDLIVEGKRVTTVSKDP
KNNSRTLIFPYIPDKAVYNAIVKVVVANIGYEGQYHVRIINQDINTKDD

IsdH^{N2N3}-K391N-FYHYA→YYHYF- IT-loop6

SADESLQDAIKNPAIIDKEHTADNWRPIDFQMKNDKGERQYYHYFSTVEPATVIFTKTGPIIELGLNTASTWKKFEVYEGDKKLPVELVSYSPSPE
DHAYIRFPVSNGTREVKIVSSIEIGENIHTDYDYTLMVFAQPITNNPDDYVDEETYNLQKLLAPYHKAKTLERQVYELEKLQEKLPEKYKAEYKKK

LDQTRVELADQVKSAVTEFENVTPTNDQLTDLQEAHFVVFESEENSESVMDGFVEHPFYTATLNGQKYVVMKTKDDSYWKDLIVEGKRVTTVSKDP
KNNSRTLIFPYIPDKAVYNAIVKVVVANIGYEGQYHVRIINQDINTKDD

IsdH^{N2N3}- FYHYA→YYHYF-Y642A

SADESLQDAIKNPAIIDKEHTADNWRPIDFQMKNDKGERQYYHYFSTVEPATVIFTKTGPIIELGLKTASTWKKFEVYEGDKKLPVELVSYDSDKD
YAYIRFPVSNGTREVKIVSSIEYGENIHEDYDYTLMVFAQPITNNPDDYVDEETYNLQKLLAPYHKAKTLERQVYELEKLQEKLPEKYKAEYKKKL
DQTRVELADQVKSAVTEFENVTPTNDQLTDLQEAHFVVFESEENSESVMDGFVEHPFYTATLNGQKYVVMKTKDDSYWKDLIVEGKRVTTVSKDPK
NNSRTLIFPYIPDKAVYNAIVKVVVANIGAEGQYHVRIINQDINTKDD

Appendix E. Mass spectrometry measurements of Isd proteins

Protein (m/z series)	Expected Mass (Da)	Measured Mass (Da)	Mass difference Expt-Meas (Da)	Expected Mass without methionine (Da)	Mass difference Expt(-MET)-Meas (Da)	Modification
$IsdH^{N3}$(1)	15640.5	15508.9	-131.6	15509.3	-0.5	Cleavage of N-terminal methionine(131.2Da)
$IsdH^{N3}$(2)		15687.93		15509.3	+178.63	Cleavage of N-terminal methionine(131.2Da) Glyconylation of his-tag(178Da)
$IsdH^{N3}$(3)		15766.8		15509.3	+257.5	Cleavage of N-terminal methionine(131.2Da) Phosphogluconolylation of his-tag(258Da)
$IsdH^{N2N3}$(1)	41370	41238.4	-131.6	41238.8	-0.4	Cleavage of N-terminal methionine(131.2Da)
$IsdH^{N2N3}$(2)		41854.1		41238.8	+615.3	Cleavage of N-terminal methionine(131.2Da) Haem bound(616.5Da)
IsdA	30304.6	30307.4	+2.8	-	-	Construct had his-tag cleaved
$IsdH^{N1}$	18876.8	18907	+30.2	-	-	None